CLONING AND CHARACTERISATION OF PHOSPHOLIPASE C X-DOMAIN CONTAINING PROTEINS (PLCXDS)

Stephen Alexander Gellatly

A Thesis Submitted for the Degree of PhD
at the
University of St Andrews

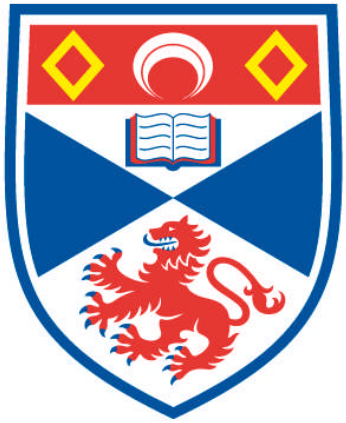

2015

Cloning and Characterisation of Phospholipase C X-Domain Containing Proteins (PLCXDs)

Steven Alexander Gellatly, B.Sc (Hons)

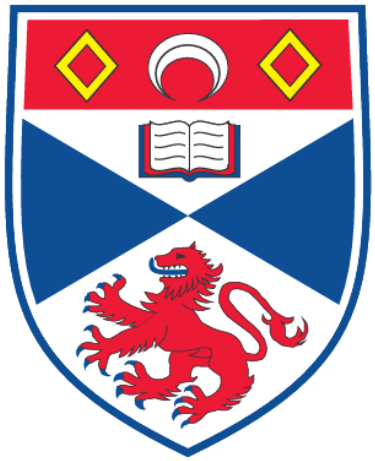

A Thesis Submitted to the University of St. Andrews for the degree of

DOCTOR OF PHILOSOPHY

School of Medicine

January 2015

Declaration

I, Steven Alexander Gellatly, hereby declare that this thesis, which is approximately 53,500 words in length, has been written by me, and that it is the record of work carried out by me or prinicipally by myself in collaboration with others as acknowldeged, and that it has not been submitted in any previous application for a higher degree.

Date……..

Signature……

I was admitted as a postgraduate research student in October 2010 and as a candidate for the degree of Doctor of Philosophy (PhD) in October 2011; the higher study for which this is a record was carried out in the University of St Andrews between 2010-2014.

Date……..

Signature……

I hereby certify that the candidate has fulfilled the conditions of the Resolutions and Regulations appropriate for the degree of PhD in the University of St Andrews and that the candidate is qualified to submit this thesis in application for that degree.

Date…….. Signature of

supervisor……

In submitting this thesis to the University of St Andrews we understand that we are giving permission for it to be made available for use in accordance with the regulations of the University Library for the time being in force, subject to any copyright vested in the work not being affected thereby. We understand that the title and abstract will be published, and that a copy of the work may be made and supplied to any bona fide library or research worker, that my thesis will be electronically accessible for personal or research use, and that the library has the right to migrate my thesis into new electronic forms as required to ensure continued access to the thesis. We have obtained any third-party copyright permissions that may be required in order to allow such access and migration. The following is an agree request by candidate and supervisor regarding the electronic publication of this thesis:

Access to printed copy and electronic publication of this thesis through the University of St Andrews.

Date……Signature of candidate……Signature of

supervisor……..

Acknowledgements

This thesis is the end of a challenging and eventful journey. Numerous friends, family and institutions have been extremely supportive and have done well to keep me travelling in the right direction for the past four years.

I express my sincere thanks and gratitude to my supervisor Dr Gordon Cramb for his support throughout the duration of the project. Gordon has been extremely supportive and has encouraged me to grow independently as a research scientist. I would also like to express my great sense of gratitude to Dr Svetlana Kalujnaia. We have shared a lot of fascinating discussions about almost everything. I have learned a lot!

I would like to thanks the Oxford Protein Production Facility for sharing their expert knowledge and experience in protein expression and purification. Dr Marisol Corral-Debrinski for supervising me on the Harlquin mouse work. It was great to have the opportunity to meet her family and enjoy dinner/wine together. Dr Stephen McMahon for his invaluable help and support with protein purification and crystallisation.

Special thanks goes to colleagues in the School of Medicine. Mary Wilson has been extremely supportive and also great fun; she is a great singer to accompany. Taciana, Katarina, Omar, Alan, Mohammad, Arif, Laura M, Richard, Petra, Elaine, Winnie (wonderful friend and neighbour), Mike, Eva, C D Owen, Christian, Anna, Rob, and many many more. I'm sorry if I have missed you……depends if you are reading this!!

Publications

Gellatly, S.A., Kalujnaia, S., Cramb, G. Cloning, tissue distribution and sub-cellular localisation of phospholipase C X-domain containing protein (PLCXD) isoforms. *Biochem Biophys Res Commun,* **424:** 651-656 (2012).

Dedication

I am dedicating this thesis to Gordon Duncan, a great friend who has unfortunately passed away. Mr D, I am sorry that we can't celebrate this occasion with a jaunt up a Munro or two but you are in my thoughts now and forever.

“Science never solves a problem without creating 10 more”

George Bernard Shaw

Abstract

Members of the phosphoinositide-specific phospholipase C (PI-PLC) enzyme family play a fundamental role in cell signalling pathways by regulating cytosolic calcium and/or the activity of several protein kinases. This thesis reports the identification, molecular cloning and characterisation of a potential seventh sub-class of the PI-PLC enzyme family, the phospholipase C X-domain containing proteins (PLCXDs), which contain only an X domain in their structure. Comparative sequence analysis has identified at least three PLCXD isoforms in the human and mouse genomes (PLCXDs 1, 2 and 3), and at least four isoforms in the European eel (PLCXDs 1-4). Key amino acid residues responsible for the catalytic properties of PI-PLCs were found to be conserved in human, mouse and eel PLCXDs 1, 2 and 3, but were absent in the sequence of eel PLCXD4. PLCXD isoforms displayed unique tissue-specific expression profiles and some similarities between species. Interestingly, in mouse PLCXD1-3 mRNA were found to be predominantly expressed in the brain, however this is yet to be confirmed in humans. Analysis of *in situ* hybridisation data in mice revealed each PLCXD to be localised in neurons within different brain regions, highly suggestive of unique roles in brain function. Furthermore, the levels of PLCXD3 protein were reduced by more than 99% in cerebella samples from a mouse model of neurodegeneration (Harlequin mouse) compared to control mice. Human PLCXD1, 2 and 3 were found to increase phosphoinositide turnover when overexpressed in the HeLa cell line, and recombinant PLCXD3, purified to homogeneity from *E. coli,* was found to interact with various phosphoinositides including $PI(4,5)P_2$. ^{31}P-NMR analysis of $PI(4,5)P_2$ and PI before and

after the addition of PLCXD3 purified from HeLa cells and *E. coli* revealed no difference in the ^{31}P spectra whereas expected chemical shifts were seen following the addition of purified bacterial PI-PLC. Significant formation of inclusion bodies was noted when human PLCXDs 1, 2 and 3 were expressed as recombinant proteins in *E. coli.* Different strategies aimed at optimising the expression of recombinant PLCXD1, 2 and 3, including the use of different fusion proteins and screening expression in *E. coli*, mammalian and insect cells had limited success, with the best soluble expression only seen with PLCXD3 in insect cells. Attempts to scale-up the purification of PLCXD3 from insect cells to provide sufficient protein for enzyme assays and crystal screens were unsuccessful. The results presented herein suggest that these novel proteins possess distinct and as yet uncharacterised tissue-specific roles in cell physiology.

Contents

List of Figures

List of Tables

Abbreviations

ADF	actin depolymerising factor
AIF	apoptosis inducing factor
AP	alkaline phosphatase
AT_1	angiotensin receptor type 1
ATCC	American type culture collection
BCR	B-cell receptor
BLAST	Basic Local Alignment Sequence Tool
BLINK	B-cell linker protein
bp	base pair
bPI-PLC	bacterial phosphatidylinositol-specific phospholipase C
BSA	bovine serum albumin
CA	Cornu Ammonis
CALM	clathrin assembly lymphoid myeloid leukemia protein
CC	coiled coil
CDP-DAG	cytidine diphosphate diacylglycerol
COS-7	CV-1 in Origin, and carrying the SC40 genetic material.
Ct	cycle time
CTP	cytidine triphosphate
DAG	diacylglycerol
DG	dentate gyrus
DGmo	dentate gyrus molecular layer
DGpo	dentate gyrus polymorph layer
DMP	dimethylpemelimidate
DMSO	dimethyl sulfoxide
ECL	Enhanced chemiluninescnece
EGF	epidermal growth factor

ENaC	epithelial sodium channels
ePI-PLC	eel phosphatidylinositol-specific phospholipase C
fMLP	Formyl-Methionyl-Leucyl-Phenylalanine
FW	freshwater
GEF	guanine nucleotide exchange factor
GPCRs	G-protein coupled receptors
GPI	glycosylphosphatidylinositol
GTP	guanosine triphosphate
HEK	human embryonic kidney
hPI-PLC	human phosphatidylinositol-specific phospholipase C
Hq	Harlequin mutant (mouse/mice)
HRP	horseradish peroxidase
IcP	cyclic inositol phosphate
IMPA	myo-inositol monophosphatase
IP_3	inositol trisphosphate
IPTG	Isopropyl β-D-1-thiogalactopyranoside
ITAM	immunoreceptor tyrosine-based activation motif
IVF	*In vitro* fertilisation
kb	kilobase
kDa	kilodalton
Kir	inwardly rectifying potassium channel
LB	Luria Broth
LTD	long-term depression
LTP	long-term potentiation
MALDI	Matrix-assisted laser desorption/ionization
MCS	multiple cloning site
MIP	myo-inositol 3-phosphate
MOB	main olfactory bulb

mPI-PLC	mouse phosphatidylinositol-specific phospholipase C
NADH	nicotinamide adenine dinucleotide reduced
NCBI	National Centre for Biotechnology Information
NGF	nerve growth factor
NLS	nuclear localisation signal
NMR	nuclear magnetic resonance
OD	Optical Density
OPPF	Oxford Protein Production Facility
PA	phosphatidic acid
Pac	puromycin N-acyl transferase
PBS	Phosphate Buffered Saline
PCR	polymerase chain reaction
PDGF	peptide derived growth factor
PE	phosphatidylethanolamine
PFA	paraformaldehyde
PH	pleckstrin homology
PIP4K	phosphatidylinositol 5-phosphate 4-kinase
PIP5K	phosphatidylinositol 4-phosphate 5-kinase
PI-PLC	phosphatidylinositol-specific phospholipase C
PKC	protein kinase C
PLC	phospholipase C
PLCXD	phospholipase C X-domain containing protein
PS	phosphdatidylserine
PVDF	polyvinylidene fluoride
RA	Ras-association
Rac 1	Ras-related C3 botumlinum toxin substrate 1
Rac 2	Ras-related C3 botumlinum toxin substrate 2
RACE	Rapid Amplification of cDNA Ends

Rpl-P0	ribosomal protein large P0
RTK	receptor tyrosine kinase
RT-PCR	reverse transcriptase polymerase chain reaction
RT-qPCR	real-time quantitative polymerase chain reaction
SOC	Super Optimal Broth
SEM	standard error of the mean
Sf-9	*Spodoptera frugiperda-9*
SH2	Src homology 2
SH3	Src homology 3
SNP	single-nucleotide polymorphism
SW	seawater
TB	Terrific Broth
TE	tris-EDTA
TEV	Tobacco Etch Virus
TIM	triose phosphate isomerase
TS	transition state
VSG	variant surface glycoprotein
WT	wildtype

CHAPTER 1: INTRODUCTION

1.1. Signal transduction

The survival of all organisms is governed by their dynamic ability to coordinate constantly their activities with environmental changes. Successful communication with the environment is achieved through a number of signal transduction pathways that receive and process signals from the external environment, from other cells within the organism and also from different regions within the cell. Signal transduction pathways coordinate a wide range of physiological activities including: cell growth and division; differentiation and development; cell motility and morphology; and cell metabolism. A deep appreciation and understanding of the different signal transduction pathways and the interplay between them is therefore essential for the development of approaches to correct abnormal cell functions.

1.2. Discovery of phosphoinositides

Inositol-containing phospholipids, also known as phosphoinositides, comprise a group of membrane lipids with different arrangements of phosphate groups attached to the polar inositol head-group. Although together they only represent a small fraction of the total cellular phospholipid pool, enzymatic regulation of the abundance of the different inositol phospholipids is a fundamental component of one of the many signal transduction pathways found in animal cells (Balla, 2013). Initial identification and characterisation of the various phosphoinositides began with the observation that inositol can be incorporated into some lipids present within mycobacteria (Anderson and Roberts, 1930). Furthermore, analysis of lipid extracts prepared from bovine brain identified inositol phospholipids that contain phosphate groups in approximate ratio of 2:1 with inositol. These lipids were named diphosphoinositides and were found to

be present in a number of different cells and tissues (Folch, 1949). Our understanding of the complexity of the inositol phospholipid family was extended following the identification of mono and tri-phosphorylated derivatives of inositol phospholipids in lipid extracts, giving a total of three major classes known as the mono-, di-, and tri-phosphoinositides. Characterisation of these lipids revealed that they all had similar chemical structures consisting of a diacyglycerol backbone (two fatty acids esterified onto glycerol) attached through a diester phosphate to the 1-hydroxyl of the inositol ring (Mitchell, 1975). Cartoon structures of these lipids are shown in Figure 1.1.

These lipids were also found to be present in many types of cells and tissues and were therefore thought to be essential for the normal functions of most cells. These lipids are now more correctly referred to as phosphatidylinositol (PI), phosphatidylinositol 4-phosphate (PI(4)P) and phosphatidylinositol 4,5-bisphosphate ($PI(4,5)P_2$) (Mitchell, 2008; Figure 1.1). The physiological importance of these lipids began to be revealed in 1953 following the observation of that acetylcholine could induce rapid changes in the abundance of certain lipids within this phosphoinositide pool in rat pancreatic slices (Hokin, 1953). The discovery of the further phosphorylated versions of phosphatidylinositol, including phosphatidylinositol 3-phosphate (PI(3)P), phosphatidylinositol 3,4-bisphosphate $PI(3,4)P_2$ and phosphatidylinositol 3,4,5-trisphosphate $PI(3,4,5)P_3$ in 1988 (Traynor-Kaplan *et al*., 1988; Whitman *et al*., 1988) and phosphatidylinositol 5-phosphate (PI(5)P) and phosphatidylinositol 3,5-bisphopshate ($PI(3,5)P_2$) in 1997 (Dove *et al*., 1997; Rameh *et al*., 1997) gave phosphoinositide research a new focus. There are now seven phosphorylated derivatives of phosphatidylinositol known to exist in mammalian cells. These are

derived through phosphorylation and de-phosphorylation of the inositol head-group by a variety of lipid kinases and phosphatases at three positions, 3, 4 and 5 (Kadamur and Ross, 2013; Figure 1.1).

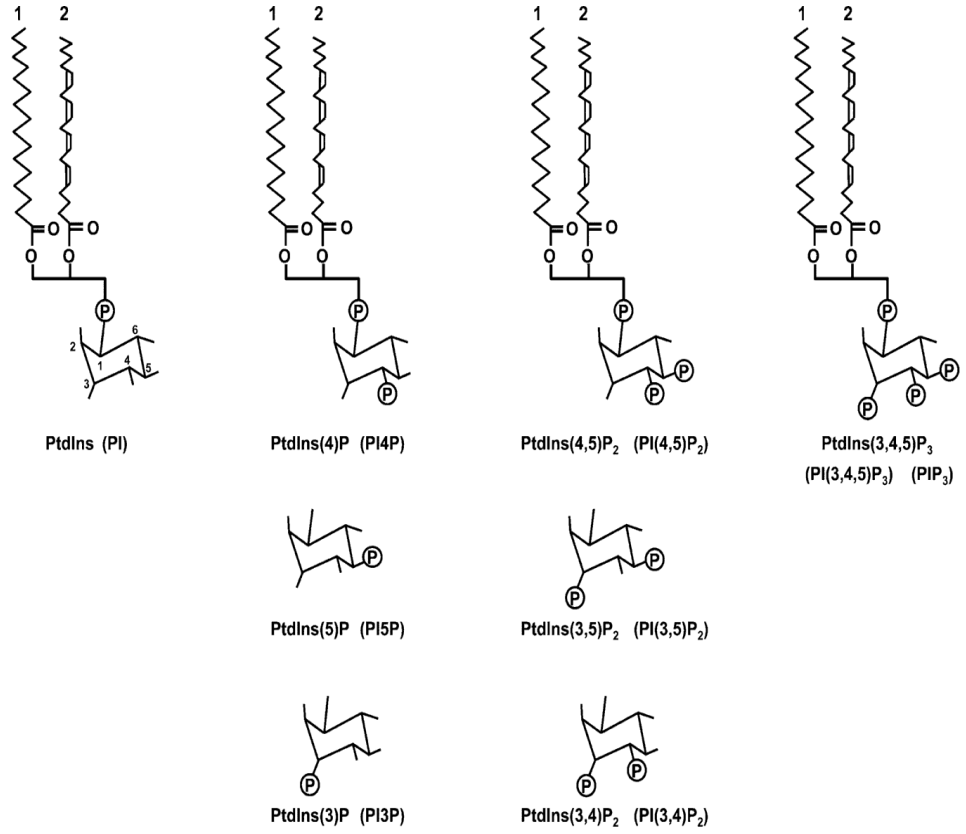

Figure 1.1: Schematic depiction of the chemical structures of the eight phosphoinositides found in mammalian cells. Each of the 8 phosphoinositides has a similar chemical structure which consists of two fatty acids esterified onto glycerol (Diacylglycerol) which is attached, through a diester phosphate, to the 1-hydroxyl of the inositol ring. The inositol moiety can be reversibly phosphorylated at positions 3, 4 and 5 of the inositol ring. Taken from Hawkins *et al*., 2006.

1.3. Pathways for phosphoinositide biosynthesis

The synthesis of phosphoinositides involves the formation of the six carbon cyclitol, inositol. In nature a total of nine possible stereoisomers of inositol have been identified to date. In eukaryotic cells *myo*-inositol is physiologically the most important

stereoisomer and is used for phospholipid synthesis (Mitchell, 2008). The biosynthesis of *myo*-inositol can occur through two pathways: the *de novo* pathway and the salvage pathway. In all organisms studied to date, the *de novo* synthesis of *myo*-inositol follows a common pathway. The NAD^+-dependent *myo*-inositol 3-phosphate synthase (MIPS) converts glucose 6-phosphate (G 6-P) to *myo*-inositol 3-phosphate (MIP), which is subsequently dephosphorylated to *myo*-inositol by inositol monophosphatase (IMPA; Nuwayhid *et al., 2006*). Alternatively, *myo*-inositol can be regenerated from any *myo*-inositol 1-phosphate recycled from the membrane phospholipid pool through the action of IMPA (Mitchell, 2008).

Once synthesized perhaps the best know fate of *myo*-inositol is as a precursor for the biosynthesis of phosphatidylinositol. In this pathway phosphatidylinositol synthase catalyses attachment of cytidine diphosphate diacylglycerol (CDP-DAG) to the D1-hydroxyl group of *myo*-inositol, forming phosphatidylinositol and releasing cytidine monophosphate (CMP; Shen and Dowhan, 1996). As with *myo*-inositol, the biosynthesis of CDP-DAG can occur through *de novo* synthesis and a salvage pathway. The former uses dihydroxyacetone phosphate derived from glucose to make glycerol 3-phosphate, which becomes acylated at carbon-1 and carbon-2 to yield phosphatidic acid (PA; Nuwayhid *et al*., 2006). Subsequently, the enzyme CDP-diacylglycerol synthase then catalyses the condensation of PA and cytidine triphosphate (CTP), eliminating pyrophosphate and forming CDP-DAG (Heacock and Agranoff, 1997). The latter involves DAG derived from the phosphatidylinositol-specific phospholipase C (PI-PLC)-mediated PIP_2 hydrolysis, which subsequently becomes converted to PA through the action of DAG kinase which is used to form CDP-DAG as described above (Li *et al*.,

2013). Phosphatidylinositol can then be reversibly phosphorylated at one or a combination of positions (3, 4 or 5) on the inositol head-group, which results in a total of eight phosphoinositide species. The levels and turnover of the different phosphoinositides are tightly regulated by families of lipid kinases and phosphatases and also phosphatidylinositol-specific phospholipase Cs (Mitchell, 2008; PI-PLCs).

1.4. The evolving physiological significance of PIP_2

Although PIP_2 represents only 1% of the total cellular phospholipid pool, it has important regulatory roles in many cellular processes. PIP_2 is mainly found in the inner, cytoplasmic leaflet of the plasma membrane but is also present in Golgi, ER and the nuclear membranes (McLaughlin *et al*., 2002). The main route leading to the production of PIP_2 is through phosphorylation of phosphatidylinositol-4-phosphate by the action of PIP5 kinase (PIP5K). However, PIP_2 can also be produced through the phosphorylation of PI(5)P by through the action of PIP4 kinase (PIP4K). The kinase involved in PIP_2 synthesis depends on the cellular location as PIP5K is mainly found at the plasma membrane whereas PIP4K is found in the cytosol, ER and the nucleus (Mitchell, 2008).

1.4.1. Phosphoinositide-specific phospholipase C-mediated PIP_2 hydrolysis

Early studies into the physiological roles of PIP_2 established a role for this lipid in the production of two second messenger molecules in the cell, diacylglycerol (DAG) and inositol trisphosphate (IP_3). An enzyme central to this process, and therefore a major regulator of PIP_2 metabolism is known as phosphatidylinositol-specific phospholipase C (PI-PLC). Following PI-PLC activation, the levels of these two second messengers

transiently rise, which themselves have a myriad of regulatory functions in mammalian cells (Kadamur and Ross, 2013). These are summarised in Figure 1.2.

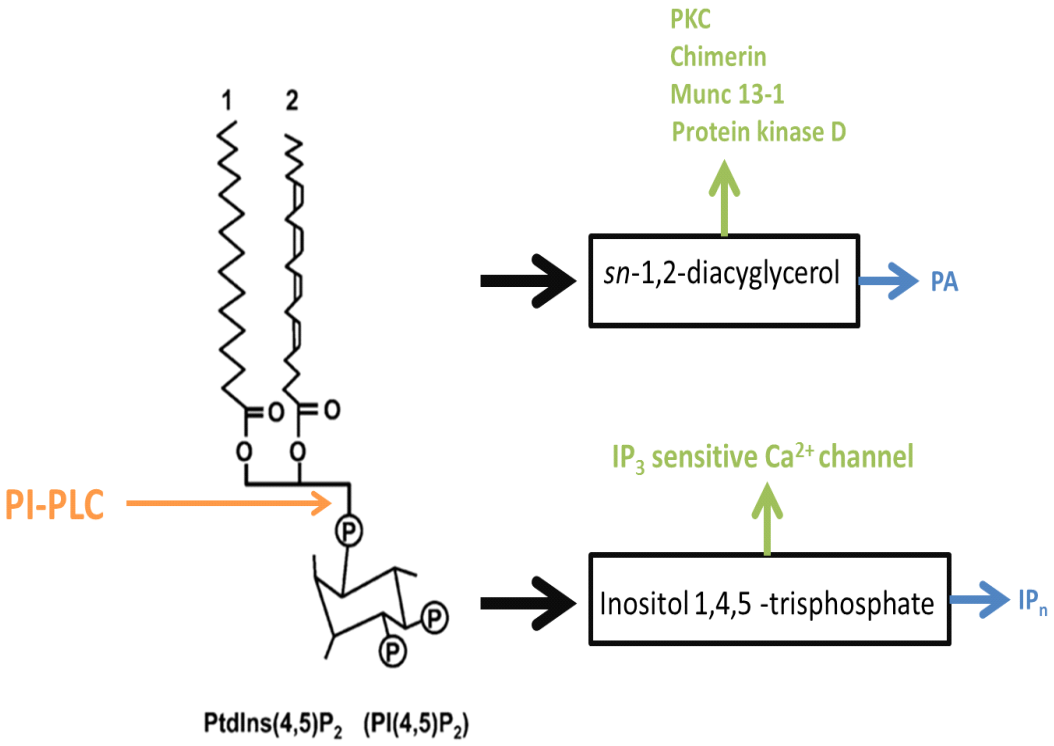

Figure 1.2: Hydrolysis of PIP_2 by phosphatidylinositol-specific phospholipase C (PI-PLC). This reaction generates both IP_3 and DAG and these second messenger molecules are known to play diverse roles in signalling pathways within mammalian cells. They also act as substrates for the formation of further signalling molecules, such as inositol phosphates and phosphatidic acid. In the above figure, the site of PI-PLC cleavage on PIP_2 is indicated with the orange arrow, the other signalling metabolites are blue, and effector molecules are green.

DAG recruits and often activates a variety of proteins containing cysteine-rich, C1 domains, and thereby influences multiple cellular processes (Hurley and Misra, 2000). Although several proteins are known to contain a DAG-binding C1 domain, protein

kinase C (PKC) isoforms have received the most attention with regards to PI-PLC-mediated signalling pathways. Activation of PKC and subsequent phosphorylation of many different proteins such as ion channels, cytoskeletal proteins and other enzymes is known to be involved in a multitude of physiological processes including cell growth, cytoskeleton reorganisation and apoptosis (Pears, 1995). In addition, a number of other C1-domain containing proteins are known to be effectors for DAG produced through PI-PLC-mediated PIP_2 metabolism. These include the chimerin family of Rho GTPase-activating proteins; the large neuronal protein Munc 13-1, which is essential for DAG-dependent augmentation of neurotransmitter release; and the serine-threonine kinase, protein kinase D, which phosphorylates numerous proteins (Brose and Rosenmund, 2002). Furthermore, DAG directly binds with DAG kinase and becomes phosphorylated to PA, which itself is an example of a signalling metabolite with far-reaching regulatory effects (Shulga *et al*., 2011). It is therefore clear from these data that the physiological effects of DAG produced through PI-PLC-mediated PIP_2 metabolism are not restricted to PKC activation, but can be mediated through many different effector molecules.

The other signalling molecule generated directly from the activation of PI-PLC is IP_3, which is known to bind and activate receptors present on intracellular calcium stores, allowing calcium to be released into the cytosol (Berridge, 2009). IP_3 mediated elevation of cytosolic calcium levels leads to the stimulation of a variety of calmodulin-dependent enzymes, such as protein kinases and phosphoprotein phosphatases (Kirk, 1990). Through its influence on intracellular calcium levels, IP_3 regulates many cellular processes, including fertilisation, apoptosis, exocytosis, cell proliferation, smooth

muscle contraction and secretion (Berridge *et al*., 2000). The ability of cells to produce a wide range of calcium signals with different spatial and temporal characteristics is not only necessary for the control and multiple functions and but underscores the versatility and importance of the calcium signalling system in physiology (Bootman, 2012).

1.4.2. Additional functions of PIP_2.

The importance of PIP_2 in cellular physiology is not restricted to its ability to produce second messengers. Recently it has become clear that PIP_2 is able to bind and regulate the molecular function of many signalling proteins, and also act as the substrate for the production of other signalling metabolites, in addition to IP_3 and DAG. PIP_2 has a number of functions in cells related to its ability to bind with signalling proteins (McLaughlin *et al*., 2002).

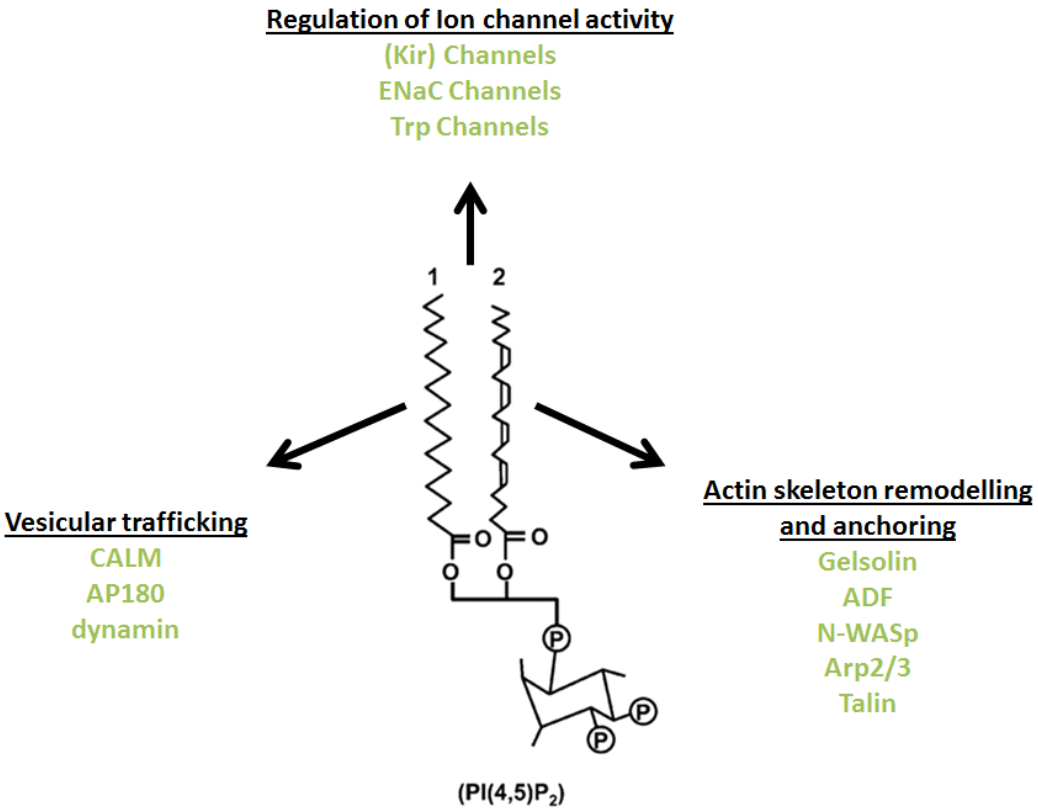

Figure 1.3: A summary of the diverse cellular functions of intact PIP_2 in mammalian cells. In addition to the production of second messenger molecules, PIP_2 has various additional cellular functions, including vesicular trafficking, cytoskeleton remodelling and regulation of ion channel activity. Clathrin assembly lymphoid myeloid leukemia protein, CALM; actin-depolymerizing factor, ADF; Neural-Wiskott Aldrich Syndrome Protein, N-WASp; actin-realted protein, Arp2/3; Adapter protein, AP180; Inwardly rectifying potassium channel, Kir; Transient receptor potential channel, Trp; Epithelial sodium channel, ENaC.

Several integral plasma membrane proteins such as ion channels and transporters are thought to be directly regulated by PIP_2 (Hilgemann *et al*., 2001). The first channel found to be regulated by PIP_2 was the inwardly rectifying potassium (Kir) channels (Hilgemann and Ball, 1996). PIP_2 activates Kir channels by stabilising its open state. A cluster of basic amino acid residues, including a highly conserved arginine, is thought to mediate the affinity of Kir channels for PIP_2, as mutation within this region prevent

normal channel activation (Huang *et al*., 1998). PIP_2 is also known to activate amiloride-sensitive epithelial Na^+ channels (ENaC), and therefore play a role in Na^+ reabsorption across the nephron with consequential effects on body Na^+ homeostasis (Ma *et al*., 2002). Although the PIP_2 binding site has yet to be clearly mapped, mutation of several lysine and arginine residues within the cytoplasmic N-terminal loops caused a severe reduction in channel activity, with no effects on surface expression (Chalfant *et al*., 1999).

Intact PIP_2 is also thought to be important in vesicular trafficking. For example, plasma membrane PIP_2 is directly implicated in clathrin-mediated endocytosis (De Camilli *et al*., 1996). This form of endocytosis is the main pathway for endocytic entry of lipids and proteins at the plasma membrane (Takei and Haucke, 2001). PIP_2 is thought to be crucial for this process as several of the proteins implicated in clathrin-mediated endocytosis are recruited to the plasma membrane through binding PIP_2. These include the brain-specific CALM (clathrin assembly lymphoid myeloid leukemia protein) homologue AP180, which mediates the assembly of clathrin coats (Ford *et al*., 2001). Other PIP_2-binding proteins involved in clathrin-mediated endocytosis include the GTPase dynamin, which is known to be crucial for the release of clathrin-coated vesicles from the plasma membrane (Bottomley *et al.,* 1999). Moreover, disruption of PIP_2 levels by sequestration or recruitment of a 5'-inositol phosphatase to the plasma membrane prevented the formation of clathrin-coated vesicles (Antonescu *et al*., 2011). PIP_2 is also thought to influence exocytosis in a number of cells, including calcium-triggered vesicle exocytosis at nerve terminals (Kabachinski *et al*., 2014). ARF6-regulated membrane trafficking is dependent on the metabolism of PIP_2.

Reduction in the PIP_2 level through inhibition of PIP5K prevents the recycling of ARF6-containing vesicles back to the plasma membrane and therefore alters exocytosis (Brown *et al*., 2001). The regulated secretion of insulin has also been shown to be negatively regulated by the inhibition of PIP_2 synthesis in pancreatic beta cells (Tomas *et al*., 2009).

A major role that has been assigned to PIP_2 is the regulation of actin cytoskeleton remodelling (Yin and Janmey, 2002). PIP_2 is known to influence actin polymerisation in a number of ways: recruiting and inhibiting the actin-severing proteins, gelsolin and ADF (actin depolymerising factor) (Sechi and Wehland, 2000); activating the branching of actin by binding N-WASp and Arp2/3 (Higgs and Pollard, 2000); mediating the removal of the caps from actin filaments and thus facilitating the addition of new actin monomers to the growing chain (Yin and Janmey, 2002). PIP_2 also binds with many other cytoskeletal proteins such as talin and vinculin and therefore facilitates the anchoring of the cytoskeleton to the plasma membrane (Chandrasekar *et al*., 2005).

1.5. Phosphatidylinositol-specific phospholipase C isozymes

Signalling pathways involving PI-PLCs have a long history that began with the observation that treatment of pancreatic slices with various cholinergic agents could induce a rapid turnover of phosphoinositides (Hokin and Hokin, 1953). Subsequently, direct hydrolysis of phosphoinositides was first observed following incubation of purified phosphoinositides with rat brain homogenates (Sloane-Stanley, 1953). A similar PI-PLC activity was observed by various other groups, and this led to the eventual partial purification of the first PI-PLC (Dawson *et al*., 1959). Currently, 13

distinct PI-PLC isoforms have been identified in mammalian cells, which have been grouped into 6 subtypes, PLCβ (β1-β4), PLCδ (δ1-δ4), PLCγ (γ1 and γ2), PLCε (ε1 and ε2), PLCη (η1- η2) and PLCζ. This classification is based on amino acid sequence homologies, overall domain structures, and the mechanisms of regulation. In addition to the presence of a number of different PI-PLC isoforms, further molecular diversity is generated by the presence of alternative splicing variants for several of these PI-PLC isoforms (Suh *et al*., 2008).

1.5.1. Domain structure of mammalian phosphatidylinositol-specific phospholipase C subtypes

The amino acid sequences of each mammalian PI-PLC subtype contain distinct modular domains that are organised around the characterised X- and Y- catalytic domain regions. They include: a pleckstrin homology (PH) domain and EF-hand like motifs, which precede the X-domain; and a single C2 domain that occurs immediately after the Y-domain. Additional subtype-specific regulatory motifs are present in γ-, ε-, β- and η- subtypes, which are thought to contribute towards specific regulatory mechanisms (Suh *et al*., 2008). These include the Ras-association (RA) and the Ras-GDP/GTP exchange factor (Ras-GEF) domains in PLCε-isoforms, the C-terminal extension region in PLCβ-isoforms, and the Src homology domains in PLCγ-isoforms (Kadamur and Ross, 2013). The domain structures of each of the 6 sub-types of PI-PLC are shown in Figure 1.4.

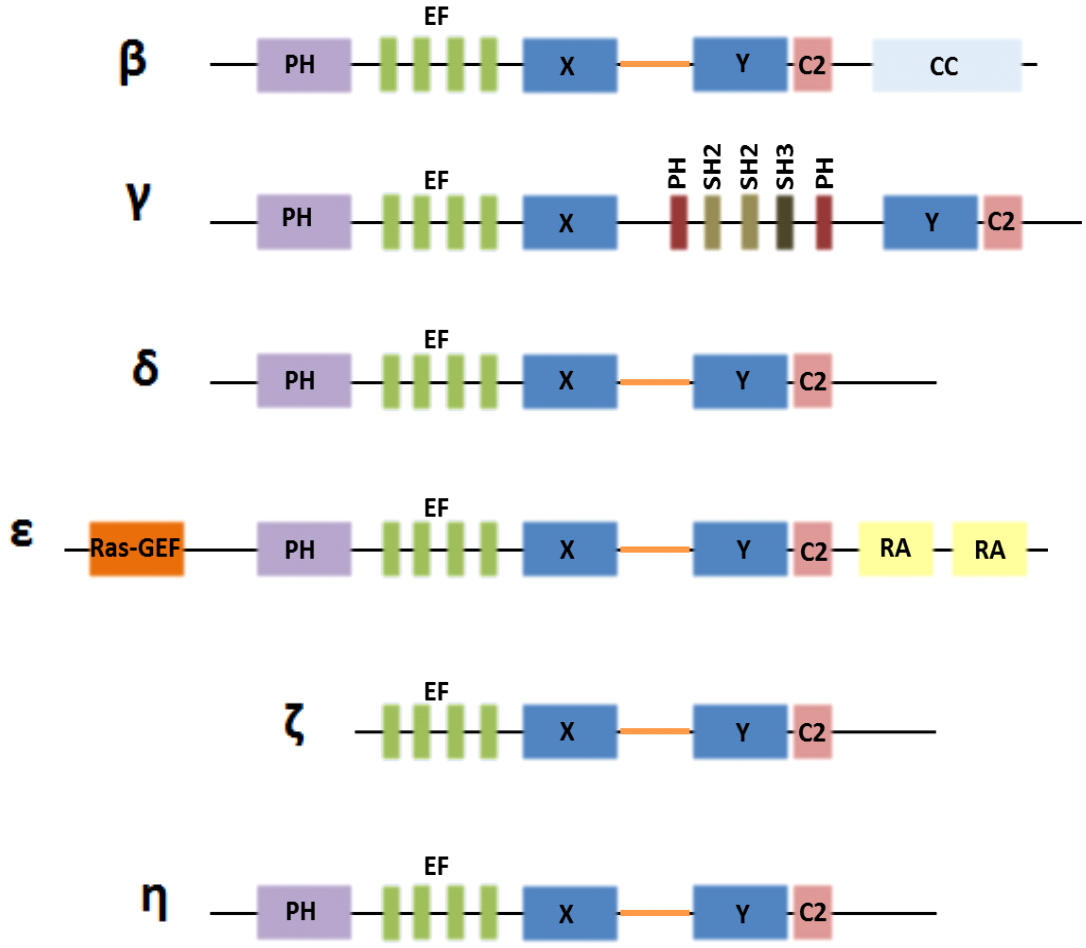

Figure 1.4: Diagrammatic representation of the domain structures of the six different mammalian PI-PLC subtypes. Each mammalian PI-PLC subtype contains distinct modular domains. The domains are abbreviated as follows: PH, pleckstrin homology; EF, EF hand domains; X and Yindicate the N and C terminal portions of the catalytic domain; SH2/SH3, Src homology 2/3; RA, Ras association; Ras GEF, Ras GDP/GTP exchange factor; CC, coiled coil.

1.5.1.1. Pleckstrin homology domain

The pleckstrin homology (PH) domain was first discovered as a short amino acid sequence occurring in various intracellular signalling proteins which showed limited homology to a region that is duplicated in the protein pleckstrin (Haslam *et al*., 1993; Mayer *et al.,* 1993) Many of these proteins that contain PH domains are known to be important in cellular processes that require association with the cell membrane,

including cell signalling and organization of the cytoskeleton. Furthermore no obvious catalytic properties have yet to be assigned to any PH domain, and therefore these domains are thought to mainly function as adaptor motifs, to recruit their host proteins to the membrane surface (Lemmon, 2007). Structural studies, involving several proteins, including PLCδ1, demonstrate that all known structural representations of the PH domain show a common fold consisting of two perpendicular anti-parallel β sheets, closed off at one end by a C-terminal α helix (Figure 1.5; Ferguson *et al*., 1995).

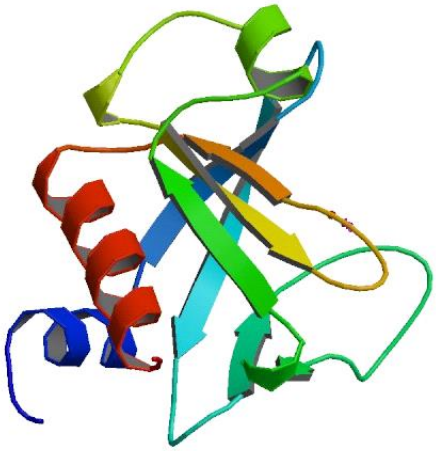

Figure 1.5: Cartoon diagram of the pleckstrin homology domain structure from Phospholipase Cδ1. The canonical structure of the PH domains consists of two perpendicular anti-parallel β sheets, occluded at one end by a more C-terminal α helix. Image from the RCSB PDB of PDB ID 1MAI (Ferguson, K.M *et al*., 1995).

With the exception of PLCζ isoforms, all PI-PLCs contain at least one PH domain at the N-terminus. PLCγ contains an additional PH domain, which is split by two SH2 domains and a single SH3 domain (Suh *et al.,* 2008). The PH domains of PLC-subtypes can bind phosphoinositides within biological membranes and also certain proteins including the βγ subunits of heterotrimeric G proteins, and PKC (Varnai *et al.,*

2002; Wang *et al.,* 2000). The PH domains of different PI-PLC subtypes exhibit disparate ligand binding specificities and therefore diverse modes of membrane interactions. Through these domain interactions, PLC-subtypes are recruited to different membranes, enabling them to interact with appropriate cellular compartments or allowing them to interact with other components of signalling pathways (Singh and Murray, 2003). These disparate interactions and how they regulate the catalytic function of individual PLC-subtypes will be discussed in Section 1.5.2.

1.5.1.2. The C2 domain

The C2 domain is a calcium-binding motif found within more than 100 proteins involved in signal transduction and the cytoskeleton, including PKC, synaptotagmin and various phospholipases. The C2 domain is thought to be involved in calcium-dependent phospholipid binding and membrane targeting processes such as subcellular localisation (Nalefski and Falki, 1996). The three-dimensional structure of the C2 domain of PLCδ1 has been reported, and consists of a β-sandwich composed of two four-stranded anti-parallel β-sheets, with a variable loop linking each of the β-strands (Essen *et al.,* 1997). A schematic depiction of this structure is shown in Figure 1.7. Two of the loops (highlighted in green; Figure 1.6) contain conserved aspartate residues which co-ordinate the binding of Ca^{2+} to the C2 domain (Rizo and Sudhof, 1998). At least two Ca^{2+} ions have been shown to bind to the C2 domain of PLCδ1, however the exact number is still unknown (Lomasney *et al.,* 2012).

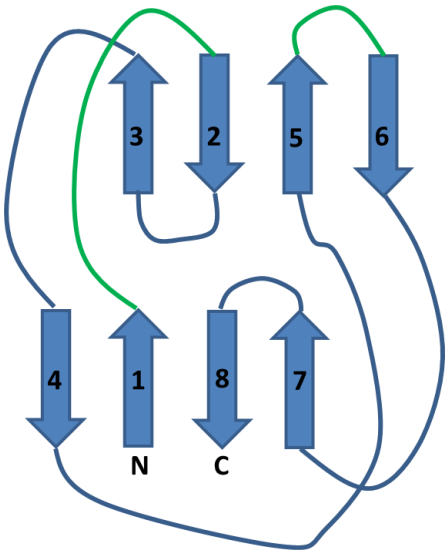

Figure 1.6: Schematic representation of the structure of the C2 domain from PLCδ1. The atomic structure of the PLCδ1 consists 8 anti-parallel β-sheets which are linked by intervening amino acid loops. The Ca^{2+} binding regions are highlighted in green. The arrows represent each of the eight β-strands. Adapted from Essen *et al*., 1997.

A single C2 domain, of around 130 amino acids, is present in all six mammalian PI-PLC isoforms (Suh *et al*., 2008). Studies of PLCδ1 suggest that Ca^{2+} binding to the C2 domain can induce a conformational change within this region, which may permit the subsequent binding of the protein to phospholipids. Also, the calcium binding loops of PLCδ1 are negatively charged due to the presence of a number of acidic residues and therefore the binding of Ca^{2+} ions is thought to confer a switch in the electrostatic characteristics of this region so that it can attract negatively charged membranes (Grobler *et al*., 1996). As with the PH domain, evidence suggests that the C2 domains of different PLC-subtypes show disparate ligand binding specificities, reflecting their unique modes of regulation (Suh *et al*., 2008). The importance of the C2 domains in the regulation of the catalytic activities of PLC-subtypes is considered further in Section 1.5.2.

1.5.1.3. The EF-hand domain

Many calcium-binding proteins are evolutionary related and share a specific type of calcium-binding domain known as the EF-hand motif (Nelson *et al.*, 2002). This structural motif was first discovered by Krestinger, following derivation of the crystal structure of parvalbumin (Krestinger and Nockolds, 1973). In this structure, the EF-hand is a 29-residue polypeptide calcium-binding motif consisting of two α-helices (helices E and F in parvalbumin) flanking an inter-helical Ca^{2+}-chelation loop (Figure 1.7) (Moews and Kretsinger, 1975). The secondary structure and the putative calcium-coordinating residues are highly conserved across EF-hand proteins such as troponin C and calmodulin (Nelson *et al.*, 2002).

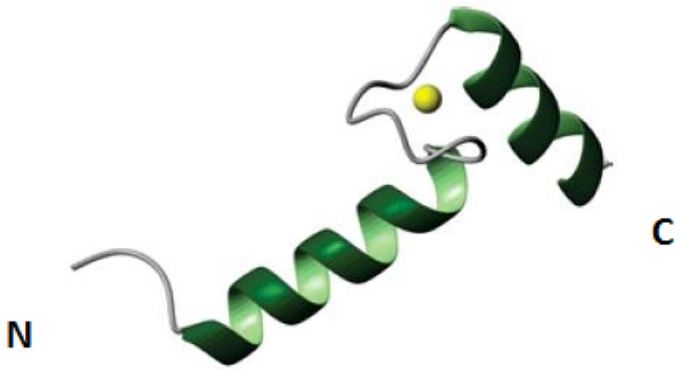

Figure 1.7: A single EF hand domain from calmodulin demonstrating the canonical structure of a single EF hand domain. The EF hand consists of an N-terminal 9-residue helix, a 9-residue calcium-binding loop and an 11-residue C-terminal loop. The yellow ball represents a calcium ion. The N- and C-terminal regions of the domain are also shown. Figure adapted from Gifford *et al.*, 2007

The first description of EF-hand motifs in PI-PLC subtypes occurred following analysis of the crystal structure of PLCδ1, which revealed the presence of the characteristic helix-loop-helix motifs (Essen *et al*., 1996). Subsequent sequence analysis revealed the presence of a total of four EF-hand motifs (EF1-4) in all mammalian PI-PLC subtypes. In these enzymes, the EF-hand domain forms part of the catalytic core, which consists of the EF-hand motif, X and Y catalytic domains and the C2 domain. In contrast to other proteins, the EF-hand domains of many PI-PLC subtypes may have limited or no ability to bind calcium (Suh *et al*., 2008). Key exceptions include PLCζ and PLCη isozymes, both of which exhibit high sensitivities to calcium, which is thought to be directed by their EF-hand domains (Nominkos *et al*., 2005; Popovics *et al.,* 2014).

1.5.1.4. The catalytic domain

The catalytic properties of PI-PLCs have been extensively studied and reveal many common characteristics shared by all mammalian enzymes (Kadamur and Ross, 2013). These studies reveal that all mammalian PI-PLCs can hydrolyse many polyphosphoinositides with a preference for PIP_2, and that their catalytic activity is entirely dependent on the presence of a calcium cofactor. The central catalytic core of PLC is composed of an X-box and Y-box domain separated by a short sequence known as the X-Y linker. Although the overall sequence similarity between PI-PLC isoforms is low, the X-box and Y-box domains are well conserved across the different subtypes, with an overall amino acid sequence homology of ~60% among all the isozymes. An even greater homology is seen within individual PLC-subtypes (Kadamur and Ross, 2013). X-ray crystallographic studies of PLCδ1 revealed the catalytic core to consist of alternating α-helices and β-strands resembling an incomplete triose phosphate

isomerase (TIM) α/β-barrel (Figure 1.9). This barrel is composed of two lobes, which are formed from the X-box and Y-box domains (Suh *et al.,* 2008). Additionally, structural analysis reveals a cluster of hydrophobic amino acids at the entrance to the active site, forming a spout like structure, which enables the enzyme to penetrate into the phospholipid bilayer, facilitating membrane interaction and introduction of the substrate into the catalytic core. The catalytic activity of all eukaryotic PI-PLCs is dependent on the presence of calcium as a cofactor (Essen *et al*., 1996).

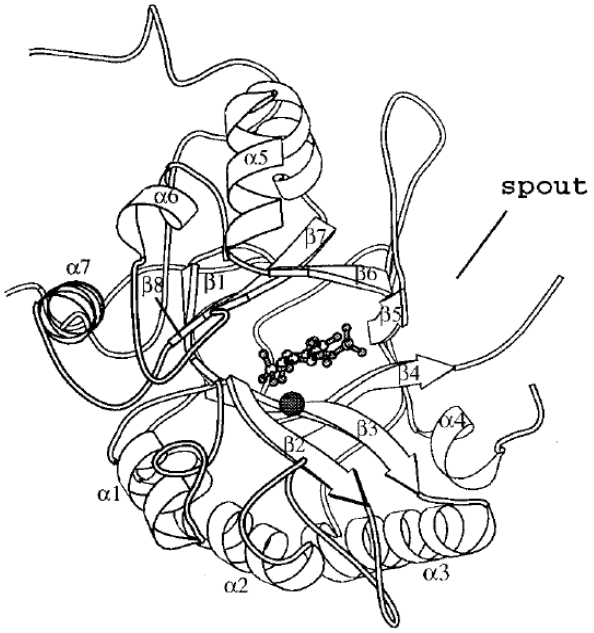

Figure 1.8: Depiction of the structure of the catalytic domain of rat phospholipase Cδ1 in the presence of IP_3. The catalytic domain folds as a TIM barrel. The active site, all catalytic residues, and a Ca^{2+} binding site are found within the TIM barrel. Bound calcium is shown as a sphere, and IP_3 is represented in ball-and-stick form. Depicted also is the "spout" which represents a clutch of hydrophobic residues that allows PIP_2 to penetrate the active site. Taken from Essen *et al*., 1996.

These crystallographic studies together with supporting data from mutational and kinetic studies have identified key residues within the catalytic core of PLCδ1 that are involved in substrate binding, interactions with calcium and have provided a structural

model for the mechanism of calcium-dependent hydrolysis (Figure 1.11). These data support a two-step, sequential mechanism that involves general acid-base catalysis. The first step is a phosphotransferase step that involves de-protonation of the 2-OH group of inositol by residue able to accept hydrogen ions (general base) which leaves an oxyanion which nucleophillically attacks the phosphate group attached at position 1 of the inositol ring forming a pentacovalent transition state intermediate. This is followed by protonation of the 1-phosphate of inositol by a residue able to donate hydrogen ions (general acid) and release of DAG and the more stable substrate intermediate cyclic inositol phosphate (Ins (1:2cyc)P; Heinz *et al*., 1998). In mammalian PI-PLCs, His356 has been identified as the general acid whereas the identity of the general base remains unclear, with Glu341 and Glu390 as the most likely candidates (Figure 1.11; Heinz *et al*, 1998)). The crystal structure of PLCδ1 shows that His311 forms a hydrogen bond with the 1-phosphate of inositol and this is thought to stabilise the Ins(1:2cyc)P intermediate. In mammalian PI-PLCs, calcium is also present within the active site and interacts with the 1-phosphate and 2-OH group of inositol. These interactions are thought to stabilise the Ins(1:2cyc)P intermediate and lower the pKa of the 2-OH group of inositol (Heinz *et al*., 1998). The side-chains of Asn312, Asp343, Glu341 and Glu390 (Human PLCδ1 numbering) are also known to co-ordinate the binding of calcium within the active site and mutation of any of these result in an increase in the concentration of calcium required for catalysis (Essen *et al*., 1996; Ellis et al., 1998). The second step (phosphodiesterase step) results in the hydrolysis of the cyclic intermediate forming the acyclic inositol phosphate product. This reaction is

much slower than the phosphotransferase step and the roles of the general base and acid are reversed resulting in the formation of an acyclic IP_3 (Heinz *et al.*, 1998).

Given the highly conserved nature of the X- and Y- catalytic domain, the catalytic mechanism of substrate hydrolysis deduced for PLCδ1 is expected to be common to all mammalian PI-PLC isoforms. All the residues identified in PLCδ1 as forming important contact with the substrate and binding calcium (described above) are strictly conserved in all mammalian PI-PLCs and mutation of any one of these severely reduces the catalytic activity of PLCδ1 towards substrate PIP_2 (Kadamur and Ross, 2013).

1.5.1.5. X-Y linker region

The X and Y domains are joined by a highly disordered intervening sequence, known as the X-Y linker region. As the X-Y linker is known to act as an auto-inhibitor of PLC-subtypes, with activation of these enzymes requiring removal of the X-Y linker from the active site. This linker varies in length between different PLC-subtypes, consisting of 40 to 110 residues in β and δ-subtypes, 190 residues in PLCε and the much longer sequence in PLCγ isoforms (~400 residues) as it also includes two Src homology 2 (SH2) domains and one SH3 domain (Suh *et al*., 2008).

1.5.2. Regulation and physiological functions of mammalian PI-PLCs

Given the sheer number of physiological processes that rely on the activity of PLC it is not surprising that a number of PI-PLC subtypes have evolved, each with a different number of isoforms and associated spliceforms. While all isozymes have similar catalytic properties, different subtypes are characterised by distinct modes of

regulation. This distinctiveness is in part due to the presence of subtype-specific domains but also due to differences in the binding specificities of common domains.

1.5.2.1. PLCβ isoforms

Currently four mammalian β-isoforms (PLCβ1-4) and additional spliced variants are known to exist (Rebecchi and Pentyala, 2000). Analysis of expressed sequence tags and subsequent experimental verification by *in situ* hybridisation and quantitative RT-PCR reveals PLCβ1 mRNA to be widely expressed, with the highest levels being detected in the cerebral cortex and hippocampus (Homma *et al*., 1989). In contrast, the expression of PLCβ2 mRNA is restricted to cells of hematopoietic origin (Sun *et al*., 2007). PLCβ3 mRNA is expressed in the brain, liver and parotid gland (Jhon *et al*., 1993) and PLCβ4 is predominantly expressed in cerebellar Purkinje and granule cells, and the retina (Adamski *et al*., 1999). Activation of the different PLCβs can take place through the absorption of photons or by the binding of certain odorant molecules or numerous hormones to a variety of G-protein coupled receptors (GPCRs) that are linked to the activation of specific isoforms (Kadamur and Ross, 2013). Figure 1.9 shows a diagrammatic representation describing the standard model of G protein activation of PLCβ isoforms.

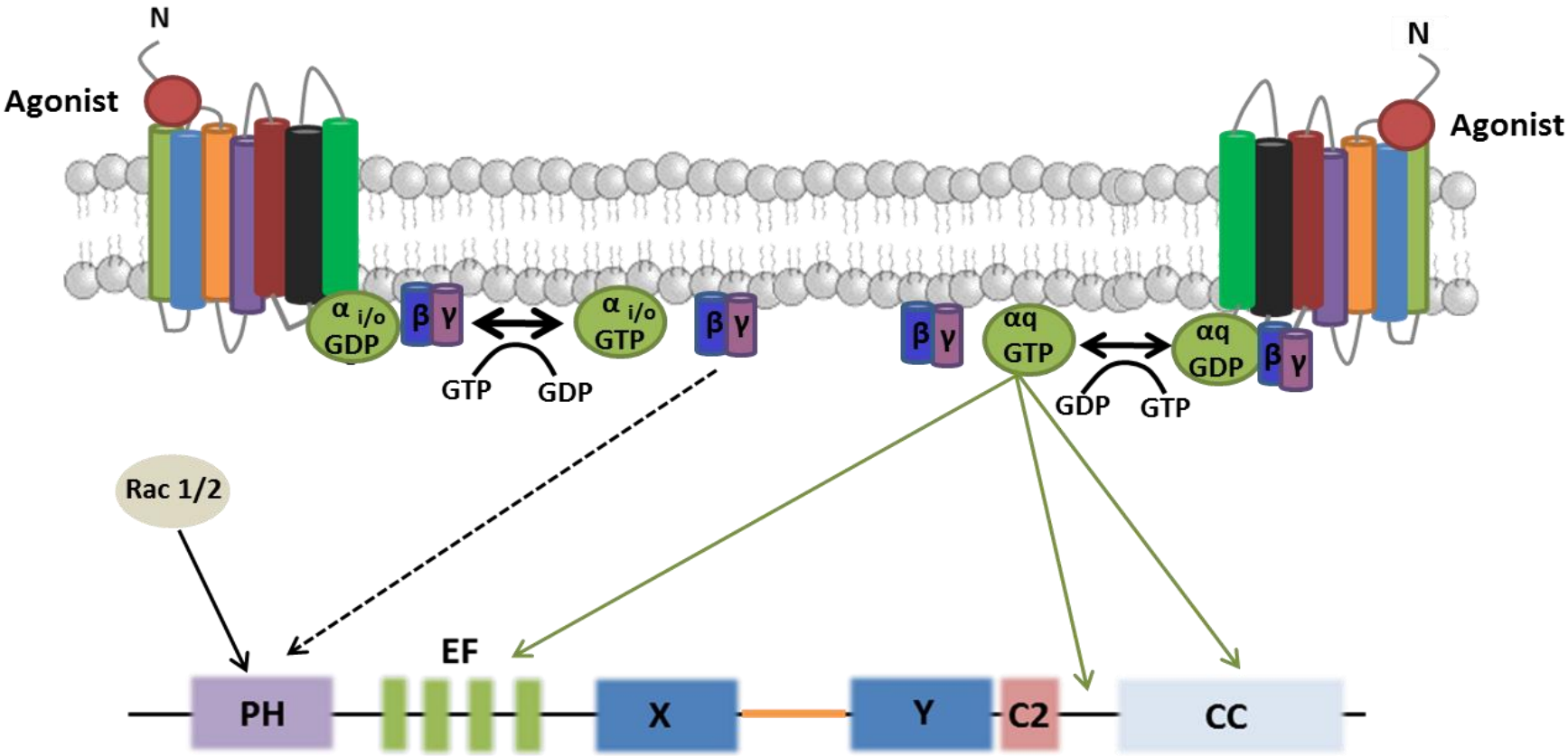

Figure 1.9: Schematic representation of the regulation of PLCβ by G protein-coupled receptors (GPCRs). Gαq stimulates PLCβ and Gβγ-subunits released from $G_{i/o}$ can also activate PLCβ. Green arrows represent the known sites on PLCβ that mediate regulation by G proteins. The black dashed line points to the potential site on PLCβ that interacts with Gβγ. Recent evidence also suggest that PLCβ can be directly activated by the small GTPases Rac 1/2, and the solid black line represents the PLCβ domain responsible for these interactions. PH, pleckstrin homology; EF, EF hand domains; X and Y indicate the N- and C-terminal portions of the catalytic domain; CC, coiled coil domain.

GPCRs are associated with heterotrimeric G proteins and upon agonist binding they facilitate the exchange of bound GDP for GTP on the α-subunit of the G protein. Once charged with GTP, the α-subunit separates from the Gβγ heterodimer in the plane of the membrane and the α-subunit, the βγ heterodimer or both increase the catalytic activity of PLCβ (Kadamur and Ross, 2013). The Gq class of α-subunits, which consists of five different isoforms (αq, α11, α14, α15 and Gα16), are known to activate PLCβ isoforms (Taylor and Exton, 1991; Lee *et al*., 1992). Recent derivation of the crystal structure of PLCβ3 in complex with Gαq has provided a greater understanding of the mechanism whereby Gαq activates PLCβ isoforms. This structure highlighted the EF hand domain, the region between the catalytic domain and the C2 domain, and the coiled coil (CC) motif C-terminal to the C2 domain of PLCβ3 as forming contact points with Gαq (Waldo *et al*., 2010). Interestingly, comparison of this high-resolution structure of activated PLCβ3 with that of non-activated PLCβ3 revealed no conformational rearrangements within the core structure of PLCβ3. It has therefore been proposed that Gαq-mediated activation of PLCβ isoforms does not involve any conformational changes to the core of the protein but instead Gαq acts to anchor and orient PLCβ at the surface of the membrane. Owing to the negative charge of the membrane, such interactions are thought to push the X-Y linker away from the catalytic core effectively removing its auto-inhibitory effect (Hicks *et al*., 2008). PLCβs 1, 2 and 3 can also be activated by Gβγ subunits and are therefore responsive to G_i-coupled GPCRs. PLCβ4 is however, not activated by Gβγ subunits (Park *et al*., 1993). The PH domains of PLCβ1-3 are thought to mediate the activation by Gβγ subunits (Wang *et al*., 1999). This is based on evidence that removal of the PH domain blocks

activation by Gβγ and a chimeric form of PLCδ1 containing the PH domain of PLCβ2 can be activated by Gβγ (Wang *et al*., 2000A). To date, no X-ray structure of PLCβ in complex with Gβγ exists and therefore the ability of the PH domain to directly bind Gβγ is unknown.

Individual PLCβ isoforms are also activated by various other regulatory ligands, such as phosphatidic acid and the small GTP-binding protein, Rac (Illenberger *et al*., 1998). PLCβ2 is directly activated by multiple, small-GTP-binding proteins such as Rac1, Rac2 and Cdc42 (Illenberger *et al*., 1997). Both biochemical and structural studies have suggested that the PH domain of PLCβ2 mediates the binding of Rac. The core structure of PLCβ2 bound to Rac1 is essentially identical to that of PLCβ2, and therefore it has been suggested that the binding of Rac does not involve any conformational changes in PLCβ2 (Jezyk *et al*., 2006). The exact mechanism by which PLCβ2 becomes activated by Rac remains to be fully characterised.

Phenotypes associated with transgenic mice and flies lacking individual β-isoforms have revealed important insights into how these enzymes are integrated into normal physiology. Mice lacking PLCβ1 experience epileptic-like seizures leading to sudden death. These mice are also much more sensitive to drugs that induce convulsions, which together with the spontaneous seizure phenotype, suggest that PLCβ1 is involved in brain inhibitory pathways (Kim *et al*., 1997). Owing to the predominant expression in immune cells, phenotypes associated with the lack of PLCβ2 are entirely different. Within immune cells, PLCβ2 couples to GPCRs for a number of chemokines, including those for C5a, fMLP and interleukin-8 (Jiang *et al.,* 1996A). In line with these

biochemical characteristics, chemokine signalling pathways are disrupted in mice lacking PLCβ2, however the outcomes are different depending on the specific immune cell involved (Jiang *et al*., 1997). Neutrophils from mice lacking PLCβ2 are insensitive to the chemoattractant fMLP and chemotaxis is inhibited (McNeill *et al*., 2007). In eosinophils from these animals, chemotaxis is enhanced suggesting in these cells PLCβ2 actually inhibits chemotaxis and that alternative pathways couple chemokines receptors to cell locomotion (Sano *et al*., 2001). Mice lacking PLCβ4 showed ataxia that was linked to defects in the normal development of the cerebellum (Jiang *et al*., 1996). The authors suggest that this phenotype was due to attenuated glutamate signalling through metabotropic glutamate receptor 1 (mGluR1) in cerebellar Purkinje cells (Jiang *et al*., 1996) In contrast to other β-isoform-knock-outs, PLCβ3-null mice die very early on in their development (Xie *et al*., 1999). It is therefore clear that the individual absences of each β-isoform gives rise to different phenotypes reflecting their unique roles in cell physiology. Further studies are required to unravel the physiological roles of the alternatively spliced variants of the each β-isoform.

1.5.2.2. PLCγ isoforms

The PLCγ family of mammalian PI-PLCs consists of two members known as PLCγ1 and 2 (Kadamur and Ross, 2013). PLCγ1 mRNA is expressed in various tissues. It is highly expressed in the brain where it is found in neurons, oligodendrocytes and astrocytes (Mizuguchi *et al*., 1991). In contrast, PLCγ2 mRNA is expressed primarily in immune cells with expression also being found in the Purkinje and granule cells found in the cerebellum (Tanado and Kondo, 1994). For PLCγ1 two alternative splicing variants have been identified thus far, and these differ in their C-terminal sequences. To date,

a single spliced variant of PLCγ2 has been identified in mouse. PLCγ isoforms are unique among other mammalian PI-PLCs in that they contain two tandem SH2 domains, a SH3 domain, and a split PH domain in region between the X and Y domains (Suh *et al*., 2008).

PLCγ isoforms can be activated downstream of receptors which possess intrinsic tyrosine kinase activity, such as those for platelet-derived growth factor (PDGF), epidermal growth factor (EGF) and nerve growth factor (NGF) (Kadamur and Ross, 2013). Figure 1.10 shows a schematic diagram summarising the pathways leading to activation of PLCγ isoforms.

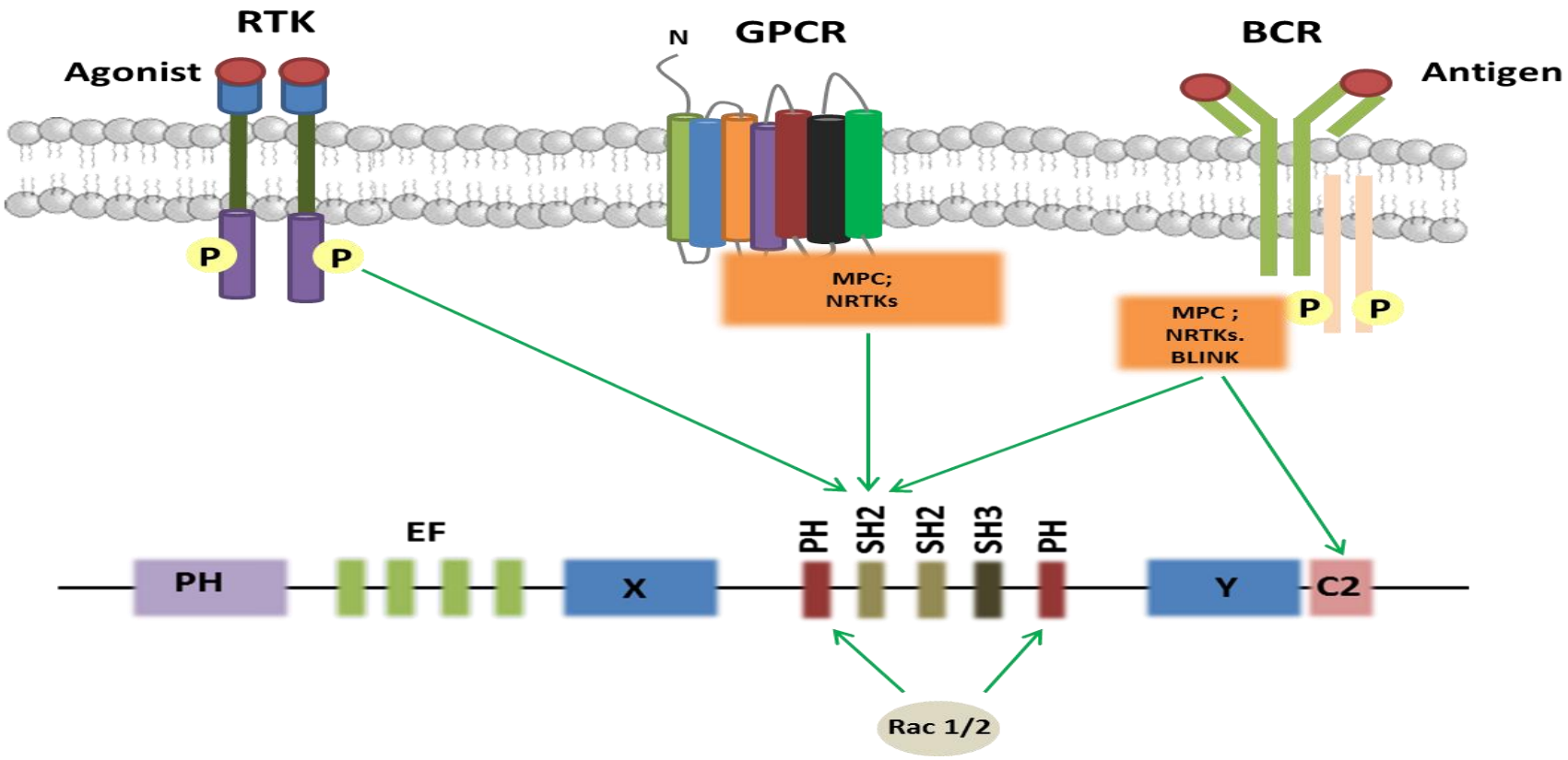

Figure 1.10: PLCγ-isoforms are regulated by tyrosine phosphorylation mediated by various different tyrosine kinases, included receptor tyrosine kinases (RTKs) and non-receptor (soluble) tyrosine kinases (NRTKs). Some NRTKs are recruited to the membrane following activation of the B cell receptor by multiprotein complexes (MPCs) that assmeble on the cytoplasmic tails of the activated receptor. Critical tyrosine residues present within the SH2 are the site of phosphorylation of PLCγ isoforms and when phosphorylated, the SH2 recruits PLCγ to the membrane. Interestingly, GPCRs are also able to regulate PLCγ functions by recruiting NRTKs to the membrane. Green arrows indicate the PLCγ domains that experimentally indicated to mediate interactions with the different regulatory inputs.

These receptors dimerize upon binding of their ligand, triggering autophosphorylation on specific tyrosine residues. These phosphorylated residues subsequently act as docking sites to recruit various SH2 containing proteins, such as PLCγ isoforms to the cell surface (Suh *et al*., 2008). A receptor may contain one or more docking sites for the recruitment of PLCγ isoforms, and mutation of these residues prevents PLCγ activation (Rebecchi and Pentyala, 2000). For the PDGF receptor, PLCγ1 specifically binds to phosphorylated Tyr-1021 (Valius *et al*, 1993) whereas PLCγ2 can bind with five preferred autophosphorylated tyrosine residues on the EGF receptor (Sorkin *et al*., 1991). Subsequently PLCγs can be phosphorylated on a number of tyrosine residues within the N-terminal SH2 domain (nSH2), but only one (Tyr-783 in PLCγ1 and Tyr-759 in PLCγ2) is essential for the stimulation of activity (Sekiya *et al*., 2004). The phosphorylated Tyr-783/Tyr-759 has been shown to associate with the C-terminal SH2 (cSH2) domain within the same PLCγ1 molecule and this interaction is thought to cause significant conformational changes resulting in the re-orientation of the X-Y linker with respect to the core enzyme (Poulin *et al*. 2005). This conformational change is thought to remove the auto-inhibition caused by the X-Y linker (Kadamur and Ross, 2013).

PLCγ isoforms are also activated downstream of receptors that lack intrinsic tyrosine kinase activity, including the angiotensin II receptor-type 1 (AT_1) and the B-cell receptor (BCR). As with the receptor tyrosine kinases (RTKs; described above), PLCγ1 and PLCγ2 activation is also mediated by tyrosine phosphorylation at Tyr-783 or Tyr-759 respectively but this time by non-receptor tyrosine kinases. In the case of the AT_1 receptor (a GPCR), coupling of PLCγ to the activated receptor and subsequent tyrosine phosphorylation is likely to occur in the context of a membrane-bound, multiprotein

complex containing a soluble tyrosine kinase (Marrero *et al*., 1994). The exact molecular identities of the proteins involved are yet to be fully characterised. In the case of the BCR, antigen binding is known to recruit and activate the catalytic activity of PLCγ2. Activation of the BCR receptor by antigen binding induces the recruitment of the Src family of protein tyrosine kinases (PTKs) to the two immunoreceptor tyrosine-based activation motifs (ITAMs) present in each of BCR accessory protein molecules Igα and Igβ (Avalos and Ploegh, 2014). Src PTKs such as Lyn, Fyn and Blk are subsequently activated which then phosphorylate all tyrosine residues present in each ITAM. These phosphotyrosine residues then recruit the SH2 domains of the PTK, Syk, which then phosphorylates a number of adapter proteins, such as BLINK (B-cell linker protein; Kim *et al*., 2004). Phosphorylated BLINK is known to recruit the C2 domain of PLCγ2, and the BCR-associated PLCγ2 becomes phosphorylated at Tyr-759 and subsequently activated; however the PTK responsible for this phosphorylation is currently unknown (Kim *et al*., 2004).

PLCγ isoforms respond to multiple regulatory inputs in addition to tyrosine phosphorylation. Piechulek *et al.* 2005 showed that PLCγ2 could be stimulated through binding to the small GTPases, Rac1 and Rac2, and that this stimulation does not involve phosphorylation of any tyrosine residues on PLCγ2 (Piechulek *et al*., 2005). Structural and biochemical studies of PLCγ2 in the presence of Rac2 identified the split PH (sPH) domain of PLCγ2 as the Rac-binding surface (Bunney *et al.,* 2009). Whether or not the binding of Rac to PLCγ2 moves the X-Y linker away from the catalytic site remains to be determined.

Loss of function in PLCγ1 and PLCγ2 gene-deficient mice has revealed the function of these isoforms *in vivo*. Consistent with its high expression in immune cells, PLCγ2-deficient mice have defects in the normal physiology of many cells of the immune system, including B lymphocytes, platelets, mast cells and natural killer cells (Suh *et al*., 2008). Furthermore, loss of PLCγ2 activity in human B lymphocytes has been observed in immunodeficiency syndromes such as X-linked agammaglobulinaemia (Satterwaite *et al.,* 1998). In contrast, the PLCγ1 is more widely expressed and is thought to regulate numerous cellular functions. Consistent with these findings, transgenic mice lacking PLCγ1 die early on in development, stressing the widespread importance of this enzyme (Ji *et al*., 1997). PLCγ1 has been shown to be required for the terminal differentiation of normal human keratinocytes from the oral cavity (Oh *et al.,* 2003), and is known be important for the survival of cardiomyocytes in response to oxidative stress (Mangat *et al.,* 2006). As mentioned previously, PLCγ1 mRNA is highly expressed within the brain and this isoform is thought to be important for brain function. Consistent with the ability of PLCγ isoforms to be activated through growth factor stimulation, in neurons PLCγ1 activity is stimulated by signalling through the fibroblast growth factor receptor and the Trk family of RTKs and this is thought to be involved in neuronal differentiation and neurite outgrowth (Bae *et al.,* 1998; Lin *et al.,* 1998). Furthermore, there is evidence that PLCγ1 activity is important for neural networks that underlie features of brain function such as memory and motor activity (Blum and Dash, 2004; Bolanos *et al.,* 2005), and polymorphisms in the human PLCγ1 gene have been linked to the pathogenesis of bipolar disorder (Turecki *et al.,* 1998).

1.5.2.4. PLCδ isoforms

In general, the single polypeptide chain of PLCδ isoforms consists of a PH domain, an EF-hand region, a catalytic X/Y domain and a C2 domain (Suh *et al*., 2008). Simple organisms such as yeast and slime moulds contain at least one PLCδ isoform, whereas three δ-isoforms (δ1, 3 and 4) have been identified in higher plants and mammals (Kadamur and Ross *et al*., 2013). A number of alternative splicing variants exist for mice PLCδ genes, increasing the number of specific isoforms. Two alternative splicing variants exist for mouse PLCδ1, known as PLCδ1a and PLCδ1b. Compared with PLCδ1a, mouse PLCδ1b has a deletion of 274 residues which results in a truncated Y domain, potentially rendering it catalytically inactive. There are two alternative splicing variants of mouse PLCδ3 (PLCδ3a and PLCδ3b), with PLCδ3a containing an additional 18 residues between the PH and EF-hand domains. Three alternative splicing variants exist for PLCδ4 (δ4a, δ4b and δ4c), with PLCδ4a containing an extra 32 amino acid residue in the linker region between the catalytic X and Y domains (Suh *et al*., 2008).

RT-PCR experiments show PLCδ1 mRNA to be mainly expressed in brain, heart, lung, skin and testes (Lee *et al*., 1999). Furthermore, using *In situ* hybridisation, the same researchers found mouse PLCδ1 to be present in almost all regions of the brain, and to be particularly enriched in spermatogonia. Northern blot analysis revealed PLCδ3 mRNA to be predominantly expressed in the heart and skeletal muscle, followed by brain and placenta (Lin *et al*., 2001). PLCδ4 mRNA is predominantly expressed in the brain, skeletal muscle, testis and kidney (Lee *et al*., 1996).

Following the homogenisation of tissues and cultured cells, PLCδ1 is mainly present in the cytoplasmic fraction. Given that PIP_2 is enriched in membranes, translocation of PLCδ1 from the cytosol to the membrane is necessary for enzyme activation and this is driven by PIP_2 binding by the PH domain and calcium by the C2 domain (Kadamur and Ross, 2013). Several studies have highlighted the functional role of the PH domain in the activation of PLCδ1 (Lemmon *et al*., 1995; Ferguson *et al.,* 1995). In cells depleted of PIP_2, PLCδ1 is localised in the cytoplasmic fraction, and deletion of the N-terminal residues corresponding to the PH domain prevents membrane association and abolishes the catalytic activity of PLCδ1 (Cifuentes *et al*., 1993). In addition to the PH domain-dependent PIP_2-mediated membrane association, the binding of calcium by the C2 domain is also required for membrane association and stimulation of the catalytic activity of PLCδ1 (Lomasney *et al.,* 1999). Although substrate hydrolysis by all eukaryotic enzymes is dependent on the presence of calcium as a cofactor within the active site, the crystal structure of PLCδ1 reveals the presence of three calcium-binding sites in the C2 domain (Essen *et al*., 1997). Membrane binding studies with the isolated C2 domain of PLCδ1 show that calcium promotes membrane association through electrostatic interactions with the anionic lipid phosphatidylserine (PS) (Lomasney *et al.,* 1999). Whether these interactions regulate enzyme activity by stabilising membrane-targeted PLCδ1, by directly stimulating enzyme activity or a combination of both is currently unclear. No other regulators of PLCδ1 activity have been identified to date and given that these enzymes are regulated by calcium, PLCδ1 may serve to amplify rather than initiate calcium mobilising signals (Kadamur and Ross, 2013).

Phenotypes associated with mice deficient in PLCδ isoforms, and human diseases associated with these isoforms have provided important insights regarding the physiological functions of these subtypes. Lack of PLCδ1 in mice is associated with the induction of skin inflammation (Ichinohe *et al*., 2007). PLCδ1 null mice show an increased expression of the pro-inflammatory cytokines IL-1β and IL-6, and the epidermis becomes infiltrated with a number of white blood cells, including macrophages, granulocytes and T lymphocytes. These defects could be cancelled by treatment with anti-inflammatory drugs. These results suggest that PLCδ1 is involved in the regulation of the immune system in the skin (Ichinohe *et al*., 2007).

PLCδ1 has also been implicated in some neurodegenerative disorders. PLCδ1 protein levels are elevated in Alzheimer's patients, and abnormally accumulate in the neurofibrillary tangles (Shimohama *et al*., 1995). Western blot analysis has also confirmed the presence of PLCδ1 in filamentous plaques of other neurodegenerative disorders, including Picks disease and Lewy body disease (Shimohama *et al*., 1993). PLCδ1 may therefore play a role in the formation of filamentous plaques in human neurodegenerative disease.

Disruption of PLCδ4 expression leads to male infertility, whereas female mice remain fertile. Immunohistochemical analysis of the sperm from wild-type mice reveals that PLCδ4 is located at the tip of the sperm, a region known as the acrosome (Fukami *et al*., 2001). The primary function of this region is to allow the sperm to penetrate the outer covering of the egg, known as the acrosome reaction (Wassarman *et al*., 1999). The zona pellucida and progesterone are known to stimulate and maintain a sustained

influx of calcium, which is essential for the normal acrosome reaction (Jackson *et al*., 2002). Interestingly, calcium transients associated with fertilisation are absent or delayed in sperm from PLCδ4 null mice, and fewer eggs become activated when inseminated with these sperm (Fukami *et al*., 2003). Together, these data indicate that PLCδ4 has an essential role in the acrosome reaction during natural fertilisation.

1.5.2.3. PLCε isoforms

PLCε was first discovered in 1998 during a yeast two-hybrid screen of a *Caenorhabditis elegans* library to identify novel Ras-binding proteins. The nematode protein, called PLC120, was shown to bind to the *C. elegans* Ras homologue, LET-60, resulting in the activation of its PLC activity (Shibatohge *et al*., 1998). A mammalian PLCε orthologue was later cloned and identified by three independent research groups (Song *et al*., 2001; Lopez *et al*., 2001; Kelley *et al*., 2001). PLCε is the largest of the PLC family members discovered to date, with a calculated molecular mass of 250 kDa and contains two domains that are not found in other PLC family members. The N-terminal CDC25-homology domain functions as a guanine nucleotide exchange factor for Ras, whereas the two C-terminal RA domains (RA1 and RA2) mediate a GTP-dependent interaction with Ras (Kadamur and Ross, 2013). The expression of mRNA coding for PLCε is highest in the heart, with expression also present in the brain, colon and lung (Lopez *et al.,* 2001). Two alternative splicing variants of PLCε exist in humans, known as PLCε1a and PLCε1b, which differ at the amino terminus (Suh *et al*., 2008). Northern blot and RT-PCR analysis suggests that PLCε1a and PLCε1b mRNA have different tissue distributions. PLCε1a was found to be present in most tissues tested, except for peripheral blood leukocytes, whereas PLCε1b could only be detected in the spleen,

lung and placenta. These differences in the expression of PLCε1a and PLCε1b are also mirrored in cell lines (Smrcka *et al*., 2012). Sorli *et al.* 2005 detected PLCε1a mRNA in most cell lines that they tested, including SKOV3 (derived from human ovary adenocarcinoma), Saos2 (dervived from a primary osteosarcoma), 293A (Human Embryonic Kidney; HEK), and 293T (HEK), whereas PLCε1b mRNA was only detected in 293T cells.

PLCε is activated by GTP-bound members of the Ras family such as Ras, Rap1, Rap2, Ral, and Rho (Kadamur and Ross, 2013). These proteins are a related group of small GTP-binding proteins that regulate crucial cellular processes such as proliferation, differentiation, apoptosis, migration and adhesion (Takai *et al*., 2001). Various ligands that regulate these GTP-binding proteins, including growth factors, adrenaline, thrombin, lysophosphatidic acid (LPA) and sphingosine-1-phosphate (S1P), are known to stimulate PLCε (Smrcka *et al*., 2012). Structural and biochemical analyses have shown the second C-terminal RA domain, RA2, to be predominantly responsible for the binding of Ras, Rap and Ral to PLCε (Kelley *et al*., 2001). Rho-dependent PLCε activation does not involve the RA domains, but instead requires an amino acid motif within the catalytic domain, which is unique to PLCε (Wing *et al*., 2003; Seifert *et al.,* 2004). Recently, PLCε has been shown to be activated by Gα12 and Gα13 subunits released from activated G protein-coupled receptors. This mode of regulation is indirect in that Gα12 and Gα13 firstly activate RhoA, which subsequently stimulates PLCε. The molecular mechanism linking the binding of members of the Ras family of GTPases to PLCε activation is currently unclear (Harden *et al*., 2009). Given that these small GTPases are membrane-associated proteins, this mechanism could involve

translocation of PLCε from the cytosol to the membrane. Based on the structural information for PLCβ, this membrane association could potentially remove the auto-inhibitory loop from the catalytic core of PLCε, leading to enzyme activation (Kadamur and Ross, 2013).

Important insights regarding the physiological functions of PLCε have been made following the analysis of the phenotypes associated with transgenic mice lacking PLCε. In line with their predominant expression in the heart, PLCε null mice develop many heart cardiac defects, including abnormal semilunar valve development, associated ventricular dilation and heart enlargement, and abnormal cardiac contraction in response to β-adrenergic stimulation (Tdano *et al*., 2005). In addition, PLCε null mice are less susceptible to carcinogen induced tumour formation (Bai *et al*., 2005). Further insights into how PLCε is integrated into animal physiology have also been provided by genome-wide association (GWAS) studies and human genetic analysis. PLCε mutations are associated with childhood nephritic syndrome and may cause abnormal glomerular development (Hinkes *et al*., 2006). Furthermore, PLCε single nucleotide polymorphisms (SNPs) have been associated with oesophageal squamous cell carcinomas (Abnet *et al*. 2010).

1.5.2.5. PLCζ isoforms

PLCζ contains the core domains common among mammalian PI-PLCs but lacks a PH domain (Suh *et al*., 2008). PLCζ was initially identified as the mammalian sperm-induction factor that initiates calcium oscillations necessary for the maturation and subsequent development of a fertilised egg (Saunders *et al*., 2002). Three alternative

splice variants have since been reported for PLCζ, known as ζ1a, ζ1b and ζ1c (Suh *et al*., 2008; Kouchi *et al.,* 2004). Northern blot analysis of mouse tissues revealed PLCζ mRNA (all isoforms) to be only detectable in the testes. RT-PCR detection of PLCζ in cDNA prepared from mouse testis devoid of spermatids suggested that PLCζ expression is specific to sperm and not another part of the testis (Kouchi *et al*., 2004).

Calcium is the only known regulatory ligand of PLCζ activity identified to date, with the purified enzyme exhibiting an EC_{50} for calcium-dependent PIP_2 hydrolysis of around 30 nM (Kadamur and Ross, 2013). Experimental evidence has highlighted the EF-hands and the C2 domain as being important for PLCζ activation as deletion of either one of these domains prevents calcium-dependent PIP_2 hydrolysis (Kouchi *et al*., 2005; Nomikos *et al.,* 2005). As mentioned previously, the association of PLC subtypes with the membrane fraction is essential for substrate interaction and subsequent PIP_2 hydrolysis. In other PLC family members, membrane association is either driven by protein-protein and/or protein-lipid interactions mediated by the PH domains of these proteins. Given that PLCζ lacks a PH domain, it is currently unclear how this PLC family member interacts with membranes and anchors to PIP_2.

In addition to the lack of a PH domain, PLCζ differs from other PLC family members in that its X-Y linker carries a positive charge, due to the presence of a cluster of basic residues not present in other PLC family members (Kadamur and Ross, 2013). Experimental evidence suggests that these residues may target PLCζ to PIP_2-enriched membranes as they have significant affinity for PIP_2 and reduction of the net positive charge of the X-Y linker significantly affects calcium-oscillation-inducing activity *in vivo*

and interaction of PLCζ with PIP_2 *in vitro* (Nomikos *et al*., 2007). In contrast, the negatively charged X-Y linkers of other PLC family members are thought to repel the negatively charged plasma membrane. This is thought to induce movement of the X-Y linker away from the catalytic domain, opening up the catalytic cleft. Removal of the X-Y linker region of PLCζ causes inhibition (Nomikos *et al*., 2007).

Prior to fertilisation, mature oocytes are halted in the second meiotic metaphase stage (M11) of the cell cycle. Upon binding of a single sperm, IP_3-mediated calcium release from intracellular calcium stores alleviates oocytes from M11 arrest, a process known as oocyte activation (Jones, 2005). A number of studies support the notion that PLCζ is responsible for IP_3-mediated calcium release and oocyte activation. Injection of complementary RNA (cRNA) encoding mouse and human PLCζ into mouse eggs initiates calcium oscillations (Saunders *et al*., 2002). Furthermore, human sperm extracts devoid of PLCζ fail to induce calcium release and are unable to initiate the first steps of embryogenesis (Yoon *et al*., 2008). Given the proposed importance of PLCζ as the mammalian sperm-inducing factor, defects in sperm PLCζ may underlie certain types of male infertility and oocyte activation failure. Recently it has been shown that sperm from men, which fail IVF, are unable to produce calcium oscillations following intracytoplasmic injection into mouse oocytes. These sperm exhibited reduced levels of PLCζ expression (Heytens *et al*. 2009). Currently, a PLCζ-deficient mouse model is yet to be established.

1.5.2.6. PLCη isoforms

Two PLCη isozymes, PLCη1 and PLCη2, were simultaneously identified by two independent research groups in 2005 (Hwang *et al*., 2005; Stewart *et al*., 2005). Currently, four alternative splice variants of PLCη1 have been identified in both humans and mice. These variants have been denoted η1a-d and display sequence variations at the C-terminal region (Hwang *et al*., 2005; Suh *et al*., 2008). For PLCη2, a total of five splicing variants have been reported in humans, and three splicing variants in mice (Zhou *et al*., 2005). RT-PCR experiments show PLCη1 mRNA to be highly expressed in the brain and kidney, with expression levels also detectable in the lungs, spleen, intestine, pancreas and thymus (Hwang *et al*., 2005). PLCη2 mRNA levels are restricted to the brain and intestine (Zhou *et al*., 2005; Nakahara *et al*., 2005). In common with other PLC family members, primary sequences of PLCη isozymes contain a PH domain, four EF-hand motifs, the C2 domain and the catalytic X and Y domains (Suh *et al*., 2008).

Recent studies suggest that PLCη isoforms are activated through GPCR stimulation. Co-expression of PLCη2 with Gβ1 and Gγ2 caused an increase in PLC activity in COS-7 cells (Zhou *et al*., 2005). Furthermore, purified extracts of PLCη2 were stimulated by G protein βγ subunits through interaction with the PH domain (Drin *et al*., 2006). *In vitro* experiments demonstrate that all PI-PLCs can be stimulated by Ca^{2+}, however PLCη1 and PLCη2 are more sensitive to Ca^{2+} compared to other isozymes, with maximal activity of both enzymes being achieved at Ca^{2+} concentrations of 1μM (Hwang *et al*., 2005). PLCη1 and PLCη2 may act to amplify the signalling events of other PI-PLCs with

the C2 domain thought to direct the calcium sensitivity of these enzymes (Popovics *et al*., 2014).

1.6. Bacterial (b)PI-PLCs: Phospholipase C X-domain containing proteins (PLCXDs)

Bacterial PI-PLCs have been isolated from various pathogenic species, including *Bacillus cereus* (Kuppe *et al,*, 1989) *B. anthracis* (Klichko *et al.,* 2003) *B. thuringiensis* (Volwerk *et al.,* 1989) and *L. monocytogenes* (Mengaud *et al.,* 1991), and also non-pathogenic species, including *Streptomyces antibioticus* (Yugo *et al*., 1994). Bacterial PI-PLCs have much smaller molecular masses (30-35 kDa) than mammalian PI-PLCs and consist of only an X-domain and hence are also known as phospholipase C X-domain containing proteins (PLCXDs). Furthermore, the bacterial PI-PLCs are secreted while mammalian PI-PLCs are intracellular enzymes and biochemical studies suggest that bPI-PLC has a role in calcium independent cleavage of PI and not its polyphosphorylated derivatives (Essen *et al*., 1998). Many bacterial PI-PLCs, including *B. cereus, B. anthracis* and *S. aurues* are also able to hydrolyse 6-glycosylated PI which can cause the release of proteins tethered to the membrane by glycosylphosphatidylinositol (GPI) anchors (Low, 1989; Low 1990). The catalytic activity of PI-PLC is thought to be important for the virulence of many pathogenic bacteria. *B. thuringiensis* is an important insect pathogen, and previous work has identified mutants lacking PI-PLC as avirulent (Camilli *et al*., 1991). *L. monocytogenes* are intracellular pathogenic bacteria that infect and multiply within macrophages. As an important part of their virulence, *L. monocytogenes* must escape from the phagosome and enter the cytoplasm of the macrophage (Pamer, 2004). Studies

demonstrate the importance of the *L. monocytogenes* PI-PLC activity in facilitating this escape through the production DAG and subsequent activation of PKC (Poussin *et al*., 2009).

With regards to the three-dimensional structure of bacterial PI-PLCs, *B. cereus* and *B. thuringiensis* have received the most attention. Sequence alignment analysis shows around 98% similarity between the two Bacillus PI-PLCs. Structural analysis using X-ray crystallography shows both enzymes consist of a single domain which folds as a distorted βα-TIM barrel, similar with to the catalytic domain of mammalian PI-PLCs. The enzymes are thought to co-ordinate substrate binding through the formation of hydrogen bonds with hydroxyl groups at positions 2, 3, 4 and 5 of the inositol ring. No hydrogen bonds are present between the protein and the hydroxyl groups at positions 1 or 6 of the inositol ring (Essen *et al*., 1998).

1.6.1. Mechanistic comparison of bacterial and eukaryotic PI-PLC

Bacillus PI-PLCs follow a general acid-base catalytic mechanism, similar to that for mammalian PI-PLCs, that involves two conserved histidine residues. In the Bacillus enzymes, these histidine residues are His32 and His82, which are conserved in other bacterial PI-PLCs. Similar to mammalian PI-PLCs, catalysis proceeds in two steps: a stable cyclic phosphodiester intermediate is created following a phosphotransfer reaction which is followed by a phosphohydrolysis reaction which creates acyclic inositol phosphate. In bPI-PLCs, His32 and His82 were identified as the general base and general acid, respectively (Heinz *et al.,* 1998). The essential roles for His32 and

His82 in this catalytic mechanism have been confirmed by mutagenesis studies (Hondal *et al*., 1997).

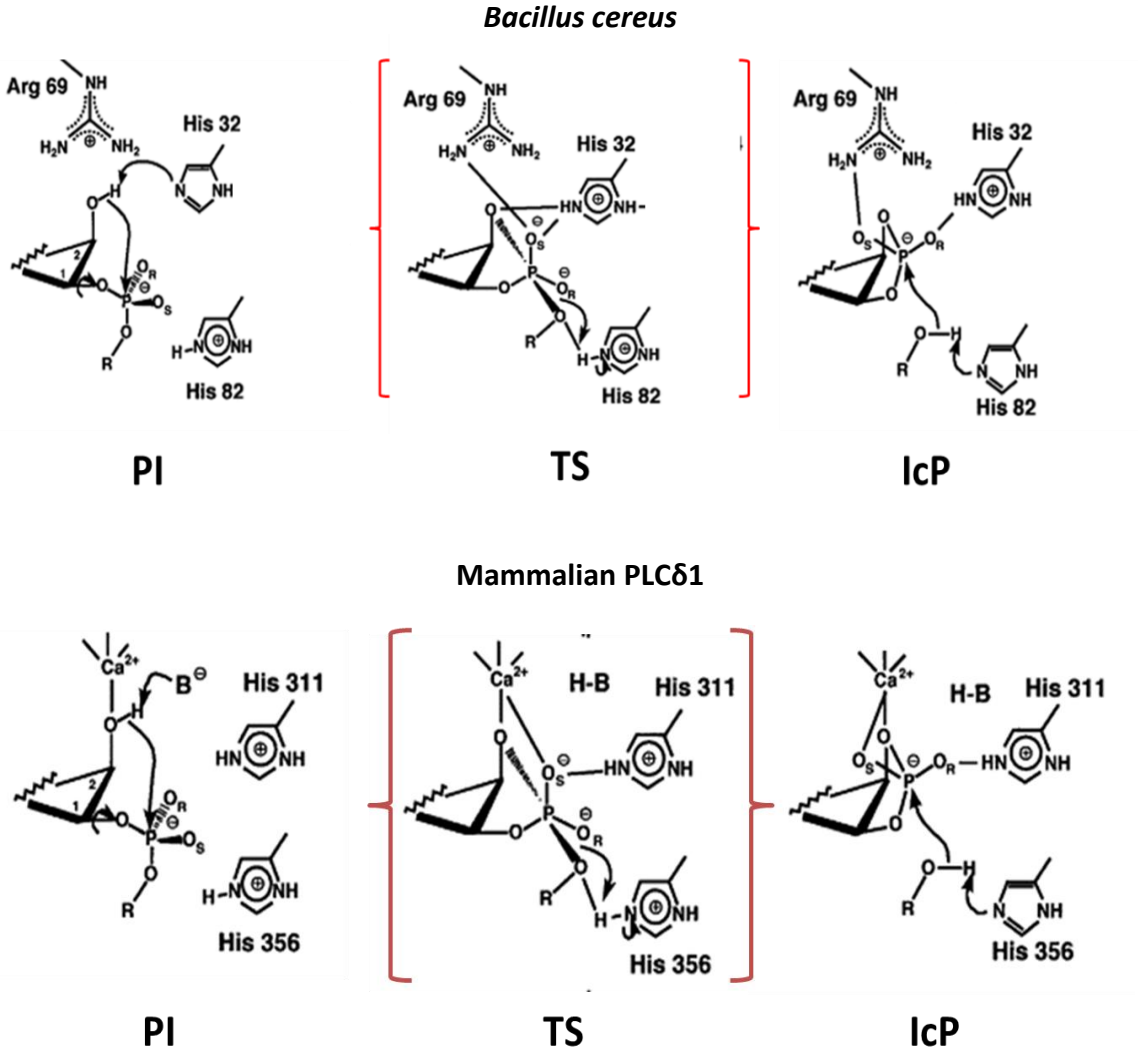

Figure 1.11: Comparison of the catalytic mechanism of the calcium-independent bacterial PI-PLCs (bPI-PLC) and the calcium-dependent mammalian PI-PLCs. This mechanism is based on structural data of PI-PLC from *Bacillus cereus* (bacterial; top on diagram) and human PLCδ1 (bottom on diagram) in complex with a number of substrate analogues. For Bacillus, His32 and His82 act as the general base and general acid, respectively and Arg69 stabilises the pentacovalent and cyclic inositol phosphate substrate intermediates. For PLCδ1, His356 acts as the general acid whereas the identity of the general base (B^-) is currently unclear. PI, phosphatidylinositol; TS, pentacovalent transition state; IcP, Ins(1:2cyc)P. Adapted from Heinz *et al*., 1998.

A striking difference between the catalytic mechanism of bacterial and eukaryotic PI-PLCs is the utilisation of calcium within the active site. The presence of calcium is a hallmark of the active site of eukaryotic PI-PLCs, and it is co-ordinated by the side-chain of a number of different amino acids (Section 1.4.1.4). These residues are not conserved in Bacillus PI-PLC enzymes, which have been confirmed to be calcium-independent enzymes. Calcium is thought to stabilise the cyclic inositol phosphate substrate intermediate within the active site of mammalian PI-PLCs. This stabilisation of the cyclic inositol intermediate by calcium is thought to provide an explanation why mPI-PLCs are able to bind this substrate intermediate with high affinity and therefore produce the acyclic inositol phosphate as the primary product of catalysis. In contrast, electrostatic stabilisation of the substrate intermediate is achieved by a basic residue, Arg69, and not calcium in Bacillus PI-PLCs and is much weaker than that of mPI-PLCs. Due to this lower affinity for the substrate intermediate, bPI-PLCs release most of the bound Ins(1:2cyc)P before the second reaction (phosphodiesterase) is complete, which is therefore the principal product of catalysis (Heinz *et al.,* 1998). The basic residue, Arg69, is well conserved among bPI-PLCs, and mutational studies demonstrate its essential role in catalysis (Essen *et al*., 1998).

1.7. Phospholipase C X-domain containing proteins (PLCXDs)

Much of the available literature on the existence and molecular functions of PLCXD proteins exist only for bacterial orthologs. It is, however, becoming increasingly clear that genes encoding PLCXD proteins are present in the genomes of eukaryotes. The first evidence of this came following the isolation and characterisation of a glycosylphosphatidylinositol-specific PLC (GPI-PLC) from the human parasite

Trypanosoma brucei (Webb *et al*., 1994). In contrast to other eukaryotic PI-PLCs, this enzyme is only 39 kDa and consists of only an X-domain. Like bacterial PI-PLCs it is also metal independent and can hydrolyse GPI anchored proteins and PI, but not PIP_2, using a similar catalytic mechanism. When using PI as a substrate, GPI-PLC generates DAG and a cyclic inositol-phosphate (Webb *et al.*, 1994). The cell surface of *T. brucei* found in the mammalian bloodstream, has a densely packed protein coat composed of a single polypeptide, the variant surface glycoprotein (VSG), anchored to the exterior surface of the plasma membrane by a GPI anchor. Cleavage of this anchor by the GPI-PLC causes a rapid release of VSG from the plasma membrane (Hanrahan *et al*., 2009). Although a definitive function for GPI-PLC has yet to be identified, evidence suggests that the release of VSG from the plasma membrane by the GPI-PLC may be important for the pathogenicity of *T. brucei* (Webb *et al.*, 1997; Sharom and Lehto, 2002).

Recently, the presence of PLCXD proteins in higher vertebrates and mammals has been confirmed. As a result of a microarray screen, a PLCXD was identified as a candidate gene showing differential expression between the different developmental stages of the European eel (*Anguilla anguilla*) (Kalujnaia and Cramb, unpublished). Comparative analysis with available databases revealed the presence of PLCXD orthologs in the genomes of virtually all species sequenced to date, including at least three isoforms in the human genome. What is more interesting is that no information exists regarding the functions of these ubiquitous proteins.

1.8. Aims of the Thesis

To date, all current information regarding the characterisation of members of the PI-PLC enzyme family has focussed on six sub-classes, with each sub-class having a different number of isoforms; PLCδ (δ1-δ4), PLCβ (β1-β4), PLCγ (γ1 and γ2), PLCε (ε1 and ε2), PLCζ and PLCη (η1 and η2). Owing to the the importance of these enzymes in cell signalling, their molecular structures, tissue distributions, mechanisms of activation and disparite physiological functions have been extensively investigated over the past 50 years with over 20,000 manuscripts currently published in the scientific literature. In contrast, PLCXDs have received less attention with information only available for bacterial PLCXDs, generally regarded as virulence factors, and the PLCXD, known as VSG lipase, present in *Trypanosoma brucei* and *Trypanosoma cruzi.*

The aim of this thesis are:

- To further characterise the putative European eel PLCXD gene indentified in the previous microarray by elucidating its full-length sequence, tissue distribution and mRNA/protein expression in the intestine of the different developmental stages of the European eel (Yellow and silver) following salinity transfer.
- To confirm the presence of three mammalian PLCXD isoforms (PLCXD1-3) and characterise their tissue distribution (mouse and human) and cellular localisations (HeLa cells; human PLCXDs).
- To characterise the mRNA and protein expression levels of PLCXDs in the cerebella and retinal samples from a mouse model of neurodegeneration (The Harlquin mouse) compared to control mice.
- To define the optimal conditions required for the production of recombinant human PLCXD proteins and characterise the enzymatic and structural properties of these proteins *in vitro.*

CHAPTER 2: MATERIALS AND METHODS

2.1 Animals

Prior to the onset of this project, adult freshwater "yellow" and "silver" eels were netted from rivers in the River Tay catchment area by Dr Gordon Cramb in collaboration with a local supplier based in Blairgowrie, UK. Briefly, fish were transported to the Scottish Oceans Institute, University of St Andrews, where they were initially kept in holding tanks containing FW (0-10 mOsm kg^{-1}) at ambient temperature (5-10 °C) on a 12h:12h light:dark photoperiod prior to the onset of experiments. Eels (n=6) were then transferred to separate experimental tanks containing 100 L of FW and salinity transfer was performed by reducing the water level of each tank to approximately 5% followed by a gradual re-filling (over a period of 1 h) back to 100 L with either SW (SW acclimation; 960-1020 mOsm kg^{-1}) or FW (controls). Eels were kept at ambient temperatures (5-10 °C) under a natural photoperiod (12h:12h light:dark) in running aerated FW or SW water. After 6 months, groups of FW-maintained and SW-acclimated yellow and silver eels were killed, decapitated and pithed before the removal of tissues.

Wild-type male mice on a B6CBA background and mice heterozygous for the X-linked harlequin mutation (*Pdcd8*^{Hq}) on the same genetic background were bred and maintained by Dr Marisol Corrall-Debrinski at the Institut de la Vision, Paris, France, as described in Bouaita *et al*., 2011. Frozen cerebellar tissue samples and retinal RNA samples were prepared from 6-month old mice (n=6 wild type; n=6 *Hq*) by Dr Marisol Corrall-Debrinski and kindly sent to St Andrews for analysis of PLCXD expression.

2.2 Microbiology

2.2.1 Growth of *E. coli* strains

E. coli strains used in this thesis are listed in Table 2.1. The different medium and antibiotic supplements used for the growth of *E. coli* are listed in Tables 2.2 and 2.3, respectively. For the growth of bacterial cultures, single colonies were selected from freshly streaked selective agar plates and used to seed up to 10 mL of selective medium and grown at 37 °C with vigorous shaking (210 rpm) overnight (16-18 h). The following day, the overnight culture was used to extract plasmid DNA (Section 2.7.2) and/or to prepare glycerol stocks for long-term storage (Section 2.2.2). For protein expression, the overnight culture was diluted 1/1000 into a larger volume of selective medium and incubated at 37 °C with shaking (210 rpm) until an optical density at 600 nm (OD_{600}) of 0.6-0.8 was reached. These cultures were then used for expressed protein purification, according to Section 2.2.5. For growth on agar plates to obtain single colonies, the desired clone was streaked from a glycerol stock (Section 2.2.2) or a freshly transformed cell suspension (Section 2.2.4) onto a freshly prepared selective agar plate and the plates were incubated upside down (agar up) over night at 37 °C.

2.2.2 Cryopreservation and resuscitation of *E. coli* cells

For long-term storage at -80 °C, glycerol stocks were prepared for *E. coli* cell suspensions. 500 µL was removed from overnight liquid cultures of *E. coli* (prepared as above) and mixed thoroughly with an equal volume of filter-sterilised freezing media (LB, 30% v/v glycerol) and stored frozen at -80 °C. For the recovery of bacteria from a glycerol stock, an aliquot of frozen cells was streaked onto an LB-agar plate

containing the appropriate antibiotic to check for the presence of selective markers, and incubated as described above.

Strain	Description
One Shot TOP10 (Invitrogen)	Chemically competent *E. coli.* Used for high-efficiency cloning and plasmid propagation.
One Shot OmniMAX™ 2 T1^{R} (Life Technologies)	Chemically competent cell line used for cloning applications. *TonA* genotype for resistance against T1 and T5 phage infection. These were provided by the Oxford Protein Production Facility (OPPF).
Rosetta™ (DE3) pLysS (Novagen)	**(DE3)** indicates that the strain carries a chromosomal copy of the T7 RNA polymerase under the control of the IPTG-inducible promoter, *lacUV5.* **pLysS** strains express T7 lysozyme which supresses basal expression of T7 polymerase prior to induction. This plasmid also carries a chloramphenicol resistance gene. These strains were a gift from Dr Arif Sheikh, University of St Andrews.
Lemo21 (DE3) competent *E. coli* (Invitrogen)	Strains contain a chromosomal copy of T7 lysozyme which is under the influence of an L-rhamnose-inducible promoter. When strains are grown without L-rhamnose they perform the same as a pLysS containing strain. Optional addition of L-rhamnose tunes the expression of the protein of interest. These were provided by the OPPF.
OverExpress C43(DE3) plysS (Lucigen)	Strains are lysogenic for the DE3 λ prophagend express the T7 RNA polymerase through IPTG induction controlled by the LacUV5 promoter. These strains also carry a chloramphenicol-resistant plasmid encoding the T7 lysozyme. These cells contain a mutations which confers toxicity tolerance and therefore they are used to express toxic proteins. These were a generious gift from Dr Arif Sheikh, University of St Andrews.

Table 2.1: *E.coli* strains and their properties.

Media type	Description
Luria-Bertani broth (LB)-Lennox (Sigma-Aldrich, Poole, Dorset, UK)	Dissolve 20 g of powder in 1 L water. Autoclaved for 15 min at 121 °C
LB agar (Sigma-Aldrich, Poole, Dorset, UK)	35 g of powder was added to 1 L water and heated to boiling whilst stirring to fully dissolve the powder. Autoclaved 15 min at 121 °C to sterilise. Was allowed to cool before making any additions, such as antibiotics. 30 ml poured into petri dishes and allowed to solidify.
Terrific broth (TB) (Sigma-Aldrich, Poole, Dorset, UK)	Dissolved 47.6 g and 8 mL glycerol in 1 L distilled water and autoclaved for 15 min at 121 °C.
Power Broth™ (AthenaES™)	52 g dissolved in I L distilled water. Glycerol (4 mL) was added and then the solution was autoclaved for 15 min at 121 °C. This was prepared by OPPF.
Overnight Express™ Instant TB Medium (Millipore)	Dissolved 60 g powder in 1 L distilled water, supplemented with 10 mL glycerol and then autoclaved for 15 min at 121 °C. This was prepared by OPPF.
SOC Medium (Invitrogen)	Supplied as 10 mL bottles of liquid medium used for the growth of bacteria in the final step of transformation.

Table 2.2: The different media used to culture *E. coli*.

Antibiotic	Descirption
Ampicillin sodium salt (Sigma-Aldrich, Poole, Dorset, UK)	Stock concentration of 100 mg/mL prepared in MilliQ water. Working concentration of 100 µg/mL.
Kanamycin sulphate (Sigma-Aldrich, Poole, Dorset, UK)	Stocks prepared at 50 mg/mL in MilliQ water and then diluted to 50 µg/mL working concentration.
Chloramphenicol (Sigma-Aldrich, Poole, Dorset, UK)	Stocks prepared at 34 mg/mL in 100% ethanol and used at a working concentration of 34 µg/mL

Table 2.3: Antibiotics used for selective growth of bacteria

2.2.3 Preparation of chemically competent *E. coli*

Within this thesis, only the Rosetta™ (DE3) pLysS and OverExpress C43 (DE3) pLysS strains were made chemically competent using the procedure described below; all other strains (Table 2.1) were purchased as chemically competent cells. A glycerol stock of Rosetta (DE3) pLysS and OverExpress C43 (DE3) pLysS strains were obtained from Dr Arif Sheikh and used to streak fresh LB-agar plates to obtained single colonies, as described in Section 2.2.1. These LB-agar plates contained 34 µg/µL chloramphenicol (prepared according to Table 2.2) to select for strains containing the pLysS plasmid. A single colony was then inoculated into 1 mL of LB medium supplemented with 34 µg/mL chloramphenicol and grown, as described in Section 2.1.1. On the following day, the starter culture was diluted 1/1,000 to a final volume of 100 mL with fresh selective LB medium (Table 2.2) and incubated with shaking until an OD_{600} of 0.25-0.3 was reached. The culture was then chilled on ice for 15 min and the cells were harvested by centrifugation at 4,000 rpm for 10 min at 4 °C in 50 mL conical tubes using the Avanti J-26PI centrifuge with a JA-25.50 fixed angle rotor (Beckman Coulter, Inc.) The supernatant was discarded and the bacterial cell pellet was resuspended in 40 mL ice-cold sterile 0.1 M $CaCl_2$ (powder obtained from Sigma-Aldrich) and incubated on ice for 30 min. The cells were then harvested as above and the pellet resuspended in 6 mL 0.1 M $CaCl_2$ containing 15 % glycerol (diluted from 100% stock in MillQ H_2O; Sigma-Aldrich, Poole, Dorset, UK). The cell suspension was fractionated into 50 µL aliquots and stored frozen at -80 °C in sterile 1.5 mL Eppendorf tubes (Thermo Fisher Scientific, Loughborough, UK).

2.2.4 Heat-shock transformation of competent *E. coli*

The ability of bacteria to directly uptake, incorporate and express exogenous genetic material from its surrounding is known as transformation. For transformation, 5-50 ng of plasmid DNA was added to a vial of chemically competent cells (50 µL), and the cell-DNA mixture was incubated on ice for 30 minutes. This step was followed by a brief "heat shock", which opens the pores of the cell membrane allowing entry of the plasmid. "Heat shock" was carried out at 42 °C for 30 s followed by immediate transfer to ice for 2 min. The transformed cells were then incubated with rotation for 1 h at 37 °C in 200 µL of SOC media (Table 2.1) to allow the bacteria to recover from the heat shock and to express the antibiotic resistance gene present on the plasmid DNA. A sample of the recovered bacteria (50-100 µL) was then grown and maintained on a pre-warmed selective agar plate, as described in Section 2.2.1. Single colonies were used to inoculate 10 mL of LB medium and grown overnight (Section 2.2.1) to prepare sufficient cells for plasmid purification, glycerol stock preparation (Section 2.2.2) and further growth for protein expression, as described in Section 2.2.5.

2.2.5 Recombinant expression in *E. coli*

Initially expression constructs were created for human PLCXD1, 2.1, and 3 (pETM11 and pET22b+; Section 2.7.10.1) and used to transform Rosetta™ (DE3) pLysS and C41 BL21 *E. coli* strains (Section 2.2.4). Towards the end of the project, human PLCXD1, 2.1 and 3 were sub-cloned to the pOPIN expression vectors (Section 2.7.10.2) and transformed to Rosetta™ (DE3) pLysS and Lemo21 E. coli cells (Section 2.2.4). This latter work was carried out in collaboration with the Oxford Protein Production Facility (OPPF). Small-scale expression experiments were carried out first to assess the effect

of different variables (Section 2.2.5.1) on the expression levels and solubility of recombinant proteins. Large-scale expression experiments were performed once the optimum expression parameters for a given target were obtained (2.2.5.2).

2.2.5.1 Small-scale expression in *E. coli*

Initially the levels of expression and solubilities of recombinant PLCXD isoforms were assessed in different *E. coli* host strains (Rosetta™ (DE3) pLysS and C41 BL21) using different induction temperatures (25 °C and 37 °C). Single colonies containing recombinant vector DNA for each clone were used to inoculate 10 mL of selective growth medium and grown overnight (Section 2.2.1). The following day, the starter culture was diluted 1/1,000 to a final volume of 50 mL with fresh selective TB medium and incubated with shaking until an OD_{600} of 0.6-0.8 was reached. Protein expression was induced by the addition of 1 mM isopropyl β-D-1-thiogalactopyranoside (IPTG; Sigma-Aldrich, Poole, Dorset, UK) directly to the cell suspension. Expression was induced for either 4 h at 37 °C or 20 h at 25 °C with shaking at 210 rpm. Following incubations the cells were harvested by centrifugation at 4,000 rpm at 4 °C for 10 min using the Avanti J-26PI centrifuge with a JA-25.50 fixed angle rotor (Beckman Coulter, Inc.). Supernatants were decanted and bacterial pellets were weighted and then stored frozen at -20 °C until protein extraction (Section 2.8.5).

Further small-scale expression trials were also carried out at the Oxford Protein Production Facility (OPPF), to test the effect of different fusion proteins on the level of soluble expression of recombinant of human PLCXD1, 2.1 and 3 in *E. coli*. Single colonies verified to contain recombinant vector DNA were used to inoculate 0.7 mL of

selective Power Broth (Table 2.2) the cultures were grown overnight in deep-well blocks (BD Falcon 353966) at 37 °C with shaking at 250 rpm. For the induction of protein expression in Power Broth, 250 µL of the overnight culture was diluted with fresh 3 mL Power Broth and incubated with shaking until an OD_{600} of 0.5 was reached. The cultures were then cooled by shaking at 240 rpm at 20 °C for 20 min and protein expression was induced following the addition of 1 mM IPTG to each well and growth overnight by shaking at 250 rpm at 20 °C. For auto-induction, individual colonies were picked and grown in Power Broth as before. A sample (0.25 mL) of this cell suspension was then diluted in 3 mL of Overnight Express Instant TB medium (Table 2.2) supplemented with the appropriate antibiotic as before. The cell suspension was incubated at 37 °C with shaking until an OD_{600} of 0.5 was reached. At this point, the temperature of the shaker was reduced to 25 °C and the cell suspension was incubated with shaking at 250 rpm for a further 20 h to induce protein expression.

2.2.5.2 Large-scale expression in *E. coli.*

For large-scale expression in *E. coli,* single colonies of each clone were picked and used to inoculate a 10 mL overnight culture, as described before. In-order to yield enough cells to seed a 12 L culture for protein expression, the starter culture was used to inoculate a further overnight culture of 200 mL. The following day, the second overnight culture was diluted 1/1,000 in fresh 1 L of selective TB medium (x12 for a 12 L culture) and incubated at 37 °C with shaking (as before) until an OD_{600} of 0.6-0.8 was reached. Recombinant protein expression was induced and the cells were harvested and stored as described in Section 2.2.4.1.

2.3 Mammalian Cell Culture

2.3.1 Maintenance of cell lines

Adherent cell lines (ATCC) were maintained at 37 °C in a humidified atmosphere at 95% air/5% CO_2 in the appropriate media (Sigma-Aldrich, Poole, UK) as shown in Table 2.4. Cells were grown in 75 cm^2 flasks and seeded at a density of 10,000 cells per cm^2. Cells were split into a new 75 cm^2 flask once they covered ~80% of the bottom of the flask, as assessed by eye. The media was removed and the cells were washed twice with 10 mL sterile 1 x Phosphate Buffered Saline (PBS pH 7.4; GIBCO). Cells were then detached from the plastic with 2 mL pre-warmed Trypsin-EDTA (Life Technologies, Paisley, UK). The cells were then suspended to homogeneity in 10 mL fresh media to inactivate the trypsin. An aliquot (0.5-2.5mL) of the cell suspension was added to a new 75 cm^2 flask containing 15 mL of fresh media.

Cell type	Origin	Media used
HeLa (ATCC)	Immortalised cervical cells derived from Henrietta Lacks	DMEM (Dulbecoos' modified Eagles's medium) supplemented with 10% (v/v) Fetal Calf Serum (FCS; Invitrogen), 100 units/mL of penicillin/streptomycin (Invitrogen, Life Technologies, Paisley, UK)
HEK293T (Human Embryonic Kidney cells). Gift from Dr Jelena Andrejeva, University of St Andrews	Immortalised cells transformed from human embryonic kidney cells.	DMEM supplemented with 10% (v/v) FCS and 100 units/mL of penicillin/streptomycin mixture (Invitrogen, Life Technologies, Paisley, UK)

Table 2.4: The maintenance of different mammalian cell lines.

2.3.2 Storage and resuscitation of cell lines

Following trypsinisation of a confluent 75 cm^2 flask, the cell suspension was centrifuged at 1,000 rpm for 3 min at 4 °C. The cell pellet was then resuspended in 4 mL freezing medium (Life Technologies) and 1 mL aliquots were added to cryovials (Thermo Fisher Scientific, Loughborough, UK). The cells were stored at -20 °C for 24 h and then -80 °C for 24 h and were stored under liquid nitrogen for long-term storage. Cells stored under liquid nitrogen were quickly thawed at 37 °C and added to 10 mL fresh growth media. The cells were harvested by centrifugation and resuspended in 25 ml of fresh medium and transferred to a 75 cm^2 flask and grown as previously described.

2.3.3 Transient expression screen in HEK293 cells

This work was carried out in collaboration with OPPF. The level of soluble expression of PLCXD1, 2, and 3 was tested in HEK293 cells by the transfection of pOPIN vector

constructs encoding PLCXDs tagged to different fusion proteins. Each PLCXD was sub-cloned into 10 different pOPIN vectors as described later in Section 2.7.10.2. Cells (1 mL; 1.5-2 x 10^5 cells/mL) were seeded in antibiotic-free DMEM (Invitrogen, Life Technologies, Paisley, UK) into 2 x 24-well plates, and incubated overnight as previously described. Following incubation, 1 mL of fresh DMEM with 2% FCS was added to each well of cells. A transfection cocktail was prepared containing 2 µL of 1.33 mg/mL GeneJuice, 60 µL of serum-free DMEM and 1 µg of plasmid DNA and incubated at room temperature for 10 min. The transfection cocktail was added to cells and incubated at 37 °C for 3 days.

2.3.4 Lentivirus-based overexpression in HeLa cells

This work was carried out in collaboration with Dr Svetlana Kalujnaia, at the University of St Andrews. Briefly, over-expression of PLCXDs in HeLa was achieved by construction of recombinant lentiviral particles containing each PLCXD isoform. Lentiviruses were generated by co-transfecting HEK293T cells with the CMV (pCMVR8.91), VSV/G (pMD_VSVG) and pdlNotI'nPk'MCS'R plasmids (Section 2.5.4). The CMV plasmid encodes the viral proteins Gag, Pro-Pol, Rev and Tat which are controlled by the CMV promoter. The VSV/G plasmid encodes the viral envelop glycoprotein from the vesicular stomatitis virus under the control of the CMV promoter. The pdlNotI'nPk'MCS'R plasmid carried the target gene and the pac (puromycin N-acyl transferase) gene, both of under the control of the SFFV promoter sequence (Section 2.6.4). Only the pdlNotI'nPk'MCS'R plasmid carried the viral packaging signal sequence and therefore complete lentiviral particles will only carry target gene and the puromycin resistance gene.

Prior to transfection, HEK293T cells were passaged and 8 x 10^6 cells were seeded in a 6 x 75 cm^2 flask and incubated overnight. The following day, HEK293T cell confluence was assessed by eye and only flasks that had 80-85% confluence were used for virus preparation. Recombinant lentiviruses expressing each PLCXD isoform were prepared by transfecting the pdlNOT/PLCXD construct together with CMV (pCMVR8.91) VSV/G (pMD_VSVG) using FuGENE®6 (Promega, Southampton, UK) according to the manufacturer's protocol. The culture medium containing the lentiviruses was removed two days after transfection and new medium was added to the cells and removed 24 h later. Medium from 2 and 3 days post transfection was pooled and centrifuged at 2,000 rpm for 10 min to remove cell debris. The supernatant was filtered through a 0.45 µm syringe filter unit (Millipore) and stored at -70 °C as the disabled lentivirus stock in 500 µL aliquots. HeLa cells were cultured in T75 cm^2 to a confluence of 25-25%, as assessed by eye, and then incubated with 500 µL the lentivirus stock in the presence of 8 µg/mL polybrene (Sigma-Aldrich, UK). Two days after infection, the virus-containing media was replaced with media supplemented with 2.5 µg/mL puromycin (Gibco®). Stocks of stable cell lines were stored frozen at -80 °C, according to Section 2.3.2.

2.4 Insect cell culture

2.4.1 Maintenance of *Sf9* cell lines

The maintenance of *Spodoptera frugiperda*-9 (*Sf9*; Life Technologies) cell lines was carried out by Ms Nahid Rahman at the Oxford Protein Production Facility. Briefly, these cells were maintained in Sf-900™ II medium (Life Technologies) at 27 °C in a non-

humidified incubator. Suspension cultures were seeded between 3-5 x 10^5 cells/mL and grown at 27 °C (as above) with shaking at 120 rpm until they reached 2-3 x 10^6 cell/mL (3-4 days) and then passaged. Adherent cultures were seeded at a density of 2-3 x 10^6 cells/mL with 10 mL of Sf-900™ II medium in a 25 cm^2 flask and incubated as above without shaking for 5-7 days. For storage, suspension cultures were grown to a density of 2-3 x 10^6 cell/mL and then centrifuged at 100 rpm for 5-10 min and the cell pellet was resuspended in the same volume of cell freezing medium (70% Sf900™ II/20% FCS/10% DMSO) as the original culture. 1.5 mL fractions of the cell suspension was added to each cryovial (Thermo Fisher Scientific, Loughborough, UK) and frozen at -80 °C for 2-3 days. The vials were transferred to liquid nitrogen for long-term storage. For resuscitation, 3-4 vials of frozen cells were rapidly thawed in a water bath at 37 °C and added to a single 125 mL shake flask containing 25 mL of Sf900™ II media. The cell suspension was grown and passaged as described above.

2.4.2 Baculovirus-based expression in *Sf9* cells

This work was carried out in collaboration with OPPF. The level of soluble expression of the different fusion constructs for PLCXD1, 2.1, and 3 was tested in *Sf9* cells using the Baculovirus expression system. In-order to create the expression vector, the full-length coding sequence of human PLCXDs was inserted into the pOPIN vector suite as described in Section 2.7.10.2. Co-transfection of linearized baculovirus shuttle vector or bacmid (BaculoGold™-Baculovirus DNA; PharMingen, BD) and the expression vector containing viral polyhedron sequences flanking the PLCXD insert allowed homologous recombination to take place (See vector map; 2.6.5). Sf-9 cells (500 µl; 5 x 10^5 cells/mL) were seeded in 24-well culture plates (Corning® Costar®cell culture plates; Sigma-

Aldrich) and left to attach for 1 h at room temperature. An aliquot containing 250 ng of bacmid was gently mixed with 100-500 ng of expression vector DNA and 50 µL of Sf900II. To this mixture 0.75 µL FuGeneHD (Roche) was added and the mixture was incubated for 30 min at room temperature. The entire transfection mixture was added slowly to the appropriate well of *Sf9* cells and incubated for 5-6 days as above. Following incubation, the baculovirus-containing media was removed (P0 virus stock) and was stored frozen at -80 °C. In-order to create P1 virus particles, *Sf9* cells were seeded at 1 x 10^6 cells/mL in 24-well plates and left to attach as before. To each well, 5 µL of the P0 virus stock (as prepared above) was added and the cells were incubated for 6 days as previously described. The media was removed (containing the P1 virus) and this was stored in 1 mL aliquots at 4 °C in the dark. For long term storage sterile BSA (Sigma-Aldrich) was added to 10% and the virus stock was stored frozen at -80 °C. Small scale expression screening was performed in suspension culture using 24 deep well plates (BrandTech Scientific, Inc., UK) with 5 mL of Sf-9 cells (1 x 10^6 cells/mL). To the cell suspensions, either 5 or 50 µL of the P1 virus was added and incubated for 2-3 days at 27 °C with shaking at 250 rpm. A 1 mL sample was taken from each well and centrifuged for 15 min at 5,500 rpm and the cell pellet was stored frozen at -80 °C for protein extraction and purification (described later in Section 2.8.9).

2.5 Cell assays and treatment

2.5.1 [^{3}H] Inositol-phosphate release assays

This assay was carried out in collaboration with Dr Svetlana Kalujnaia. HeLa cells were virally-transfected and maintained as previously described. Control, non-transfected, and PLCXD1, 2.1 and 3 overexpressing cell lines were seeded in 6-well plates (Sigma-

Aldrich) until they reached 70-80% of confluence, as assessed by eye. The inositol phospholipid pools were then radio-labelled by incubating the cells in inositol-free DMEM (MP Biomedicals, IIIkrich, France) containing 1 µCi/mL myo-D-[^{3}H]-inositol (GE Healthcare, Buckinghamshire, UK) for 24 h. The cells were then extensively washed in complete media and were incubated for 2 h at 37 °C in HEPES-buffered DMEM (MP Biomedicals, IIIkrich, France) containing 10 mM LiCl (inhibitor of endogenous inositol monophosphatases) to determine the rate of turnover of the phosphoinositide pool by the accumulation of [^{3}H]-inositol phosphate in the cell cytosol. Incubations were also conducted in the presence of LiCl plus the calcium ionophore A23187 (Sigma-Aldrich). The reaction was terminated by removal of the medium and the addition of 1 mL 10 mM ice-cold formic acid (Sigma-Aldrich) to each well and incubating on ice for 30 min. The soluble [^{3}H]-inositol phosphates were isolated from the formic acid extract by passing the cell extract through a column of Dowex AG resin (prepared by addition of a 0.5 ml 50% slurry in water; Bio-Rad Laboratories, Hemel Hempstead, UK, to 2 mL plastic columns). The resin was washed with 0.5 mL water and 0.5 mL of 60 mM ammonium formate/ 5 mM sodium tetraborate before eluting the [^{3}H]-inositol phosphates with 1 mL of 1 M ammonium formate/0.1 M formic acid. An 800 µL sample of the eluate was transferred into scintillation tubes and mixed with 2.5 mL Optiphase Hisafe 3 (Perkin Elmer Biosystems, Cambridge) and the activity was quantified with a MicroBeta^2 scintillation counter (PerkinElmer Biosystems, Cambridge, UK).

2.5.2 Immunocytochemistry and fluorescent microscopy

HeLa cells exhibiting stable overexpression of Pk/V5-tagged hPLCXD1, 2.1 and 3 were created and grown (Section 2.3.1) to sub-confluence on sterile coverslips (R&D

Systems, Inc, Minnesota) in 6-well plates (Sigma-Aldrich). The media was removed and the cells were washed in PBS. The cells were fixed with 4% formaldehyde (Sigma-Aldrich) in 1 x PBS for 10 min and were washed three times in 1 x PBS. To enable the antibodies to gain access to the cell interior, the cell were permeabilised with 0.5% NP-40 (Tergitol®; Sigma-Aldrich) in PBS for 10 min and the cells were washed 3 times in PBS. The cover slips were then incubated with 1% goat serum (Cell Signalling Technology™) in PBS for 1 h at room temperature to block non-specific binding of protein. Cover slips were then incubated with 1/200 dilution of the mouse anti-Pk tag (Abcam antibody gifted by Dr Jelena Andrejeva, University of St Andrews) in 5% BSA in PBS for 1 h at room temperature followed by 3 washing steps in PBS. Secondary antibody (Alexa Fluor 633-labelled donkey anti-mouse polyclonal antibody; ThermoScientific) was diluted 1:1000 in 5% BSA in PBS for 1 h at room temperature followed by extensive washing in PBS. Cover slips were washed briefly in PBS and mounted in ProLong gold antifade reagent containing DAPI (Sigma-Aldrich) according to manufacturer's instructions. Slides were examined with a Zeiss fluorescent microscope system with a 63x oil emersion objective.

2.6 Vector Maps

2.6.1 pCR® 4-TOPO® vector

The pCR 4-TOPO vector was purchased from Invitrogen, Life technologies, Paisley, UK. Linearized vector is supplied with 3'-thymidine (T) overhangs for TA cloning. The vector contains ampicillin and kanamycin resistant genes for positive colony selection using 100 µg/mL and 50 µl/mL of the antibiotic, respectively. Priming sites for M13 and T7 primers which are present for sequencing reactions.

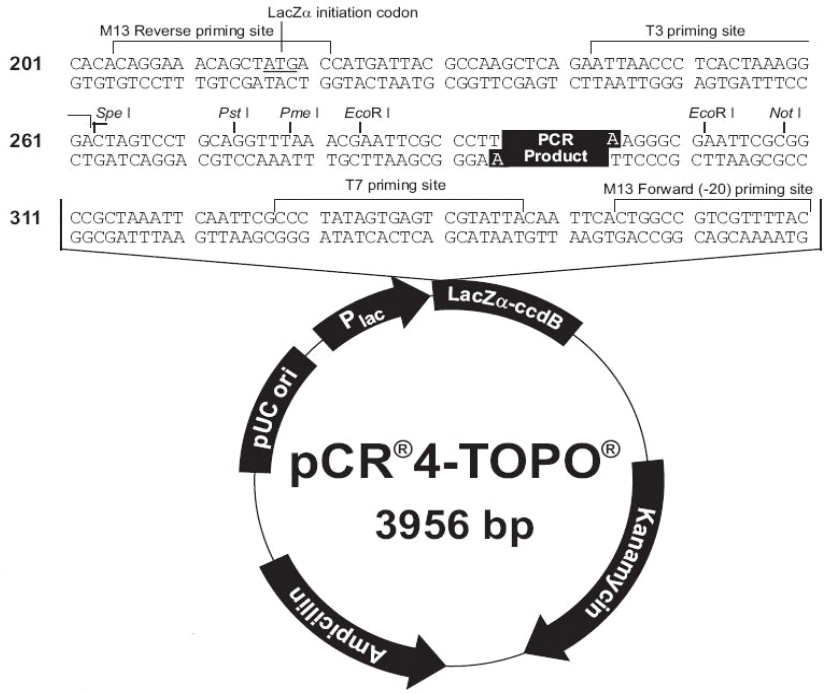

Figure 2.1- Vector map of the pCR 4-TOPO vector showing the cloning site and primers sequences used to confirm the presence of a gene insert.

2.6.2 pET M11 vector

The pET M11 vector was provided as a 0.5 mg/mL purified stock from Dr Arif Sheikh, University of St Andrews. The pET M11 vector is derived from pET backbones (Novagen). The vector has an N-terminal $(His)_6$-tag which is cleavable by Tobacco Etch Virus (TEV) protease and the functional multiple cloning site (MCS) starting with the NcoI recognition site. The NcoI has the start codon ATG that can be used for the expression of the protein of interest. The target gene is inserted downstream of the T7 promoter.

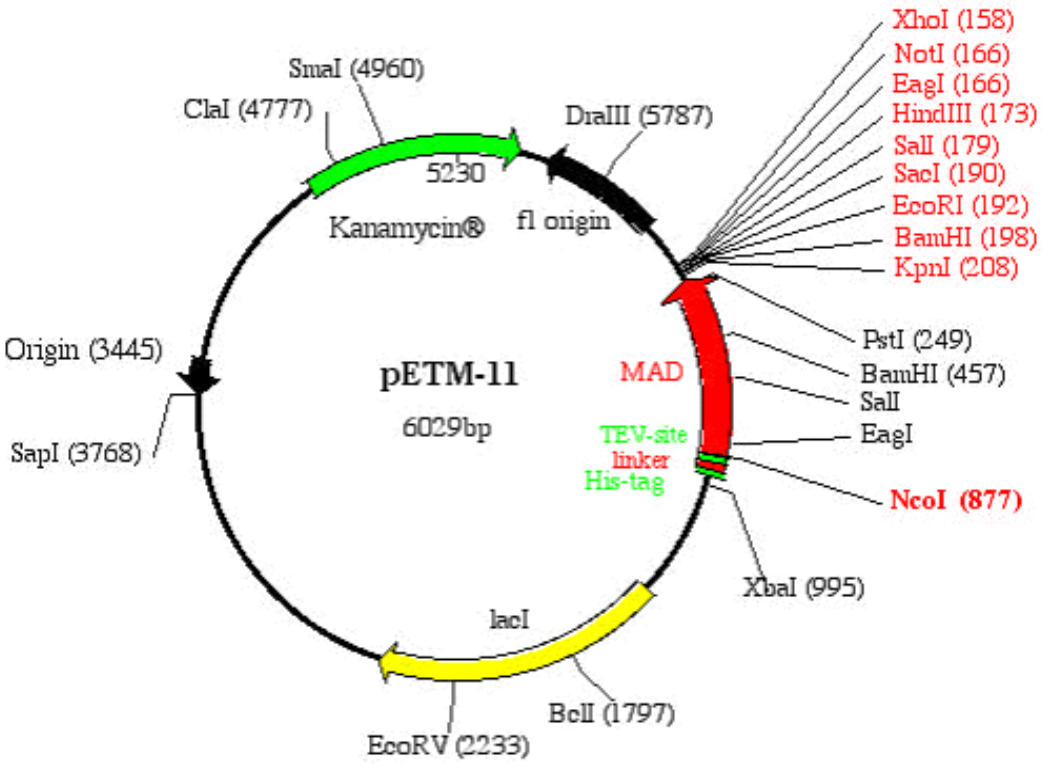

Figure 2.2- pETM11 vector map show the multiple cloning site and other elements responsible for the expression of a gene of interest.

2.6.3 pET 22b+ vector

The pET 22b+ vector was provided as a 0.5 mg/mL purified stock from Dr Arif Sheikh, University of St Andrews. The pET 22b+ is also derived from pET backbones (Novagen). It includes a C-terminal $(His)_6$-tag which is not cleavable by any proteases. For protein expression without a signal sequence, the gene of interest is sub-cloned into the MCS using NdeI and XhoI restriction sites. This places the gene downstream of the T7 promoter which allows for inducible protein expression through by the action of IPTG.

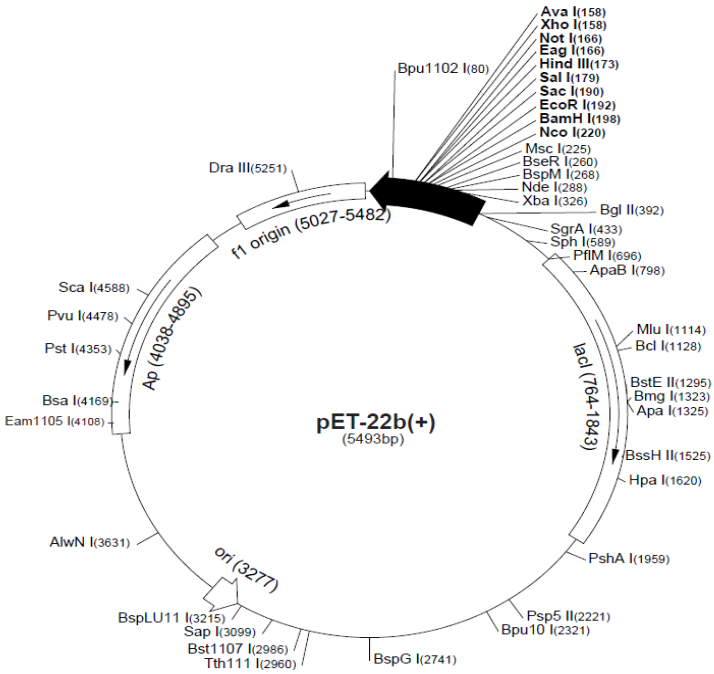

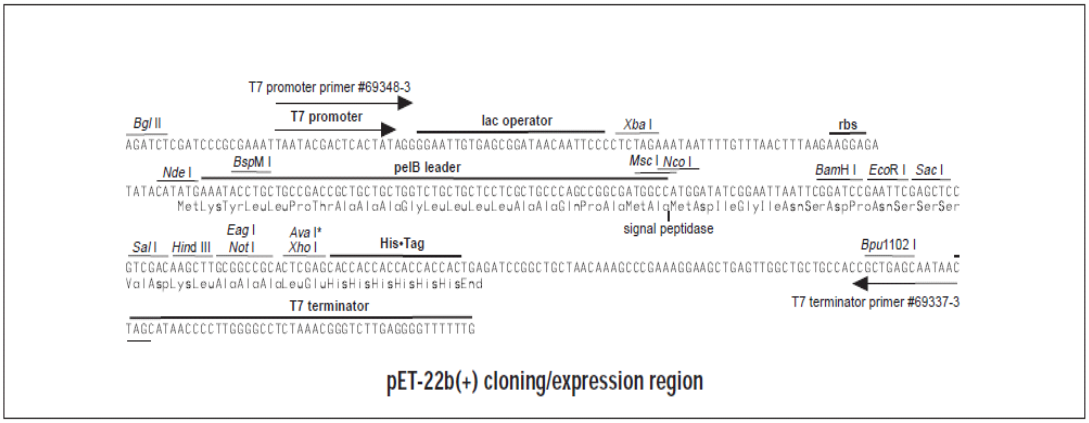

Figure 2.3- pET-22b+ vector map showing the multiple cloning site (MCS)

2.6.4 pdlNotI'nPk'MCS'R

The HIV-1-based lentiviral vector pdlNotI'nPk'MCS'R was provided as a 1 mg/mL stock by Dr Jelena Andrejeva, University of St Andrews. The vector was used to generate HeLa stable cell lines expressing N-terminally Pk/V5-tagged PLCXD-1, 2.1 and 3. The vector carries an ampicillin resistance gene for selection in E. coli and a puromycin

resistance gene (pac) for selection of transfected mammalian cells. Figure 2.4 summarises the features of the vector used for protein expression in HeLa cells.

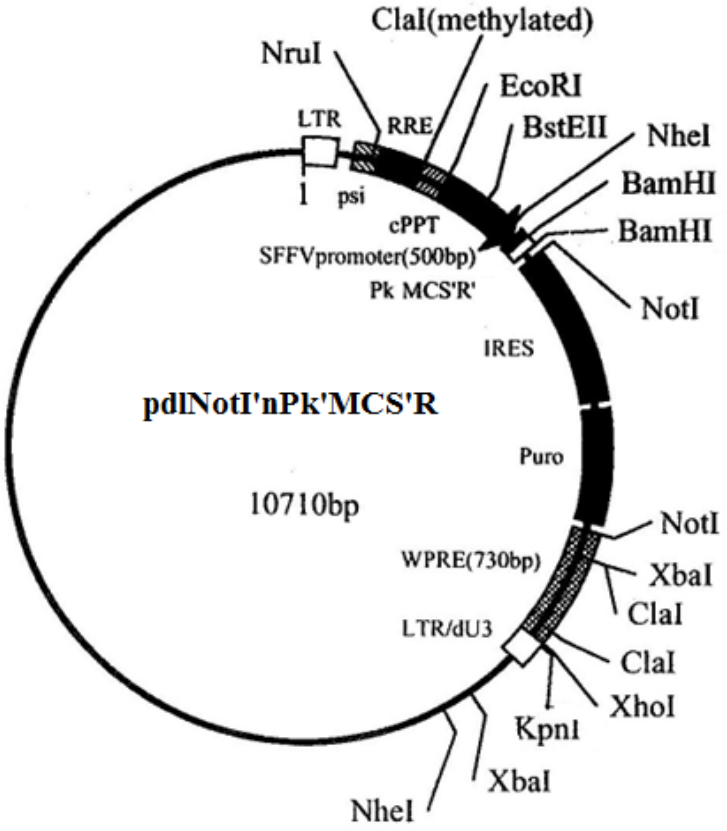

Figure 2.4- Vector map showing features of the pdINotI'nPk'MCS'R vector allowing for sub-cloning and expression of a gene of interest. 5' and 3' Long Terminal Repeats (LTF) for integration into the host genome; the psi viral packaging signal sequence; central polypurine tract (cPPT) which improves vector integration into the host genome; the spleen focus-forming virus (SFFV) promoter; internal ribosome entry site (IRES) for the initiation of translations; the woodchuck hepatitis virus post-transcriptional regulatory element (WPRE) for RNA processing and nuclear import.

2.6.5 pOPIN vector suite

The pOPIN vector suite is a series of expression vectors for the fusion of the target protein at its N- and C-terminus with a number of different fusion partners. These plasmid vectors were originally constructed by Dr Louise Bird, Oxford Protein Production Facility. The pOPIN vectors utilised for the expression of PLCXD fusion proteins in this thesis are shown in Table 2.3. The pOPIN vectors allow for the parallel screening of protein expression in multiple hosts (*E. coli*, HEK293T cells and Sf-9 insect cells; Figure 2.5). Each vector carries an ampicillin resistance gene for positive selection of colonies.

The presence of a T7 polymerase promoter with *lac*O operator allows for inducible expression in *E. coli* strains containing the DE3 prophage. The vector also contains a number of elements necessary for the protein expression in eukaryotic cells. The cytomegalovirus (CMV) early enhancer element, chicken β-actin promoter and the rabbit β-globin poly A site sequences together drive the high level expression in eukaryotic cells. Initiation of translation in eukaryotic hosts is driven by the presence of a Kozak consensus sequence. The p10 promoter and the *lef2*/ORF 603 and the ORF 1629 baculoviral recombination sites allow for insertion into the baculovirus shuttle vector and for transfection of Sf-9 insect cells (Bird, 2011; Figure 2.8)

Vector	Fusion Protein	Sense primer extension	Anti-sense primer extension
pOPINF	$(His)_6$-3C-POI	AAGTTCTGTTTCAGGGCCCG	ATGGTCTAGAAAGCTTTA
pOPINS3C	$(His)_6$-SUMO-3C-POI	AAGTTCTGTTTCAGGGCCCG	ATGGTCTAGAAAGCTTTA
pOPINTRX	$(His)_6$-TRX-SC-POI	AAGTTCTGTTTCAGGGCCCG	ATGGTCTAGAAAGCTTTA
pOPINMSYB	$(His)_6$-MSYB-3C-POI	AAGTTCTGTTTCAGGGCCCG	ATGGTCTAGAAAGCTTTA
pOPINHALO	$(His)_6$-HALO7-3C-POI	AGGAGATATACCATG	CAGAACTTCCAGTTT
pOPINM	$(His)_6$-MBP-3C-POI	AAGTTCTGTTTCAGGGCCCG	ATGGTCTAGAAAGCTTTA
pOPINTF	$(His)_6$-TF-3C-POI	AAGTTCTGTTTCAGGGCCCG	ATGGTCTAGAAAGCTTTA
pOPINNUSA	$(His)_6$-NUSA-3C-POI	AAGTTCTGTTTCAGGGCCCG	ATGGTCTAGAAAGCTTTA
pOPINE*	POI-$(His)_6$	AGGAGATATACCATG	GTGATGGTGATGTTT
pOPINE-3C-HALO7*	POI-3C-HALO7-$(His)_6$	AGGAGATATACCATG	CAGAACTTCCAGTTT

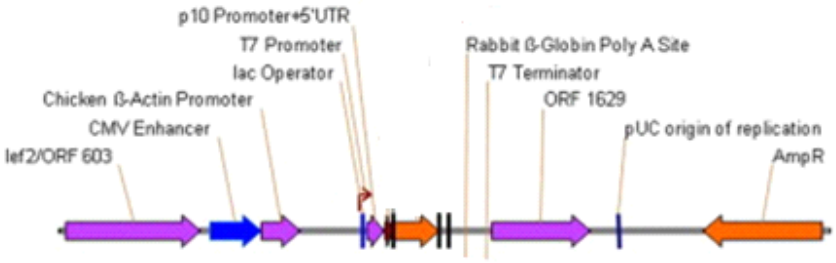

Figure 2.5: Features of the pOPIN vector suite allowing for parallel expression in *E. coli*, mammalian (HEK293T) and insect (Sf-9) cells.

2.7 Nucleic acid techniques

2.7.1 RNA Extraction

Total RNA was extracted from numerous animal tissues and cultured cells using TRIzol reagent (Invitrogen, life Technologies, Paisley, UK). The TRIzol reagent is a solution of phenol and guanidinium isothiocyanate that solubilises biological material and denatures proteins. Frozen tissue samples (50-100 mg) were homogenised with 6 x 2.8 mm ceramic beads using a Precellys 24 homogenizer (4 X 20 s at 6,500 rpm; PeqLab, Fareham, UK) in ice-cold TRIzol. For cultured cells (25 cm^2 flask), media was aspirated off, cells were then rinsed once with ice-cold 1X PBS and resuspended in 500 µL of ice-cold TRIzol. After tissue/cell disruption, homogenates were centrifuged at 10,000 rpm for 1 min at 4 °C to pellet insoluble particulate matter. The supernatant was removed and thoroughly mixed with chloroform:isoamyl alcohol (24:1 v:v) (0.2 ml per ml of TRIzol; Sigma-Aldrich) in a fresh tube, which was then centrifuged at 14,000 rpm at 4 °C for 15 min in-order to separate the RNA-containing aqueous phase (top) from the organic phase (proteins and high molecular weight DNA being denatured at the interphase). The aqueous phase was then removed and RNA was precipitated by adding 500 µL isopropanol (Sigma-Aldrich). The sample was then centrifuged at 14,000 rpm at 4 °C for 10 min and the RNA pellet was washed once with 75% ethanol (Sigma-Aldrich) and left to air dry. The RNA pellet was resuspended in MilliQ- water to a final concentration of 2 µg/µl. The concentration and purity of RNA was determined by measuring its optical density (OD) at 260 nm (Nanovue; Section 2.7.3). RNA integrity was assessed by electrophoresis in 1 % agarose gels (Sigma-Aldrich; Section 2.7.8),

with samples containing well-defined 18S and 28S ribosomal bands being deemed acceptable (Figure 2.6).

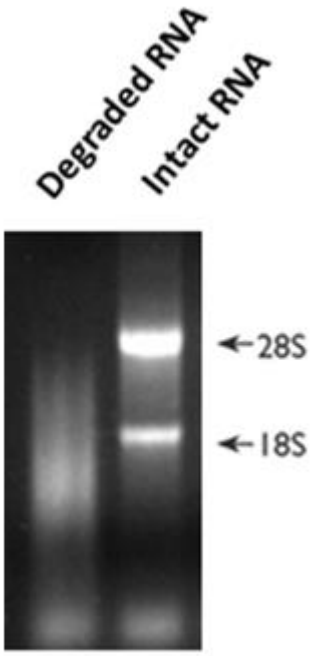

Figure 2.6- Purified RNA was electrophoresed (Section 2.6.8) to monitor the integrity of extracted RNA. A total of 2 µg of RNA was separated alongside the 1 kb New England Biolabs molecular markers (NEB; Lane 1) on a 1% agarose gel. Both the 28S and 18S RNA bands are visible in the intact RNA (Lane 3). Degraded RNA appears as a smear (Lane 2). This image is representative of all RNA extractions, with only intact RNA being used for further experimental manipulation.

2.7.2 Plasmid DNA extraction from *Escherichia coli*.

Bacterial colonies were picked grown as described in Section 2.2.1. Following incubation, the cells were harvested via centrifugation at 4,000 rpm at 4 °C for 10 min. Pelleted cells were washed once with ice-cold 1X PBS to remove excess culture media. Plasmid extraction and purification was then carried out using the QIAprep-Spin Miniprep kit (Qiagen, Mancester, UK) following the manufacturer's instructions. The

concentration and purity of extracted plasmid DNA was then estimated, as described below.

2.7.3 Measuring the concentration and purity of nucleic acids

The concentration and purity of RNA and DNA was measured using a NanoVue Plus Spectrophotometer (GE Healthcare). The ratio of absorbance at 260 nm and 280 nm (A_{260}/A_{280}) was used as an indicator of the purity of RNA and DNA. A A_{260}/A_{280} ratio of ~2.0 and ~1.8 were accepted as "pure" for RNA and DNA, respectively. An aliquot (2 µL) of the reference sample (same solution that RNA and DNA are suspended in) was used to blank the absorbance and then 2 µL of the appropriate RNA or DNA sample was used for quantification.

2.7.4 First strand cDNA synthesis

Prior to cDNA synthesis, RNA samples were DNase treated to remove any contaminating genomic DNA. To a 2 µg sample of RNA, 1 unit of DNase I enzyme (Promega, Southampton, UK) and 1.6 µL of 5 X DNase buffer (Promega, Southampton, UK) were added to a final volume of 8 µL with MilliQ H_2O. This reaction was mixed thoroughly by flicking the tube and then incubated for 30 min at 37 °C. Heat inactivation of DNase I was then performed at 70 °C for 10 min. After DNase treatment, 1 µL of MilliQ H_2O and 1 µL of Oligo dT primer (500 µM) were added and the samples were incubated at 70 ° C for 5 min then placed on ice for 2 min. A volume of 5 µL First Strand Buffer (5X; Promega, Southampton, UK), 1.5 µL 10 mM dNTPs, 0.5 µL RNase inhibitor (RNAsin; Promega, Southampton, UK), 1 µL Moloney-Murine Leukaemia Virus reverse transcriptase (1 unit; M-MLV RT; Promega, Southampton, UK) and 7 µL MilliQ

H_2O were then added and thoroughly mixed. The samples were then incubated in the following conditions: 42 °C for 50 min, 55 °C for 10 min, 70 °C for 10 min (inactivation of M-MLV) and 4 °C for storage. For semi-quantitative and real-time PCR, cDNA was diluted 1:20 with MilliQ H_2O. In-order to clone and sequence the full-length of eel PLCXD-4, intestinal cDNA was synthesized using the Marathon cDNA Amplification Kit (Clontech, Saint-Germain-en-Laye, France) according to manufacturer's protocol.

2.7.5 Primers and primer design

A number of different primers were used for PCR amplification and DNA sequencing. All primers were purchased from Eurofins MWG Operon. Primers were designed according the following specifications: sense and antisense primers were designed to have approximately the same melting temperature of 60-65 °C; and each primer had a GC content close to 50-60%. The melting temperature was calculated using the following equation: Tm = 4 x (G+C) + 2 x (A +T). For molecular cloning in *E. coli,* specific restriction sites were added to ends of the sense and antisense primer according to the cloning strategy. For relative quantitative PCR, primers of 18-24 nucleotides in length were designed across exon-exon boundaries to amplify fragments of 150-200 bp in length. A full list of primers used in this thesis can be found in the Appendices A-F.

2.7.6 Reverse transcriptase Polymerase Chain Reaction (RT-PCR)

RT-PCR selectively amplifies a specific region of cDNA using a pair of primers that bind to the target sequence. In this thesis, RT-PCR methods are used for the cDNA cloning of the PLCXD isoforms (Section 2.7.9), sub-cloning to different vectors (Section 2.7.10)

and to determine their tissue expression patterns. The sequence of sense and antisense primers used are shown in Table 2 (Appendices). All primers were designed to have an annealing temperature of between 63 and 65 °C. In general, RT-PCR was performed in a total reaction volume of 20 µL consisting of 1 µL of a diluted (1:20) cDNA, 300 nM each of gene-specific forward and reverse primers, 1 X Taq DNA polymerase buffer (Biogene; supplemented with 1.5 mM $MgCl_2$), 200 nM dNTPs and 1 unit of Taq DNA polymerase. The following PCR cycle was repeated for 35 cycles: 94 °C for 10 sec (denaturation), 60 °C for 30 sec (annealing), and 72 °C for 1 min (elongation). For the amplification of the full-length open-reading frames of PLCXD isoforms and sub-cloning into different vectors, the proof-reading DNA polymerase, Platinum *Pfx* (Invitrogen, Life Technologies, Paisley, UK) was used and the sequences were verified according to Section 2.6.9.

For high-throughput PCR reactions performed at OPPF, RT-PCR was performed in a total volume of 50 µL consisting of 40 ng template DNA, 300 nM of each sense and antisense primer, 200 nM dNTP mix, 1 x KOD buffer (Millipore, UK; supplemented with 1.5 mM $MgCl_2$) and 1 unit of KOD Hot start DNA polymerase (Millipore, UK), made up to the final volume with MilliQ H_20. The mixture was first heated to 98 °C for 30 sec to active the KOD DNA polymerase and then the following PCR cycle was repeated for 29 cycles: 98 °C for 10 sec (denaturation), 60 °C for 30 sec (annealing), 68 °C for 1.5 min (elongation). The PCR products were then stored at 4 °C until further use.

2.7.7 Rapid Amplification of cDNA Ends (RACE)

5'-rapid amplification of cDNA ends (RACE) DNA fragments were amplified from RNA extracted 6-month SW-acclimated yellow eel intestine with a Marathon cDNA

amplification kit, as previously described (Section 2.5.3). 5'-RACE products were amplified in nested reactions using eel PLCXD-4 specific antisense primers (Appendix A) in combination with the Marathon kit AP1 and AP2 primers (Table 1; ClonTech, Saint-Germain-en-Laye, France), according to Section 2.5.4 using *Pfx*. PCR products produced by 5'-RACE amplification were cloned and sequenced as described in Section 2.6.9.

2.7.8 Detection of nucleic acids

Gel electrophoresis was used to separate and visualise DNA/RNA. Agarose (1 g) was dissolved in 100 mL 1 x TAE buffer (40 mM Tris, 20 mM acetic acid, 1 mM EDTA, pH 8.0) by heating in a microwave until boiling. This solution was cooled and a stock 1 mg/mL ethidium bromide (Life Technologies) was added to give a final concentration of 0.1 µg/ml. The agarose gels were then cast in a 10 x 20 cm gel tank (BioRad) with a 24-well gel comb and allowed to set. Gel electrophoresis was carried out in a horizontal tank containing 1 x TAE as running buffer and run at 120 V for 1.5 h. Gels were imaged using the Gel Doc XR System (Bio-Rad). For estimation of fragment size, a 100 bp or 1 kb ladder (Invitrogen, Life Technologies, Paisley, UK) with known fragments sizes and concentrations was used.

2.7.9 Molecular cloning in *E. coli* for sequencing

2.7.9.1 Purification of PCR product

When multiple PCR products are present following agarose gel electrophoresis, products within the expected size range were purified by gel extraction. DNA bands were excised from the gel as 100 mg agarose slices using a sterile scalpel blade. PCR

products were then purified using the QIAquick gel extraction kit (Qiagen) according to the manufacturer's instructions. DNA was eluted from the QIAquick spin column upon addition of 30 µL of TE buffer (10 mM Tris-HCl, 1 mM EDTA, pH 7.5). Where only a single PCR product was detectable following gel electrophoresis, the product was purified directly from the reaction mixture using SOPE resin (QuickStep 2 SOPE Resin; EdgeBio, UK) according the manufacturer's protocol. The concentration of DNA recovered was then quantified, as described in Section 2.7.3.

2.7.9.2 Ligation of PCR fragments in pCR4- TOPO.

For all sequencing reactions, PCR amplified fragments were cloned into pCR4-TOPO using the TA Cloning Kit (Invitrogen, Life Technologies, Paisley, UK), as per the manufacturer's instructions. PCR fragments amplified with Platinum *Pfx* were SOPE cleaned and incubated with 10 mM dNTPs and 1 unit of Taq polymerase in 1x Taq buffer for 10 min at 72 °C to add 3' deoxyadenosine (A) overhangs for TA cloning. A 5 µL aliquot of the PCR product was added to 0.5 µL of the vector along with 1 µL of high salt solution and incubated at room temperature for 10 minutes. The entire TOPO cloning reaction was added into an aliquot (50 µL) of One Shot TOP10 chemically competent *E.coli* (Invitrogen, Life Technologies, Paisley, UK) and heat shock transformation conducted as previously described (Section 2.2.4).

2.7.9.3 Selection of Colonies and sequencing

Colonies were selected and used to inoculate 10 mL of selective LB medium and grown overnight, as described in Section 2.2.1. The following day, 5 mL of the overnight was used for plasmid extraction (Section 2.7.2) and the remaining cell suspension was used

to create glycerol stocks for each clone (Section 2.2.2). For sequencing, the PCR insert was amplified from the purified plasmid DNA (1 ng) using M13 sense and antisense primers (Appendix D). Amplified fragments were purified by SOPE resin (Section 2.7.9.1) and 40-50 ng used for sequencing using the Big Dye di-deoxy chain termination method (Applied Biosystems, Foster City, CA), according to manufacturer's protocol, using the nested T3 forward and T7 reverse primers (Appendix D).

2.7.10 Molecular cloning in *E. coli* for protein expression

Sequenced verified clones of hPLCXD1, 2.1 and 3 genes were selected and sub-cloned into a number of vectors for protein expression in *E.coli*, insect (*Sf*9) and mammalian (HeLa and HEK-293) cells.

2.7.10.1 Sub-cloning of human PLCXDs in pET M11, pET 22 b+, pdl NotI

The full-length sequences of human PLCXD-1, 2.1 and 3 were amplified with gene-specific sense and antisense primers containing appropriate restriction sites for eventual insertion into either pET M11 (PLCXD 1 and 3), pET 22b+ (hPLCXD2.1) or pdl NotI. Details of the primer sequences and restriction sites are presented in Appendix A. The products of the PCR were first cloned in pCR4-TOPO for sequence verification, as described above. Plasmids containing the PLCXD isoforms and the target plasmids for protein expression were double digested with both restriction enzymes. All restriction enzymes were purchased from Promega. As a general protocol, 1 µg of each plasmid DNA was mixed with 1 unit of enzyme, 2 µg bovine serum albumin (BSA) and 1 x buffer (Multi core B; Promega, Southampton, UK) made up to a final volume of 20 µL with MilliQ water. For double digestions, a buffer was chosen which was optimal

for both enzymes. The samples were incubated at 37 °C for 2-3 h followed by 65 °C for 10 min to inactivate the enzymes. After digestion, 4 µL of 6 x Gel loading buffer was added to each reaction and the samples were electrophoresed in 1% agarose gels, according to Section 2.7.8. Bands corresponding to the excised PLCXD product were gel extracted, purified and the amount of DNA quantified, as described previously. For the ligation of digested vector DNA and target insert DNA, a total of 100 ng of DNA (with a molar ratio of insert to vector of 3:1) was mixed 2 µL 10 X ligation buffer (Promega, Southampton, UK), 1 µL 1 unit T4 DNA ligase (Promega, Southampton, UK) and MilliQ H_20 to to 20 µL. The samples were mixed gently with a micropipette, centrifuged briefly and then incubated at 16 °C overnight.

2.7.10.2 In-Fusion cloning of human PLCXDs to the pOPIN vector suite

PLCXDs were cloned from a HeLa cDNA library using primers designed for In-Fusion cloning, as described in Section 2.5.4. The PCR products were purified using AMPure XP Magnetic beads (Beckmann Coulter) according to the manufacturer's protocol. In a total volume of 10 µL, 100 ng of purified PCR product was mixed with 100 ng of the appropriate linearized pOPIN vector (depending on the primers used in amplification) and then transferred to a dry-down In-Fusion plate and mixed by pipetting. The entire reaction contents were then transferred to a clean 96-well PCR plate and heated at 42 °C for 30 min. Once the incubation was complete, the In-Fusion reaction was transferred to ice and diluted with 40 µL of Tris-EDTA (TE) pH 8.0. A 5 µL aliquot of the diluted In-Fusion mixture was then immediately transformed into OmniMaxII cells by the heat-shock method (Section 2.2.4) and 50 µL of transformed cells were grown on agar plates supplemented with antibiotic, 40 µg/mL X-Gal and 0.1 mM IPTG. White

colonies were selected and grown in 1.2 mL Power Broth in deep-well blocks at 37 °C overnight with shaking at 250 rpm. Glycerol stocks were prepared according to Section 2.2.2, and the remaining cells were harvested following centrifugation at 4,000 rpm for 10 min. The media was decanted and the bacterial pellet was lysed and the plasmid purified according to the QIAquick Miniprep protocol (Qiagen) using a Bio-Robot 8000.

2.7.11 Real-time quantitative PCR

The relative expression of all PLCXD isoforms in different tissues was measured by quantitative RT-PCR using SYBR Green PCR Master Mix (Applied BioSystems, Foster City, CA) and amplification and analysis on an Applied Biosystems 7300 Cycler running propriatory SDS detection software (Applied Biosystems, Foster City, CA). The PCR was carried in a total volume of 20 µL consisting of: 1 µL cDNA template (diluted 1/20; Section 2.7.4); 300 nM of each gene-specific sense and antisense primer (Appendices); 1x SYBR green master mix (Applied BioSystems, Foster City, CA); MilliQ water to 20 µL. Amplification was started with an initial 10 min denaturation at 95 °C, followed by 40 cycles of denaturation (95 °C, 30 s), primer annealing at the temperature appropriate for each primer (55-60 °C, 45 s) and primer extension (72 °C, 45 s) ending with melting curve analysis to validate the specificity of the PCR products. Template negative controls (NTC) were performed, using MilliQ water instead of template cDNA, to verify the absence of non-specific products or primer dimers. The relative abundance values for each target gene were expressed as standard quantity of gene of interest (determined from the cycle threshold (Ct) and the efficiency curve for the target gene) divided by the standard quantity of the reference (Rpl-P0; determined as for the target gene). The PCR efficiency estimates for each primer pair were performed using five-

point, 5-fold, serially diluted template cDNA of the template cDNA ranging from 1/5-1/625. The Ct values (y-axis) were plotted against the log cDNA concentration (x-axis) and the primer efficiency was determined based on the slope of the standard curve. Slopes within the range of -3.60 to -3.10, correlating to efficiencies between 90-100%, were considered acceptable for real-time PCR. The threshold cycle (C_T) for Rpl-P0 did not vary under different experimental conditions when equal amounts of RNA were used.

2.8 Protein analysis

2.8.1 Protein extraction from animal tissues and cultured cells

Cytosolic and membrane protein fractions were prepared from tissues and cell homogenates for Western blotting analysis. Frozen tissue samples (100-150 mg) were homogenised with 6 X 2.8 mm ceramic beads using a Precellys 24 homogenizer (4 X 20 s at 6,500 rpm; PeqLab, Fareham, UK) in ice-cold extraction buffer (50 mM Hepes, 1 mM $MgCl_2$, 0.25 M sucrose pH 7.4 containing 1 X EDTA-free cOmplete protease inhibitor cocktail (Roche Diagnostics Ltd., West Sussex, UK). For cultured cells, media was aspirated off and the cells were rinsed once with 1 X PBS. The cells were then trypsinised, as previously described in Section 2.3.1, and pelleted by centrifugation in 15 mL falcon tubes at 1,000 rpm (Eppendorf Centrifuge 5810 R, swing-bucket rotor A-4-62; Eppendorf, UK) at 4 °C for 1 min. The cell pellet was rinsed once in 1 X PBS to remove trypsin and resuspended in 0.5-1 mL ice-cold extraction buffer and homogenized with 0.7g X 1.7 mm ceramic beads as described above. After tissue/cell disruption, homogenates were centrifuged at 10,000 rpm (Eppendorf centrifuge 5417C, fixed-angle rotor FA-45-30-11) for 10 s to pellet insoluble particulate matter

and the supernatant were re-centrifuged at 20,000 rpm (Eppendorf centrifuge 5417C, FA-45-30-11 rotor) for 40 min at 4 °C to gain the cytosolic fraction. The membrane pellets were resuspended in extraction buffer (0.2 x the original volume). The Bradfords method (Bio-Rad Laboratories, Hercules, CA, USA) was used to determine protein concentrations, according to the manufacturer's protocol. Both the cytosolic and membrane protein fractions were aliquoted at 2 mg/mL and stored frozen at -20 °C.

HEK293T cells transiently transfected with pOPIN-PLCXD constructs were harvested after 3 days of growth to screen to monitor the expression of the different fusion constructs of PLCXDs. The media was removed from the cells and the 24-well plate was frozen at -80 °C for 30 min. The cells were then defrosted at room temperature for 10 min and lysed using 250 µL of lysis buffer (NP1-10, DNase, 1x Roche protease inhibitors). The mixture was pipetted up and down repeatedly to detach the cells from the plastic and the mixture was then centrifuged at 5,000 rpm for 30 min in 1.5 mL Eppendorf tubes (Thermo Fisher Scientific, Loughborough, UK) using an 5417C Eppendorf centrifuge with the FA-45-30-11 rotor (Thermo Fisher Scientific, Loughborough, UK). A 20 µL aliquot of the supernatant was then mixed with 20 µL of SDS sample buffer, denatured at 95 °C for 10 min and the proteins were separated and analysed by western blotting using anti-his primary antibody, as described below.

2.8.2 Antibodies

Studies described in this thesis utilised both commercially available and custom made primary antibodies alongside enzyme (HRP and AP) and fluorophore (Alexa Fluor)-

conjugated secondary antibodies. These are detailed in Table 2.4. Custom-made primary antibodies were generated by Dr Gordon Cramb in collaboration with Pepceuticals, Leicester, UK. Briefly, a synthetic peptide was generated that reflected a sequence region sharing the lowest level of homology with other PLCXDs (See Table below). The synthetic peptide was conjugated to the keyhole limpet haemocyanin (KLH) carrier protein and then used to generate the specific polyclonal antisera in rabbits (Pepceuticals, Leicester, UK). Antibodies were subsequently affinity purified from a total of 20 mL of antisera using the specific peptide antigen cross-linked to activated thiol Sepharose 4B, following the manufacturers protocol (Amersham Biosciences).

Antibody	Species	Antigen	Source	Experiment
Pk/V5-tag	Mouse	Pk/V5-tag	Dr Jelena Andrejeva	Co-IP (Chapter 6) and Immunocytochemistry (Chapter 4)
ePLCXD4	Mouse	eelPLCXD4; aa's 27-48-C-LEKLDLPNGHEVNWMMSIDDET	Pepceuticals, Leicester, UK.	Western blotting (Chapter 3)
α-tubulin	Rabbit	Mouse α-tubulin	Abcam	Western blotting (Chapters 3 and 5)
hPLCXD3	Rabbit	Human PLCXD3;aa's 1-16-MASSQGKNELKLADW-C	Pepceuticals, Leicester, UK.	Lipid binding studies (Chapter 6)
Alexa Fluor 633	Donkey	Mouse IgG	Invitrogen, Life Technologies, Paisley, UK	Immunocytochemistry (Chapter 4)
HRP-conjugated	Donkey	Mouse IgG	Abcam	Western blotting (Chapter 3)
AP-conjugated	Donkey	Rabbit IgG	Abcam	Western blotting (Chapter 4 and 6)

Table 2.5: List of antibodies used in this thesis.

2.8.3 SDS Polyacrylamide gel electrophoresis (PAGE)

Extracted protein samples (2 mg/mL) were diluted 1:1 with 2 X SDS sample buffer (125 mM Tris-HCl, 4% SDS, 20% glycerol and 90 mM β-mercaptoethanol, pH 6.8) and incubated at 95 °C for 10 min before being loaded (10 µg) onto NuPAGE precast polyacrylamide gradient gels (4-12%; Invitrogen, Life Technologies, Paisley, UK). Samples were separated at a constant voltage of 160 V for 1 h in a 1 x Mes running buffer (Invitrogen, Life Technologies). A sample (5 µL) of SeeBlue Plus2 pre-staining molecular weight standards (Invitrogen, Life Technologies, Paisley, UK) was used for molecular size estimation. Once electrophoresed, the gel was either stained with Coomassie blue (Section 2.8.3) or the proteins were transferred onto a PVDF membrane for Western blotting analysis (Section 2.8.4).

2.8.4 Coomassie blue staining of proteins

Within this study Coomassie blue dye was used to visualise proteins separated by SDS PAGE. Following electrophoresis the gel was incubated at room temperature with constant shaking in a solution of Coomassie brilliant blue stain (0.1% Coomassie Brillant Blue R-250, 50% methanol and 10% glacial acetic acid) for 5 minutes. The gel was then washed with a destaining solution (10% methanol, 10% glacial acetic acid) at room temperature with constant shaking for 10 minutes. This washing step was repeated several times to enable the visualisation of individual protein bands.

2.8.5 Western blotting analysis

Proteins separated by SDS-PAGE were electroblotted onto PVDF membranes (VWR, Leicestershire, UK) for 1 h at 120 Volts in 1 x NuPAGE transfer buffer (Invitrogen, Life Technologies, Paisley, UK), supplemented with 10% methanol and 0.01% SDS. Immediately before transfer the PVDF membrane was incubated in methanol for 1 min prior to washing in water and then transfer buffer for 10 min. Following transfer, the membranes were incubated in blocking buffer (10% non-fat milk in PBS containing 0.2% Tween-20) for 1 h at room temperature with gentle rocking. Membranes were then incubated in 1% non-fat milk in PBS containing 0.5% Tween-20 and the primary antibody overnight at 4 °C. Primary antibody incubation was followed by washing for 3 x 10 min in PBS, 0.2% Tween-20. Generally, the secondary antibody was diluted 1/10,000 in blocking buffer, which was added to the membrane for 1.5 h at room temperature. This thesis used two types of secondary antibody: alkaline phosphatase (AP)-linked secondary antibodies and horseradish peroxidase-conjugated antibodies (Table 2.5). For the former, bound antibodies were visualised by incubating membranes in Western blue phosphate substrate solution (Promega, UK) for approximately 5 min to allow the development of immunoreactive bands. For horseradish peroxidase-conjugated secondary antibodies, detection was performed using the ECL detection method, as described by the manufacturer (Pierce Dura ECL, Thermo Fisher Scientific, and Loughborough, UK). Densitmetric analysis was carried out using Aida Image analyser software.

2.8.6 Purification of recombinant proteins from *E. coli*

Following expression recombinant proteins contained an N-terminal 6X His-tag. Cell pellets were thawed on ice and resuspended in 10 mL of lysis buffer (50 mM Tris-HCl, 500 mM NaCl, 10 mM imidazole, pH 8.0) per gram of wet cell pellet. The lysis buffer was supplemented with 1 X EDTA-free cOmplete protease inhibitor cocktail (Roche Diagnostics Ltd., West Sussex, UK) and 5 µg/mL DNAseI (New England Biolabs). The cells were mixed into a homogenous suspension in lysis buffer, and then sonicated six times for 10 s at 10 s intervals keeping on ice throughout. Total cell lysate was partitioned into soluble and non-soluble protein fractions by centrifugation for 30 minutes at 20,000 rpm at 4 °C in 50 mL conical centrifuge tubes (Termo Fisher Scientific, Loughborough, UK) using the Avanti J-26PI centrifuge with a JA-25.50 fixed angle rotor (Beckman Coulter, Inc.). After centrifugation, the soluble fraction was filtered through a 0.22 µm syringe filter unit (Millipore) and the target protein was purified with a Ni^{2+} -affinity column (HisTrap™ HP column; GE Healthcare), according to the manufacturers' instructions', using the Akta Purifier chromatography system (UPC 10; GE Healthcare). Purification of target proteins was confirmed by SDS-PAGE and Coomassie staining.

2.8.7 $(His)_6$-tag cleavage

Excess imidazole was removed following dialysis of pooled eluate samples in lysis buffer in the presence of dithiothreitol (DTT). TEV (Tobacco Etch Virus) protease was added (1 µg protease for 1 mg target protein at 4 °C overnight). Following digestion, the protein sample was analysed by SDS-PAGE to check the efficiency of TEV protease digestion. Protein samples were then loaded into the nickel column as before.

Successful cleavage of the $(His)_6$-tag from the protein means that it should not bind to the column and therefore the target proteins should be eluted in the flow-through. The flow-through was then dialysed against 25 mM Tris-HCl containing 150 mM NaCl and concentrated using a Sartorius™ Vivaspin™ 20 centrifugal concentrator with a 10,000 Da molecular weight cut-up (Thermo Fisher Scientific, Loughborough, UK) to prepare the samples for further purification by gel filtration column chromatography.

2.8.8 Gel filtration column chromatography

Gel filtration column chromatography is a method used to separate protein primarily based on molecular size. A sample volume of up to 5 mL was loaded onto a HiprepTM 16/60 SephacrylTM S-200 column (GE Healthcare) according to the manufacturer's protocol. Columns were run using the Akta Purifier chromatography system (GE Healthcare) and samples were collected into 1.5 mL fractions. Samples from the observed peaks were collected and analysed by SDS-PAGE.

2.8.9 Pk-tag co-immunopreciptation (pull-down)

Vector containing a PLCXD3 insert was virally transfected into HeLa as previously described. As a control, non-transfected wild-type HeLa cells were used. Transfected and control cells were seeded into 4 x 75 cm^2 flasks each and grown until 80-85% of confluence as previously described. Cells were then washed twice in PBS and lysed with 500 µL of protein extraction IP buffer (25 mM Tris-HCl pH 7.4, 150 mM NaCl, 1mM EDTA, 1% NP-40 and 5% glycerol) per flask for 10 min on ice. Samples from each of the 4 flasks were transferred into a 1.5 mL microfuge tube and spun for 40 min, 14,000 rpm at 4 °C using the Avanti J-26PI centrifuge with a JA-18.1 fixed angle rotor (Beckman

Coulter, Inc.). The supernatants were then pooled together (~2 mL) and transferred into two 1.5 mL microfuge (1 mL of supernatant in each) and a 10 µL sample was taken to assess the protein concentration by the Bradfords method. Prior to cell lysis, the primary Pk antibody was immobilised to Protein G Sepharose resin (GE Healthcare) using dimethylpimelimidate (DMP; Pierce). A 1 mL aliquot of protein G Sepharose was pelleted by centrifugation at 1,000 rpm for 3 min in a bench microfuge and resuspended and then washed three times with 1 mL PBS. The beads were resuspended with 500 µL of PBS and 20 µg of the anti-Pk primary antibody was then added to the Sepharose and incubated for 30 min on a rotary shaker at room temperature. The sample was centrifuged (as before) and the anti-Pk antibody-bound Protein Sepharose was then washed three times with crosslinking buffer (0.2M tris ethanolamine, 0.1 M sodium borate, pH 9) and incubated with 20 mM DMP in crosslinking buffer for 45 min with rotation at room temperature. The crosslinking reaction was stopped by washing 3 times in crosslinking buffer without DMP. The beads were then incubated with IP elution buffer (0.1 M acetic acid, 0.15 M NaCl, pH 3.0) to wash away any Pk antibody that was not bound covalently to the beads. The beads were then washed three times with PBS and the bound antibody concentration was determined by the Bradford's method. The beads were resuspended and stored in 500 µL PBS containing 0.02% azide at 4 °C until use. Extracted protein (0.5 mg) from both transfected and control HeLa cells was added to 100 µL of cross-linked bead slurry prepared above and incubated overnight at 4 °C with rotation. The beads were then washed three times with IP buffer and the protein was eluted using 3 x 20 µL of IP elution buffer (as above) and neutralised by adding an equal volume of Tris pH 8.0.

Protein concentration was quantified using Bradford's method and samples were checked by SDS-PAGE analysis followed by Western blotting.

2.8.10 Ni^{2+}-NTA expression screen protocol

Frozen Sf-9 or *E. coli* cells expressing the different fusion constructs for PLCXDs were completely resuspended in 210 µL of Lysis Buffer (50 mM NaH_2PO_4, 300 mM NaCl, 10 mM imidazole, 1% v/v Tween-20, pH 8) containing 3 units/mL of benzonase and 1 mg/mL lysozyme. The deep-well blocks were then incubated at room temperature for 15 min with shaking at 500 rpm. The cell lysate was transferred to a 96 deep-well block and a 20 µL sample was added to 20 µL SDS loading buffer (whole cell expression). The remaining lysate was cleared of cell debris and insoluble material following centrifugation at 4,000 rpm for 30 min in a bench microfuge. Before the end of the centrifugation, 20 µL of Ni-NTA magnetic bead suspension (Qiagen, Mancester, UK) was pipetted into a flat-bottomed microtitre plate (Greiner 655101) and then washed 3 times with lysis buffer. In between each wash step the plate was placed on a 96-well magnet (QIAgen) for 1 min to pellet the beads and the supernatant was removed. Following centrifugation of the cell lysate, the supernatant was then mixed with the pre-equilibrated Ni-NTA agarose beads and incubated for 30 min at room temperature with shaking at 600 rpm. The insoluble pellets were kept in case no soluble expression was observed. The plate was then placed on a magnet (as before) for 5 min to pellet the beads. The supernatant was removed and the beads were sequentially washed with 200 µL of lysis buffer, 200 µL wash buffer (lysis buffer with 0.05% v/v Tween-20 and 20 mM imidazole) and then 60 µL elution buffer (lysis buffer with 0.05% Tween and 250 mM imidazole). The Ni-NTA beads were pelleted between each wash by

transferring the plate to the magnet. A 20 µL sample of the supernatant (eluate) was then mixed with 20 µL of SDS sample buffer and analysed by SDS-PAGE for the presence of soluble recombinant proteins.

2.8.11 Detection of protein-lipid interactions by PIP strips™

PIP strips are hydrophobic membranes that have been pre-adsorbed with 100 pmol of all eight phosphoinositides (See Chapter 1) and seven other important phospholipids, including lysophosphatidic acid, lysophosphocholine, phosphatidylcholine, sphingosine 1-phosphate, phosphatidic acid, phosphatidylethanolamine and phosphatidylserine (Echelon Biosciences Inc). Membranes were blocked for 1 h at room temperature with PBS supplemented with 3% BSA and 0.1% Tween-20 (Sigma-Aldrich, Poole, Dorset, UK; known as blocking buffer). The membranes were then incubated with 0.5 µg/mL of purified PLCXD-3 (Section 2.6.3) in the blocking buffer. For detection of protein-lipid interactions, membranes were incubated with monoclonal mouse anti-PLCXD-3 primary antibody (1/1,000 in blocking buffer) for 1 h at room temperature. The membranes were then washed in blocking buffer for 3 x 10 min and then incubated with donkey anti-mouse HRP-conjugated secondary antibody for 1 h at room temperature. Following washing, as above, bound secondary antibody was visualised using the SuperSignal West Dura chemiluminescent substrate, as previously described (Section 2.8.4).

2.8.12 PLCXD3 activity towards purified lipids

This assay was conducted with help from Dr Tomas Lebl (Department of Chemistry, University of St Andrews). Recombinant PLCXD3 overexpressed in *E. coli* and HeLa cells

and purified as described previously (Sections 2.8.5 and 2.8.8). Soluble homologues of phosphatidylinositol- 4,5- bisphosphate ($PI(4,5)P_2$; 1 mg) and phosphatidylinositol (PI; 1 mg) containing truncated fatty acid chains (dCi8) were purchased from Echelon Biosciences. These lipids were resuspended to 1 mg/mL in 50 mM Tris-HCl pH 8.0, containing 150 mM NaCl and 1 mM $MgCl_2$ and stored frozen at -20 °C until use. Samples for ^{31}P-NMR were prepared with 250 µg of the substrate lipid, 1 µg of purified PLCXD-3 (prepared from HeLa pull-down assay and *E. coli* expression), 11% D_2O, and same buffer as the lipids to a final volume of 600 µL in 5 mm NMR tubes (Norwell). Prior to the addition of purified PLCXD-3, a 1 dimensional ^{31}P-NMR spectra was obtained for each lipid using a Bruker AVANCE III 500 with 1,000 scans for approximately 30 min. Purified PLCXD-3 was then incubated with each lipid for 30 min at 28 °C and the 1D ^{31}P-NMR spectra was analysed as above.

2.8.13 Protein Crystallisation

Following gel filtration chromatography, purified proteins were concentrated to 10 mg/mL using Vivaspin™ sample concentrators (GE Healthcare). A number of commercially available crystal screens were used to test the conditions required for crystal formation, including JCSG+ (Qiagen), Index (Hampton Research), Wizard I+II (Emerald Biosciences) and PEGs (Qiagen). These screens were kindly provided by Dr Stephen McMahon. School of Biology, University of St Andrews. Crystal plates were set-up using a nano-drop crystallisation robot (Cartesian HoneyBee, Genomic Solutions) with 150 nL of protein and 150 nL of buffer per well. Plates were then incubated at room temperature and regularly checked for the presence of crystals. Initial hits were optimised in the attempt to gain better quality crystals, and this was

achieved by varying the concentration of salt and protein in the appropriate screen and also varying the amount of precipitant used.

2.8.14 X-ray crystallography

Suitable crystals chosen for X-ray data collection were cryoprotected in the original crystallisation buffer containing 15-30% (v/v) of glycerol. The work was carried out by Dr Stephen McMahon, School of Biology, University of St Andrews. Briefly, protein crystals were picked using a crystal loop and then dipped in 5 µL of the cryoprotection buffer. The crystal was then exposed to X-rays at 100K using an in-house Rigaku/MSC MicroMaz-007HF rotating anode with a Saturn 944+ CCD detector at wavelength 1.54178 A.

2.8.15 PLCXD4 Immunohistochemistry in eel intestine

The anterior, mid and posterior regions of the intestine were removed from a 3-month SW-acclimated silver eel and fixed overnight in 4% paraformaldehyde in PBS and stored at 4 °C in PBS. These tissues were mounted in paraffin and 4 µm sections were cut and mounted onto slides courtesy of Professor David Harrison, School of Medicine, University of St Andrews. Tissue sections were de-waxed by immersion in xylene (Sigma-Aldrich, Poole, Dorset, UK) for 10 min and then re-hydrated in graded ethanol solutions (100%, 80% and 50%) for 5 min each and then rinsing in running water for 5 min. De-waxed and re-hydrated slides were subjected to heat-induced antigen retrieval for 15 min in a pressure cooker with boiling citrate buffer (10mM Sodium citrate, 0.2% Tween-20, pH 6.0) using a microwave at 700 w. Once full pressure had been reached (10 min), the pressure was maintained for a further 5 min before

removing the heat and rapidly cooling whilst releasing the pressure. The slides were then washed 3 x 5 min in wash buffer (1 x PBS, 0.2% Tween-20) with gentle agitation. The slides were incubated in 0.3% H_20_2 (Sigma-Aldrich, Poole, Dorset, UK) in PBS for 10 min and then washed 3 x 5 min in wash buffer. The slides were then incubated in blocking solution (Protein Block; Dako) for 30 min at room temperature. The slides were drained and excess blocking solution was removed from the sections with tissue paper. Droplets (30 µL) of the eel PLCXD4 primary PLCXD4 antibody (Table 2.4) was diluted 1/500 in antibody diluent (Dako) and incubated overnight at 4 °C in a humidified chamber. Following 3 x 5 min rinses with wash buffer, the sections were incubated for 1.5 h in droplets containing a 1/1,000 dilution of secondary, Alexa Fluor 633-conjugated donkey anti-mouse antibody (Invitrogen, Life Technologies, Paisley, UK) in antibody diluent (Dako). Following extensive rinsing with washing buffer, sections were mounted with Prolong gold anti-bleaching medium containing DAPI (Sigma-Aldrich, Poole, Dorset, UK). Sections were viewed with a fluorescence microscope (Zeiss Axioplan, Welwyn Garden City, Hertfordshire, UK) and images collected and analysed using Ziess Axiovision Aoftware. Control sections were incubated with blocking solution without the primary antibody.

Immunohistochemistry was also performed to investigate the distribution of PLCXD3 in the retinas of wild type and Harlequin mutant mice (n=6 for each condition). This work was carried out in collaboration with Dr Marisol Corrall-Debrinski at the Institute de la Vision. Fixed retinal sections were prepared from both wild type and Harlequin mice (n=6 for each genotype) as described in Bouaita *et al*., 2011. These sections were

prepared for Immunohistochemistry using anti-PLCXD3 antibody sent from St Andrews by Marisol Corrall-Debrinski as described in Bouaita *et al*., 2011.

2.9 Bioinformatics

Available PLCXD amino acid sequences were obtained from NCBI and Esembl and amino acid identity and similarity were calculated using MatGat2.01 software. For the construction of the phylogenetic tree, amino acid sequences were aligned using ClustalW and automatically edited in the software. The Mega 5 software was used for tree construction and visualisation using the p-distance of the neighbour-joining (N-J) method (Tamura *et al*., 2011).

2.10 Statistical analysis

Values are presented as means +/- SEM. For RT-qPCR and Western blot analyses, statistical significance was determined using a nonpaired Student's *T*-test and significanct differences were considered within $P < 0.05$.

CHAPTER 3: Cloning, sequencing and characterisation of a *PLC-like* gene from the European eel (*Anguilla anguilla*)

3.1. Introduction

The European eel (*Anguilla anguilla*; Anguillidae) is a euryhaline teleost fish and therefore is able to inhabit both freshwater (FW) and seawater (SW) environments. The life cycle of the European eel is complex and begins in the western part of the North Atlantic known as the Sargasso Sea. Following spawning, the eggs use oceanic currents to drift towards freshwater systems of Europe and North Africa, including rivers, ponds and brackish water (Van Ginneken and Maes, 2005). During this migration, the eggs hatch releasing larvae, which eventually develop into the transparent, leaf-shaped lepthocephali larvae. Once these larvae reach the continental shelf of Europe they undergo their first metamorphosis to form "yellow eels", so called due to their yellow, dark green pigmentation (Munk *et al.,* 2010). In freshwater systems of Europe the "yellow eels" begin to feed on invertebrates, crustaceans and other fish. Towards the end of this phase of development (2-15 years for male; 4-20 years for females), the eels undergo a second metamorphosis (also referred to as "silvering") to form the sexually mature “silver eels”, which begin the *c.* 6000 km migration back to the Sargasso Sea (Van Gubbeken and Maes, 2005). Physiologically, the differences between the "yellow" and "silver" stages are important for survival with physiological and anatomical adaptations linked to the transition between fresh and salt water, and preparation of the *c.* 6000 km migration back to the Sargasso sea to breed (Van Ginneken *et al*., 2007). These adaptations include changes in expression of specific genes involved in the regulation of energy resources and initiation of the reproductive development (Durif *et al.,* 2005). Numerous other changes occur during the silvering developmental transitions which are suggestive of “anticipation

adaptation" to life in the deep sea, including an increase in the ocular index, new retinal pigments, modification/recruitment of gill chloride cells, colour modification with the body turning silvery white and increased thickness of their skin (Van Ginneken *et al*., 2007).

Previous microarray studies in this laboratory identified various genes exhibiting differential expression following the "yellow" to "silver" developmental transition of the *A. anguilla.* One gene identified as showing a decrease in expression during this developmental transition was denoted *PLC-like* in that the partial sequence obtained contained only an X-domain and was devoid of all other domains commonly found in eukaryotes PI-PLC isozymes. Thus, investigations described in this chapter aimed to determine the full-length sequence of the *PLC-like* gene identified in the microarray and perform sequence comparisons with other known PI-PLCs to predict its cellular functions. Furthermore, quantitative analysis of the mRNA levels of the *PLC-like* gene were performed using tissues extracted from both "yellow" and "silver" eels to clarify the microarray data and strengthen a potential role of this gene in the development of the European eel.

3.2. RT-PCR amplification and sequencing of the eel *PLC-like* gene from the European eel

Prior to the onset of this project, a partial sequence for the *PLC-like* cDNA was cloned and sequenced by Dr Svetlana Kalujnaia (unpublished data; See Appendix A for sequence). As a starting point, cloning experiments were then performed in this project to obtain the full-length coding sequence of the eel *PLC-like* gene using the

Marathon 5' RACE RT-PCR technique (Chapter 2, Section 2.7.6). Using the proof-reading *Pfx* DNA polymerase, RT-PCR was performed using Marathon cDNA synthesised from the intestine of the yellow eel (Chapter 2, Section 2.7.4) using gene-specific antisense primers designed near the existing 5' end of the *PLC-like* cDNA fragment. Successive nested PCR reactions were then performed in combination with the kit AP1 and AP2 primers. Primers sequences are detailed in Appendix A. For RACE 1 reactions, amplifications were carried out with the AP1 Clontech kit primer and three gene-specific antisense RACE1 primers (AS1, 2 and 3, Figure 3.1). A fragment of approximately 480 base pairs was successfully amplified only with the gene-specific AS3 primer. This PCR product was used as a template and re-amplified with the AP2 primer and the gene-specific antisense 1 and 2 RACE 2 primers (Lane 2 and 1 respectively, Figure 3.1). Following the nested RACE reactions, a fragment of around 280 base pairs (bp) was produced corresponding to the combined expected size difference between the RACE 1/RACE 2 and AP1/AP2 fragments (Figure 3.1; Lane 2). The 280 bp PCR product obtained by RACE 2 PCR reactions was subsequently sub-cloned to pCR4-TOPO and the recombinant vector was transformed into TOP 10 cells for propagation of the 280 bp fragment (Chapter 2, Section 2.7.9). Colony PCR was performed using M13 forward and reverse primers (Appendix E) to check for the presence of the gene insert and four positive colonies with the most intense bands of the expected size were selected and sequenced using T3 and T7 (Appendix E). The 5' RACE eel *PLC-like* sequences were then aligned with the original partial fragment using GENE JOCKEY II software (Biosoft) and one continuous sequence was created. The derived amino acid sequence was then determined and an interleaved

nucleotide/amino acid sequence produced (Figure 3.2). The open-reading frame of the eel *PLC-like* cDNA consists of 959 nucleotides, which encodes a protein containing 319 amino acids. The nucleotide sequence reported herein appears in the GenBank nucleotide database under accession number JX101676.

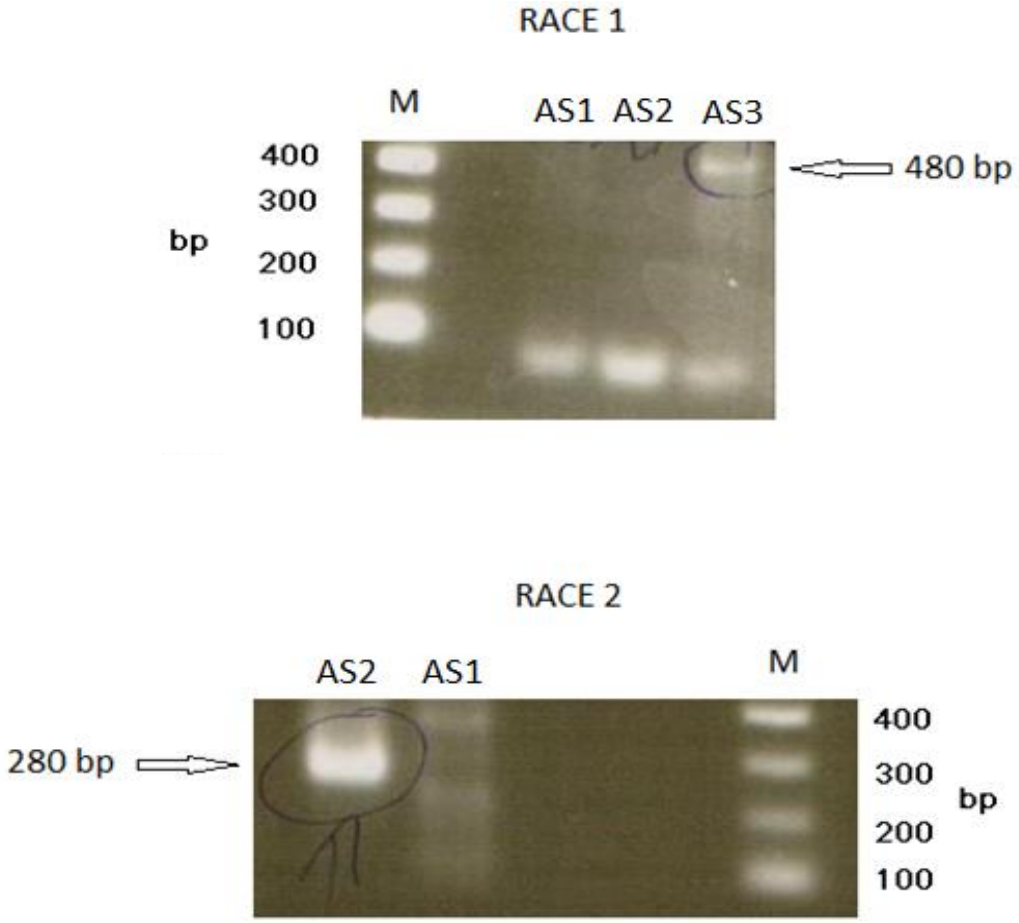

Figure 3.1: Results of the RACE 1 and RACE 2 RT-PCR reactions for the amplification of the 5' end of the eel *PLC-like* gene. For RACE 1 reactions, amplifications were carried out with the AP1 Clontech kit primer and either the gene-specific antisense 1, 2 or 3 primers (AS1, AS2 and AS3; Lane 1, 2 and 3 respectively). For the RACE 2 reactions, the AP2 primer was used in combination with either antisense 1 or 2 gene-specific primers (AS1/2).

Met Glu Phe His Leu Cys Val Leu Leu Tyr Phe Val Ile Leu Phe Ala Gly Ser Glu Gly Asp Pro Tyr Phe Asn Asp Leu Glu Lys Leu Asp Leu Pro Asn Gly His Glu 37

1 ATG GAA TTC CAC CTG TGT GTT CTG CTG TAC TTT GTA ATA CTT TTC GCT GGC AGT GAA GGG GAT CCC TAT TTC AAT GAT TTA GAA AAG CTT GAT CTC CCA AAT GGT CAT GAA

Val Asn Trp Met Lys Ser Ile Asp Asp Glu Thr Leu Leu Ser Ala Val Thr Ile Pro Gly Thr Cys Gln Ser Met Lys Met Asn Thr Leu Asp Gln His Gln Ala Trp Thr 74

38 GTA AAC TGG ATG AAA AGT ATA GAT GAT GAA ACA CTT CTC TCA GCA GTC ACC ATT CCA GGC ACA TGC CAA AGC ATG AAA ATG AAT ACT CTT GAT CAA CAC CAA GCA TGG ACA

Val Thr Gln Gln Phe Thr Ala Gly Val Arg Phe Phe Asp Ile Ser Leu Asp Asn Ser Val Val Lys Asp Gly Ser Leu Thr Arg Arg Lys Phe Ala Asp Val Met Glu Lys 111

75 GTA ACA CAG CAG TTT ACA GCA GGG GTG CGA TTC TTT GAT ATC TCC CTG GAT AAT TCA GTT GTC AAA GAT GGT TCT CTT ACA CGT AGA AAA TTT GCA GAT GTC ATG GAA AAG

Met Arg Glu Arg Leu Ile Ala His Pro His Glu Val Ile Leu Ile Arg Leu Thr Pro Glu Asn Gly Lys Ala Glu Lys Glu Ile Glu Lys Phe Ile Gln Val Asn Asp Asn 148

112 ATG AGA GAA CGT TTG ATT GCT CAC CCT CAT GAA GTA ATT TTG ATA AGA TTG ACC CCA GAA AAT GGC AAA GCT GAA AAG GAA ATA GAA AAA TTC ATA CAA GTG AAT GAC AAT

Val Trp Lys Asp Lys Lys Val Pro Lys Met Lys Glu Val Arg Gly Lys Ile Val Leu Val Gln Ser Ser Lys Phe Ser Lys Gly Leu Pro Val Asp Leu His Val Gly Gly 185

149 GTG TGG AAG GAT AAA AAA GTG CCC AAA ATG AAA GAA GTA AGG GGT AAG ATA GTG TTG GTG CAG AGC AGC AAG TTC AGT AAA GGG CTC CCG GTG GAC CTT CAT GTG GGT GGG

Lys Glu Phe Lys Asp Lys His Ser Lys Lys Tyr Met Glu Ala Ile Tyr Asn His Phe Lys Asp Lys His Ser Lys Lys Tyr Met Glu Ala Ile Tyr Asn His Leu Lys Ala 222

186 AAG GAG TTT AAA GAT AAG CAC TCA AAA AAG TAC ATG GAA GCG ATT TAT AAT CAT TTT AAA GAT AAG CAC TCA AAA AAG TAC ATG GAA GCG ATT TAT AAT CAT CTA AAG GCA

Ala Glu Asn Ala Gly Asp His Ile Val Val Thr Glu Thr Ser Ala Tyr Phe Gly Phe Thr Lys Ser Ser Lys Asn Ala Ala Val Lys Ile Asn Pro Met Leu Gln Lys Tyr 259

223 GCA GAA AAT GCA GGT GAC CAT ATT GTA GTG ACT GAA ACA AGC GCA TAT TTT GGA TTC ACA AAA TCA TCA AAA AAT GCA GCT GTA AAA ATT AAT CCC ATG CTC CAA AAA TAC

Ile Asp Asn Gln Pro His Ala Asn Lys Pro Lys Gly Leu Gly Val Ile Val Met Asp Tyr Pro Gly Ile Asp Leu Ile Gln Lys Ile Ile Asp Ile Asp Ile Asn Pro Lys 296

260 ATA GAC AAC CAG CCG CAT GCT AAT AAA CCA AAA GGT TTG GGG GTG ATT GTC ATG GAC TAT CCA GGC ATT GAT CTC ATC CAG AAA ATC ATA GAT ATA GAT ATC AAC CCT AAA

Ser Glu Gly Ser Pro Glu Ser Ser Pro Glu Glu Gly Glu Asn Pro Pro Glu Thr Asp Gly Glu Pro Glu Stop 320

297 TCA GAA GGC TCA CCT GAA TCC TCC CCA GAA GAA GGT GAG AAC CCA CCT GAA ACT GAT GGG GAA CCC GAA TGA

Figure 3.2: The interleaved nucleotide and derived amino acid sequences of the coding region of the *PLC-like* gene from *Anguilla anguilla*. Blue lettering denotes the predicted nucleotide and amino acid sequences of the X-domain. Numbers present on the left and right margins refer to the nucleotide and amino acid sequences, respectively. Underlined is a signal sequence predicted by the SignalP 4.0 server (Peterson *et al*., 2011).

3.3. Sequence analysis and comparison of PLCXD isoforms in the European eel with other species.

The deduced 319-amino acid protein has a predicted molecular mass of 33.9 kDa and an isoelectric point of 5.84. An N-terminal signal peptide of 20 amino acids was predicted by the SignalP 4.1 Server (ExPASy; Petersen *et al.,* 2011). The presence of a signal peptide suggests that the eel *PLC-like* gene may be targeted to the secretory pathway or a specific organelle within the cell; however this remains to be determined experimentally. The deduced amino acid sequence of the *PLC-like* gene was predicted to contain only a PI-PLC X-domain following sequence comparisons with the Prosite protein domain database (motif entry code PS50007, Gly^{35}- $Lysine^{278}$ region). The presence of an only an X-domain suggests that the *PLC-like* gene identified is more similar in primary structure to bacterial PI-PLCs (Chapter 1, Section 1.6).

The deduced amino acid sequence of the *PLC-like* gene was searched against the complete non-redundant protein (nr) database on NCBI (http://blast.ncbi.nlm.nih.gov/Blast.cgi). BLAST analysis showed the greatest homology (33%) with a 33.4 kDa uncharacterised predicted protein from the bicolor damselfish (*Stegastes partitus*; probability with BLAST, 3×10^{-38}). Other proteins which scored high in the BLAST search included 15 uncharacterised predicted proteins from zebrafish (*Danio rerio*; probabilities with BLAST between 7×10^{-36} and 2×10^{-20}) and bacterial phosphatidylinositol-specific phospholipases from *Listeria monocytogenes* (GenBank accession no. AFA26313.1, 1×10^{-19} *Bacillus thuringiensis* (GenBank accession no. X14178.1, 2×10^{-10}) and *Bacillus cereus* (GenBank accession no. X64141.1, 2×10^{-10}). All proteins identified from this BLAST search were of a similar molecular

size to the eel *PLC-like* protein (30-35 kDa) and only contained an X-domain. A second BLAST search was performed against the complete non-redundant protein sequence database in mammals. This search identified a number of homologous proteins which had previously been characterised as members of a distinct PI-PLC subtype which contain only the X-domain of the other multi-domained members of this enzyme family and hence known as mammalian phospholipase C X-domain containing proteins (PLCXDs). To date, BLAST analysis reveals the presence of three PLCXD isoforms (PLCXD1, 2 and 3) in the genomes of most mammals, including human and mouse. The deduced amino acid sequence of the eel *PLC-like* gene showed less than 20% sequence identity with mammalian PLCXD isoforms (Figure 3.3). With the aim of identifying further PLCXD sequences in *A. anguilla*, BLAST analysis against the recently sequenced eel genome was performed using the PLCXD1, 2 and 3 nucleotide sequences identified in humans. Eel PLCXD1, 2 and 3 homologues were identified and their full-length sequence reconstructed by Dr Svetlana Kalujnaia, University of St Andrews. The deduced amino acid sequence of the eel *PLC-like* gene identified herein displays 17.6%, 17.3% and 19% amino acid sequence identity with the predicted eel PLCXD1, 2 and 3 respectively. The sequences of eel PLCXD1, 2 and 3 are yet to be experimentally verified. Given the low sequence homology with other PLCXDs, the eel *PLC-like* gene and others identified in the first BLAST search were denoted PLCXD4. In-order to verify the presence of additional PLCXD isoforms in vertebrates, a phylogenetic tree was constructed with a number of the PLCXD amino acid sequences identified through BLAST searching. Phylogenetic analysis indicates that the vertebrate PLCXD proteins group into four distinctive clusters (Figure 3.3). The PLCXD-like sequences identified in

the first BLAST search were subsequently denoted PLCXD4 as they did not group with any of the PLCXD1, 2 or 3 sequences.

Although functional characterisation of vertebrate PLCXDs has yet to be performed, PLCXD sequences found in prokaryotes such as *Bacillus cereus* and *Bacillus thuringenesis* have been shown to be active lipases involved in the hydrolysis of phosphatidylinositol (PI) and glycosylated phosphatidylinositol (GPI) substrates (Heinz *et al*., 1998). The catalytic mechanism of *B. cereus* and *B. thuringiensis* has been well characteristed and the invariant histidine 32 (His32), histidine 82 (His82) and arginine 69 (Arg69) amino acids, present within the X-domain, have been shown to be essential for catalysis (Chapter 1, Section 1.4.3.1) Sequences corresponding to the X-domains of PLCXDs from different vertebrates were aligned with the X-domain sequences of *B. cereus* and *B. thuringenesis* to screen whether these key catalytic residues are conserved in the vertebrate PLCXD isoforms (Figure 3.4). Indeed, His32, His82 and Arg69 were found to be conserved in the X-domain sequences of vertebrate PLCXD enzymes including eel PLCXD1, 2 and 3 isoforms, suggestive of the retention of similar catalytic properties to the bacterial PI-PLCs. In contrast, these residues were not found to be conserved in the X-domain sequence of eel PLCXD4.

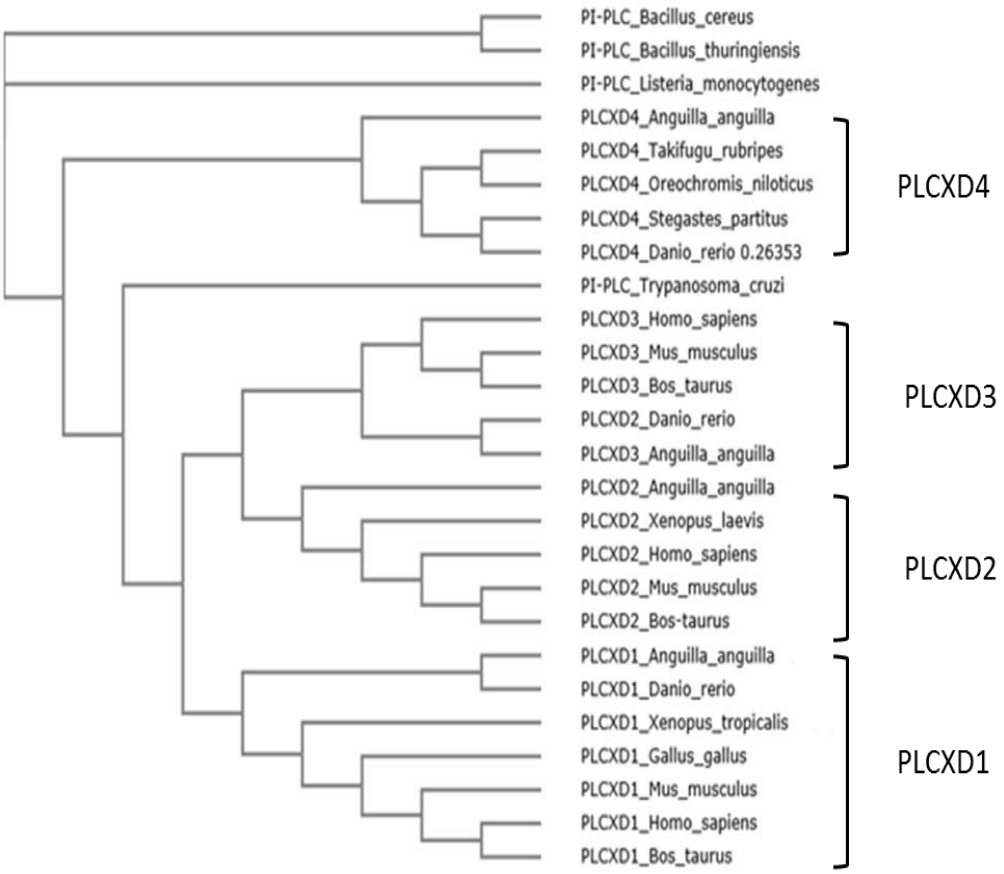

Figure 3.3: Phylogenetic analysis of PLCXDs. This tree was constructed using the neighbour-joining method, with each bar representing the p distance of the N-J method. NCBI/EMBL accession numbers are detailed in Appendix B.

Figure 3.4: Alignments of the derived X-domain amino acid sequences from a various vertebrate and non-vertebrate species. Symbols in the alignment are as follows: (*) indicates where there is a conserved amino acid; (:) indicates an amino acid position with conserved similarity; (.) indicates a semi-conserved amino substitution has occurred; (-) indicates spaces introduced to optimise the alignment. Conserved residues known to be important for the catalytic function of bacterial PI-PLC's are highlighted in yellow. The NCBI Accession numbers where available in Appendix B.

3.4. Tissue expression of eel PLCXD isoforms

Quantitative RT-PCR (Chapter 2, Section 2.7.11) was used to determine the distribution and relative levels of expression of all four PLCXD mRNAs in tissues extracted from one FW-maintained and one SW-acclimated silver eel. RNA isolation and cDNA conversion were performed using standard protocols (Chapter 2, Sections 2.7.1 and 2.7.4) and cDNAs from the same tissue were pooled together from the FW and SW silver eel. The sequences of the primers used for amplifications are detailed in Appendix A. Normalised expression values were obtained for PLCXD1, 2, 3 and 4 in each tissue and were subsequently presented as a bar graph (Figure 3.5 A, B, C and D). PCR analyses clearly indicated that PLCXD1, 2, 3 and 4 mRNAs show distinct tissue expression patterns. The eel PLCXD1 homologue has a wide tissue distribution with the highest mRNA expression in the gill and oesophagus. Similarly, expression of eel PLCXD4 mRNA was found in most of the tissues tested, with the highest expression being found in the intestine. In contrast, the eel PLCXD2 homologue showed a narrower tissue distribution, with mRNA expression only detectable in the eye. Melting curve analysis and gel electrophoresis were performed after each amplification to test the specificity of the gene-specific primers. A single peak and a single band of the expected size were obtained following amplification of PLCXD1, 2, 3 and 4 indicating that the results represent the amplification of the gene of interest (data not shown). No amplification was observed in the no-template and reverse transcriptase negative controls indicating no nucleic acid contamination in the PCR reactions (data not shown). It is important to note that due to problems obtaining sufficient eels for tissue extraction the mRNA expression values for each tissue were

obtained using a cDNA sample pooled from n=1 FW-maintained eel and n=1 SW-acclimated eel. Further tissue extractions from a larger sample of European eel is therefore required to verify the observed mRNA expression patterns.

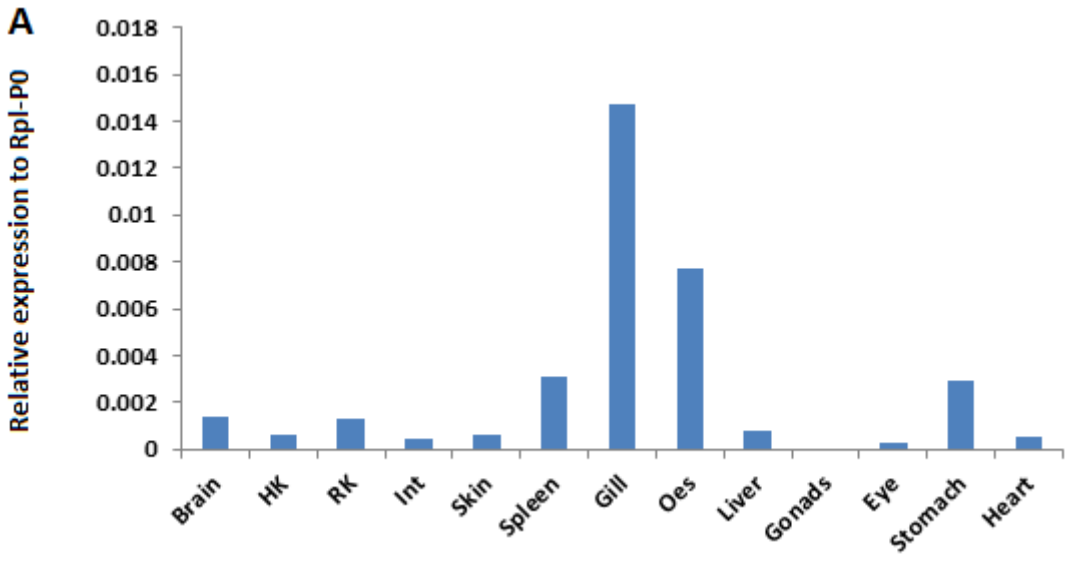

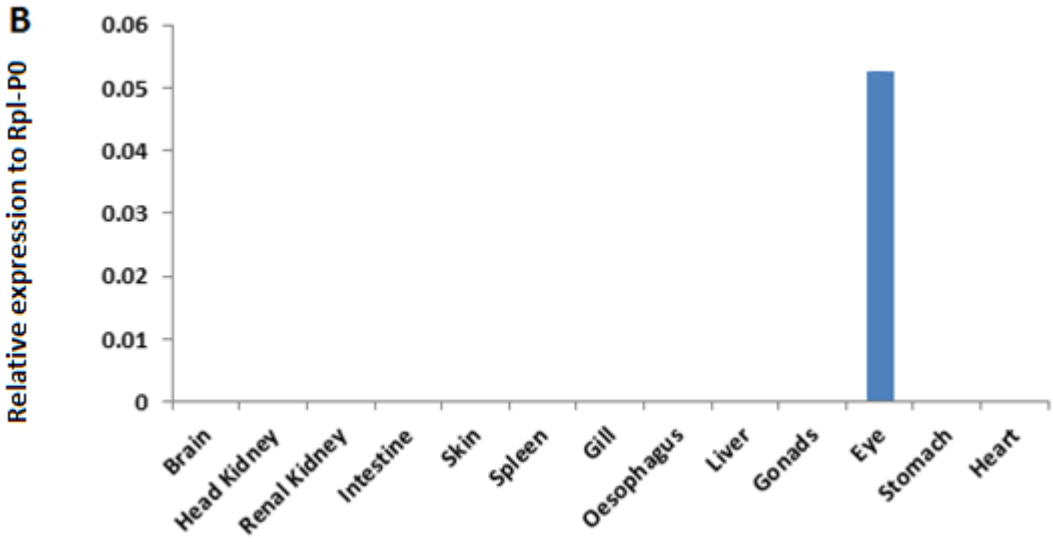

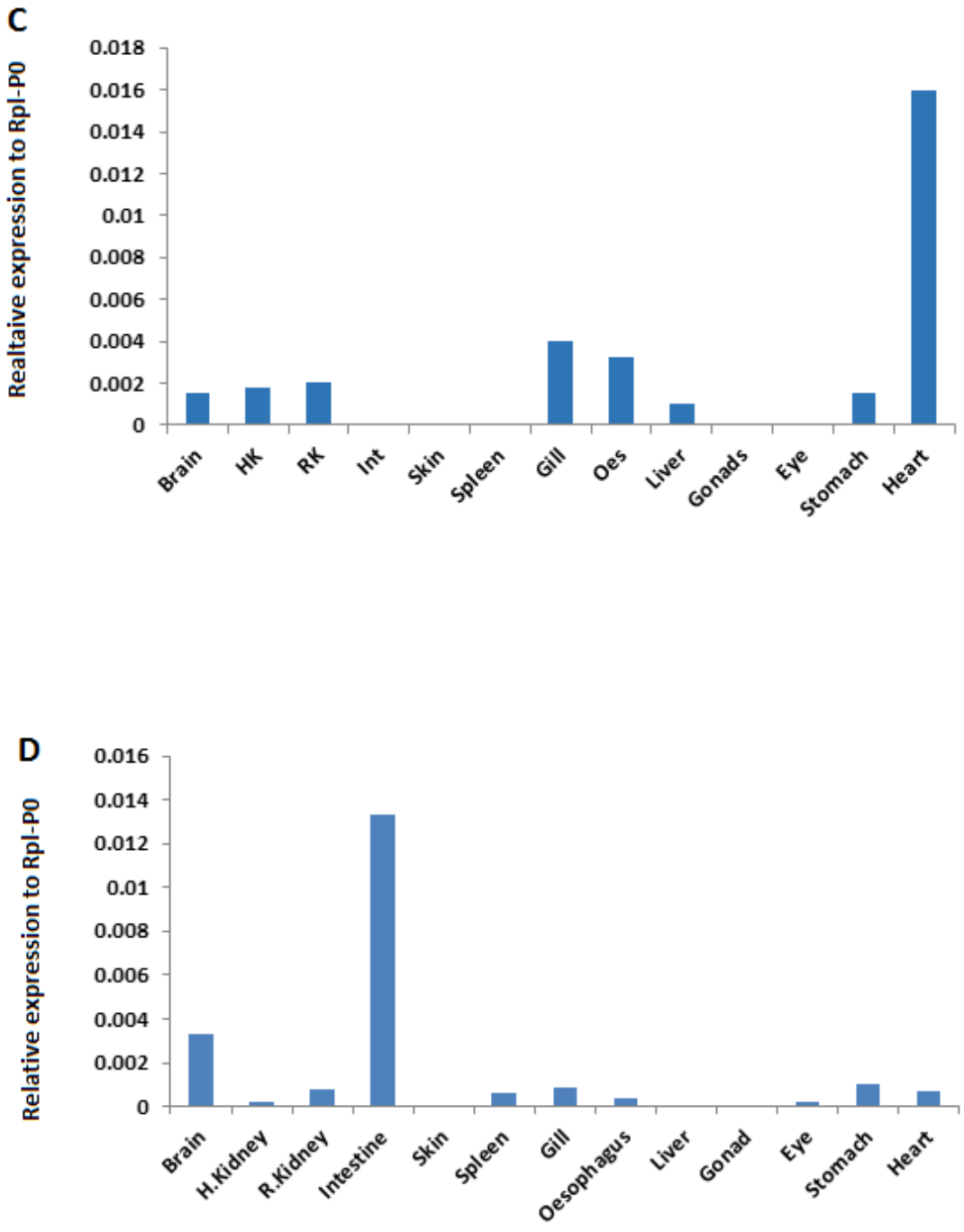

Figure 3.5: Relative expression of ePLCXD-1, 2, 3 and 4 mRNAs in selected eel tissues (A-D respectively). Expression of PLCXD mRNAs was determined from Ct values obtained and normalised to Rpl-P0 expression in each tissue as detailed in the Chapter 2, Section 2.6.11. For each tissue, cDNA was pooled from n=1 FW-maintained and n=1 SW-acclimated silver eels. For both the gene of interest and Rpl-P0, each PCR reaction was run in triplicate with the average Ct value being used to calculate the relative expression value.

3.5. Quantitative mRNA expression and protein expression of eel PLCXDs in FW- and SW-acclimated yellow and silver eel intestine

The previous microarray study found the eel PLCXD4 to exhibit higher expression in the intestine of the yellow eel compared with that of the silver eel (unpublished). In-order to further confirm this, quantitative RT-PCR was performed to test the levels of PLCXD4 mRNA in the intestine of FW-maintained and 3 month SW-acclimated yellow and silver eels. The primers used were the same as those for the determination of tissue distribution, and their sequences are detailed in Appendix A. RNA was isolated from six FW-maintained and six SW-acclimated for both yellow and silver eels and was subsequently converted to cDNA. Normalised levels of PLCXD4 mRNA were calculated for each fish and an average value for the six FW-maintained and six SW-acclimated yellow and silver eels obtained. PLCXD4 mRNA levels were found to be 30-fold higher in the intestine of yellow eels compared with that of silver eels and were unaffected by salinity transfer suggesting that PLCXD4 mRNA expression is dependent on the developmental stage of the eel (Figure 3.6).

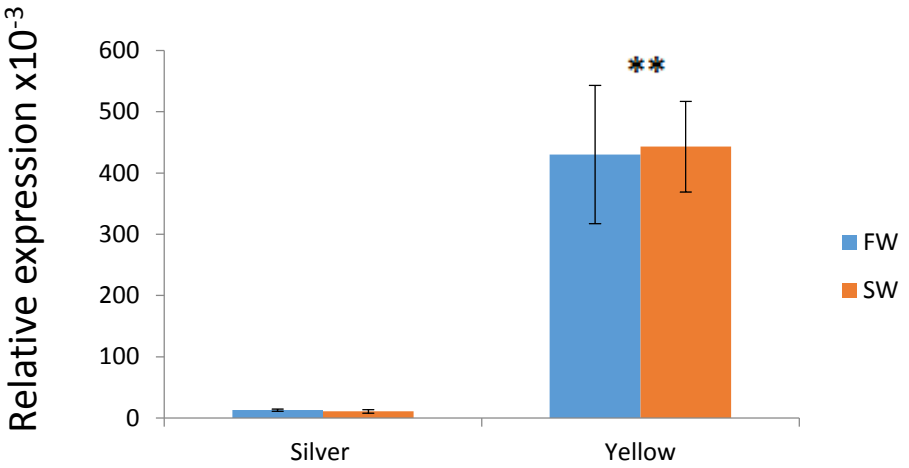

Figure 3.6: Relative expression of eel PLCXD4 mRNA in the intestine of FW-maintained and 3-month SW-acclimated yellow and silver eels. A total of 12 silver eel and 12 yellow eels (6 FW and 6 SW) were used. Ct values were averaged from 6 fish in each condition and expressed relative to Rpl-P0 (x 10^{-3}). Samples were run in triplicate and the error bars represent SEM across fish. ** P< 0.01.

In order to test whether PLCXD4 protein levels also change during developmental transitions, western blot analysis (Chapter 2, Section 2.8.5) was performed using supernatant protein samples extracted from the intestine (Chapter 2, Section 2.8.1) of FW-maintained and 3 month SW-acclimated yellow and silver eels. Custom-made antibodies raised against the N-terminal 15 amino acid peptide antigen from ePLCXD4 were generated, as described in Chapter 2, Section 2.8.2. In proteins samples extracted from yellow eels an immunoreactive protein band of the expected molecular weight (36 kDa) was detected in both FW-maintained and SW-acclimated fish. Western bot analysis also revealed the presence of a prominent lower molecular weight band of 34 kDa. The presence of these bands was highly variable among individual yellow eels with most fish containing both bands and some fish containing either the 34 or 36 kDa bands (Figure 3.7).

The intensity of the combined 36 and 34 kDa immunoreactive ePLCXD4 bands and α-tubulin was determined in each sample by densitometry (Chapter 2, Section 2.8.5) and revealed no significance difference in ePLCXD4 levels between FW-maintained and SW-acclimated yellow eels (Figure 3.7B). Similarly, two immunoreactive protein bands (34 and 36 kDa) corresponding to ePLCXD4 were detected in the protein samples extracted from silver eel intestine. The intensity of the immunoreactive bands corresponding to ePLCXD4 appeared to be greater in SW-acclimated fish compared to FW-maintained fish and this was confirmed by densitometric analysis of the proteins blot (Figure 3.7). Immunoprecipitation of crude intestinal extracts, prepared from SW-acclimated Silver eels, followed by mass spectrometry confirmed the specificity of the PLCXD4 antibody for the 36 kDa protein band. Matched peptides of eel PLCXD4 identified by mass spectrometry are shown in Figure 3.7C.

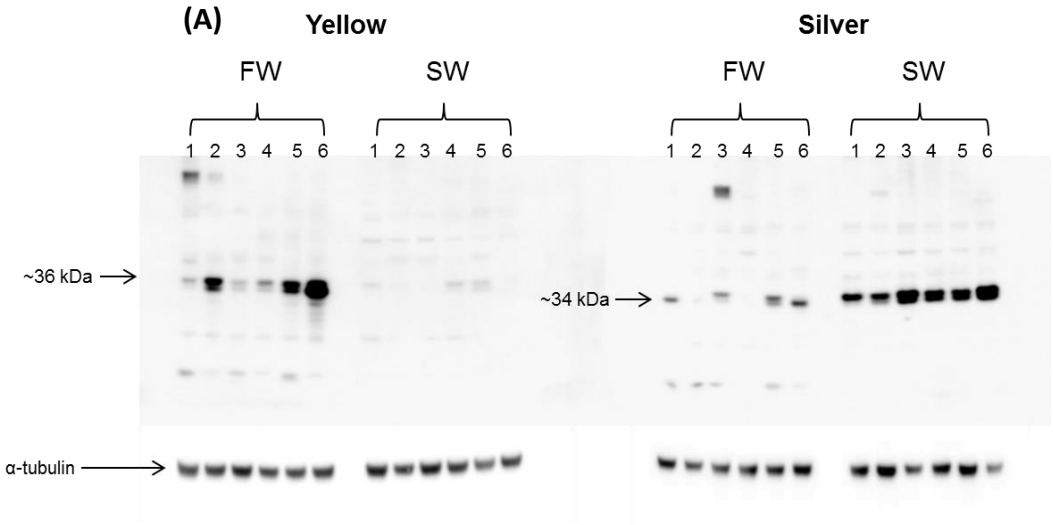

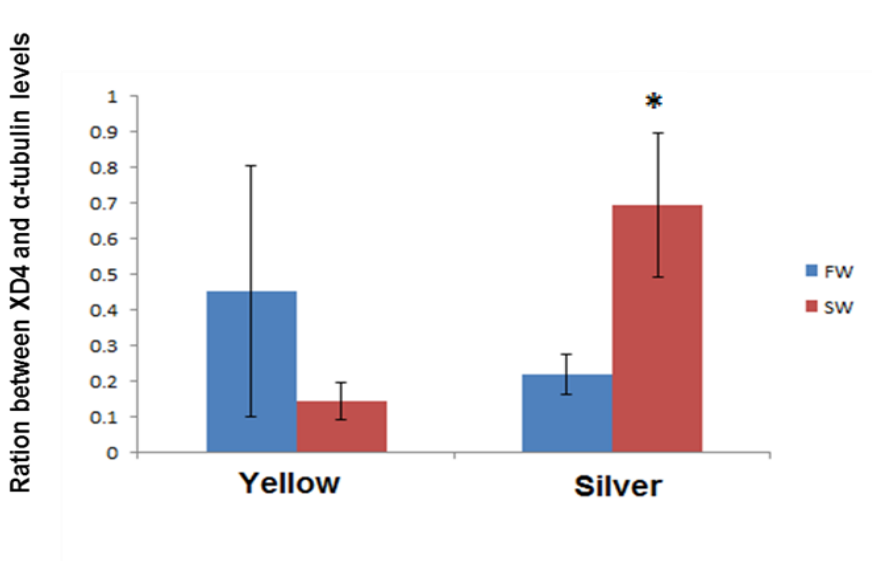

(C)

MEFHLCVLLYFVILFAGSEGDPYFNDLEKLDLPNGHEVN
WMKSIDDETLLSAVTIPGTCQSMKMNTLDQHQAWTV
TQQFTAGVRFFDISLDNSVVKDGSLTRRKFADVMEKMR
ERLIAHPHEVILIRLTPENGKAEKEIEKFIQVNDNVWKDK
KVPKMKEVRGKIVLVQSSKFSKGLPVDLHVGGKEFKDKH
SKKYMEAIYNHLKAAENAGDHIVVTETSAYFGFTKSSKN
AAVKINPMLQKYIDNQPHANKPKGLGVIVMDYPGIDLI
QKIIDIN PKSEGSPESSPEEGENPPETDGEPE

Figure 3.7: (A) Western blot analysis of the expression of ePLCXD4 and α-tubulin in the intestines of FW-maintained and SW-acclimated yellow and silver eels (*n*=6 eels for each condition). 10 µg of protein was loaded to each well. **(B)** Densitometric analysis of western blot data. Results are expressed as the ration between ePLCXD4 and α-tubulin (*n*=6 fish; mean +/- S.E.M.) The data was further analysed by Students T-test. * P<0.05. Samples FW1-6 and SW1-6 for both yellow and sliver eels are the same as in Figure 3.6. **(C)** Matched peptides of eel PLCXD4 indentified by mass spectrometry.

3.6. Cellular localisation of PLCXD4 protein by immunofluorescence light microscopy

Immunohistochemistry (Chapter 2, Section 2.8.15) was used to determine the cellular location of PLCXD4 peptide in the anterior, middle and posterior intestine of a 3-month SW-acclimated silver eel and a FW-maintained yellow eel. PFA fixation and paraffin embedding procedures yielded good antigenicity and good structural preservation (Figures 3.8 and 3.9). In both the 3-month SW-acclimated silver eel and the FW-maintained yellow eel, PLCXD4 immunoreactivity was restricted to irregular shaped cells that appeared randomly at the base and in between the more columnar epithelial cells where fluorescence was present throughout the entire cell. The precise nature of these cells awaits further investigation. Immunofluorescence studies showed high levels of consistency across the anterior, middle and posterior sections of both the FW-maintained yellow eel and the 3-month SW-acclimated silver eel. As expected, control sections incubated with only a secondary antibody showed no fluorescence.

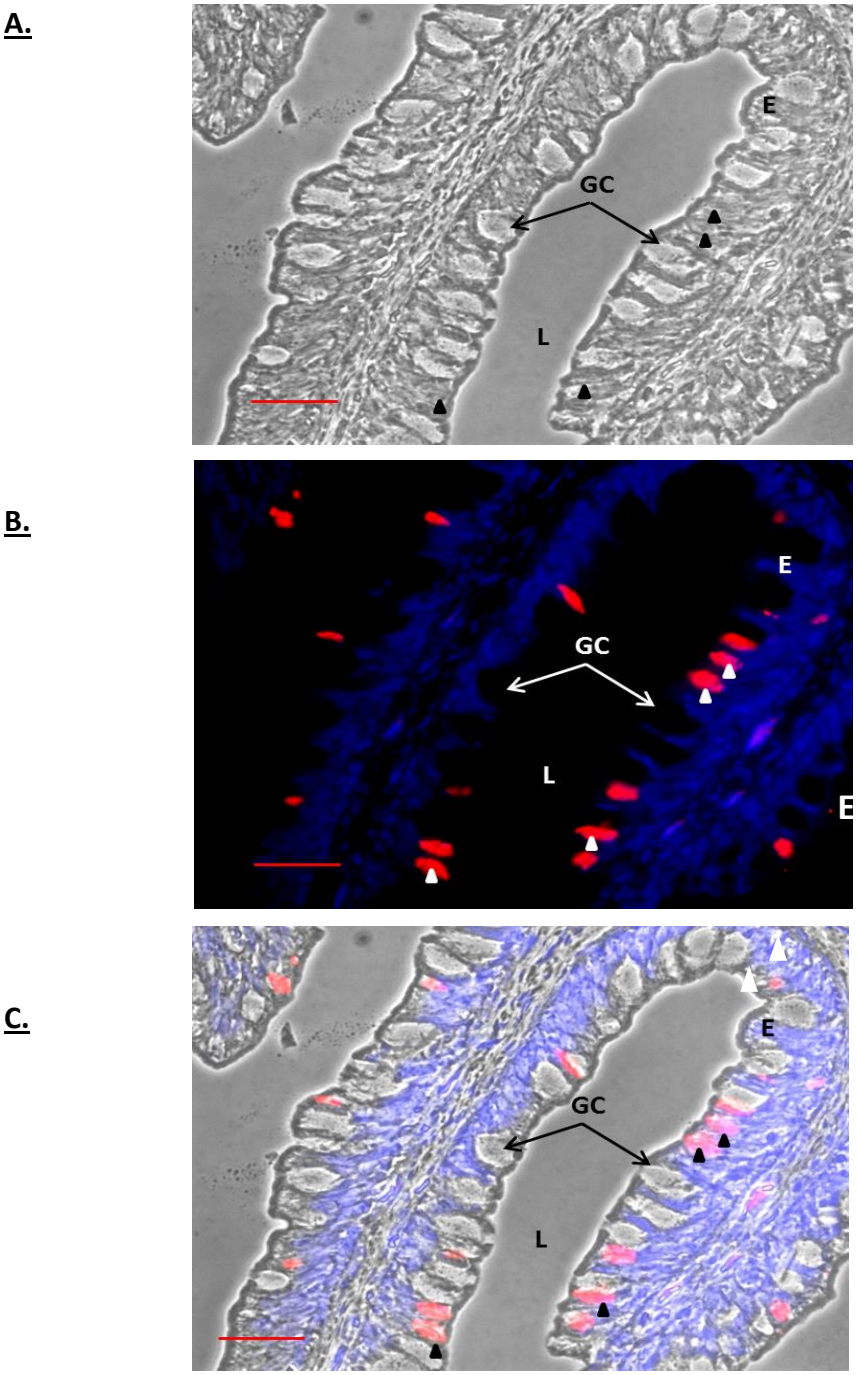

Figure 3.8: Immunolocalisation of eel PLCXD4 in transverse intestinal sections from a FW-maintained yellow eel. PLCXD4 localises to irregular intra-epithelial cells. Eel intestine sections were taken from the middle gut and probed with the affinity-purified mouse anti-ePLCXD4 primary antibody and the Alexa Fuor 633-labelled donkey anti-mouse polyclonal antibody. Scale bar indicates 100 µm. (A) Phase contrast image, (B) Fluorescence image, (C) merge. Goblet cells, GC; Lumen, L; Epithelium, E. Images are representative of at least 10 microscope fields of view for 3 sections taken from one fish.

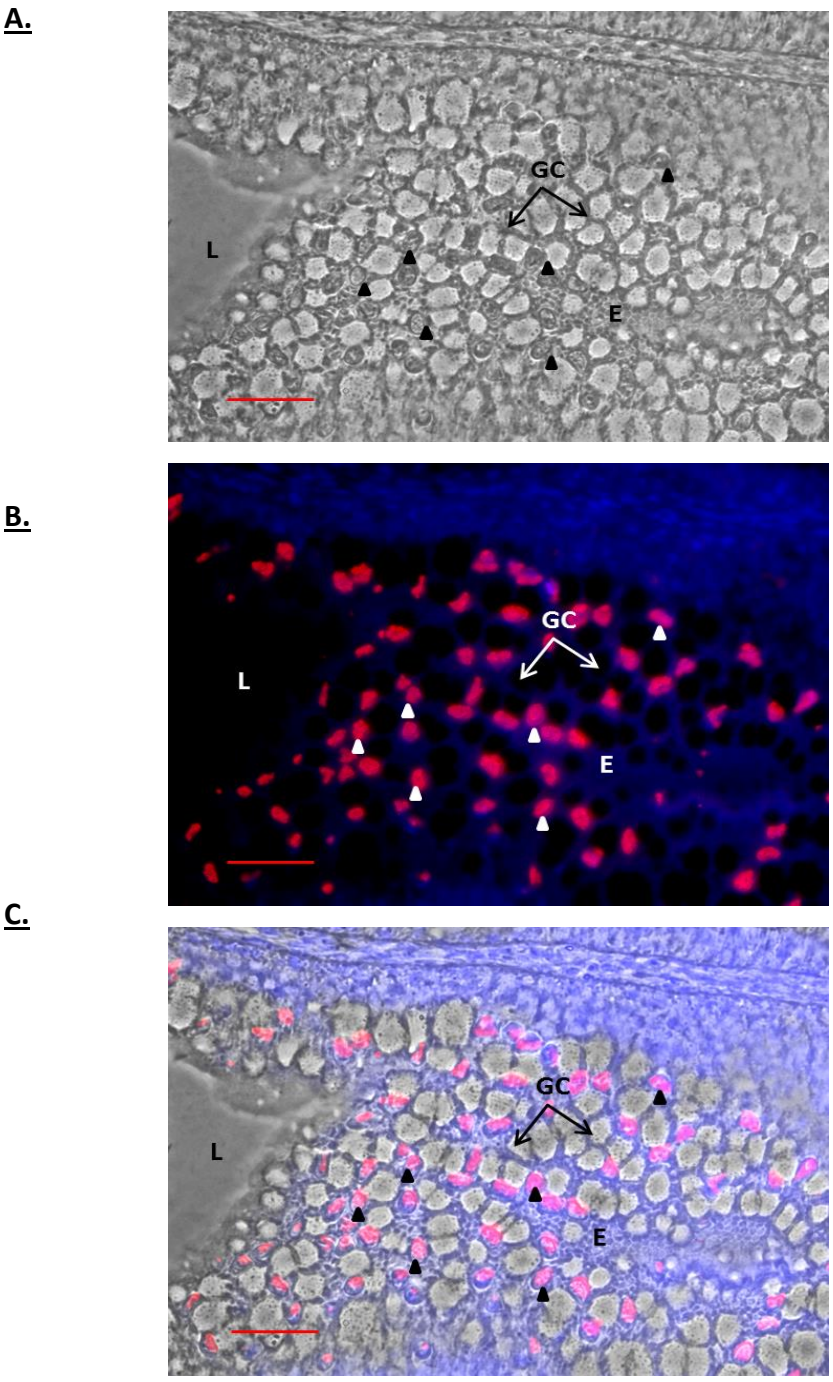

Figure 3.9: Immunolocalisation of PLCXD4 in the middle intestine from a 3-month SW-acclimated silver eel. As with the yellow eel, PLCXD- localises to irregular shaped intra-epithelial cells in close proximity to goblet cells. Sections were probed with affinity-purified N-terminal anti-ePLCXD4 antibody. Scale bar indicates 100 µm. (A) Phase contrast image, (B) Fluorescence image, (C) merge. Goblet cells, GC; Lumen, L; Epithelium, E. Images are representative of at least 10 microscope fields of view for 3 sections taken from one fish.

3.6. Discussion

Inositol phospholipids are integral components of increasingly complex signalling pathways found in all animal cells. A variety of extracellular signalling molecules including many hormones, neurotransmitters and growth factors responsible for the regulation of a wide range of metabolic processes within a spectrum of cell types, mediate their actions through co-ordinated changes in inositol lipid metabolism. A family of enzymes central to these signalling pathways are known as phospholipase Cs (PLCs). These enzymes are responsible for the hydrolysis of phosphatidyl inositol 4, 5 bisphosphate (PIP_2) producing DAG and IP_3, both of which serve as second messengers within the cell. DAG is a potent activator of protein kinase C signalling pathway, and IP_3 mediates the release of calcium from intracellular stores (See Chapter 1). To date, all current information regarding the characterisation of members of this enzyme family have focussed on six sub-classes of PLCs, with each sub-class having a different number of isoforms. As a result of the importance of these enzymes in cell signalling their molecular structures, tissues distributions, mechanisms of activation and disparate physiological functions have been extensively investigated (See Chapter 1).

Previous microarray studies in this laboratory identified various genes exhibiting differential expression following the “yellow” to “silver” developmental transition of the *A. anguilla.* One gene identified as showing a decrease in expression during this developmental transition was denoted *PLC-like* in that the partial sequence obtained contained only an X-domain. In this study, the full-length sequence of the coding region of the *PLC-like* gene was obtained by 5’ RACE RT-PCR reactions using Marathon cDNA cloning. *In silico* analyses indicated the *PLC-like* gene as being a member of a

novel PI-PLC subtype which contain only the characteristic X-domain of the other multi-domained members of this enzyme family and hence are known as phospholipase C X-domain containing proteins (PLCXDs). Although the molecular and physiological functions of vertebrate PLCXD isoforms remain to be characterised, PLCXD homologues present within *B. cereus* and *B. thuringiensis* are considered to be virulence factors and are capable of hydrolysing the phosphodiester bonds found in both phosphatidylinositol (PI) and also glycosylphosphatidylinositol (GPI)-anchored proteins within mammalian cells (See Chapter 1; Heinz *et al.,* 1998). The chapter details results of the initial characterisation of the amino acid sequence and homologies, tissue and cellular distribution and protein expression patterns.

3.6.1 Sequences of eel PLCXD proteins

The present study describes the isolation, full-length sequencing and characterisation of a *PLC-like* gene from the intestine of the European eel. Analysis of the deduced amino acid sequence of the *PLC-like* gene suggests that it's a member of the phosphatidylinositol-specific phospholipase C (PI-PLC) superfamily of phosphodiesterases. Unlike other eukaryotic PI-PLCs (See Chapter 1), the *PLC-like* gene characterised herein is predicted to only contain an X-domain and is subsequently much smaller than other eukaryotic PI-PLCs with a predicted molecular weight of 33.9 kDa. Screening of amino acid sequences from public databases (most notably the NCBI database) has identified homologues of the *PLC-like* gene in the genomes of a number of species from bacteria to humans. These proteins are members of a distinct PI-PLC subtype known as phospholipase C X-domain containing proteins (PLCXDs) as they only contain an X-domain. BLAST analysis and subsequent phylogenetic analysis within

this thesis has identified three PLCXD isoforms (PLCXD1, 2 and 3) in most mammals and at least four in teleost fishes. To date, eukaryotic PI-PLCs have been divided into six subtypes each of which contain a multi-domain structure, as previously described in Chapter 1. Given that PLCXDs only contain an X-domain, these proteins are more similar in primary structure to bacterial PI-PLCs and therefore potentially represent a seventh subtype of the PI-PLC superfamily of phosphodiesterases.

From the structure of the complexes, supporting data from enzyme kinetics, and site-directed mutagenesis, bacterial PLCXD isozymes are known to utilise general base/acid catalysis with the invariant His-32, His-82 and Arg-69 residues (present within the X-domain) known to be essential for catalytic activity (Heinz et al. 1998). Alignments of the X-domain sequences of eel PLCXD1, 2, 3, and 4 with that of *B. cereus* and *B. thuringiensis* found the key catalytic residues (His32, His82 and Arg69) of bacterial PLCXD enzymes to be conserved in eel PLCXD1, 2 and 3 isoforms, suggestive of the retention of catalytic properties similar with the bacterial PLCXD enzymes. In contrast, none of these residues were conserved in the X-domain sequence of PLCXD4 suggesting that this isoform may be an inactive phosphodiesterase or possess a yet uncharacterised catalytic mechanism unique from other phospholipase C enzymes. Indeed, site-directed mutagenesis of His32, His82 and Arg69 abolishes the catalytic activity of PI-PLC from *B. cereus* (Heinz *et al.,* 1998). The conservation of these key catalytic residues within the X-domains of eel PLCXD1, 2 and 3 is highly suggestive of the retention of PLC-related catalytic functions. Future studies should aim to test the ability of recombinant proteins of all eel PLCXD isoforms to hydrolyse PI and PI(4,5)P_2 and also test their lipid binding properties.

3.6.2 Tissue expression of eel PLCXD isoforms

Quantitative real-time PCR using RNA isolated from various tissues from the European eel was used to determine the tissue-specific expression of eel PLCXDs 1, 2, 3 and 4 mRNA in *A. anguilla*. Previously we characterised the tissue distribution of human PLCXDs 1, 2 and 3 isoforms (Gellatly *et al*., 2012). Similarly with human PLCXD isoforms, eel PLCXDs 1, 2, 3 and 4 display distinctive mRNA expression patterns. Unlike the human PLCXD isoforms, the mRNA expression levels of eel PLCXDs 1, 2, 3 and 4 were not found predominantly in the brain. For eel PLCXD1, mRNA expression was found in virtually all the tissues tested with the highest level being found in the gill. The tissue distribution of eel PLCXD2 mRNA was restricted to the eye with no detectable signal being present in any other tissue. In contrast, a wider mRNA expression pattern for PLCXD2 was observed in human tissues. The tissue distribution of eel and human PLCXD3 isoforms was similar with expression primarily within the heart. Given that the European eel PLCXD1, 2, 3 and 4 isoforms have obvious tissue specificity, these proteins potentially have distinctive yet uncharacterised physiological roles. The lack of consistency in the tissue distribution of eel and human PLCXDs 1, 2 and 3 isoforms suggests that each PLCXD isoform may exhibit species-specific physiological functions. To our knowledge, this is the first report describing the tissue-specific mRNA expression pattern of any PLC subtype in the *A. anguilla*.

3.6.3 Quantitative mRNA expression and protein expression of eel PLCXDs in FW- and SW-acclimated yellow and silver eel intestine

Consistent with our previous microarray data, quantitative expression studies showed PLCXD4 mRNA levels to be significantly more abundant (30-fold) in the intestine of

yellow eels compared to silver eels and unaffected by salinity transfer. These results suggest that some, as yet unknown, developmental changes associated with the "yellow" to "silver" transition (also known as silvering) may be responsible for the changes seen in PLCXD4 mRNA expression in the eel intestine. Whether PLCXD4 mRNA expressed in other tissues of the *A. anguilla* is similarly affected by the yellow to silver developmental transition remains to be characterised. We further evaluated the expression of PLCXD4 protein levels in the intestine in both FW-maintained and SW-acclimated yellow and silver eels using western blot analysis. Immunoreactive protein bands of 36 kDa (expected size) and 34 kDa were detected and confirmed by co-IP to be ePLCXD4. The presence of these bands were highly variable among individual yellow and silver eels with most fish containing both bands and some fish containing either the 34 or 36 kDa bands. Relative quantification of ePLCXD4 protein bands, normalised to α-tubulin, revealed similar levels of ePLCXD4 in the intestine of FW/SW yellow and FW silver eels. However, there was marked variability in the expression of the ePLCXD4 proteins between different fish with the same group, particularly FW-maintained yellow eels, causing difficulties in the interpretation of the data. More accurate determination of ePLCXD4 protein levels requires an increase in the number of intestinal samples tested; however the declining population numbers of the European, close to the level of extinction has therefore made it difficult to gain sufficient eel samples for experimental purposes. In silver eels, densitometry revealed an almost 2-fold increase in the level of ePLCXD4 in the intestine of the SW-acclimated fish compared with FW-maintained fish. The increase in expression was not seen in the mRNA levels and therefore the observed increases in protein expression level is

likely due to as yet uncharacterised post-transcriptional changes. One explanation for the observed increase in ePLCXD4 protein level in SW-acclimated silver eels could be that this protein is involved in the molecular mechanisms underlying osmoregulation in the European eel. Given that no changes in ePLCXD4 protein levels were detected when yellow eels were transferred to SW, this explanation seems unlikely. A more likely explanation is that ePLCXD4 is linked to the series of morphological and physiological changes that occur late on during the silvering process as the eel enters the sea (See Section 3.1).

3.6.4. Immunolocalisation of PLCXD-4 in middle intestinal sections

In the previous section, western blot analysis revealed that PLCXD4 protein levels were detectable in the intestine using an affinity-purified N-terminal PLCXD4 antibody. In-order to further characterise PLCXD4 protein expression in the intestine of the European eel and to shed light on possible physiological functions, immunohistochemistry was used to examine the localisation of PLCXD4 within the intestine. PLCXD4 immunoreactivity was restricted to irregular shaped cells that appeared randomly at the base and in between the more columnar epithelial cells. Immuno-fluorescence was present throughout the entire cell. No specific fluorescence was observed in the smooth muscle and connective tissue layers of the intestine. The intestinal epithelium is a single cell layer which consists mainly of absorptive columnar cells, referred to as enterocytes, with the inclusion of mucus-secreting goblet cells, and various intraepithelial endocrine /neuroendocrine cells and lymphocytes (Clarke and Witcomb, 1989). The presence of a various different cell types within the intestinal epithelium is thought to underlie the multifunctional nature of the gut which has been

shown to be involved in diverse functions in the eel including nutrient, water and ion uptake, and therefore osmoregulatory processes, as well as being the first line of defence against harmful agents entering the lumen (Grosell *et al*., 2010). The precise nature of these cells awaits further co-localisation experiments with antibodies recognise proteins specific for endocrine, neuroendocrine or immune cells. Although the precise functional role of PLCXD4 in the eel intestine is currently unknown, future experiments could characterise the expression, cellular localisation and effect of gene knockdown and over-expression in cultured primary epithelial cells from the intestines of European eels. These molecular approaches will offer a better comprehension of the cellular/potential physiological functions of PLCXD4 in the intestinal epithelium. Given that only very low PLCXD4 expression was detected in western blots using the intestine of FW-maintained silver eels, it would be interesting to carry out immunofluorescence studies of PLCXD4 protein expression using intestinal sections from this group of fish. Currently intestinal sections from the yellow eel are unavailable.

CHAPTER 4: Cloning, tissue distribution and characterisation of human and mouse PLCXD isoforms

4.1. Prediction and characterisation of human PLCXD genes

With the goal of identifying human and mouse PLCXD isoforms, BLAST searching against the non-redundant NCBI protein database was used to identify sequences with homology to eel PLCXDs. Three genes, denoted PLCXDs 1, 2 and 3, were identified and their corresponding nucleotide sequences were submitted to the BLAT search engine on the Santa Cruz genome browser. In human, the PLCXD1 sequence is present on both X (Xp22.33) and Y (Yp11.32) chromosomes whereas PLCXD2 and 3 sequences mapped to positions 3q13.2 and 5p13.1 respectively. Interestingly, the Ensembl database predicted the presence of two transcripts for PLCXD2, designated ENST00000393934 and ENST00000477665, each containing an open-reading frame consisting of four exons. The predicted sequences of exons 1-3 were found to be identical, whereas the sequence of exon 4 is different. The presence of two different PLCXD2 transcripts may result from alternative splicing events within exon 4, and ENST00000393934 and ENST00000477665 were subsequently denoted PLCXD2.1 and 2.2 (Figure 4.1).

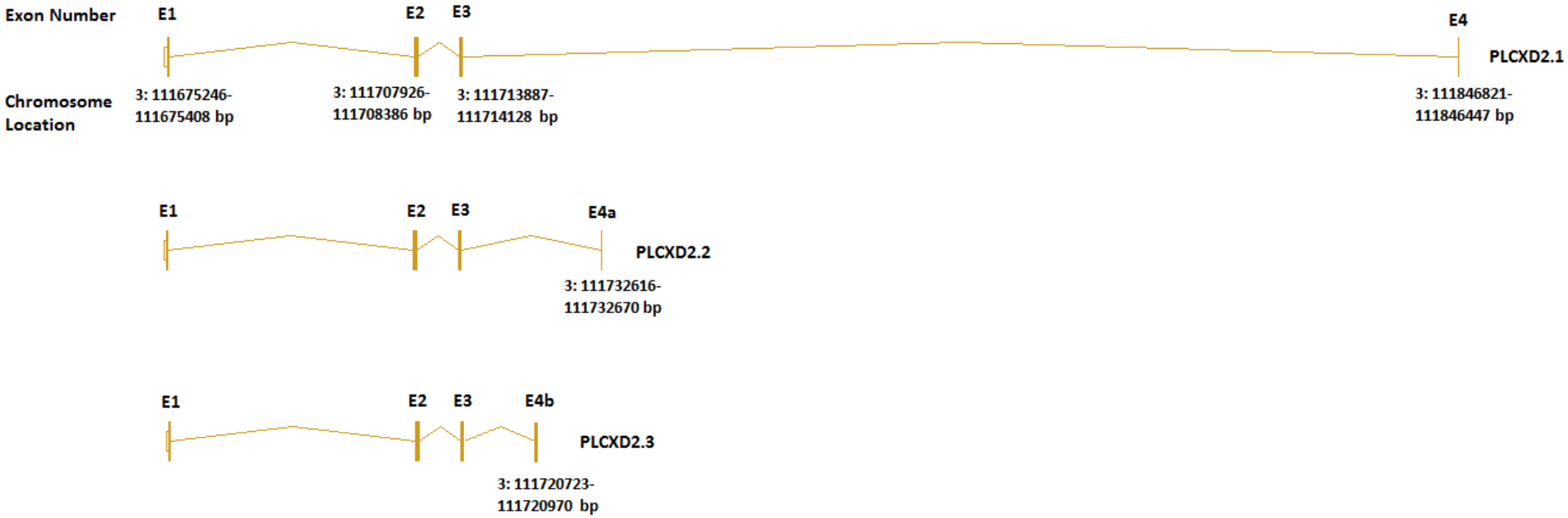

Figure 4.1: Schematic diagram of exonic sequences present in different PLCXD2 mRNA isoforms. Boxes and lines represent the exons and introns, respectively. Human PLCXD2 is found on band q13.2 of chromosome 3. The location of each exon sequence on chromosome 3 is indicated below each exon (See Esembl). The nucleotide sequences of PLCXD2.1 and PLCXD2.2 were originally obtained from the Esembl database and subsequently confirmed following sequencing of RT-PCR products cloned from HeLa first strand cDNA. PLCXD2.3 was initially identified during RT-PCR amplification of PLCXD2.2 and its full-length sequence was later obtained using Marathon cDNA prepared from the HeLa cell line.The nucleotide sequence of Exons 1-3 are identical in each splice variant, whereas the sequence of Exon 4 is different.

In-order to confirm the predicted sequences of all human PLCXDs, including the splice variants of PLCXD2, RT-PCR was used to amplify the entire open-reading frames of all human PLCXD transcripts from a HeLa cell cDNA pool (Chapter 2, Section 2.7.6). The sequences of primers used are detailed in Appendix C. PCR products of around 1000 base pairs were obtained corresponding to the expected molecular sizes of PLCXD1 and 3 (Figure 4.2). Following gel purification and TOPO cloning reactions (Chapter 2, Section 2.7.9), the predicted sequences of human PLCXD1 and 3 were confirmed. For PLCXD2, PCR products of around 1000 base pairs were obtained corresponding to the full-length open reading frames of PLCXD2.1 and 2.2 (Figure 4.2). Sequencing reactions confirmed these sequences to be identical to those present within the database. Additionally, a larger band of just over 1000 base pairs was detected following amplification with primers specific to PLCXD2.2, which sequencing reactions and alignment analysis showed to be highly similar to PLCXD2.1 and 2.2 with differences only present at the 3'-end (Figure 4.1 and 4.2). Cloning and sequencing of this additional band was carried out in collaboration with Dr Taciana Kasciukovic, University of St Andrews. This additional band therefore represents a further PLCXD2 transcript with a divergent 3'-end which was subsequently denoted PLCXD2.3.

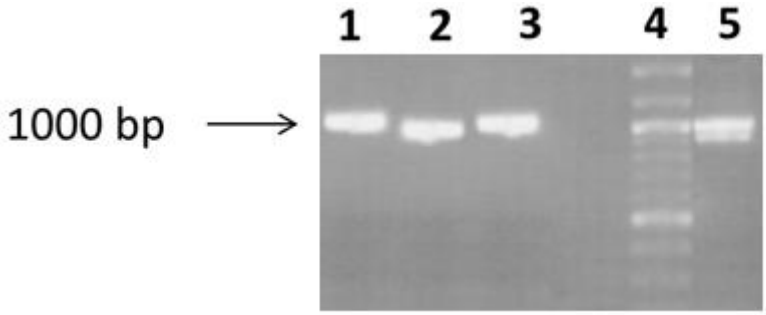

Figure 4.2: RT-PCR amplification of human PLCXDs using cDNA synthesized from HeLa cells. Gel electrophoresis analysis with ethidium bromide staining shows the amplification of PCR products of the expected size for human PLCXD1, PLCXD2 and PLCXD3 (Lanes 1, 2 and 3, respectively). Included in the analysis was a predicted alternative splicing variant of PLCXD2, PLCXD2.2, shown in Lane 5. Interestingly, a larger band was also amplified alongside PLCXD2.2 which sequencing has confirmed as a further alternative splicing variant of PLCXD2, denoted PLCXD2.3. The molecular markers for size estimation is shown in lane 4.

The presence of conserved protein domains was predicted using the SMART databases (Smart Architecture Research Tool; http://smart.embl.de/). Based on predictions by SMART, amino acids 30-206, 42-215 and 22-197 of PLCXDs 1, 2 and 3 respectively have homology with X-domain sequences of the normal X and Y catalytic domains found in all known eukaryotic PI-PLC. No other domain homologies were predicted using SMART databases. Previous phylogenetic analysis of PLCXD proteins from different species showed PLCXD1, 2 and 3 sequences to cluster into separate groups with each isoform being highly conserved across species, suggestive of conserved functions. Additionally, previous sequence alignments of PLCXD proteins from different species including the functionally characterised bacterial PLCXD homologs revealed the conservation in all human PLCXDs of two key catalytic histidines and an arginine residue suggestive of the retention of similar catalytic properties in human proteins (Chapter 3, Figure 3.5).

4.3. mRNA expression and tissue distribution of mouse and human PLCXD1, 2 and 3

Quantitative RT-PCR (Chapter 2, Section 2.7.11) was used to determine the distribution and relative levels of mouse PLCXD1, 2 and 3 mRNAs in a range of different tissues. Primer sequences used are detailed in Appendix D. As shown in Figure 4.3A, B and C, PCR analyses clearly indicated that PLCXD1, 2, 3 mRNAs show distinct tissue expression patterns. For all PLCXD isoforms, the highest mRNA expression levels were observed in the brain. PLCXDs 1 and 3 mRNAs were observed in virtually all tissues tested indicating potential fundamental roles in cell function.

In the case of human PLCXD isoforms, mRNA expression levels were analysed using semi-quantitative RT-PCR in a restricted number of tissues (Figure 4.3D). Human PLCXD1 mRNA expression levels were observed in virtually all tissues tested. Although PLCXD3 mRNA expression was detectable in most of the tested tissues, a particular strong signal was found in the heart. PLCXD2 mRNA expression levels (probe for all spliceforms) was restricted to the leukocytes and thymus.

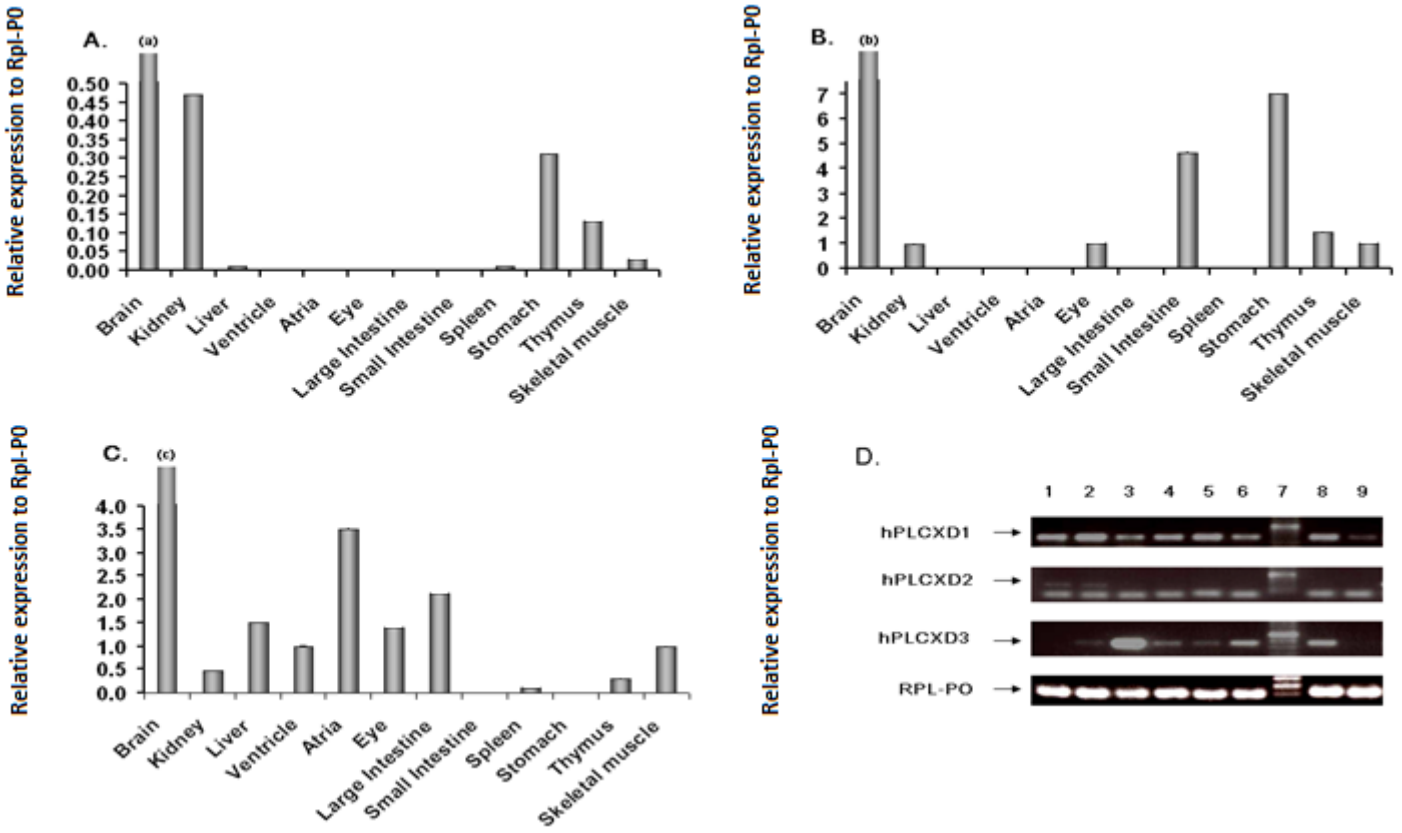

Figure 4.3: Relative expression of mPLCXD-1, 2.1 and 3 transcripts in a range of mouse tissues (A-C) taken from n=1 mouse. Relative levels were calculated using Rpl-P0 as the normalizing gene, as detailed in the materials and methods. PCR amplifications were run in triplicate and the mean values are reported. Mean values for brain samples (a), (b) and (c) are 1.0, 100 and 20, respectively. Values on the Y-axis indicate relative expression to Rpl-P0 ($x10^{-3}$). (D) Semi-quantitaive expression levels of hPLCXD1, 2 and 3 transcripts by RT-PCR analysis from a restricted number of human tissues (1- leukocytes, 2- thymus, 3- heart, 4- small intestine, 5- colon, 6- kidney, 7- molecular weight markers, 8- lung and 9- skeletal muscle.

4.4. The distribution of PLCXD1, 2 and 3 in the mouse brain

Analysis of the expression of PLCXD1, 2 and 3 in different areas of the mouse brain has been previously characterised by *in situ* hybridisation experiments and this data was accessed from the Allen Brain Atlas. This comprehensive analysis was undertaken by the Allen Institute for Brain Science (AIBS) and is the first large scale project to map the expression of approx. 20,000 genes in the mouse brain by *in situ* hybridisation. The expression of these genes was detected and quantified and subsequently stored in a database, allowing for comparisons of gene expression patterns. All data present within the database was taken from 8-week-old adult C57BL/6J male mice. In this chapter, the database was used to reveal the PLCXD1, 2 and 3 mRNA expression patterns in different brain regions to further characterise the predominant expression of these transcripts previously observed in the mouse brain (see Figure 4.4). The expression pattern of each PLCXD isoform is represented in a heat map, where the level of gene expression is indicated by different colours (blue: low, green: medium, red: high expression level), as determined by *in situ* hybridisation using digoxigenin-labelled probes. For PLCXD1, a strong signal was present in the hippocampal formation, in particular the pyramidal cells of the regions CA1-3 and granule cells of the dentate gyrus (Figure 4.4). Additionally, a strong signal for PLCXD1 was evident in the purkinje layer of the cerebellum. For PLCXD2, a particularly strong signal within periglomerular cells and the mitral cells layer of the olfactory bulb (Figure 4.5). PLCXD2 staining was also evident in visual cortex and various regions of the mid-brain including the *inferior colliculus,* and the *lateral posterior nucleus* of the thalamus (Figure 4.7). Localisation observed in nervous tissues was in the nerve cell, but not in the glial cells as revealed

at higher magnification. Interestingly, no detectable expression was observed for PLCXD3, which is inconsistent with our previous findings.

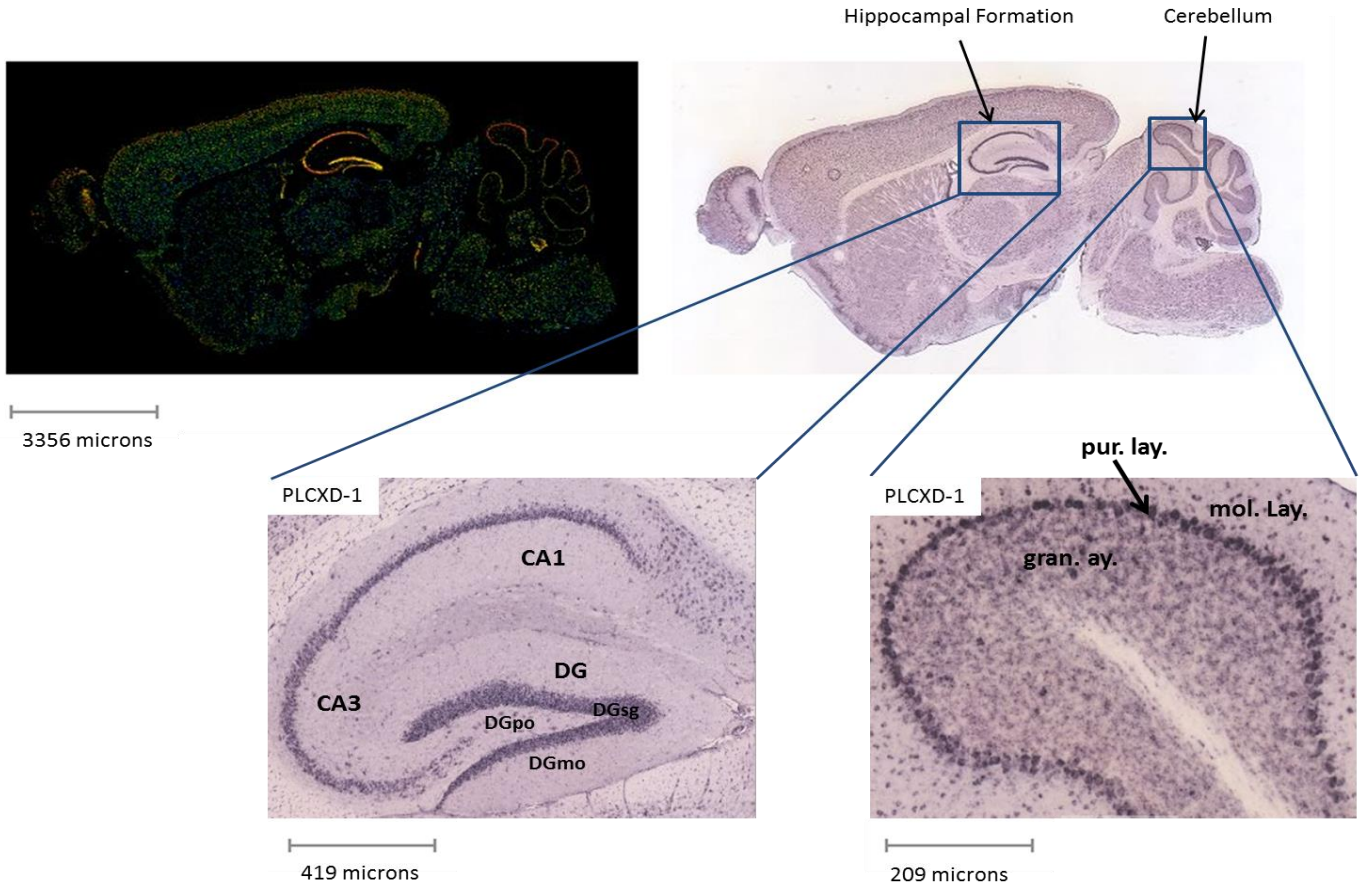

Figure 4.4: Analysis of the expression of PLCXD1 in different regions of brain of 8-week-old adult C57/BL/6J male mice by *in situ* hybridisation. This data is stored within the Allen Brain Atlas (http://www.brain-map.org/). Expression is also represented as a heat map (Top left; blue: low, green: medium, red: high expression). Hippocampal formation: *Cornu Ammonis* area 1 and 3 (CA1 and CA3), dentate gyrus (DG), dentate gyrus polymorphic layer (DGpo), dentate gyrus granule cell layer (DGsg), dentate gyrus molecular layer (DGmo). Cerebellum: purkinje layer (pur. lay.) and granule cell layer (gran. lay.).

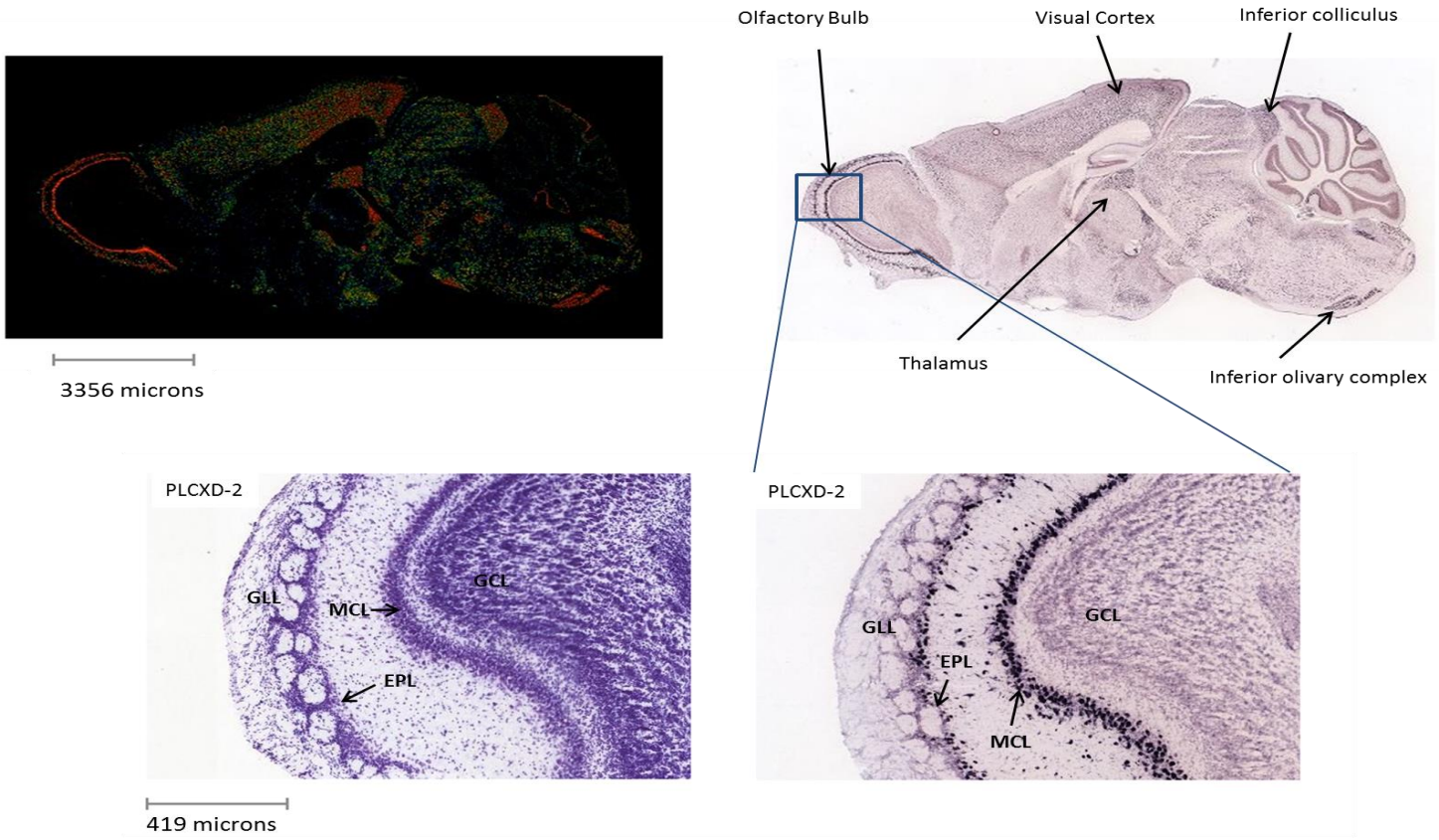

Figure 4.5: Analysis of the expression of PLCXD2 in different regions of brain of 8-week-old adult C57/BL/6J male mice by *in situ* hybridisation. This data is stored within the Allen Brain Atlas (http://www.brain-map.org/). Expression is also represented as a heat map (Top left; blue: low, green: medium, red: high expression). Bottom left shows Nissl-staining. Glomerular layer (GLL), external plexiform layer (EPL), mitral cell layer (MCL), granule cell layer.

4.5. Sub-cellular localisation of PLCXD1, 2 and 3 isoforms in the HeLa cell line

The most basic question of where human PLCXD isoforms are located within the cell can be investigated with immunofluorescence microscopy. HeLa cells stably expressing Pk/V5-tagged forms of PLCXD1, 2 and 3 were created in collaboration with Dr Svetlana Kalujnaia, University of St Andrews, using a lentiviral-based expression system, as described in the Section 2.3.4. Successful over-expression of each PLCXD isoform was confirmed by Western blot analysis (Figure 4.6) using the mouse monoclonal anti-Pk/V5 antibody (1/500 dilution; See Table 2.5) and a secondary alkaline phosphatase-conjugated donkey anti-mouse polyclonal antibody (1/10,000 dilution; See Table 2.5). Wild-type cells (non-transfected) and HeLa cells exhibiting stable overexpression of Pk/V5-tagged hPLCXD-1, 2.1 and 3 were grown and prepared for immunocytochemistry and fluorescent microscopy, as described in Chapter 2, Section 2.5.2. When transfected HeLa cells were probed with an anti-Pk/V5 antibody followed by a secondary labelled Alexa Fluor 633-labelled donkey anti-mouse polyclonal antibody, the most prominent signals were present in uncharacterised cytoplasmic and perinuclear vesicles suggestive of endoplasmic reticulum and/or Golgi apparatus (Figure 4.7 B and D). In contrast, transfected PLCXD2.1 protein was found to be entirely nuclear (Figure 4.7C). No staining was observed in control non-transfected HeLa cells, therefore confirming the specificity of both the primary and secondary antibodies.

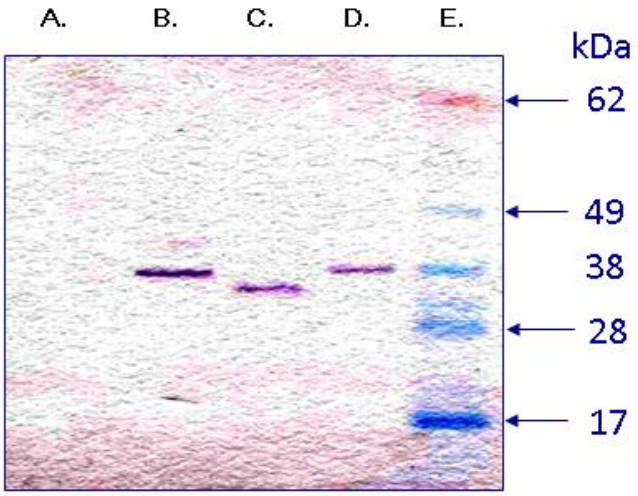

Figure 4.6: Western blotting analysis of HeLa cells stably expressing Pk/V5-tagged PLCXD1, 2.1 and 3 (B, C and D respectively). Primary antibody: mouse anti-Pk/V5 tag; 1/500 dilution. Secondary antibody: Alkaline phosphatase-conjugated donkey anti-mouse. No bands were detected in control non-transfected cells (control; Lane A). Lane E: Standard protein marker (Fermentas). This image is a representation of 3 separate experiments.

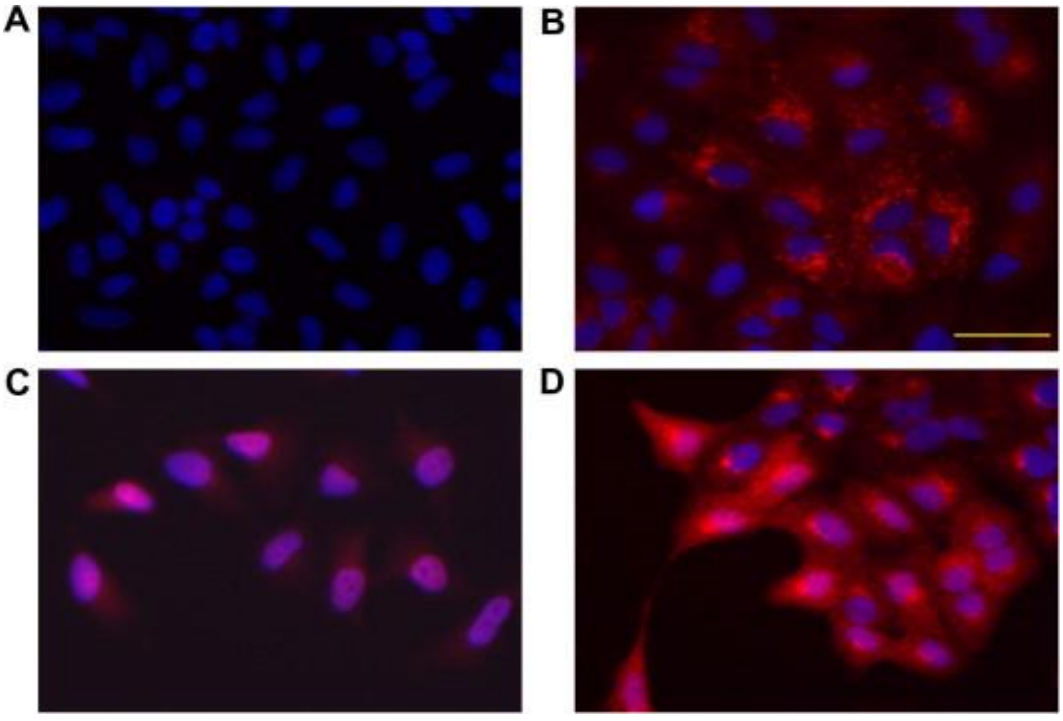

Figure 4.7: Sub-cellular localisation of hPLCXD isoforms (red) in HeLa cell lines stably transfected with Pk-tagged hPLCXD1 (B), 2.1 (C) or 3 (D), respectively. Non-tranfected (Control) cell lines (A). DAPI stained nucleus is shown in blue. Photomicrographs were captured using a Zeiss Axiocam light microscope x40 objective. These images are representative of at least 10 microscopic fields of view for 3 separate experiments. Scale bar indicates 50 µm.

4.6. *In vivo* phospholipase C assays

A cell-based [^{3}H]-inositol-phosphate release assay was performed (Chapter 2, Section 2.5.1) to investigate the potential role of hPLCXDs acting as functional PI-PLCs. This assay was carried out in collaboration with Dr Svetlana Kalujnaia, University of St Andrews. The relative [^{3}H]-inositol phosphate (IP) content of non-transfected (control) HeLa cells and cells transfected with hPLCXD1, 2.1 and 3 was determined either in the presence or absence of the calcium ionophore A23187 (Chapter 2, Section 2.5.1). As shown Figure 4.8, HeLa cells transfected with hPLCXD constructs all exhibited significant (2.5- to 7-fold) increases in basal turnover of the phosphatidylinositol pool compared to the non-transfected control cells. Interestingly, compared with both PLCXD1 and PLCXD2.1 transfected cells, the turnover of PI-phospholipids was significantly higher in cells transfected with PLCXD3. Western blot analysis revealed hPLCXD1, 2 and 3 proteins to be expressed at similar levels in HeLa cells. The calcium ionophore A23187 increased PI turnover to the same extend in control and PLCXD1 and PLCXD2.1 transfected cells but failed to enhance the already high turnover in cell over-expressing hPLCXD3. These data suggest that over-expression of all three hPLCXD isoforms increased endogenous phospholipase C activity in cultured HeLa cells in a calcium-independent manner.

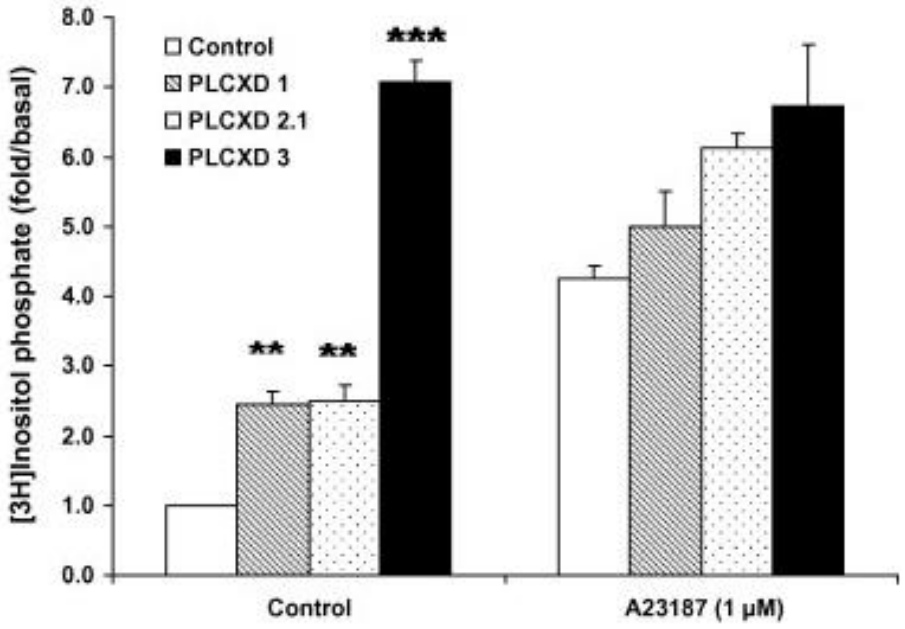

Figure 4.8: Relative [^{3}H]-IP content of non-transfected (control) HeLa cells and cells overexpressing hPLCXD1, hPLCXD2.1, hPLCXD3, following a 2 h incubation with 10 mM LiCl plus or minus the calcium ionophore A23187. Bars indicate the fold difference over non-transfected, control cells. Error bars indicate SEM for n=3 replicates.

4.7. Discussion

4.7.1. Identification of PLCXD homologs in the human genome

Human and mouse sequences belonging to the PLCXD class of genes were identified, analysed and several important observations were made. Previous observations in the European eel showed PLCXD genes to be segregated into four groups (PLCXDs 1, 2, 3 and 4) on the basis of sequence similarity, coincident with their position within a phylogenetic tree. Current investigations within this chapter have resulted in the identification of PLCXD1, 2 and 3 orthologues in humans and mice. In humans, the PLCXD1 gene is unusual, in as much as it is one of only 29 pseudo-autosomal genes that are present on both X (Xp22.33) and Y (Yp11.32) chromosomes. As with all

pseudo-autosomal genes that escape X-inactivation, this highlights PLCXD1 as potentially being linked to the variety of physical and mental disorders associated with sex chromosome aneuploidy, such as found in Triple X syndrome (Blaschke and Rappold, 2006).

Sequence analysis has indicated that both mouse and human PLCXD isoforms have retained the amino acids known to contribute to the acid/base hydrolysis of phosphoinositides in *B. cereus* PI-PLCs as well as other mammalian PLCXDs, including His32, His 82 and Arg69 (*B. cereus* PLCXD sequence numbering; Figure 3.5, highlighted in yellow). Both mouse and human PLCXD isoforms also have a conserved arginine residue (Figure 3.5, highlighted in yellow), which is homologously positioned to Arg69 in the calcium-independent bacterial PI-PLCs. As mentioned previously (Section 1.4.3.1), Arg69 is important for stabilisation of the Ins (1:2cyc) P substrate intermediate in the active site of bacterial PI-PLCs whereas mammalian PI-PLC utilise a calcium ion to fulfil this role (Heinz *et al*., 1998). This difference is thought to be the reason that bacterial PI-PLCs can only catalyse the first step of the two-step reaction (Section 1.4.3.1) and therefore release Ins(1:2cyc)P as the principal product of phosphoinositide hydrolysis; in contrast, the principal product of mammalian PI-PLCs is the acyclic inositol phosphate (Heinz *et al*., 1998). As with eel PLCXD-1, 2 and 3, these data are suggestive of the retention of similar catalytic properties of mammalian PLCXD proteins to their homologues in bacteria. Further characterisation of the catalytic activity of human PLCXD is described in Chapter 5.

As a result of *in silico* analysis and subsequent RT-PCR and sequencing reactions, we have identified and confirmed the existence of at least three splicing variants of the

PLCXD2 isoform derived from a single gene that differ in their C-terminal sequences. Alternative splicing variants have been previously reported for several other PI-PLC isozymes including rat PLC-β1 (Bahk *et al*., 1994), human PLC-β2 (Sun *et al.,* 2007), human PLCε (Sorli *et al.,* 2005) and mouse PLC-η (Hwang *et al.,* 2005). Differences in tissue distribution and catalytic properties have been reported for most spliced variants of PI-PLC iszoymes (Rebecchi and Pentyala, 2000). The presence of splicing variants of PLCXD2 may therefore have important physiological and potential pathological consequences. Future work should aim to characterise and compare the tissue distribution and cellular localisations of the different alternative splice variant of PLCXD2 in a range of different tissues and cell lines.

Recently the crystal structures of eukaryotic and prokaryotic PI-PLCs have been determined both in complexes with substrates thus enabling comparisons of the enzymes in substrate-specificity terms. Prokaryotic PI-PLCs and the catalytic domain of eukaryotic PI-PLCs consist of alternating α- helices and β-strands that resemble an incomplete triose phosphate isomerase α/β-barrel (TIM-barrel; Section 1.4.1.4). The first half of the barrel displays large structural similarity between the prokaryotic and eukaryotic PI-PLCs, however the enzymes display a much weaker similarity in the second half of the barrel. The higher degree of structure conservation in the first half of the barrel correlates with the presence of all catalytic residues, including the two catalytic histidine residues, in this portion of the enzyme. The second half of the TIM-barrel contains the amino acid residues contributing to the substrate binding pocket. The distinctive nature of the second half of the TIM-barrel in prokaryotic and eukaryotic enzymes is known to contribute to their different substrate preferences

(Heinz et al. 1996; Heinz *et al.,* 1998). In-order to predict whether mouse and human PLCXD proteins contain amino acids enabling interaction with inositol containing substrates, a structural model of mammalian PLCXDs was constructed using the known structures of *B. cereus* PI-PLC and the catalytic site of mammalian PLC-δ1. Due to low amino acid sequence homology this model was not robust and therefore whether mammalian PLCXDs have retained the amino acids known to contribute to the binding of either $PI(4,5)P_2$ or PI is currently unknown.

4.7.2. mRNA expression of PLCXD1, 2 and 3 in different mouse tissues and regions of the mouse brain

Analysis of the tissue-specific mRNA expression patterns of the different PLCXD isoforms in mice and humans show PLCXD1, 2 and 3 to have distinct tissue distributions. Indeed the distribution of other mammalian PI-PLC subtypes and their different isoforms is well characterised and has similarly been shown to be tissue- and organ-specific (Suh *et al*., 2008). For instance, northern blot analyses of mouse tissues and EST sequence analyses using human UniGene database showed the highest level of PLC-γ1 mRNA to be present in the brain and embryonic tissues whereas PLC-γ2 mRNA is expressed mainly in the lymph nodes (Mizuguchi *et al*., 1991). These differences in tissue distribution patterns are thought to serve as an explanation to the predominant role of PLC-γ1 in embryonic cell development and the role of PLC-γ2 in immune responses (Wang *et al*., 2000; Hashimoto *et al*., 2000). Given the specificity in distribution of PLCXD1, 2 and 3 in mouse and human tissues, it may be that each PLCXD isoform bears a unique function in the modulation of physiological responses. At least

in mice, the highest mRNA expression of PLCXD1, 2 and 3 was found within the brain suggestive of a fundamental role in nerve cell function.

The tissue-specific localisation of all three PLCXD isoforms was further described based on the data provided by the Allen Brain Atlas. PLCXDs 1 and 2 were found to have a widespread distribution in the brain with mRNA being detected within most brain regions. PLCXD1 was found to be particularly enriched throughout the hippocampal formation, with expression being detected in the neurons of the CA1-3 regions and the dentate gyrus, and the Purkinje layer of the cerebellum. The dentate gyrus appears as a V-shaped structure enveloping the end of the pyramidal cells of CA3 and is composed of three layers: molecular, granule and polymorph. PLCXD1 shows preferential expression in granule cell layer (DGsg) with little to no expression in the polymorph (DGpo) and/or the molecular (DGmo) layers. The hippocampal formation is known to play important roles in the consolidation of information from short-term memory to long-term memory and spatial navigation and neurons within this region have been extensively studied with regards to the cellular basis of “learning” (Jarrard, L.E, 1993; Izquierdo, I. and Medina, 1997). Neural circuit behaviour within and between neurons of the CA1-CA3 region and the denate gyrus is known to be modified in and experience-dependent manner involving changes in synaptic strength and neuronal excitability. These changes can be manifested in either long-term potentiation (LTP) and/or long-term depression (LTD) of neuronal transmission (Bruel-Jungerman *et al*., 2007). Multiple receptors coupled to phospholipase C have been shown to be involved in the induction of LTD. Indeed, loss of PLC-specific signalling with inhibitors such as wortmannin, and more specifically, knock-out of PLCβ1 are known to impair LTD

(Reyes-Harde and Stanton, 1998). Similarly, the synaptic strength and neuronal excitability of Purkinje cells within the cerebellum is also known to be experience-dependent and this is thought to underlie the memory processes in the cerebellum of behaving animals (Jorntel and Hansel, 2006). The mRNA expression data for PLCXD1 may therefore be suggestive of a potential role in signal transduction in the hippocampus and cerebellum and potential association with learning and memory formation within these regions. In-order to further assess the role of PLCXD1 in memory formation, future creation of a specific knock-out mouse model would be crucial. Using this model, learning tests and local measurement of synaptic transmissions in the hippocampus could be performed. Future experiments could also aim to study the expression, localisation and regulation of PLCXD1 in neurons cultured from the hippocampal formation.

High mRNA levels of PLCXD2 were detected in the main olfactory bulb (MOB) and throughout the visual cortex (Allen Brain Atlas). Within the MOB, PLCXD2 mRNA expression was enriched in the mitral and periglomerular layers with little to no expression seen in the granule cell layer. These neurons are key elements of odor/pheromone processing and are directly involved in information processing to and from the olfactory epithelium, and the olfactory cortex and associated brain areas. Indeed, PLC-η2 (Nakahara *et al.*, 2005) and PLC-β 1 (Watanabe *et al.*, 1998) have also been shown to be expressed in the same neurons of the olfactory bulb. The presence of PLCXD2 mRNA within neurons of the MOB and the visual cortex suggests that PLCXD2 might specifically be involved in neural pathways underlying the transduction

and processing of sensory stimuli within higher brain regions. Further elucidation of the role played by PLCXD2 in sensory systems awaits the creation of PLCXD2 null mice.

In summary, tissue-distribution analysis reveals PLCXD1, 2 and 3 to be predominantly expressed in the brain and further analysis (at least for PLCXDs 1 and 2) reveal this expression to be mainly restricted to neurons within specific regions of the adult mouse brain. Together, these data suggest that PLCXD isoforms may play fundamental roles in nerve tissue function. Further work is needed to clarify the cellular functions of PLCXD1, 2 and 3 by, for example, analysis of PLCXD-deficient or overexpressing cells and/or PLCXD knock-out animals.

4.7.3. Cellular localisation

In-order to further characterise the basic principles surrounding the molecular functions of human PLCXD proteins, the sub-cellular localisation of these proteins was determined following the transfection of tagged constructs into HeLa cells and subsequent visualisation by immunofluorescence. Western blotting analysis of wildtype, untransfected HeLa cell lysates probed separately with monoclonal antibodies raised against each human PLCXD isoform failed to detect a band corresponding to PLCXD1, 2 or 3. Given that endogenous protein expression was undetectable in HeLa cells, immunofluorescence experiments were performed using HeLa cells (over)-expressing each PLCXD isoform. PLCXDs 1, 2 and 3 were expressed as fusion proteins containing a Pk/V5-tag, thereby allowing detection using an anti-Pk primary antibody. PLCXDs 1 and 3 were found to be localised within uncharacterised cytoplasmic and perinuclear vesicles suggestive of endoplasmic reticulum and/or Golgi apparatus. This indicates that both proteins may be involved in unknown intracellular

functions rather than existing as part of extracellular signalling processes occurring at the plasma membrane. In contrast, transfected PLCXD2.1 was found to be associated with the nucleus. Interestingly, phosphoinositides have been shown to be enriched within the nucleus along with a number of enzymes that regulate phosphoinositide metabolism (Gonzales and Anderson, 2006). Although the lipid binding specificities and substrate specificities of PLCXD2 are currently uncharacterised, evidence detailed within this thesis suggests that this protein is able to influence phosphoinositide turnover in cultured HeLa cells. Whether PLCXD2 has a direct or indirect effect on phosphoinositide turnover remains to be fully characterised, however its association with the nucleus is suggestive of a potential regulatory role in nuclear phosphoinositide metabolism.

Currently, this is the first attempt to characterise the sub-cellular localisation of any PLCXD isoform. The distinct nature of the sub-cellular localisations of PLCXDs 1, 2 and 3 is highly suggestive of unique functions within cellular physiology. Most eukaryotic proteins are encoded in the nuclear genome and synthesized either in the cytosol or endoplasmic reticulum where they can be further sorted to other subcellular compartments. Depending on the destination, the sorting of proteins relies on the presence of a targeting sequence that is recognised by translocation machinery. Translocation of a protein to the nucleus requires a nuclear transport mechanism initiated by a nuclear localisation signal (NLS) sequence on the protein (Lange *et al*., 2007) Such signals have been found in many nuclear proteins including PLC-β, where it is present as a cluster of basic residues at the C-terminus of the protein (Irvine, 2003). Interestingly, no classical nuclear localisation signal is predicted for PLCXD2.1. It is

possible that PLCXD2.1 could “piggyback” into the nucleus by binding to a nuclear protein however the exact mechanism of PLCXD2.1 nuclear remains to be characterised. Additionally, an interesting experiment would be to examine and compare the sub-cellular localisations of PLCXD2.2 and PLCXD2.3 splice variants and test whether they are also confined to the nucleus. This, however, awaits generation of HeLa cell lines stably expressing these proteins. At least for PLCXD1 and 3, future work should attempt to co-localise these proteins with various organelle-specific markers, including Golgi and endoplasmic reticulum markers. The sub-cellular localisation of PLCXD1, 2 and 3 described here need to be further verified in a cell line where endogenous protein expression can be detected with antibodies specific to each isoform.

4.7.4. *In vivo* phospholipase C assay

To investigate the potential of human PLCXDs acting as functional PI-PLCs, an *in vivo* phosphoinositide turnover assay was performed. All three hPLCXD isoforms were found to increase the endogenous phospholipase C activity in cultured HeLa cells in a calcium-independent manner. Although it is possible that the expressed PLCXDs mediate indirect increases in expression and/or activity of the endogenous HeLa cell PI-PLCs, given the sequence similarities with the bacterial PI-PLCs it is likely that PLCXDs have their own phospholipase C activity. In-order to determine whether the observed increases in PI turnover are due to PLCXDs having their own phospholipase C activity, the PI turnover assay could be repeated with mutant PLCXDs lakcing the two catalytic histidine residues. The increased activity in all cells seen with the ionophore could be accounted for by an enhanced activity of endogenous PI-PLCs, most of which

are stimulated by increasing calcium concentrations. All existing mammalian PI-PLCs have been shown to hydrolyse $PI(4,5)P_2$ in a calcium-dependent manner whereas bacterial PI-PLCs show no metal-ion dependency and do not cleave multi-phosphorylated forms of PI (Essen *et al.*, 1997). Interestingly, the absolute increase in PI-phospholipid turnover in cells over-expressing PLCXD1 and PLCXD3 was lower in the presence of the ionophore, indicating a possible attenuation of PLCXD1 and 3 actions in the presence of excess calcium. With respect to the apparent lack of stimulation by calcium *in vivo* and the conservation of the Arg69 residue, known in bacterial PI-PLCs to occupy the location of Ca^{2+} in the eukaryotic enzymes, the human PLCXDs may be functionally more similar to bacterial PI-PLCs than other mammalian PI-PLCs. Alternatively the observed results may be due to the stress induced by protein overexpression. From this it is clear that the ability of the different human PLCXD isoforms to directly hydrolyse various PI and $PI(4,5)P_2$ needs to be investigated and these experiments are described in Chapter 5.

CHAPTER 5: Expression analysis of PLCXDs 1, 2 and 3 in the tissues of Harlequin mice.

5.1. Introduction

The Harlequin (*Hq*) mouse is a naturally occurring genetic mouse model of late-onset neurodegeneration. The phenotype of *Hq* mice is mainly characterised by progressive cerebella neuron defects, including the degeneration of granule and purkinje cells, which begins at 4 months of age and continues with progressive ataxia symptoms. In addition, progressive loss of retinal neurons is also evident in *Hq* mice, including ganglion and amacrine cells, which begins at 3 months and eventually leads to blindness (Bouaita *et al*., 2012). The *Hq* mouse carries an X-linked recessive mutation in the apoptosis-inducing factor (AIF) gene, identified as a retroviral insertion in the first intron, which severely reduces the expression of the AIF gene by 80% in mutant mice (Klein *et al*., 2002). AIF has nicotinamide adenine dinucleotide (NADH) oxidase activity and is found on the inner membrane of the mitochondria and plays a role in respiratory chain complex I biogenesis (Susin *et al*., 1999). Alternative splicing of the AIF mRNA precursor is known to give rise to four distinct isoforms (AIF1-4; Hangen *et al*., 2010). Reduced levels of both AIF1 and AIF2 is thought to increase the susceptibility of neurons to free radical damage leading to abnormal cell cycle re-entry and death of terminally differentiated cerebella and retinal neurons (Klein *et al*., 2002; Bouaita et al., 2012).

Previously we proposed hypothetical functions for PLCXDs based on high levels of expression, relative to Rpl-P0, in the mouse brain. Furthermore, expression analysis revealed, at least for PLCXD2 and 3, detectable mRNA levels within the mouse eye and *in situ* hydridisation studies revealed the presence of PLCXD1 and 3 mRNA levels within the mouse cerebellum. Given these findings, it was of interest to further characterise

the mRNA expression levels and cellular localisation of all three PLCXD isoforms in the cerebellum and retina of both wild-type (WT) and *Hq* mutant mice to establish a potential role for PLCXDs in neurodegeneration.

5.2. Analysis of mRNA expression levels and the cellular localisation of PLCXD isoforms in wild-type and the Harlequin mouse

Previous studies have shown the mRNA levels of AIF1 and AIF2 to be reduced in the retina (~96%; Bouaita *et al*., 2012) of *Hq* mice compared to control animals (Bouaita et al., 2012). In addition, the mRNA-levels of Brn3a, which is a specific marker of retinal ganglion cells, has been shown to be reduced to ~50% of control values in *Hq* retinas (Bouaita *et al*., 2012). We obtained six retina and six cerebellum samples from both control and *Hq* mutant mice (Generous gift from Dr Marisol Corral-Debrinski, Institue de la Vision, Paris). As an important first step, RT-qPCR (Chapter 2, Section 2.7.11) was performed using gene-specific primers for AIF1 and 2, and Brn3a to confirm previously the observed down-regulations associated with the *Hq* phenotype. In the retina of *Hq* mutant mice, our analysis revealed suppression of both AIF1 and AIF2 mRNAs by 96%, and Brn3a mRNA by 43% to the control samples (Figure 5.1A). We also found the levels of AIF1 and AIF2 mRNA in Hq mice to be reduced by ~70% and ~60% respectively, in the cerebellum compared to control samples (Figure 5.1B).

In-order to test whether PLCXDs 1, 2 and 3 are involved in the phenotypes associated with the *Hq* mutants, the cerebellar and retinal expressions of the gene transcripts and proteins were examined. Total RNA and protein was extracted from the cerebellum of six WT and six *Hq* mutant mice, as previously described. Unfortunately due to tissue availability only RNA was available from retinal samples of six WT and six *Hq* mutant

mice. RT-qPCR analysis of cDNA prepared from these tissues revealed PLCXD2 and 3 transcript levels to significantly decrease in the retina of *Hq* mutant mice (Figure 5.2). In contrast, PLCXD1 levels were undetectable in both the cerebellum and retina samples from WT and *Hq* mutant mice (data not shown). No significant differences in PLCXD2 and PLCXD3 transcript levels were observed between cerebellar samples of control and *Hq* mutant mice (Figure 5.3A). Interestingly, western blotting analysis using a purified antibody against the N-terminus of PLCXD3, showed PLCXD3 protein levels to be undetectable in the cerebellum of *Hq* mutant mice compared to control mice where a band of 36 kDa was obtained, corresponding to the expected molecular size of mouse PLCXD3 (Figure 5.3B).

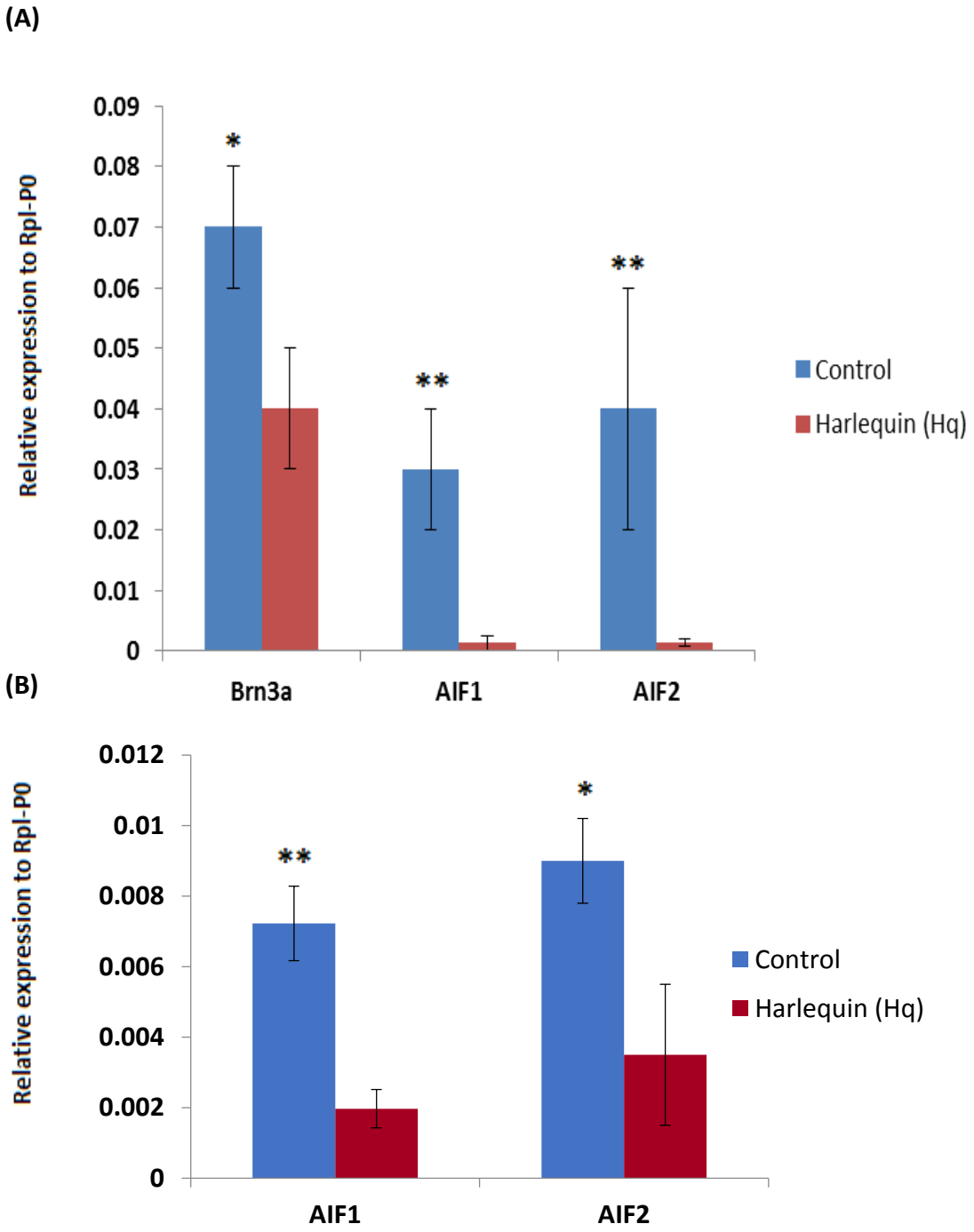

Figure 5.1: RT-qPCR analysis of the relative transcript levels of AIF1 and 2 and Brn3A in the retina (A) and the cerebellum (B) of control and *Hq* mutant mice. Total RNA was prepared from a total of six retina and six cerebellar samples from control and *Hq* mutant mice (mean +/- SEM presented). Values on the Y-axis represent relative expression to Rpl-P0. * P< 0.05, **P< 0.01

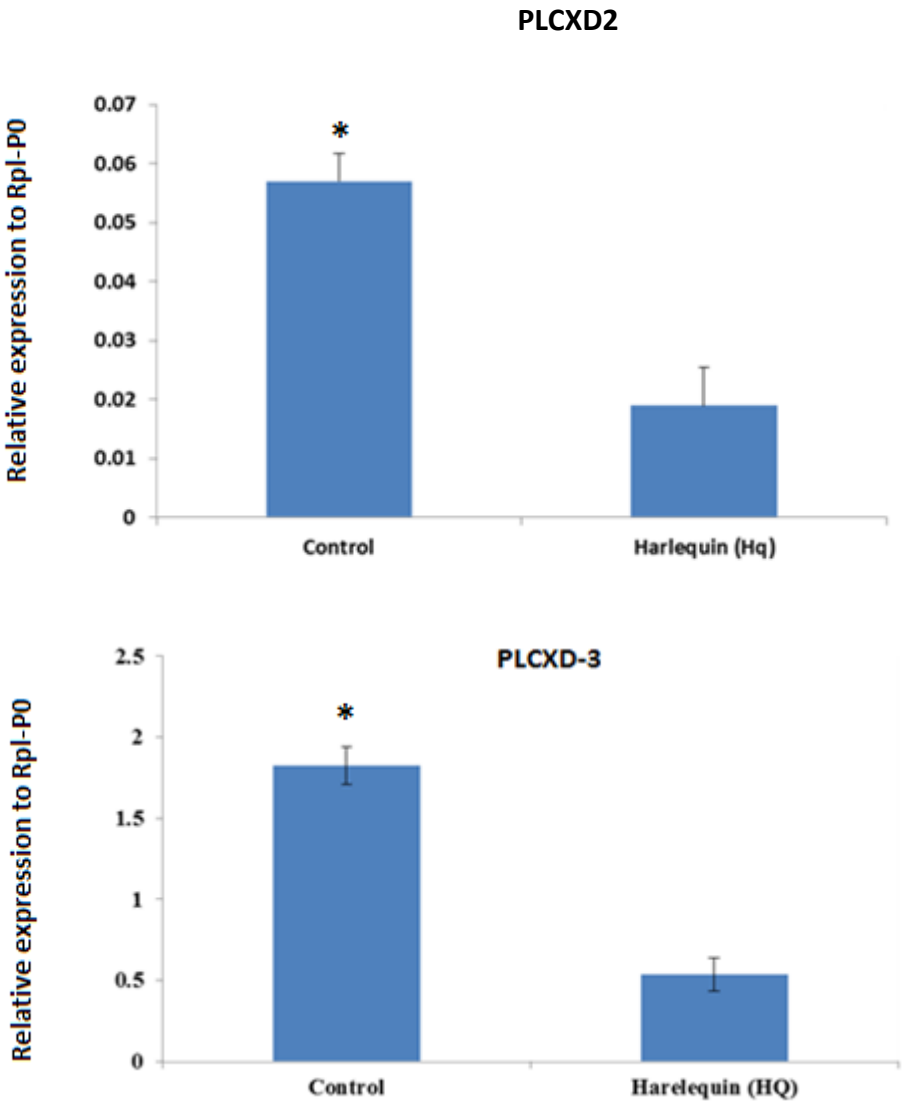

Figure 5.2: Quantification of PLCXD isoform expression in the retina. RT-qPCR assays were performed with total RNAs from retinas to determine the levels of PLCXD2 and 3 mRNAs. Six independent RNA preparations of retinas were evaluated for both wild-type and Harlequin (Hq) mutant mice (mean +/- SEM presented, ** $p < 0.01$ and * $p < 0.05$). Values on the Y-axis represent relative expression to Rpl-P0.

(A)

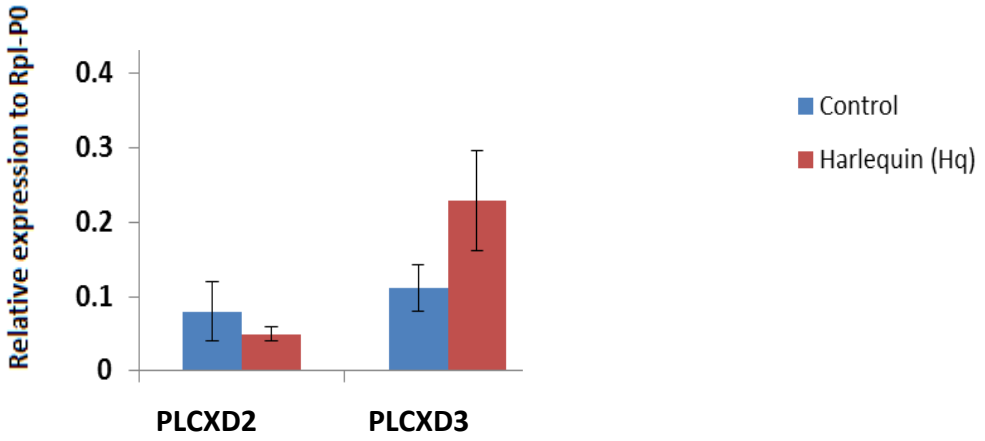

(B)

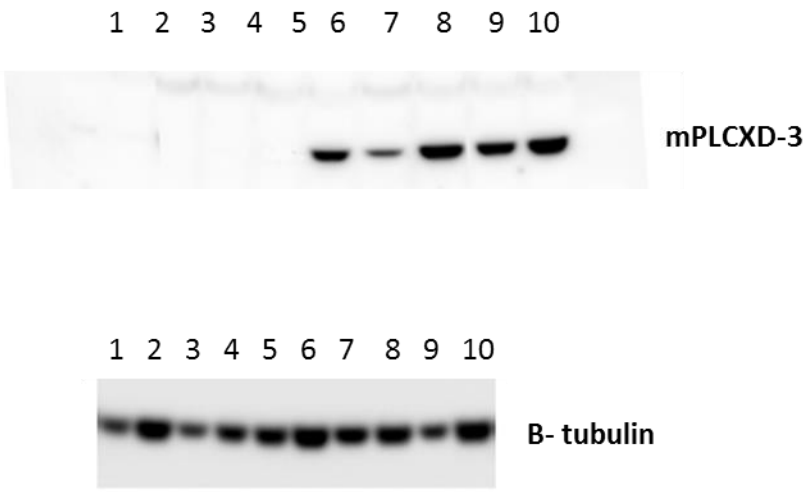

Figure 5.3: **(A)** Quantification of PLCXD2 and 3 transcript levels in the cerebellum of *Hq* mutant and control mice. Total RNA was extracted from the cerebellum of six control and six *Hq* mutant mice and cDNA conversions and RT-qPCR assays subsequently performed. Relative levels were calculated using *Rpl-P0* as the normalizing gene. **(B)** Western blot analysis of PLCXD3 protein levels in cerebellar lysates from five control and five *Hq* mutant mice. 10 µg of total protein was loaded per each lane. A standard western blotting procedure was carried out using a purifed antibody raised against the N-terminus of human PLCXD3. Alpha-tubulin was included as the loading control. Lanes 1-5 represent *Hq* mutant mice, and lanes 6-10 represent control mice, in both blots.

5.3. Immunofluorescence analysis of retinal nerves from Control and Harlequin mice

To further elucidate the functional role of PLCXD3 in the mouse retina, its subcellular distribution in retinal sections was analysed by immunostaining. This work was carried out in collaboration with Dr Marisol Corral-Debrinski, Institut de la Vision, Paris, France. Retinal sections were obtained for both wild-type and Harlequin mutant mice (n=6 for each) and were probed with an N-terminal affinity purified anti-hPLCXD3 antibody, as described in Section 2.8.4. Cells immuno-positive for PLCXD3 (green; Figure 5.4A, B and C) were found in the ganglion cell layer (GCL) and the inner nuclear layer (INL), with a decrease in the numbers of PLCXD3 positive cells in Harlequin mutant mice. To further characterise the PLCXD3 positive cells, immunolocalisation was performed for a variety of cell type-specific markers, including Brn3A (retinal ganglion cells; red Figure 5.4B), calretinin (amacrine cells; red Figure 5.4A) and paralbumin (bipolar and retinal ganglion cells; Red Figure 5.4C). Antibodies for these markers were kindly provided by Dr Marisol Corrall-Debrinski. It clearly appeared that PLCXD3 (green) expression is found in amacrine cells specifically labelled with an antibody against the calcium-binding protein calretinin (red), within the INL and GCL (Figure 5.4A). PLCXD3 positive cells were found to be negative for Brn3A and paralbumin (Figure 5.4B and C respectively). Elucidation of the immuno-localisation of PLCXD2 in retinal sections awaits antibody preparation.

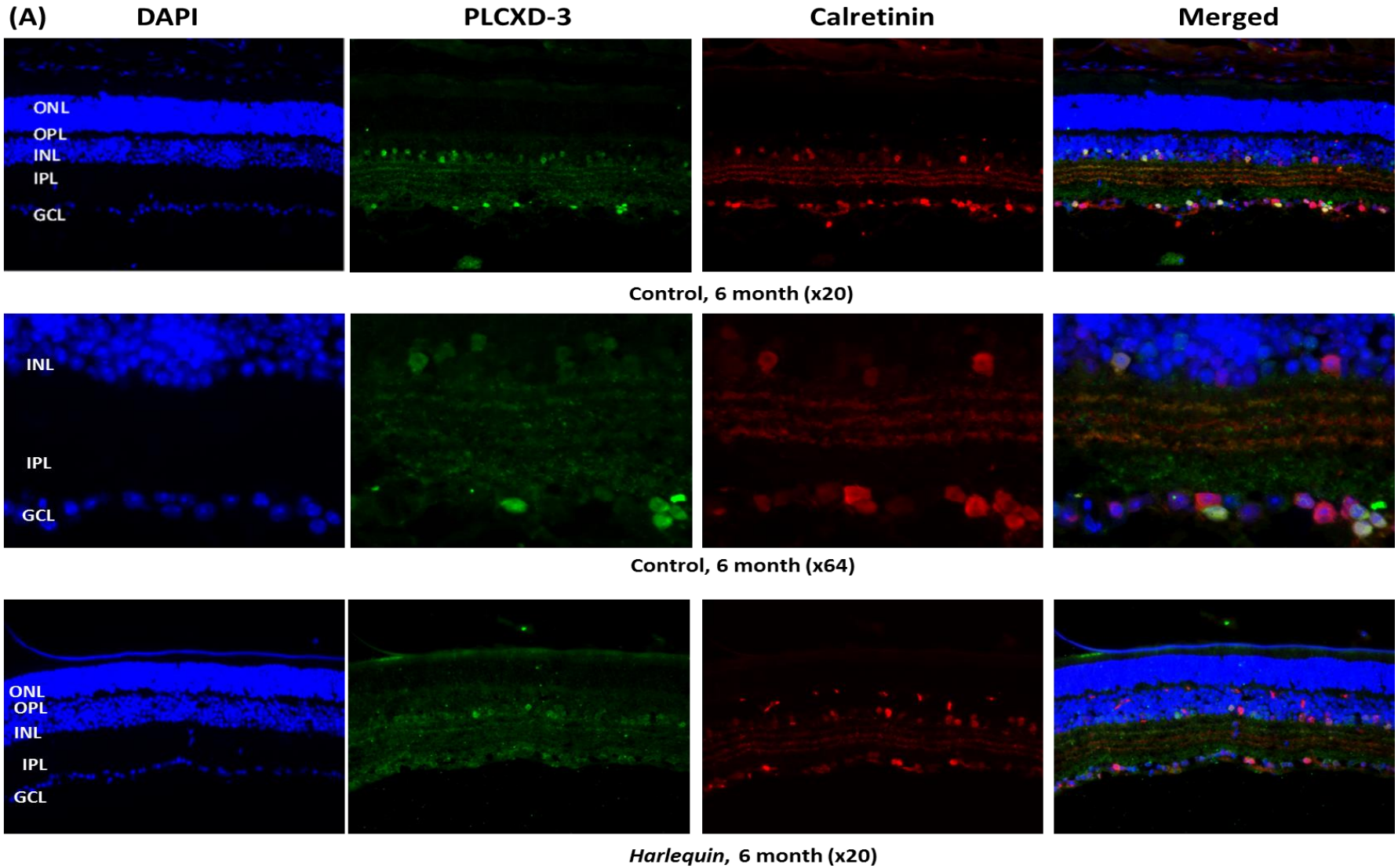
(A)
DAPI
PLCXD-3
Calretinin
Merged
ONL
OPL
INL
IPL
GCL
Control, 6 month (x20)
INL
IPL
GCL
Control, 6 month (x64)
ONL
OPL
INL
IPL
GCL
Harlequin, 6 month (x20)

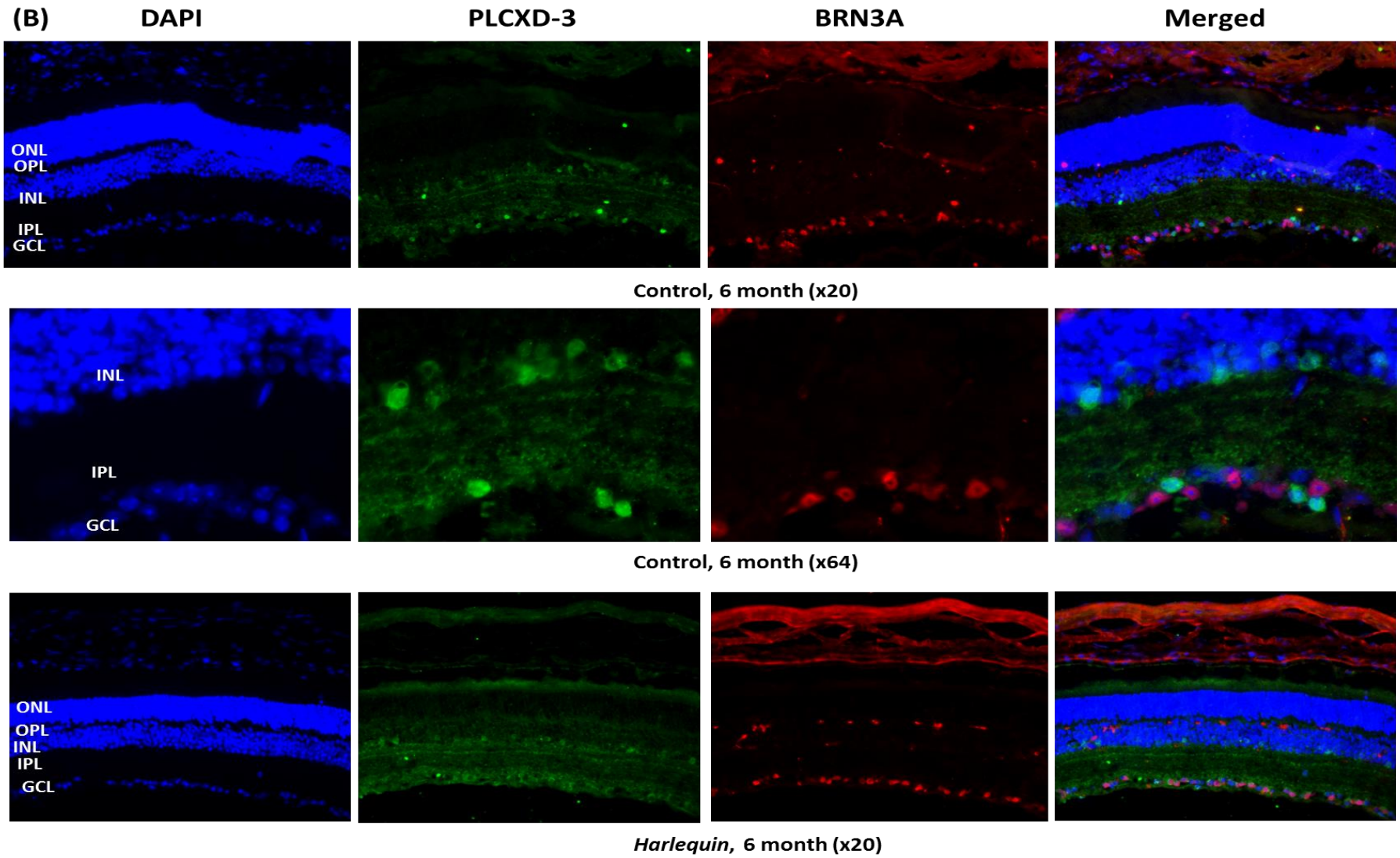
(B)
DAPI
PLCXD-3
BRN3A
Merged
ONL
OPL
INL
IPL
GCL
Control, 6 month (x20)
INL
IPL
GCL
Control, 6 month (x64)
ONL
OPL
INL
IPL
GCL
Harlequin, 6 month (x20)

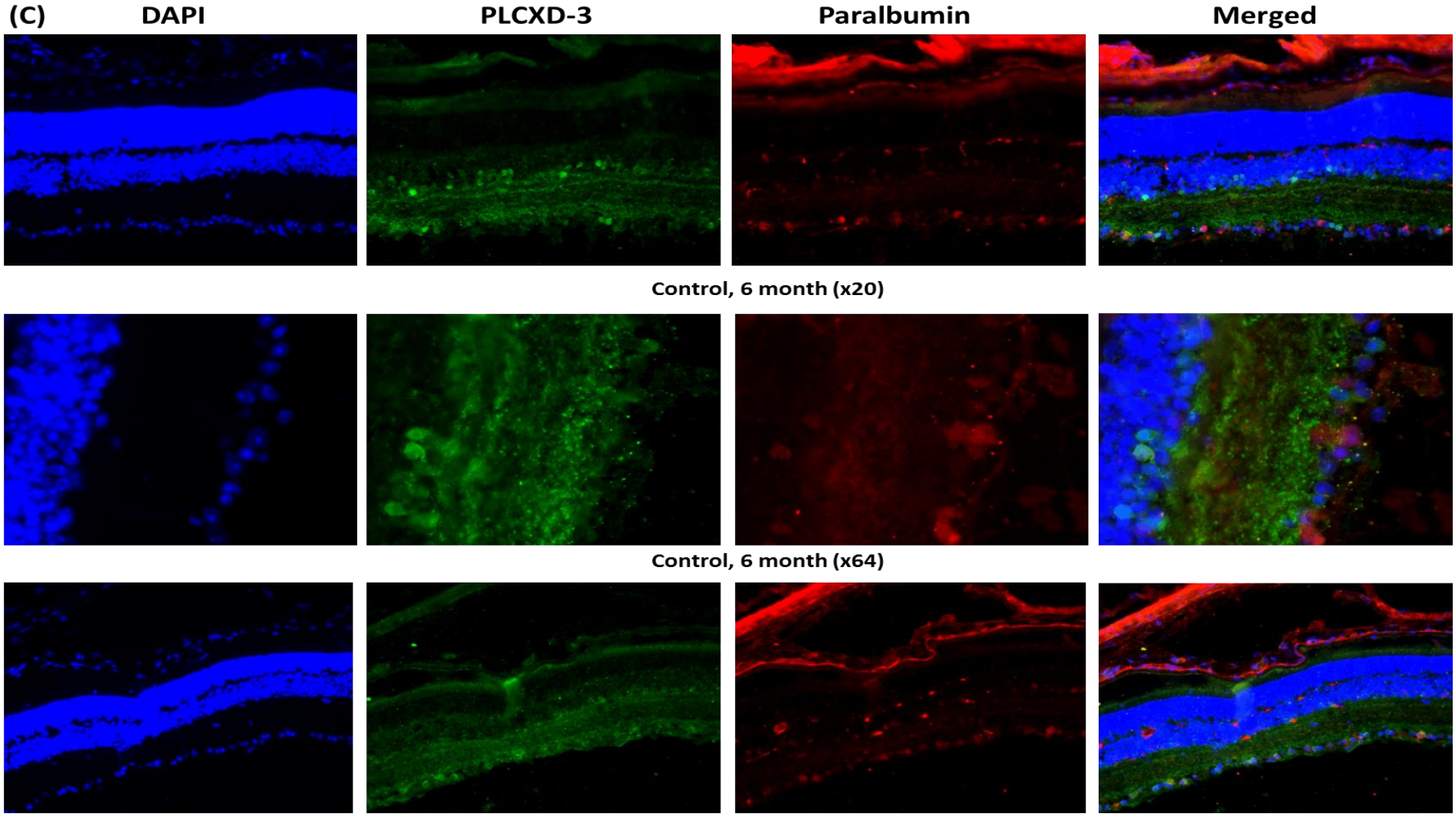
(C)
DAPI
PLCXD-3
Paralbumin
Merged
Control, 6 month (x20)
Control, 6 month (x64)
Harlequin, 6 month (x20)

Figure 5.4: Immunofluorescence analysis of retinas from control and *Hq* mice. (A, B, C) Immunostaining for PLCXD-3 (Green) and Calretinin (Red; A), BRN3A (Red; B) and Paralbumin (Red; C) in the retina from control mice aged 6 months; PLCXD-3 expression was restricted to the ganglion cell layer (GCL) and the inner nuclear layer (INL). Brn3A immunostaining has been reported as a reliable and simple method for identifying retinal ganglion cells (RGCs) in retinal cross sections; paralbum is specific for RGCs and bipolar cells; Calretinin is specific for amacrine cells. PLCXD-3 positive cells were also found to be positive for calretinin suggesting that PLCXD-3 is confined to amacrine cells. *Hq* mice experienced a decrease in PLCXD-3 expression. In the control sections, a 3-fold zoom was included to better visualise potential co-localisations. GCL, galnglion cell layer; IPL, Inner polar layer; INL, Inner nuclear layer; OPL, outer polar layer; ONL, outer nuclear layer.

5.4. Discussion

Harlequin (*Hq*) mutant mice represent a reliable genetic model for age-related neurodegeneration. Aging *Hq* mutant mice experience progressive retinal and cerebellar cell degeneration, which eventually leads to blindness (Bouaita *et al*., 2012). The *Hq* phenotype is caused by an ecotopic proviral insertion into intron 1 of the apoptosis-inducing factor (AIF) gene, resulting in a reduction in transcript and protein levels (Klein *et al*., 2002). Interestingly, AIF was first discovered as a caspase-independent apoptotic effector, which in dying cells, relocates from the mitochondria to the nucleus where it is thought to mediate chromatin condensation and large-scale DNA fragmentation (Modjtahedi *et al*., 2006). Recent elucidation of the crystal structure of both murine and human AIF proteins reveals that, in addition to a DNA binding domain, AIF contains an oxidoreductase domain, with a similar fold to the eukaryotic glutathione reductase family of enzymes (Mate *et al*., 2002) New work has been conducted to shed light on the molecular mechanisms by which mutant AIF results in neurodegeneration. Klein *et al*., 2002 have shown that cerebellar granule cells and retinal neurons from *Hq* mutant mice are more susceptible to hydrogen

peroxide-mediated cell death than their wild-type counterparts, a response that can be rescued following retroviral transduction of wild-type AIF. The mechanisms underlying AIF-mediated protection from peroxide insult in neurons are as yet unclear, with scavenging of hydrogen peroxide or maintenance of normal mitochondrial respiration being proposed (Klein et al., 2002).

Previously, we have shown mouse PLCXD isoform transcripts to be predominantly expressed in the brain, with expression also being detected in numerous other tissues including the eye. Given that the phenotypes associated with the *Hq* mouse mutant are mostly restricted to neurons within the cerebellum and retina, we were interested to further characterise the expressions of PLCXD isoforms in these tissues from both wild-type and mutant mice. Towards this aim, we examined the expression levels of PLCXD transcripts and protein in the cerebella and retinas of six wild-type and six *Hq* mutant mice. In the *Hq* mutant mice, PLCXD2 and 3 transcript levels in the retina were found to be 50-60% of their wild-type counterparts. Although protein samples from the retinas of wild-type and *Hq* mutant mice are currently unavailable, immunofluorescence suggested a reduction in PLCXD3-specific staining in retinal sections from *Hq* mutant mice. Although reductions in immunofluorescence were observed, this would need to be confirmed by quantitative immunofluorescent experiments. Immunofluorescence revealed positive staining for PLCXD3 in the ganglionic cell layer (GCL) and the inner nuclear layer (INL) of the retina which, in most cases, also stained positive for the cholinergic amacrine cell-specific marker, calretinin. However, PLCXD3 positive staining did not fully co-localise with that of calretinin. Biochemical, histochemical and pharmacological studies suggest around 30 different

amacrine cell sub-types, to exist within the mouse retina (MacNeil *et al*., 1999; Kunzevitzky *et al*., 2013) and therefore PLCXD3 positive staining that did not co-localise with the calretinin marker, may represent the expression of PLCXD3 in more than one amacrine cell subtype. Alternatively, PLCXD3 may also be localised to retinal cells distinct from amacrine cells. Full elucidation of the localisation of PLCXD3 within the retina therefore requires further co-localisation experiments with various other cell-specific markers. The transcript levels of PLCXD1 were undetectable in our assay conditions suggesting that this isoform is expressed at very low levels. Future experiments could aim to convert a higher concentration of mouse retinal RNA to cDNA in an attempt to obtain a detectable signal for PLCXD1.

In the cerebellum of *Hq* mutant mice, the transcript levels of PLCXD2 and 3 isoforms were expressed at similar levels to that of wild-type mice. Interestingly, western blot analysis showed a complete disappearance of the expression of PLCXD3 protein expression in the cerebellum of *Hq* mutant mice. Very often mRNA changes are reflected in protein levels; however it appears that in this case the two parameters change independently. Therefore for PLCXD3, results suggest that there is a decrease in protein expression within the cerebellum of *Hq* mutant mice, which is due to as yet uncharacterised post-transcriptional changes, potentially affecting either mRNA transport and/or translation efficiency.

In summary, we have demonstrated specific and significant decreases in mRNA expression of PLCXD2 and 3, and although no absolute quantitative studies have been carried out, preliminary immunofluorescence suggests a reduction in the number of

cells within the retina of *Hq* mutant mice that express PLCXD3 protein. Additionally, western blot analyses indicates a > 99% fall in PLCXD3 protein levels in the cerebellum of *Hq* mutant mice. Retinal and cerebellar neurons of *Hq* mutant mice have reduced AIF1 and AIF2 levels and this is thought to predispose these cells to peroxide-mediated cell death. Furthermore, these cells could be rescued by retroviral transfection with AIF cDNA (Klein et al., 2002). How AIF can act to reduce oxidative stress *in vivo* is currently unknown. Oxidative stress is thought to lead to neurodegeneration by inducing abnormal cell cycle re-entry in terminally differentiated neurons by an unknown mechanism. Further investigations into the role of PLCXDs in *Hq* pathologies are now needed to clarify the association between the disease phenotype and changes to PLCXD mRNA and protein expression. It would be interesting to determine whether PLCXD mRNA and protein levels are influenced by oxidative stress within neurons. This might be tested by RT-qPCR and western blotting analysis of primary neuron cultures in the presence and absence of chemically induced oxidative stress. More work is also required to establish whether a decrease in the levels of PLCXDs mRNA and/or protein are associated with the mechanisms underlying oxidative stress-induced aberrant cell cycle re-entry.

In further support of a potential role for PLCXDs in neurodegeneration, three intronic SNPs in the PLCXD3 gene have recently been shown to be associated with increased risk of variant Creutzfeld-Jakob disease (CJD) (Bishop *et al*., 2013). Sequencing revealed that these SNPs were found at the junction of intron 1 and exon 2, close to the splice site motifs (Bishop *et al*., 2013). Interestingly, exon 2 encodes the X-domain of PLCXD3, including the two putative catalytic histidine residues. Whether the

presence of these SNPs in PLCXD3 alters the functioning of the spliceosome between intron 1 and exon 2, and therefore the expression and activity of PLCXD3 is currently unknown. Future experiments should measure both mRNA and protein levels of PLCXD3 in postmortem specimens from persons with CJD. Similarly with *Hq* mutant mice, the association of oxidative stress and abnormal cycle progression has been reported in various human neurodegenerative disorders, including Alzheimers disease (AD; Klein and Ackerman, 2003). Studies of AD found many cell cycle regulators to be expressed in terminally differentiated neurons of affected regions, which led to DNA replication and subsequent progression to apoptosis and not mitosis (Nagy *et al*., 1998). Whether the accumulation of PrP^{Sc} causes abnormal cell cycle re-entry in terminally differentiated neurons is yet to be established. It would be interesting to test whether PLCXD mRNA and protein levels are altered in post-mortem specimens from persons with AD and other common neurodegenerative diseases.

Chapter 6: Recombinant expression, purification and characterisation of human PLCXD1, 2 and 3

6.1. Introduction

As highlighted in Chapter 1, eukaryotic PI-PLCs play a central role in most signal transduction cascades through the regulated hydrolysis of PtdIns(4,5)P_2 producing the IP_3 and DAG second messengers which are responsible for Ca^{2+}-mobilisation and protein kinase C-activation. By altering membrane levels of PtdIns(4,5)P_2, PI-PLC enzymes are also known to affect the membrane association and activities of many other signalling proteins (Chapter 1, Section 1.3.2.) In contrast, bacterial PI-PLCs have much smaller molecular masses (30-35 kDa), consisting of only an X-domain, and are known to hydrolyse phosphatidylinositol (PI). From the crystal structures of rat PLCδ1 and *B. cereus* PI-PLCs, it is possible that both mammalian and bacterial PI-PLCs have a similar catalytic mechanism, characterised by general acid general base catalysis. Two active site histidine residues (His32 and His 82 in *B. cereus*; His311 and His356 in PLCδ1) are strictly conserved in all catalytically active PI-PLCs. A striking difference between mammalian and bacterial PI-PLCs is the utilisation of calcium within the active site (Section 1.4.3.1.). In the calcium-independent bacterial PI-PLCs, Arg69 functions analogously to that of Ca^{2+} in the mammalian PI-PLCs (Section 1.4.3.1). This difference in calcium dependency is thought to underlie the fact that bacterial enzymes only complete the first step in catalysis and produce mainly the cyclic product, Ins(1:2cyc)P; mammalian PI-PLCs mainly produce both cyclic and acyclic inositol phosphates.

Based on the primary amino acid sequences, all cloned hPLCXD isoforms show features typical of PI-PLC enzymes and contain the two conserved His residues. In addition, similarly with bacterial PI-PLCs, hPLCXD isoforms have an arginine residue analogously positioned with Arg69 from *B. cereus*. Although bacterial and other mammalian PI-PLC

enzymes have undergone numerous biochemical and structural studies, no data exists describing the basic molecular functions of hPLCXD isoforms. Towards this aim, we have cloned full-length versions of hPLCXD1, 2.1 and 3 isoforms and expressed them as recombinant proteins in *E.coli.* This chapter describes initial attempts to express hPLCXDs as recombinant protein in *E. coli* for protein purification and subsequent biochemical and structural characterisation.

6.2. RT-PCR amplification of human PLCXD1, 2 and 3 and sub-cloning to expression vectors

In-order to express PLCXD proteins for biochemical and structural studies, large amounts of purified protein must be generated. Towards this aim, the nucleotide sequences of the coding regions of human PLCXD1, 2 and 3 were amplified from cDNA prepared from HeLa cells using standard PCR protocols (Chapter 2, Section 2.7.6.). For PLCXD1 and 3, the primers used were designed to create an *NcoI* and a *HindIII* site 5' and 3' to the initiation and termination codons, respectively, whereas primers used for PLCXD2.1 contained the restriction sites *NdeI* (sense primer) and *HindIII* (antisense primer). A table of primers is shown in Appendix C. As shown in Figure 6.1, the amplified products were all approximately 1kbp is length, which is in accordance with the length of the PLCXD1, 2 and 3 coding regions (971, 914 and 965bp respectively). These PCR fragments were purified and subsequently digested with the appropriate restriction enzymes allowing for insertion into the appropriate expression vector- pET M11 for PLCXDs 1 and 3; pET 22b+ for PLCXD2 (See Chapter 2, Section 2.6 for vector maps). The resulting constructs were used to transform TOP10 cells, as decribed in Chapter 2, Section 2.2.4. A number of colonies were selected and colony PCR was

carried out to check for the presence of each gene insert. A fragment of ~1200 bp was amplified using vector-specific sense and antisense primers (Figure 6.2; See Appendix E for primer sequences). Three colonies were selected for each PLCXD isoform, their plasmids purified and the sequence of the insert confirmed as described in Chapter 2, Section 2.6.9, using vector-specific primer sequences.

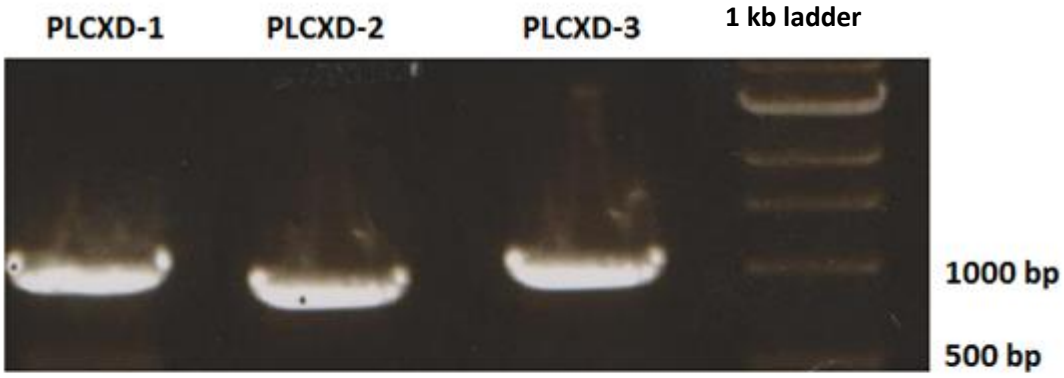

Figure 6.1: Gel electrophoresis of PCR products following amplification of PLCXD1, 2 and 3 using gene-specific primers. Total RNA was extracted from HeLa cells and converted to cDNA, which was used as a template in the amplifications. A 1kb DNA ladder molecular marker (NEB) was used for size estimation.

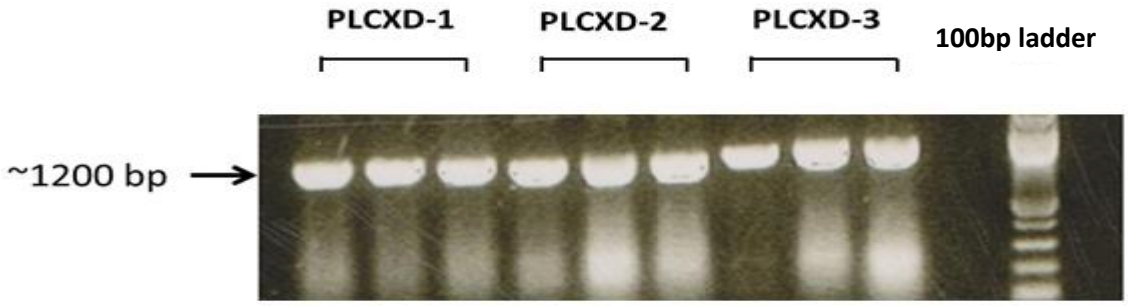

Figure 6.2: Gel electrophoresis of colony PCR products amplified using vector-specific sense and anti-sense primers (pETM11 A/AS and pET22b+ S/AS; Appendix E). PLCXD1 and 3 were inserted into the pET M-11 vector whereas PLCXD2 was inserted to pET 22b+. A 100 bp DNA ladder molecular marker (M; NEB) was used for size estimation.

6.3. Recombinant over-expression of hPLCXDs 1, 2 and 3 in *E.coli*

Sequence-confirmed expression vector constructs for hPLCXDs 1, 2 or 3 were used to transform the *E.coli* expression host, Rossetta (DE3) pLys S (See Chapter 2, Table 2.1 for more details). Initial expression trials for PLCXD1, 2 and 3 were conducted on a small scale (50 mL cultures) in order to assess the extent of induction and solubility of each PLCXD isoform when expressed as a recombinant protein in *E.coli* (Chapter 2, Section 2.2.5.1). Recombinant proteins were expressed following addition of 1 mM IPTG and the growth of cells at 37 °C for 4 hours (Chapter 2, Section 2.2.5.1.) Following induction of protein expression by addition of IPTG, bacterial cells were harvested and lysed using standard methods (Chapter 2, Section 2.8.6), and samples taken from the total lysate and the soluble extract. Equal amounts of protein (10 μg) from the total lysate and soluble extract fractions were separated and analysed by SDS-PAGE gel electrophoresis (as described in Section 2.8.3) and protein bands detected following Coomassie blue staining (as described Section 2.8.4) For hPLCXDs 1, 2 and 3, bands of the expected size (39.7, 37.8 and 39.4 kDa respectively) corresponding to $(His)_6$-tagged versions of the protein of interest, were present in the total lysates of Rosetta cells following induction at 37 °C for 4 hours. In each case, however, no soluble expression was observed for hPLCXDs 1 and 2, and only limited soluble expression was observed for hPLCXD3 (Figure 6.3). In an attempt to optimise protein solubility, the induction of protein expression was conducted at a lower temperature of 25 °C and induction time was increased to 20 hours. Additionally, the resulting solubilities of expressed hPLCXDs 1, 2 and 3 were determined following induction with the lower IPTG concentrations of 0.5 mM and 0.2 mM. No improvements in the solubility of hPLCXD1, 2 and 3 were seen

either using lower IPTG concentrations or reduced induction temperatures (data not shown). The best soluble expression was seen with hPLCXD3 when induced with 1 mM IPTG at 37 °C for 3 hours in both *E. coli* strains and therefore this condition was chosen for scale-up purification. Further optimisation of hPLCXD1 and 2 inductions is required to enable reasonable scale-up purification experiments.

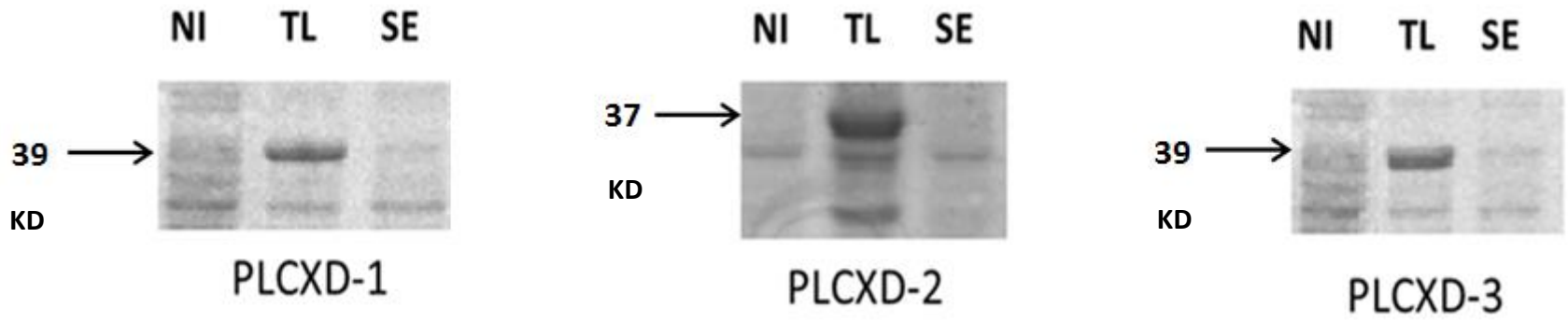

Figure 6.3: SDS-PAGE analysis of recombinant expression of PLCXD1, 2 and 3 in *E.coli* cells. Total protein was extracted from *E.coli* prior to (non-induced; NI) and following induction of protein expression with IPTG at 37 °C for 4 hours. Protein samples in the total lysate (TL) of cells extracted following induction of protein expression were subsequently centrifuged to yield a soluble fraction (soluble extract; SE). 10 µg of protein was loaded into each lane and proteins were detected with Coomassie blue. Protein bands for PLCXD1, 2 and 3 represent His-tagged versions. Similar results were obtained when human PLCXDs were expressed in Rosetta and C41 cells, with protein induction at 37 °C or 25 °C for 4 hours and 20 hours, respectively. Western blotting analysis revealed consistent results (data not shown).

6.4. Scale-up purification of human PLCXD3

The recombinant hPLCXD3 protein expression was scaled-up to a 30 litre culture using standard methods as detailed Chapter 2, Section 2.2.5.2. Bacterial cell pellets containing hPLCXD3 were harvested, pooled and re-suspended to homogeneity in lysis buffer containing a DNAse and EDTA-free protease inhibitor cocktail (Chapter 2, Section 2.8.6). Proteins were then extracted and $(His)_6$-tagged hPLCXD3 was purified using nickel chromatography (Chapter 2, Section 2.8.6.). hPLCXD3 bound to the column was eluted using an imidazole gradient and fractions containing hPLCXD3 identified by SDS-PAGE (Figure 6.4A). A protein of around 40 kDa was displaced from the Ni^{2+} column at 60 mM imidazole, corresponding to $(His)_6$-tagged hPLCXD3. Samples containing the 40 kDa band were pooled and subsequently dialysed against two changes of lysis buffer to remove any extra imidazole. In-order to remove the $(His)_6$-tag from hPLCXD3, TEV was added to the dialysis tube containing $(His)_6$-tagged PLCXD3 (1 µg protease for 1 mg) and digestion was conducted overnight at 4°C (Chapter 2, Section 2.8.7.) Following dialysis and TEV digestion, the pooled eluate fraction was loaded onto the Ni^{2+} column, as before, and the flow-through was collected and analysed by SDS-PAGE (Figure 6.4B). A protein band of 35 kDa was detected which corresponds to hPLCXD3 devoid of the $(His)_6$-tag. The flow-through was subsequently dialysed, concentrated to 3 ml and then loaded onto a gel filtration column. Corresponding fractions containing hPLCXD3 were identified and confirmed by SDS-PAGE analysis (Figure 6.4D). A major protein band corresponding to the expected size of hPLCXD3 and two additional bands at 30 and 25 kDa were detected by SDS-PAGE analysis (Figure 6.4 C). Fractions containing PLCXD3 were pooled and concentrated to 10 mg/mL, aliquoted, flash frozen and then stored at -80°C

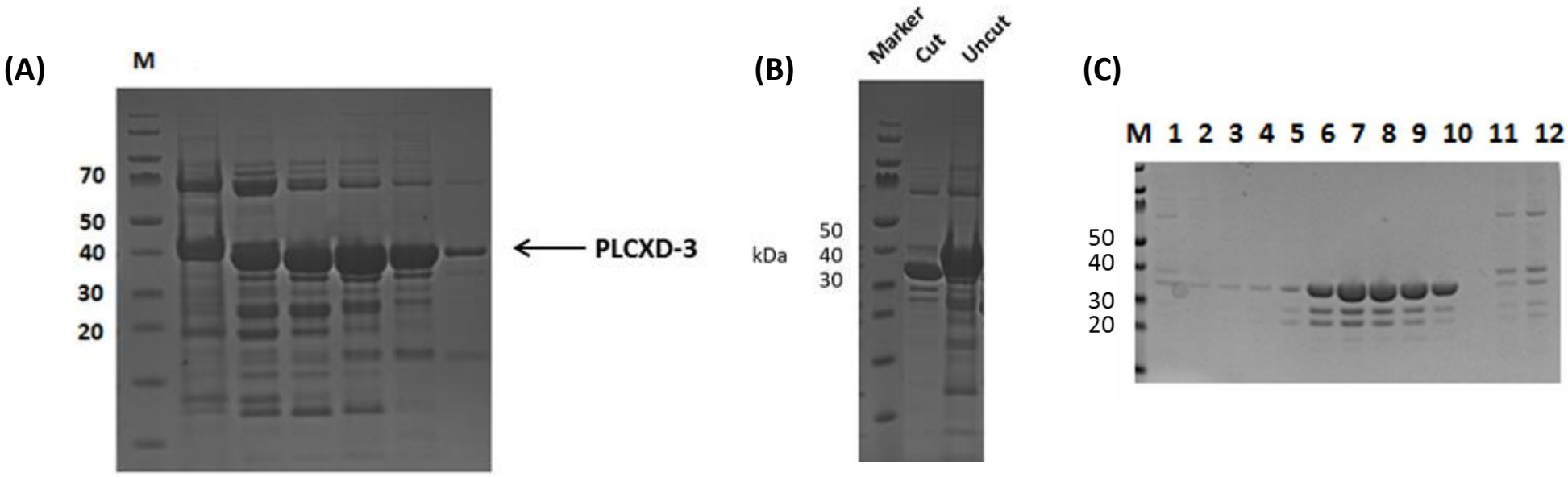

Figure 6.4: Expression and purification of human PLCXD3 protein using Ni^{2+} affinity chromatography and AKTA technology. (A) Comassie-stained SDS-PAGE gel of the proteins present in various fractions following elution of the the first Ni^{2+} column with different concentrations of imidazole; M, molecular marker. **(B)** TEV cleavage of His-tagged PLCXD3. Uncut lane, dialysed eluted protein from first Ni^{2+}-affinity column; Cut lane, flow-through of the second Ni^{2+}-affinity column following TEV digested sample of PLCXD-3. **(C)** Comassia-stained SDS-PAGE gel of the eluted proteins following gel filtration chromatography of the dialysed TEV digested fractions.

6.5. Pk/V5-tag co-immunoprecipitation (co-IP) of human PLCXD3 from HeLa

HeLa cell lines stably expressing N-terminal Pk/V5-tagged versions of PLCXD3 were previously created in collaboration with Dr Svetlana Kalujnaia using a lentivirus based-transfection approach (Chapter 2, Section 2.3.4.). For co-IP assays, wild-type (control; non-transfected) and hPLCXD3 transfected cells were grown and maintained in 4 x 75 cm^2 culture flasks, according to Sections 2.3.1 and 2.8.9. The anti-Pk/V5 antibody (Chapter 2, Table 2.5) was immobilised to Protein G sepharose resin, using a standard cross-linking protocol (Section 2.8.9). Pooled lysates were then prepared for each condition and 0.5 mg of cleared lysate was used for co-IP assays (Section 2.7.8.). The cross-linked antibody-resin slurry was then incubated with the cleared cell lysate, as described in Section 2.8.9. Following extensive washing, bound proteins were eluted from the resin into three 30 µL fractions using a glycine buffer of pH 2 (Section 2.7.8) and the eluates were immediately neutralised (Section 2.8.9) and tested for the presence of hPLCXD3 by western blotting analyses (Figure 6.5) using a rabbit anti-hPLCXD3 primary antibody and a donkey anti-rabbit AP-conjugated secondary antibody (Chapter 2, Table 2.5). A band of around 38 kDa corresponding to the expected size of Pk-tagged hPLCXD3 was obtained in each eluate of HeLa cells transfected with hPLCXD3. These bands were absent from control, non-transfected cells (Figure 6.5).

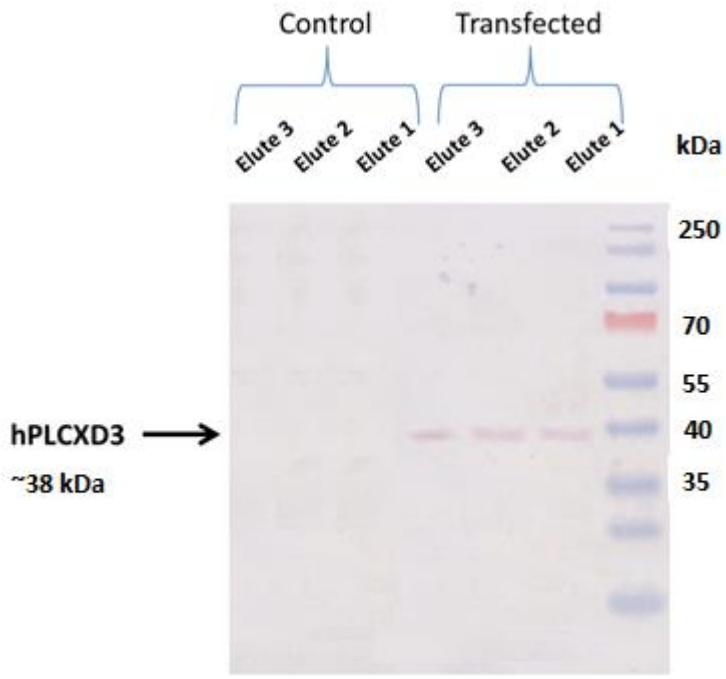

Figure 6.5: Co-immunoprecipitation (co-IP) of hPLCXD3 from HeLa. Cells stably overexpressing PLCXD3 were created as described in Chapter 2, Section 2.2.4. Anti-Pk/V5-tag antibody was conjugated to Protein G-sepharose resin, as described in Chapter 2, Section 2.2.4. Antibody-conjugated resin was then used to purify Pk/V5-tagged hPLCXD3 from total cell lysates prepared from transfected HeLa cells, as previously described. Bound protein was eluted from the resin with a glycine buffer of pH 2.0 and the samples were neutralised and samples prepared for Western blotting, as described previously. Western blotting was performed with an anti-PLCXD3 primary antibody raised against the N-terminus of the protein and a donkey anti-rabbit alkaline phosphatase-conjugated secondary antibody (Abcam). This image is representative of 3 separate experiments.

6.6. Interaction of purified hPLCXD3 with lipids

Mammalian PI-PLCs are known to hydrolyse $PI(4,5)P_2$ forming $I(3,4,5)P_3$ and diacylglycerol (DAG), whereas bacterial PI-PLCs are known to hydrolyse phosphatidylinositol to cyclic inositol phosphate and DAG. The ability of hPLCXD3 purified from *E.coli* and HeLa cells to hydrolyse soluble homologues of PI and $PI(4,5)P_2$ (diC4 PI and diC8 $PI(4,5)P_2$ respectively) was tested by ^{31}P NMR (Chapter 2, Section

2.8.12). For both phosphatidylinositol (PI) and PI(4,5)P_2 the NMR signal spectrum of the phosphate group at position 1 in the inositol ring was monitored before and after the addition of either recombinant hPLCXD3 purified from *E.coli* (Chapter 6, Section 6.4) or hPLCXD3 immunoprecipitated from HeLa cells (Chapter 6, Section 6.5), as detailed in the methods section (Chapter 2, Section 2.8.12). No changes in the chemical shifts patterns were seen following addition of 1 µg of hPLCXD3 purified by either of the above methods (Figure 6.7). Expected chemical shifts were observed following incubation of diC4 PI with 1 µg of PI-PLC commercially purified from *B. cereus* (Figure 6.6).

To investigate whether a direct interaction of membrane lipids with human hPLCXD3 could occur, hPLCXD3 purified from *E. coli* (Section 6.4 above) was used as a probe in a protein lipid overlay assay with a membrane lipid strip (Echelon) containing 15 different spotted lipids (Chapter 2, Section 2.8.11). Following detection with hPLCXD3-specific antibody, hPLCXD3 was seen to bind with varying extents to spots containing PI(3,4,5)P_3, PI(4,5)P_2, phosphatidic acid (PA), PI(3,5)P_2 and PI(3,4)P_2 (Figure 6.7 B). Control membrane strips incubated in the absence of hPLCXD3 resulted in low signals only with PA, indicating that the anti-hPLCXD3 primary and/or the anti-rabbit secondary antibodies displayed a slight non-specific interaction with this lipid.

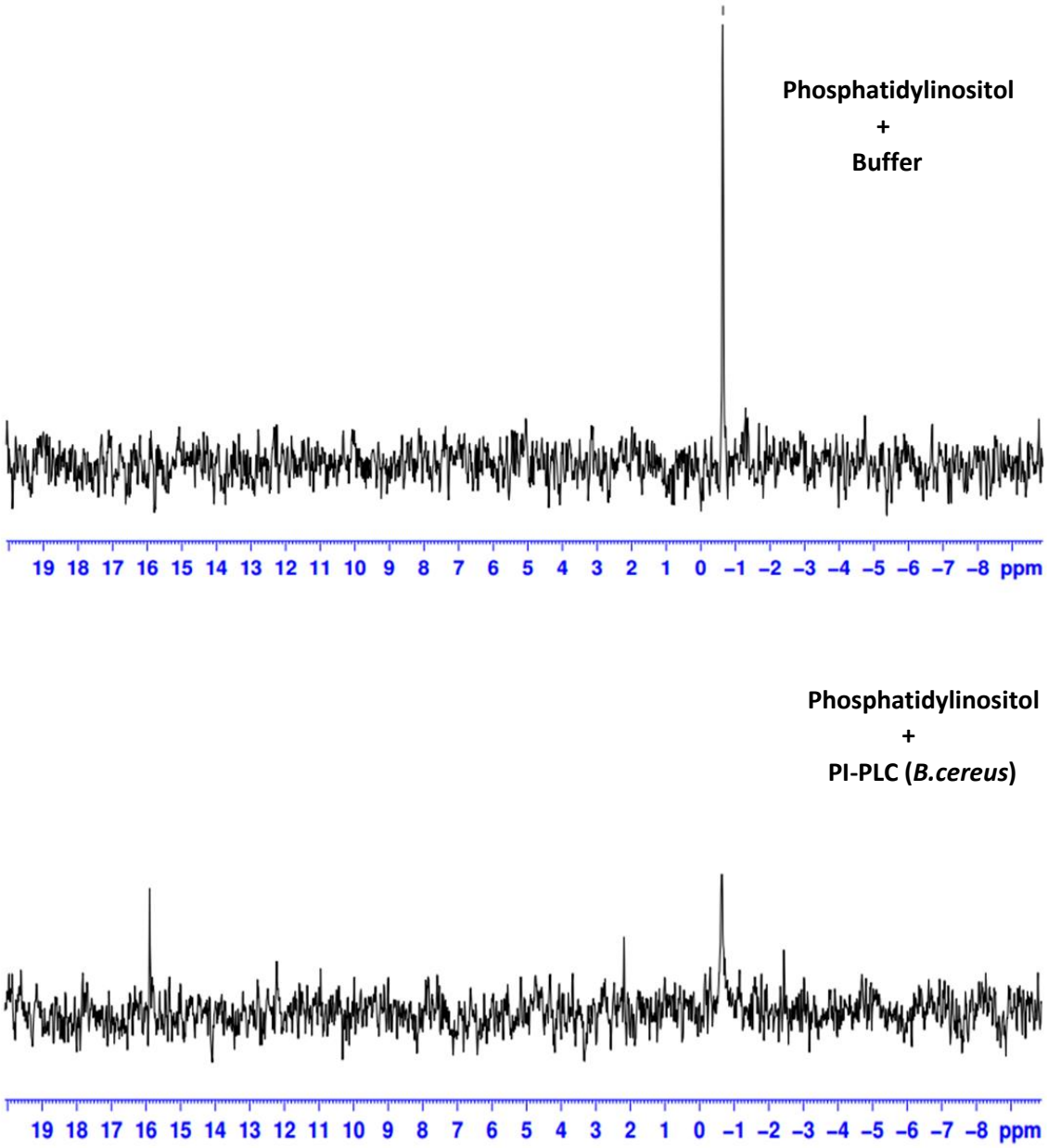

Figure 6.6: ^{31}P-NMR studies were performed to assess whether hPLCXD3 could hydrolyse short chain (diC8) PI and/or PIP_2. Both hPLCXD-3 purified from *E.coli* and insect cells were tested (A) and PI-PLC purified from *B.cereus* (B). 500 µg of substrate and 1 µg purified from either *E.coli* or insect cells were used in each assay.

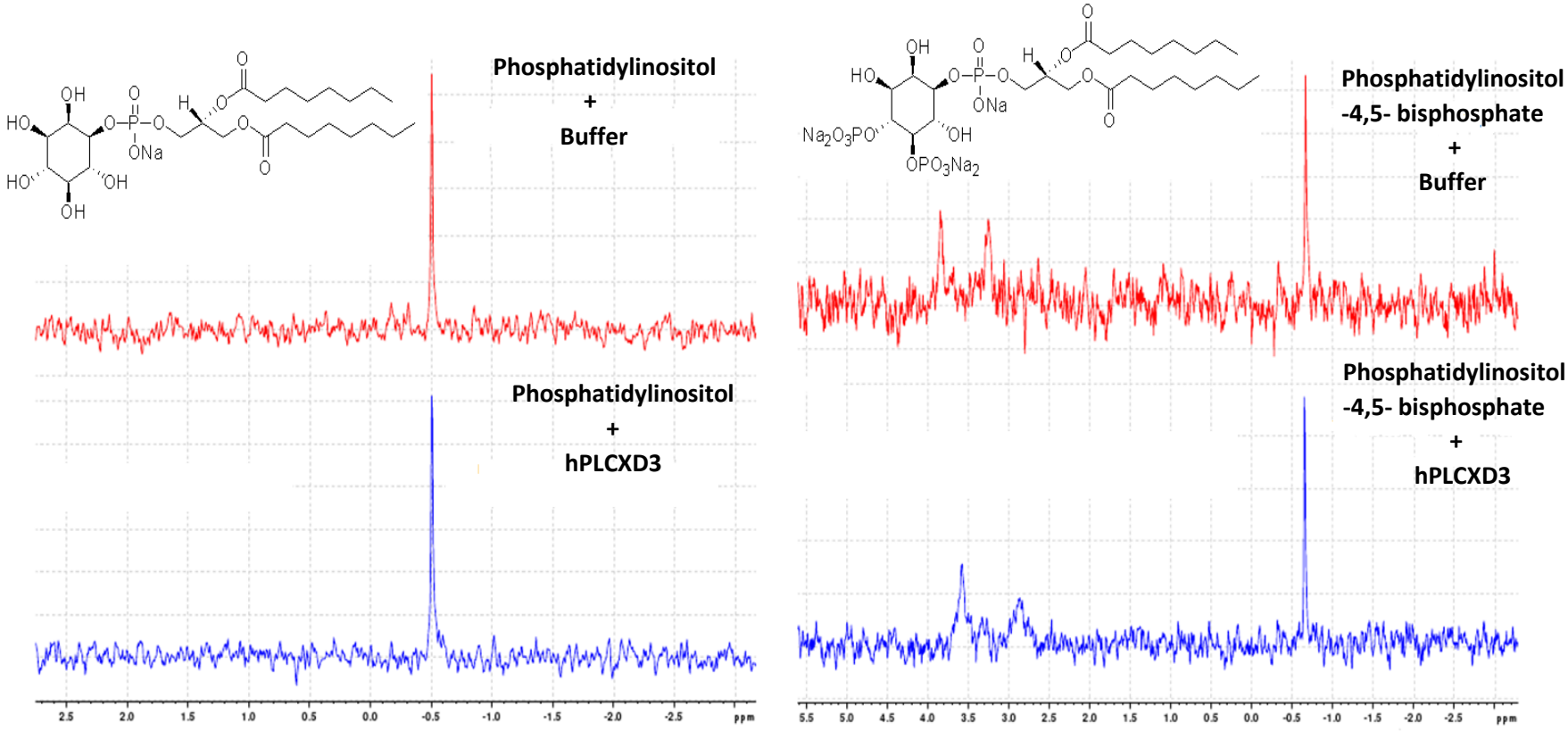

Figure 6.7: ^{31}P-NMR studies were performed to assess whether hPLCXD3 could hydrolyse short chain (diC8) PI and/or PIP_2. Both hPLCXD-3 purified from *E.coli* and insect cells were tested (A) and PI-PLC purified from *B.cereus* (B). 500 µg of substrate and 1 µg purified from either *E.coli* or insect cells were used in each assay.

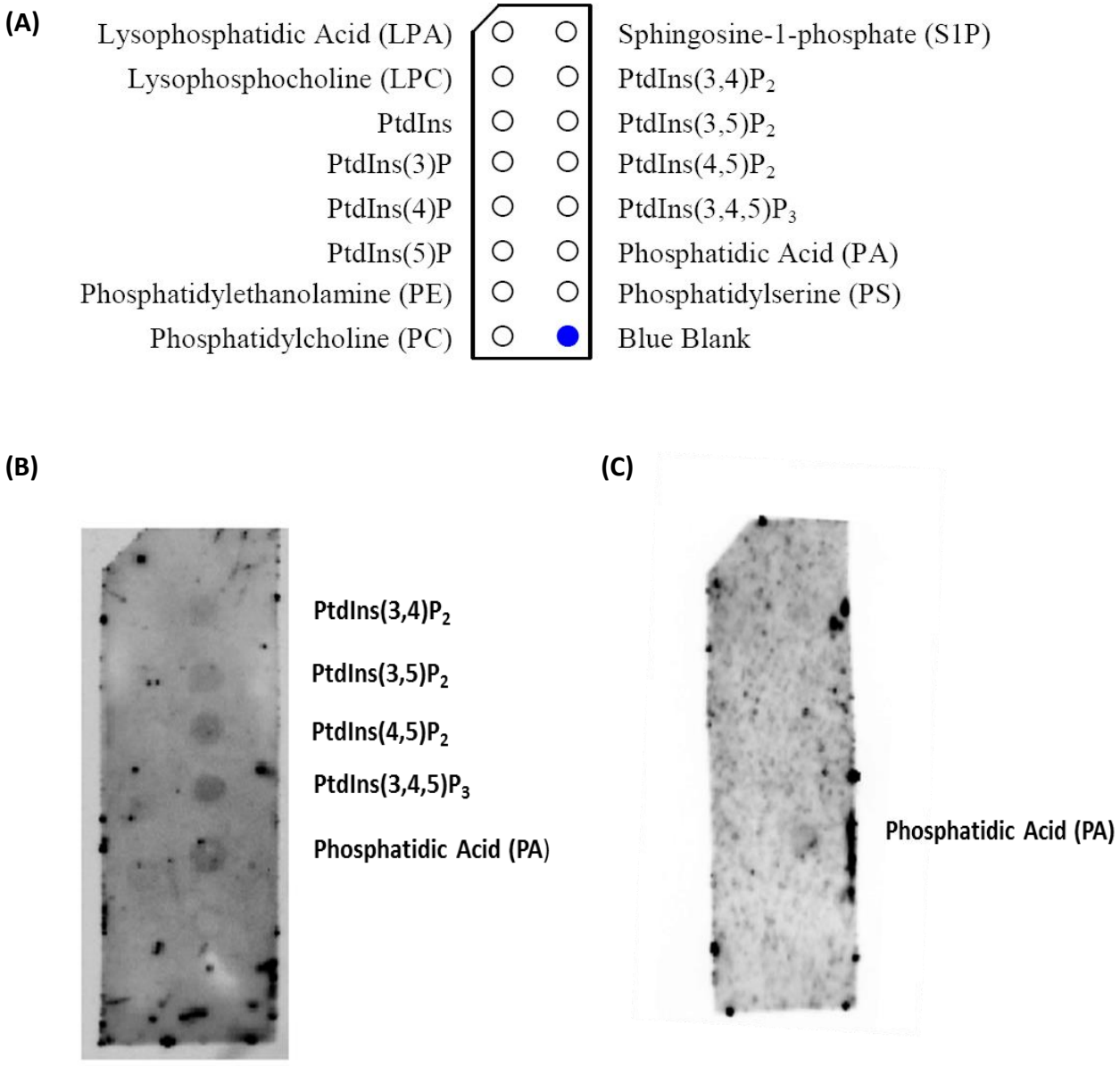

Figure 6.8: Overlay assay with hPLCXD3 incubated with membranes spotted with 100 pmol of the phospholipids indicated (Lipid strips). Proteins were expressed in *E.coli* and purified by Ni^{2+} -affinity chromatography. Lipid strips were incubated with 100 pmol of the recombinant protein overnight at 4 °C as detailed under "Experimental Procedures." After washing, PLCXD3 was visualised using the polyclonal N-terminal anti-PLCXD3 antibody. (A), shows a schematic diagram of phospholipids impregnated on each individual PIP strip. (B), shows binding of the recombinant protein to the various lipids (100 pmol/spot). (C) represents the negative control PIP strip following incubation in the absence of recombinant protein.

6.7. Crystallisation and optimisation of hPLCXD3

For crystallisation trials, a total of six different crystal screens were set up with the two concentrations (5 mg/mL and 10 mg/mL) of the recombinant protein. Crystal plates were set up using a nano-drop crystallisation robot, with 300 nL of buffer and 300 nL of protein per drop (Chapter 2, Section 2.8.13). A number of commercially available crystal screens were used to test the conditions required for crystal formation (See section 2.8.13). A single hit was obtained in the JCSG+ screen using 10 mg/mL of protein (Figure 6.8). hPLCXD3 protein crystals were picked, cryoprotected and exposed to X-rays at 100K, according to Section 2.7.13. The crystals diffracted X-rays to a low resolution of 10 A. In an attempt to gain better quality crystals, the conditions that produced the initial crystal (above) were further optimised by varying the concentration of salt and proteins and also varying the type and amount of each precipitant used. Further optimisation did not yield crystals of sufficient quality for structure determination.

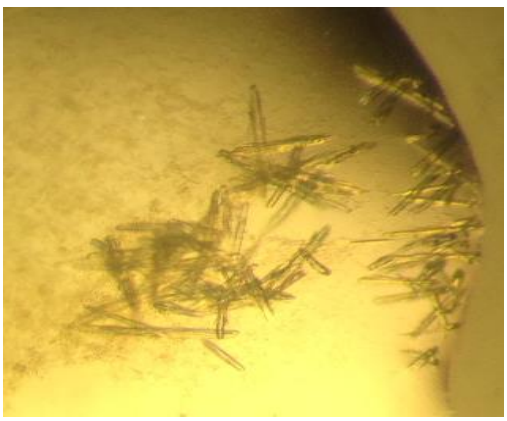

Figure 6.9: Showing protein crystals obtained with hPLCXD3 purified from *E. coli* (Section 6.4; described above). Crystal plates were set-up according to Chapter 2, Section 2.7.12 using 150 nL of 10 mg/mL purified hPLCXD3. The crystals above were obtained following 1 days of incubation at room temperature.

6.8. Discussion

6.8.1. Recombinant over- expression of hPLCXDs 1, 2 and 3 in *E.coli*

Although high levels of hPLCXDs 1, 2 and 3 were found in the whole lysates of induced cells, the levels of soluble proteins were poor, with only hPLCXD3 showing any sign of soluble expression. The efficiency of recombinant protein expression in a bacterial host organism like *E. coli* depends on numerous parameters. Important factors associated with recombinant protein expression include the expression vector used for gene cloning (including the type of promoter used) as well as other factors linked to the nucleotide and amino acid sequence of the protein of interest (including mRNA and protein stability). Given that these parameters are predefined by the choice of the expression vector and the hPLCXD sequences, initial attempts to optimise soluble recombinant protein expression of hPLCXDs 1, 2 and 3 were performed by varying parameters affecting *E. coli* cell growth (growth/induction temperatures). Induction of the expression of hPLCXDs 1, 2 and 3 at a lower temperature and reducing the IPTG concentration failed to increase the solubility of any hPLCXD isoform. It is therefore clear that further optimisation of the recombinant expression of hPLCXD1, 2 and 3 is required, details of which are detailed in Chapter 6.

The best soluble expression of the hPLCXD isoforms in *E. coli* was seen with hPLCXD3, which was therefore chosen for scale-up purification. In-order to gain enough soluble protein to enable structure determination by X-ray crystallography, a 30 litre *E. coli* culture expressing hPLCXD3 was grown. Standard affinity chromatography using nickel columns and gel filtration mainly yielded a single band of 35 kDa on SDS-PAGE. Additionally, hPLCXD3 purification contained minor contaminants which were

subsequently found by mass spectrometry to be polypeptides of 25 and 20 kDa molecular mass derived from the 35 kDa hPLCXD3. These degradation products were present at each stage during the purification process and may be due to the instability of hPLCXD3 and/or insufficient inhibition of the bacterial proteases. Fractions containing the 35 kDa hPLCXD3 enzyme were pooled together and concentrated to 10 mg/mL.

6.8.2. Interaction of purified hPLCXD3 with lipids

The potential activity of PLCXD3 as a functional phospholipase C was tested *in vitro* using a phosphorus-based NMR assay. Whereas expected chemical shifts, indicative of phospholipase C activity, were observed for commercially purified *B. cereus* PI-PLC enzyme, no phospholipase C activity was observed for hPLCXD3 purified from *E. coli* or HeLa cells with either PI or PtdIns(4,5)P_2 as the substrate. Due to expected chemical shifts being observed with PI-PLC purified from *B. cereus,* we believe the NMR assay used to be an appropriate test for phospholipase C activity. One interpretation of the results is that hPLCXD3 has no endogenous phosphodiesterase activity, at least to the substrates, PI and PIP_2. Alternatively, the observed results may suggest that hPLCXD3 can hydrolyse a substrate other than PI or PtdIns(4,5)P_2. Indeed, phospholipase C enzymes with substrate specificity for phosphatidylcholine (PC) have been identified in both bacterial and mammalian cells, however they exhibit low homologies and different domain structures when compared with hPLCXD3 and therefore PC-specific activity seems unlikely for hPLCXD3. Given that hPLCXD3 enzymes purified from two different sources both failed to show any phospholipase C activity, we believe that the lack of enzyme activity is not an artefact of the purification procedure, however this

cannot be fully ruled out until recombinant hPLCXD3 is successfully purified from further sources.

Enzymes that act on substrates such as lipid membranes often interact with more than one lipid substrate molecule. The enzymatic activity of the PI-PLC isolated from *B.cereus* has been shown to increase in the presence of organised lipid substrates, such as bilayers and micelles, containing certain phospholipids (Volwerk et al. 1994; Wehbi et al. 2003). Indeed numerous studies have demonstrated activation of mammalian PLC-δ1 and PLC-β1 following presentation of their substrate within a micelle or bilayer (Boguslavsky et al. 1994). Therefore, like other PI-PLCs, hPLCXD3 may exhibit interfacial catalysis in the presence of other, as yet unknown lipids, acting through allosteric means, required for enzyme activation. Evidence for the ability of hPLCXD3 to associate with phospholipids in a non-catalytic manner was obtained following a lipid overlay assay. The hPLCXD3 enzyme purified from *E. coli* was able to interact with the poly-phosphorylated phosphoinositides PI(3,4,5)P_3, PI(4,5)P_2, PI(3,5)P_2 and PI(3,4)P_2. A slight interaction was also seen with PA; however this was also observed in the negative control assay and therefore possibly indicates cross-reaction of the hPLCXD3 antibody with PA. Both mammalian and bacterial PI-PLC isozymes have been shown to interact with various non-substrate phospholipids and these interactions have been shown to be important for the regulation of sub-cellular localisation and enzymatic activity. The signalling phospholipid, PA, has been shown to bind to and stimulate PLC-β1 through a mechanism involving the C-terminal domain of PLC-β1 (Ross et al. 2006). For PI-PLC isolated from the virulent bacteria *B. thuringiensis*, vesicles containing PI and PC displayed enhanced hydrolysis of PI compared with

vesicles containing only PI. PC is thought to allosterically bind and activate PI-PLC by helping the enzyme anchor to the membrane in a more active conformation (Zhou et al. 1997; Qian et al. 1998). The observed lipid binding specificities of hPLCXD3 may indicate that the catalytic function of the enzyme requires allosteric activation from non-substrate phospholipids and may explain the lack of enzyme activity observed in previous NMR studies. The ability of hPLCXD3 to hydrolyse PI and PtdIns(4,5)P_2 when presented in mixed micelles containing different phosphoinositides requires future investigation. The amino acid residues involved in PLCXD3 lipid binding are yet to be characterised. Lipid hydrolysis and binding specificities for PLCXD1 and 2 awaits recombinant expression optimisation, as detailed in Chapter 7.

6.8.3. Crystallisation

Important discoveries have been made concerning the functional characterisation of eukaryotic and prokaryotic PI-PLC family members that include the crystal structures of the *B. cereus* (Heinz et al. 1995), *B. thuringiensis* (Shao et al. 2007) PI-PLCs and mammalian PLC-δ1 (Essen et al. 1996). Comparison of the crystal structures shows that prokaryotic PI-PLCs to be structurally similar to the X-domain of eukaryotic PI-PLCs in that both enzymes containing a distorted ($\beta\alpha_8$)-barrel structural motif, with a particularly large similarity for the first half of the barrel, in which all the catalytic residues, including two essential histidine residues, are located. The fact that eukaryotic enzymes, but not prokaryotic PI-PLCs require Ca^{2+} is explained by the observations that, in the bacterial enzymes, an arginine residue occupies a location close to that of the Ca^{2+} cofactor in the eukaryotic enzymes. Significant advances on the interactions of these enzymes with both substrate and non-substrate lipids have

been made and these have been described in the previous section. Given the conserved nature of PI-PLC family members, derivation of the crystal structure of human PLCXDs and subsequent comparative analysis from bacteria to man would really give some idea of the functions of these proteins.

In this chapter, we describe the initial attempts to obtain the crystal structure of human PLCXD3. Although positive hits were obtained for hPLCXD-3 with one of the crystallisation conditions tested, these crystals diffracted at an insufficient resolution for further structure determination. Additionally, crystals were obtained following optimisation of the initial crystallisation condition through variation in the concentration of hPLCXD3, precipitant and the salt; however, as with previous crystals, they diffracted to an insufficient resolution. Producing protein crystals suitable for structure determination is often a challenging task, which benefits from high-throughput screening to identify initial positive crystallisation conditions with further optimisation often required. Attempts to gain diffraction quality hPLCXD3 crystals appear to be challenging and further optimisation is clearly required. Furthermore, given that the purified fraction of hPLCXD3 was not homogeneous, with the presence of breakdown products, further optimisation of protein expression and purification protocols to gain soluble homogeneous protein may help to obtained crystals suitable for structure determination. With the aim of obtaining crystals suitable for structure determination, attempts to further optimise the expression of human PLCXDs in different host organisms have been made and are described in the next chapter.

CHAPTER 7: Small-scale recombinant expression screen of human PLCXD1, 2 and 3 isoforms using the pOPIN vectors in different host organisms

7.1. Introduction

E. coli has been utilised as the expression system of choice by many laboratories involved in the production and purification of proteins for structural genomics. Many advantages are associated with the use of *E. coli* as an expression host including its well-known physiology, ease of genetic manipulation with advanced genetic tools, rapid growth and high-levels of recombinant protein production achieving up to ~30% of total cellular proteins (Baneyx 1999). The main disadvantage, particularly for eukaryotic proteins, is the tendancy for mis-folding and aggregation into inclusion bodies as a result of lack of eukaryotic chaperones, specialised post-translational modifications and/or ability to form complexes with stabilising binding partners (Hannig and Makrides 1998). In recent years, other expression systems, utilising different host cells including the baculovirus-insect cell and HEK cell expression systems, have been used for the production of recombinant eukaryotic proteins. The expression of eukaryotic chaperones, existence of post-translational modification pathways and ability to target proteins to sub-cellular localisations are among the many advantages of the use of these expression systems for the recombinant production of eukaryotic proteins (Nettleship *et al*., 2010). In addition, the level of soluble expression of a target protein can also be altered by the addition of an N- or C-terminal fusion protein, such as maltose-binding protein (MBP), thioredoxin (Trx) and glutathione S-transferase (GST; Nettleship *et al*., 2010).

Previous attempts to express hPLCXD1, 2.1 and 3 isoforms as recombinant proteins in *E.coli* resulted in little soluble expression due to the aggregation of the highly

expressed proteins into inclusion bodies. Several strategies to enhance the folding of hPLCXD1, 2.1 and 3 into a native state in *E.coli* were tested, including lowering the temperature during induction or inducing expression with lower concentrations of IPTG, but these strategies proved unsuccessful (Chapter 6). It was therefore clear that further optimisation of hPLCXD1, 2.1 and 3 recombinant expression was required. The Oxford Protein Production Facility (OPPF) provides specialist facilities and knowledge for high-throughput cloning, expression in different host organisms and purification of target proteins for crystallography. To enable the optimisation of protein expression and solubility, the OPPF uses the pOPIN vector suite, which allows expression of a target protein with a number of different fusion tags (Chapter 2, Figure 2.5) and in multiple host organisms (*E. coli*, mammalian cells (HEK293T cells) and insect cells (*Sf9* cells)). This chapter details the high-throughput screen that was carried out at the OPPF to test the levels of soluble expression of recombinant PLCXD1, 2.1 and 3 when expressed as different fusion proteins (Chapter 2, Figure 2.5) in *E. coli*, HEK293T and *Sf9* insect cells.

7.2. InFusion cloning of human PLCXD1, 2.1 and 3 to the pOPIN expression vectors

A total of 10 pOPIN vectors (Chapter 2, Figure 2.5) were used to create expression constructs for each hPLCXD isoform. To do this, the full-length coding sequences of hPLCXDs 1, 2.1 and 3 were amplified from a HeLa cDNA library (Created by Dr Svetlana Kalujnaia) using forward and reverse primers containing appropriate nucleotide extensions for InFusion cloning to the pOPIN vector suite (Chapter 2, Section 2.7.10.2). Primer sequences are detailed in Appendix C. A total of 10 amplifications were performed for each PLCXD gene using the KOD Hot start DNA polymerase (Chapter 2,

Section 2.7.6) and the products were analysed by gel electrophoresis. As shown in Figure 7.1, a PCR product of the expected size was obtained for PLCXDs 1 and 3, and almost all of the PLCXD2.1 amplifications. No PCR product for PLCXD2.1 was observed when amplified with primers containing extension for insertion to the pOPINM vector (lane 5).

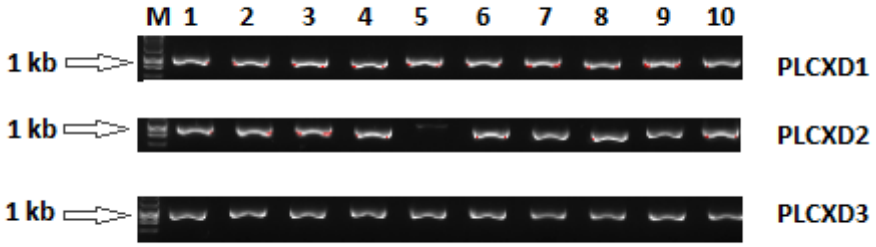

Figure 7.1: Gel electrophoresis analysis of PCR products following amplification of human PLCXDs 1, 2 and 3 with primers containing extensions for subsequent insertion into different expression vectors (1- pOPINF, 2- pOPINS3C, 3- pOPINNUSA, 4- pOPINMYSB, 5- pOPINM, 6- pOPINTF, 7- pOPINTRX, 8- pOPINHALO7, 9- pOPINE Neo, 10- pOPIN- 3C- HALO7. M denotes molecular size marker.

The PCR products were then purified using AMPure XP Magnetic beads, according to Chapter 2, Section 2.7.10.2. The purified PCR products were then inserted into 10 different pOPIN expression vectors using the InFusion cloning method (Chapter 2, Section 2.7.10.2) and the expression constructs were transformed into OmniMaxII *E. coli* cells and grown on agar plates containing X-Gal for blue/white colony screening, as described in Section 2.7.10.2. Two white colonies were selected for each construct and grown for plasmid preparation, according to Chapter 2 Section 2.7.10.2. The

purified expression constructs were then used to express different fusion versions of PLCXD1, 2.1 and 3 in *E.coli*, HEK293 and *Sf9* insect cells.

7.3. Expression trials of hPLCXD1, 2.1 and 3 in *E. coli*

The resultant 10 pOPIN expression vector constructs, made for each PLCXD isoform, were transformed into two different host strains - Rosetta (DE3) and Lemo 21 - and protein expression was induced by two expression regimes in 3 mL shaking cultures (Chapter 2, Section 2.2.5.1) giving rise to 40 samples for each hPLCXD isoform. Bacterial pellets were harvested and recombinant $(His)_6$-tagged proteins were purified using magnetic nickel beads, according to Section 2.8.10. The level of soluble protein expression was assessed by visual inspection of SDS-PAGE gels of purified proteins and is shown in Figures 7.2, 7.3 and 7.4. The expected molecular sizes of the different fusion proteins are detailed in the Table 7.1. For each hPLCXD, little to no protein was purified when the expressed construct contained an N- terminal $(His)_6$-tag, under any of the test conditions. However, with the exception of hPLCXD2.1, at least one fusion tag was found to increase the apparent solubility of the proteins when expressed in *E. coli*. For hPLCXD1, although limited success was experienced with most fusion constructs, the addition of an N-terminal trigger factor (TF) fusion tag to the full-length protein gave the best soluble expression when expressed in Rosetta (DE3) cells using the auto induction method (Chapter 2, Section 2.2.5.1); however this was not consistent across the different expression conditions (Figure 7.2). For hPLCXD3, expression of the protein with a C-terminal $(His)_6$-histidine tag increased solubility, however no soluble expression was seen with an N-terminal HIS_6- histidine tag (Figure 7.3). Additionally, expression of hPLCXD3 with either an N-terminal small ubiquitin-like

modifier (SUMO) or thioredoxin (TRX) fusion tag, also gave an increase in solubility, however only when expressed in the Lemo 21 host with IPTG induction. When the same constructs were expressed in Lemo 21 cells with auto-induction, only the SUMO fusion tag was seen to increase solubility (Figure 7.4).

	PLCXD1 (kDa)	**PLCXD2.1 (kDa)**	**PLCXD3 (kDa)**
$(His)_6$-3C (Lane 1)	**38.8**	**36.9**	**38.5**
$(His)_6$-SUMO-3C (Lane 2)	**50.4**	**48.5**	**50.0**
$(His)_6$-NUSA-3C (Lane 3)	**93.7**	**91.8**	**93.3**
$(His)_6$-MSYB-3C (Lane 4)	**53.2**	**51.3**	**52.8**
$(His)_6$-MBP-3C (Lane 5)	**82.2**	**80.3**	**81.8**
$(His)_6$-TF-3C (Lane 6)	**87.0**	**85.1**	**86.7**
$(His)_6$-TRX-3C (Lane 7)	**50.8**	**48.9**	**50.5**
$(His)_6$-HALO-3C (Lane 8)	**71.8**	**69.9**	**71.5**
3C-$(His)_6$ (Lane 9)	**38.8**	**36.9**	**38.5**
3C-HALO7-$(His)_6$ (Lane 10)	**71.8**	**69.9**	**71.5**

Table 7.1: The expected Molecular sizes of the recombinant fusion proteins for PLCXD-1, 2.1 and 3, expressed using the pOPIN vector suite.

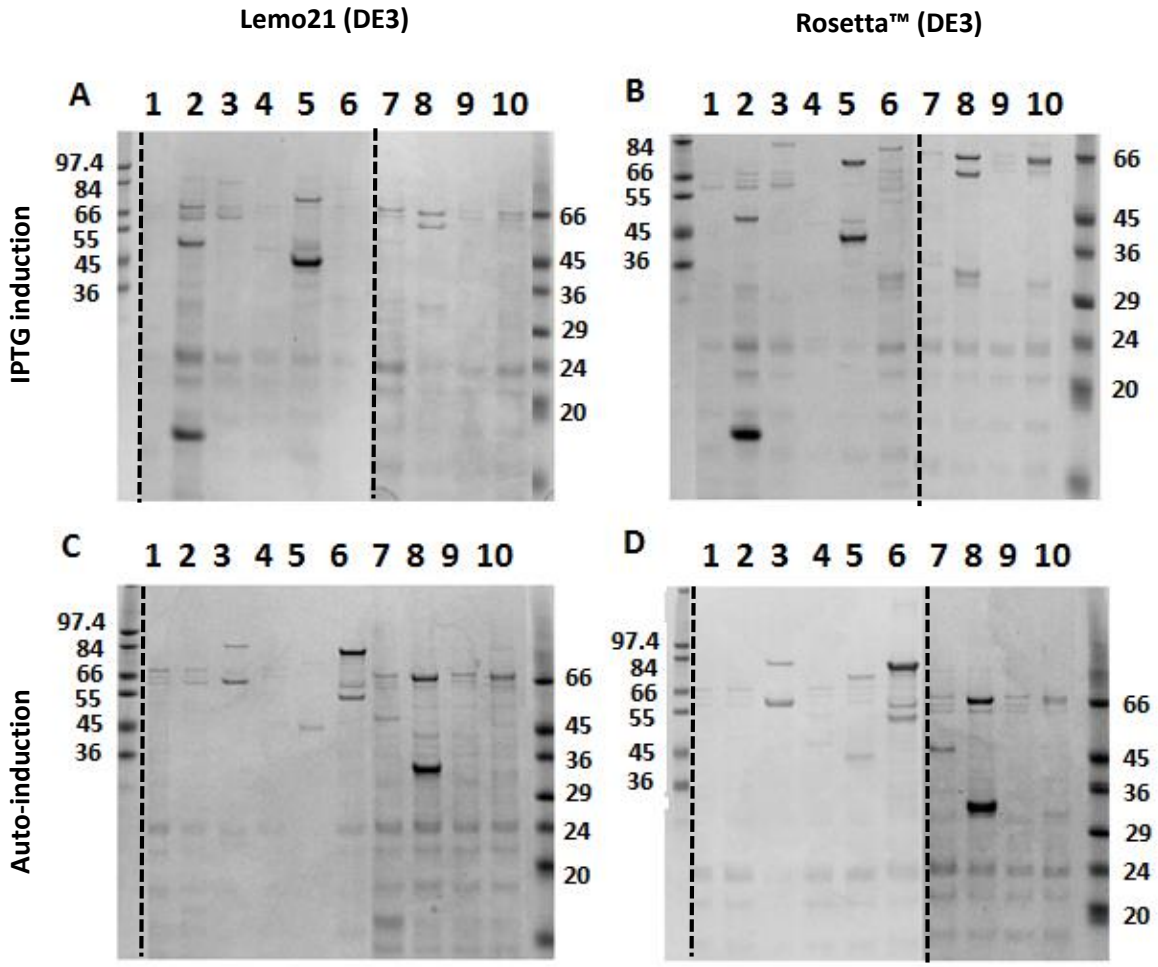

Figure 7.2: SDS-PAGE analyses of expression screens. Full-length *Homo sapiens phospholipase C X-domain containing protein 1.* A. Lemo 21 cells grown in Powerbroth with IPTG induction; B. Rosetta (DE3) cells grown in Powerbroth with IPTG induction; C. Lemo 21 cells with auto-induction using TB-Overnight express media; D. Rosetta (DE3) cells with auto-induction using TB-Overnight express media. N-terminal fusion tag: 1- $(His)_6$-3C; 2- $(His)_6$-SUMO-3C; 3- $(His)_6$-NUSA-3C; 4- $(His)_6$-MSYB-3C; 5- $(His)_6$-MBP-3C; 6- $(His)_6$-TF-3C; 7- $(His)_6$-TRX-3C; 8- $(His)_6$-HALO-3C. C-terminal fusion tag: 9- 3C-$(His)_6$; 10- 3C-HALO7-$(His)_6$. To maintain the same layout, some of the gels have been stitched together and this is denoted with a doted line.

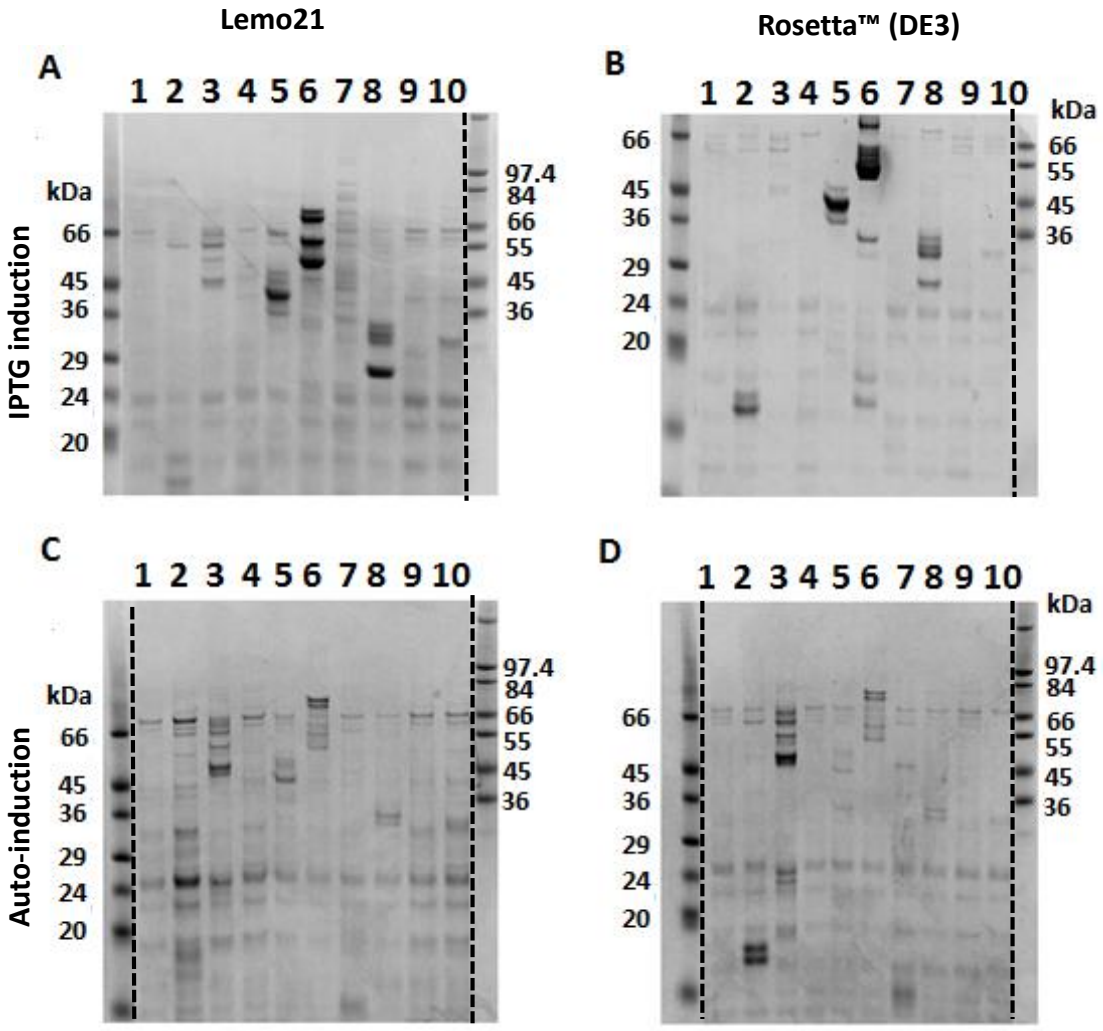

Figure 7.3: SDS-PAGE analyses of expression screen. Full-length *Homo sapiens phospholipase C X-domain containing protein 2.1.* A. Lemo 21 cells grown in Powerbroth with IPTG induction; B. Rosetta (DE3) cells grown in Powerbroth with IPTG induction; C. Lemo 21 cells with auto-induction using TB-Overnight express media; D. Rosetta (DE3) cells with auto-induction using TB-Overnight express media. Fusion tags: 1- $(His)_6$-3C; 2- $(His)_6$-SUMO-3C; 3- $(His)_6$-NUSA-3C; 4- $(His)_6$-MSYB-3C; 5- $(His)_6$-MBP-3C; 6- $(His)_6$-TF-3C; 7- $(His)_6$-TRX-3C; 8- $(His)_6$-HALO-3C. C-terminal fusion tag: 9- 3C-$(His)_6$; 10- 3C-HALO7-$(His)_6$. To make it easier to view the molecular marker some of the gels have been stitched together and this is denoted with a doted line.

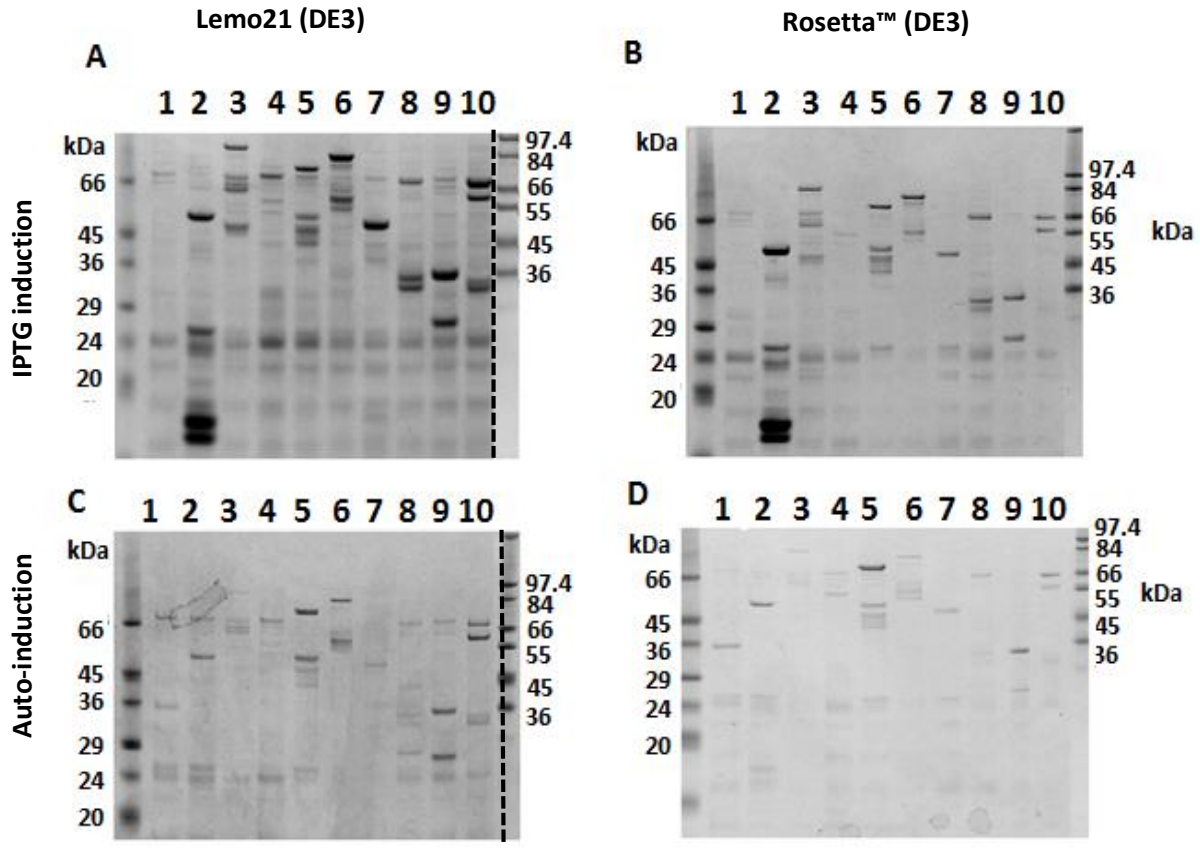

Figure 7.4: SDS-PAGE analyses of expression screen. Full-length *Homo sapiens phospholipase C X-domain containing protein 3.* A. Lemo 21 cells grown in Powerbroth with IPTG induction; B. Rosetta (DE3) cells grown in Powerbroth with IPTG induction; C. Lemo 21 cells with auto-induction using TB-Overnight express media; D. Rosetta (DE3) cells with auto-induction using TB-Overnight express media. N-terminal fusion tags: 1- $(His)_6$-3C; 2- $(His)_6$-SUMO-3C; 3- $(His)_6$-NUSA-3C; 4- $(His)_6$-MSYB-3C; 5- $(His)_6$-MBP-3C; 6- $(His)_6$-TF-3C; 7- $(His)_6$-TRX-3C; 8- $(His)_6$-HALO-3C. C-terminal fusion tag: 9- 3C-$(His)_6$; 10- 3C-HALO7-$(His)_6$. To make it easier to view the molecular marker some of the gels have been stitched together and this is denoted with a doted line

7.3. Expression trials of hPLCXD1, 2.1 and 3 in mammalian cells

The same suite of recombinant pOPIN expression vectors previously constructed for each PLCXD isoform, were tested for soluble protein expression following transfection of human embryonic kidney cells (HEK293; Chapter 2, Section 2.3.3). The different PLCXD fusion proteins were transiently expressed in HEK293 cells according to Chapter 2, Section 2.3.3. Following growth of cells for 3 days (Section 2.3.3) the cells were lysed (Section 2.8.1) and soluble protein expression was assessed by western blotting detection of $(His)_6$-tagged proteins present in the total lysate (Figure 7.5A) and soluble fractions (Figure 7.6B). Immunoreactive bands of expected sizes were observed in the total lysate of HEK293 cells transfected with most of the PLCXD3 vector constructs, however the intensity of these bands were variable. Corresponding bands were also observed in the soluble protein extract for these constructs indicating soluble expression. For PLCXD3, the highest level of soluble expression was observed with N-terminal SUMO and TRX fusion tags. Immunoreactive bands were not found to be present in either the total lysate or soluble extract fractions from HEK293 cells transfected with expression vector constructs containing either PLCXD1 or PLCXD2.1 (data not shown).

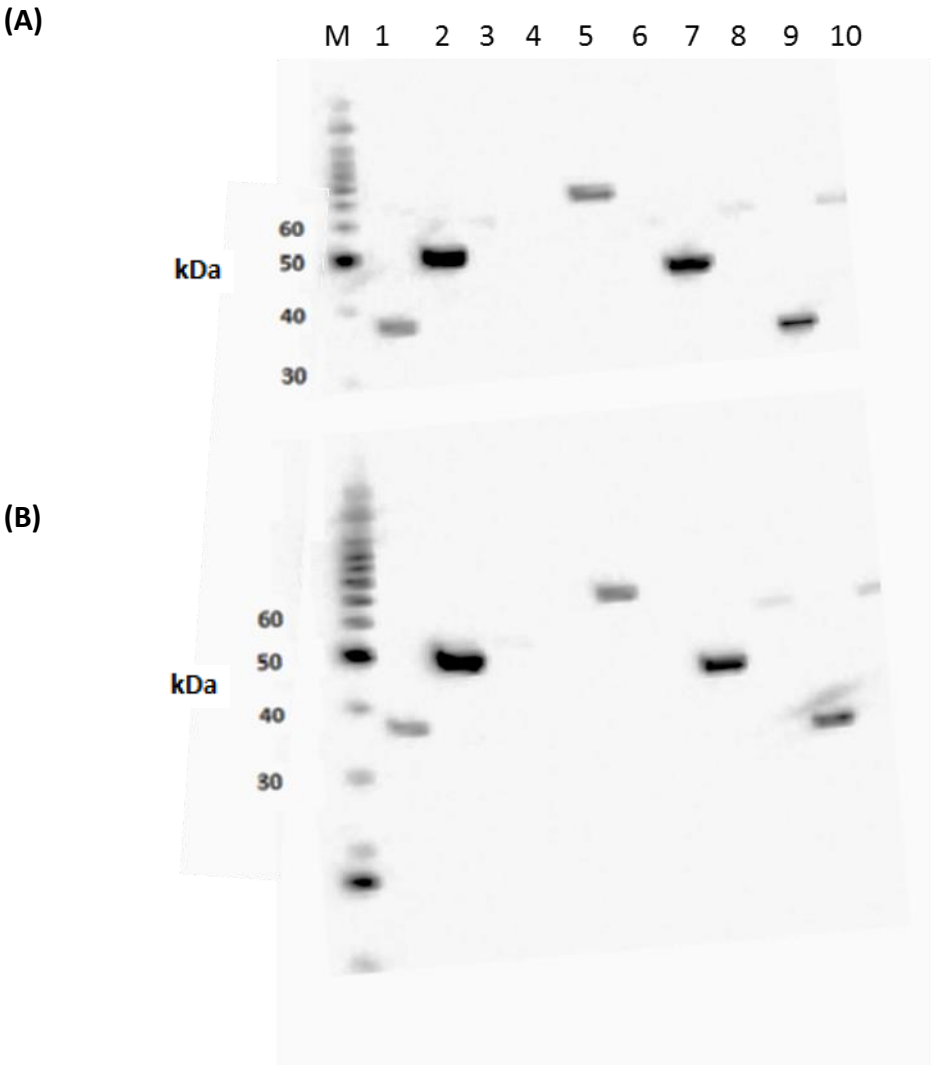

Figure 7.5: Western blot showing the results of the HEK293 cell expression screen. *Homo sapiens phospholipase C X-domain containing protein **3**.* Western blot performed using anti-His primary antibody (1/1000 dilution) with total cell lysate (A), and soluble extract (B). N-terminal fusion tags: 1- $(His)_6$-3C; 2- $(His)_6$-SUMO-3C; 3- $(His)_6$-NUSA-3C; 4- $(His)_6$-MSYB-3C; 5- $(His)_6$-MBP-3C; 6- $(His)_6$-TF-3C; 7- $(His)_6$-TRX-3C; 8- $(His)_6$-HALO-3C. C-terminal fusion tag: 9- 3C-$(His)_6$; 10- 3C-HALO7-$(His)_6$. The expected sizes of the different tagged versions of PLCXD3 are detailed in Table 7.1

7.4. Expression trials of hPLCXD1, 2 and 3 in insect cells

The suite of pOPIN vectors previously created for each PLCXD isoform were used to create recombinant baculovirus particles for protein expression in *Sf9* insect cells, as described in Chapter 2, Section 2.4.2. *Sf9* cells were transfected with either 5 µL or 50 µL of recombinant P1 baculovirus and proteins were harvested 72 and 96 hours post-infection (Section 2.8.1). As with recombinant expression in HEK293 cells, soluble recombinant protein expression was only observed for hPLCXD3 (Figure 7.6). The presence of hPLCXD-1, 2.1 and 3 was not tested in total lysates. The highest levels of soluble expression were seen when hPLCXD3 was expressed with only a $(His)_6$-tag at either the N (pOPINF construct; Lane 1) or C-terminal (pOPINE Neo construct; Lane 9). This result was consistent across the different expression conditions tested.

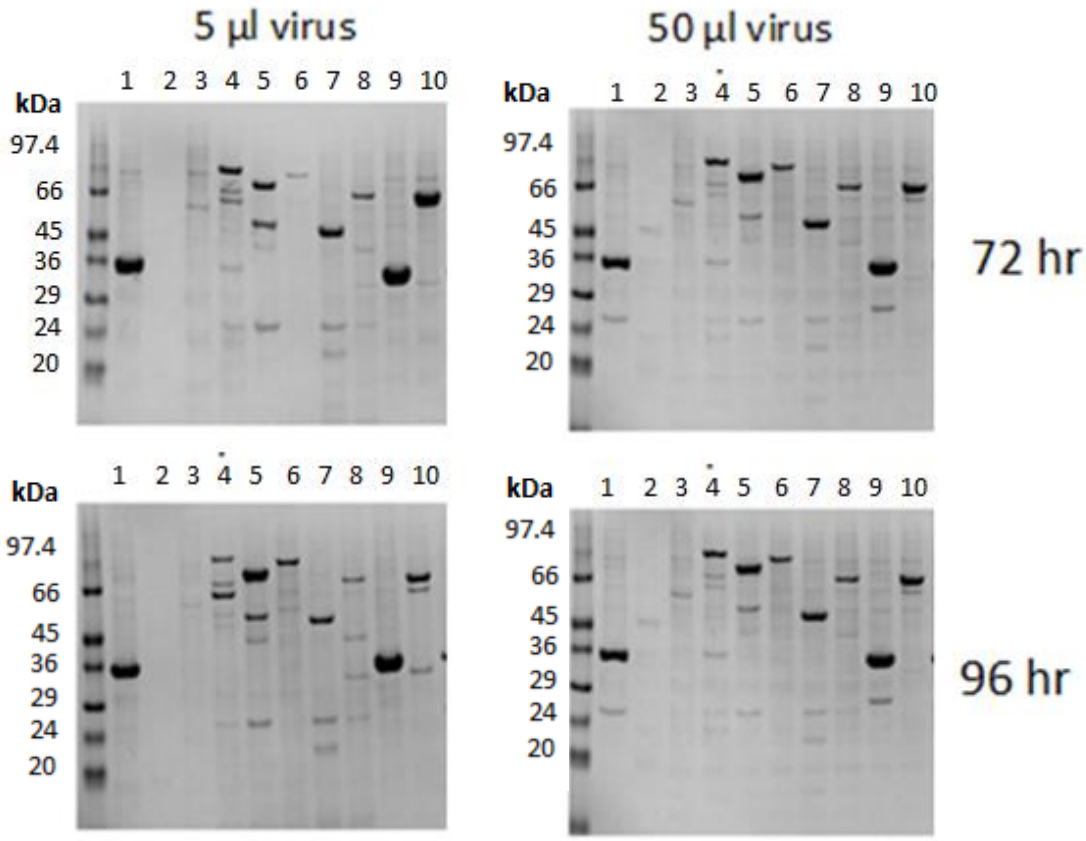

Figure 7.6: SDS-PAGE analyses of insect *Sf*9 cell expression screens. Small-scale trials were conducted to determine the optimal conditions for hPLCXD3 production in *Sf*9 cells following infection with recombinant baculovirus (BV) containing the hPLCXD3 coding sequence. N-terminal fusion tags: 1- $(His)_6$-3C; 2- $(His)_6$-SUMO-3C; 3- $(His)_6$-NUSA-3C; 4- $(His)_6$-MSYB-3C; 5- $(His)_6$-MBP-3C; 6- $(His)_6$-TF-3C; 7- $(His)_6$-TRX-3C; 8- $(His)_6$-HALO-3C. C-terminal fusion tag: 9- 3C-$(His)_6$; 10- 3C-HALO7-$(His)_6$.

7.5. Scale-up purification and crystallisation trials of hPLCXD3

Previously, small-scale expression trials were performed in *E.coli*, HEK293T and *Sf9* insect cells to test the effect of numerous fusion tags on the expression of soluble recombinant human PLCXD1, 2.1 and 3 proteins. Whereas no signs of soluble expression were detectable for hPLCXDs 1 or 2.1 under any of the conditions tested, hPLCXD3 expressed as a soluble protein with highest levels being obtained in the insect expression screen. The expression of N- and C-terminal $(His)_6$-tagged hPLCXD3 was further optimisation in *Sf9* cells by transfection with different titers of the recombinant P1 virus particles (5, 10, 15, 12 and 30 µL) created for each construct. Cells were transfected according to Section 2.3.2 and protein extraction was carried out after 1, 2, 3 and 4 days post-transfection (Chapter 2, Section 2.8.1). The soluble expression of hPLCXD3 was analysed by western blotting. The work was carried out by Ms Nahid Rahman, Oxford Protein Production Facility. For N-terminal $(His)_6$-tagged hPLCXD3, the best soluble, non-degraded expression was present in cells infected with 15-30 µL of recombinant P1 virus, that were harvested 3 days post-infection. For the C-terminal $(His)_6$-tagged construct, the best levels of expression was present in cells infected with 15-30 µL recombinant P1 virus that were harvested 1 day post-transfection. These conditions were then chosen for scale-up purification.

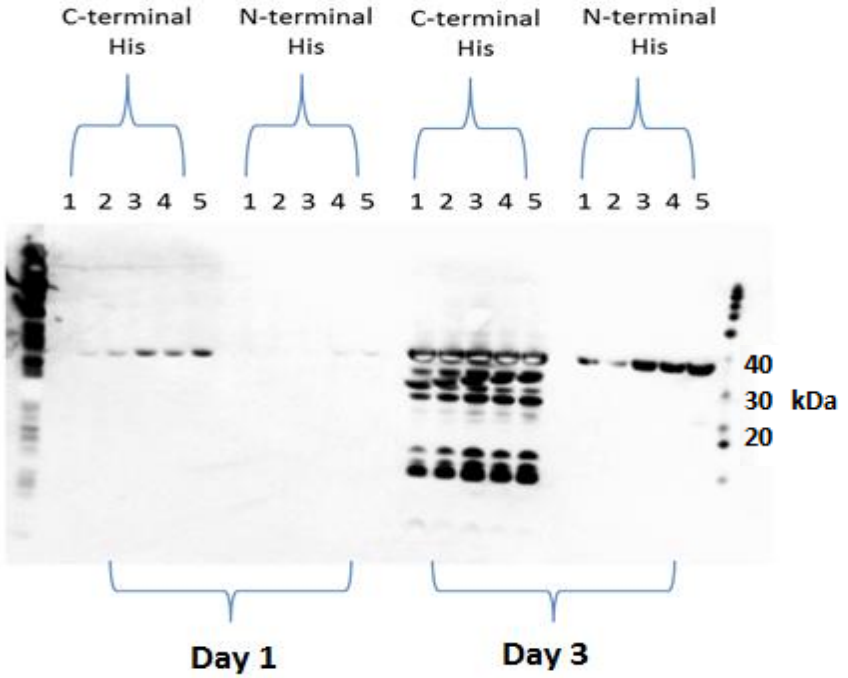

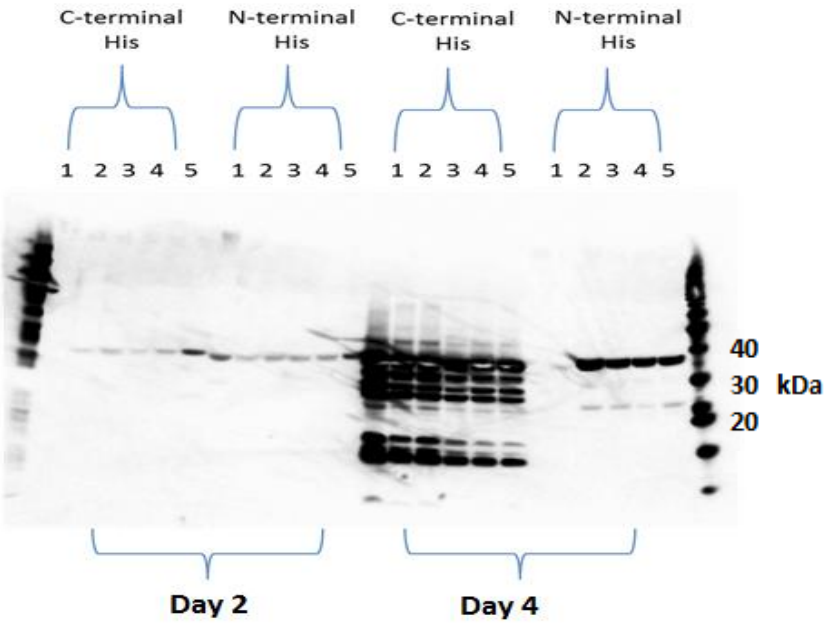

Figure 7.7- Western blot analysis of the expanded insect cell expression screen for hPLCXD3. Recombinant virus containing either the N- or C-terminal $(His)_6$-tagged version of hPLCXD3 was used to infect *Sf9* cells. The following volumes of virus were used for transfections: 5 µL, 10 µL, 15 µL, 20 µL and 30 µL (denoted 1, 2, 3, 4 and 5 above). Cells were harvested at day 1, 2, 3 and 4 and western blotting analysis was performed on extracted proteins using an anti-His primary antibody. Molecular markers are present in the first and last lanes of both blots.

For scale-up, total culture volumes of 1 litre were grown for each hPLCXD3 construct and recombinant proteins expressed according to Chapter 2, Section 2.4.2. Insect cell pellets were disrupted and $(His)_6$-tagged proteins purified from the cell lysate using standard affinity nickel-chromatography techniques, as detailed in Chapter 2, Section 2.8.6. SDS-PAGE analysis revealed the presence of a band of ~38.5 kDa corresponding to the expected size of $(His)_6$-tagged hPLCXD-3 in both the soluble extract (Lane 2; Figure 7.8A and B), and the affinity-purified eluate fractions (Lanes 6, 7 and 8; Figure 7.8A and B). The highest levels of soluble expression were seen with the hPLCXD3, N-terminal $(His)_6$-tagged protein. For both N- and C-terminal $(His)_6$-tagged hPLCXD3 proteins, eluate fractions were pooled and prepared for further purification by gel filtration chromatography (Chapter 2, Section 2.8.8). For each construct, two clear protein peaks were observed (Figure 7.9 and 7.10). The first peak corresponded to higher molecular proteins of ~2500-200 kDa, but also contained a number of proteins below 200 kDa which presumably exist of dimers in solution. The second peak comprised proteins ranging in molecular weight from ~20 to 100 kDa, including the $(His)_6$-tagged hPLCXD3. SDS-PAGE analysis of fractions spanning the second chromatogram peak revealed a band corresponding to the expected size of $(His)_6$-tagged hPLCXD3 (~38.5 kDa) for both preparations (Figure 7.9 and 7.10). For the N-terminal $(His)_6$ fusion protein, fractions containing the 38.5 kDa band were pooled and the histidine tag cleaved following incubation with the 3C protease, as previously described in Chapter 2, Section 2.8.7. Following cleavage of the N-terminal $(His)_6$-tag, the solubility of hPLCXD3 was compromised and substantial precipitate was obtained after storage of the protein at 4 °C for 24 h. SDS-PAGE analysis revealed reduced levels

of the 37 kDa band in the remaining soluble fraction. For the C-terminal $(His)_6$ fusion protein, no tag cleavage was performed and fractions containing hPLCXD3 were subsequently pooled and concentrated to 5 mg/mL, as described in Section 2.7.12. Mass spectrometric analysis of the purified protein showed no evidence of post-translational modifications. An initial crystallization screen was carried out using the commercially available JCSG+ and Wizard I+II protein crystallisation screens and the un-cleaved C-terminal fusion protein (Chapter 2, Section 2.8.13). Crystal trays were incubated at room temperature and checked for the presence of crystals each day for 6 months. No crystals were detected in any of the tested conditions.

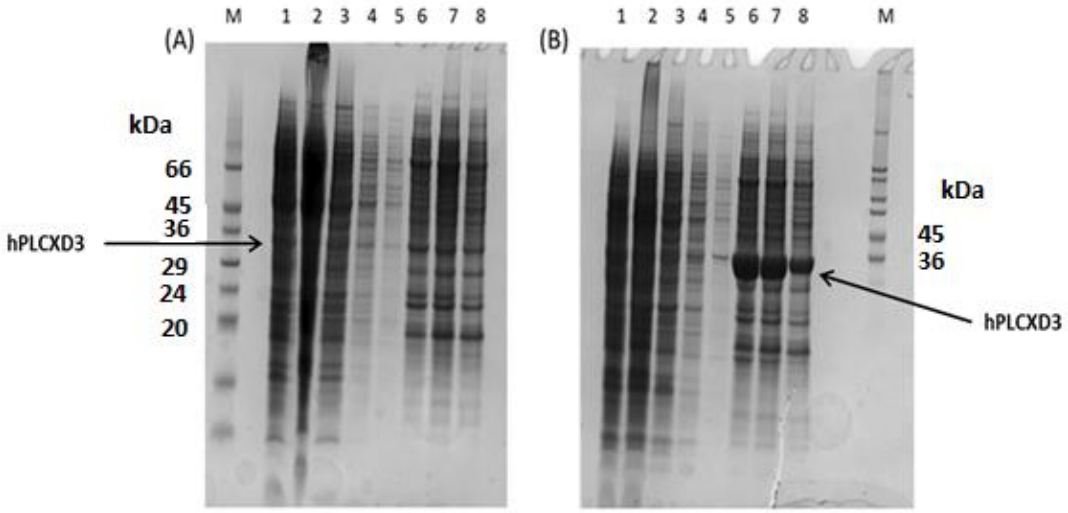

Figure 7.8: SDS-PAGE analysis, with Instant Blue staining, of the different stages purification of C-terminal (A) and N-terminal (B) $(His)_6$-tag fusions of hPLCXD3 from a 1 litre culture of *sf9* cells. Affinity purification chromatography using Nickel-beads was performed in both cases. Lanes are as follows: 1- total lysate; 2- soluble extract; 3- Ni column flow through; 4- Ni column wash 1; 5- Ni column wash 2; 6- Ni column eluate fraction 1; 7- Ni column eluate fraction 2; 8- Ni column eluate fraction 3; M- molecular weight size markers.

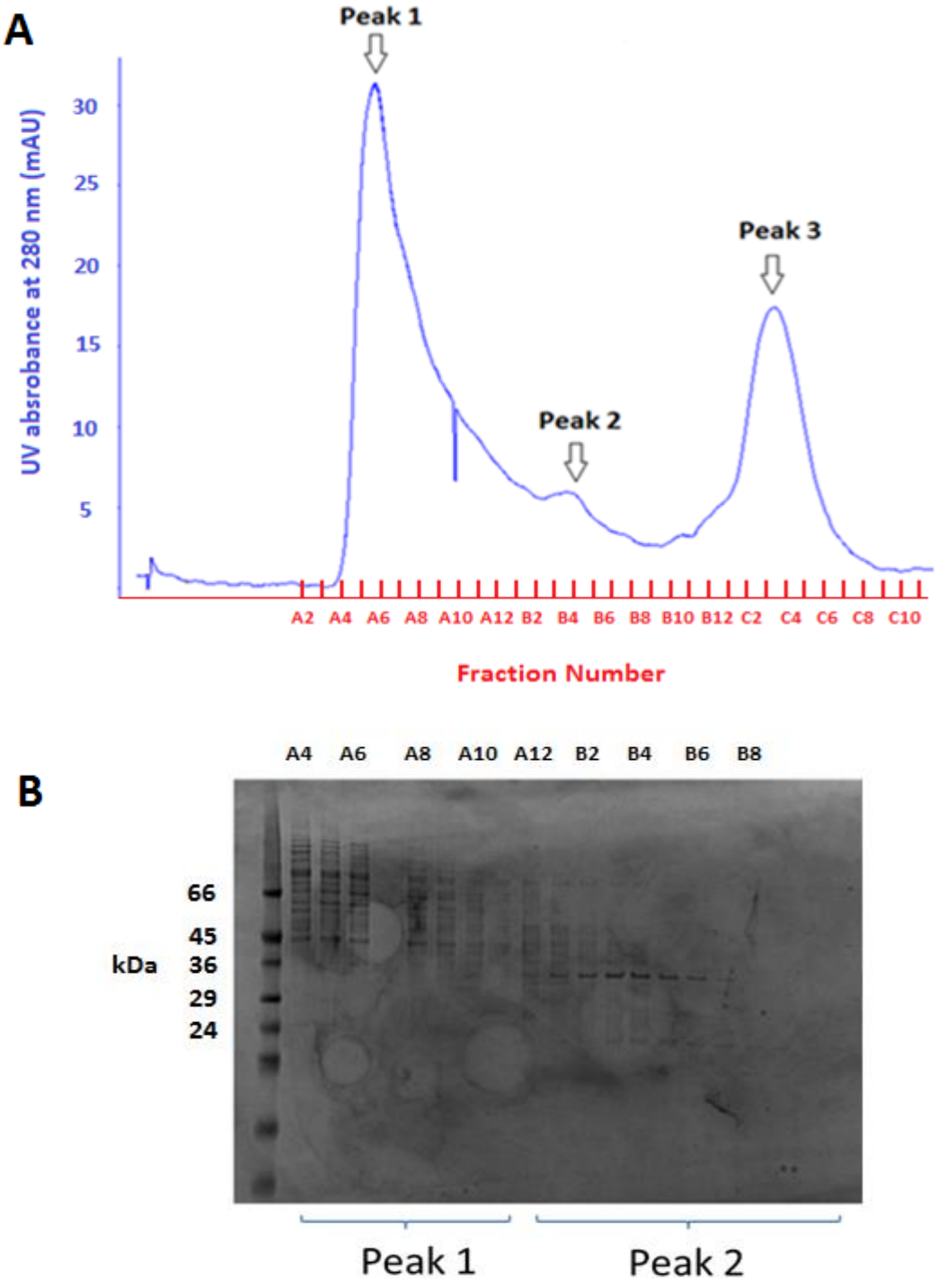

Figure 7.9: Gel exclusion chromatographic analysis of the pooled eluate fractions of the C-terminal PLCXD3 $(His)_6$-tag fusion protein expressed in Insect cells following affinity chromatography. (A) chromatographic analysis showing two protein peaks (Peaks 1 and 2) corresponding to proteins eluting from the first Ni^{2+} - affinity column chromatography and an imidazole peak (Peak 3). (B) SDS-PAGE analysis of selected fractions from the two protein peaks.

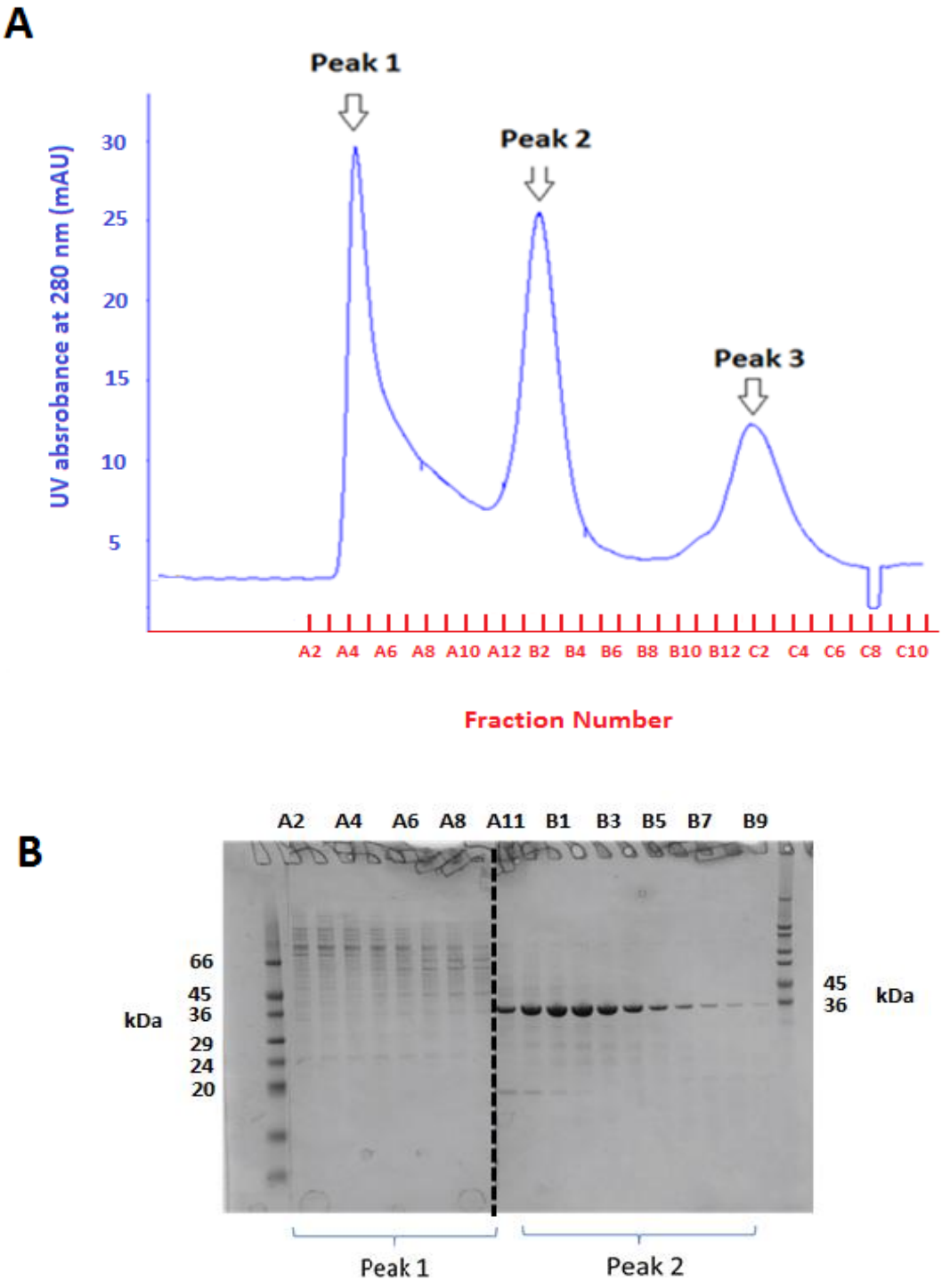

Figure 7.10: Gel exclusion chromatographic analysis of the pooled eluate fractions of the N-terminal PLCXD3 $(His)_6$-tag fusion protein expressed in Insect cells following affinity chromatography. (A) chromatographic analysis showing two protein peaks (Peaks 1 and 2) corresponding to proteins eluting from the first Ni^{2+} - affinity column chromatography and an imidazole peak (Peak 3). (B) SDS-PAGE analysis of selected fractions from the two protein peaks.

7.6. Discussion

Analysis of the data generated by the expression screens in the three different host organisms revealed a high level of variability in protein solubility, with PLCXD3 showing the highest levels of soluble expression in each host. In the *E. coli* screen the production of soluble PLCXD1 and 3 appeared to be a "hit-or-miss" affair with some fusion tags enhancing solubility but with little consistency across the different expression regimes tested, and no obvious increases in solubility of PLCXD2. The HEK293 mammalian expression screen was also met with limited success with soluble expression only experienced with some fusion tagged versions of PLCXD3. The baculovirus-insect cell expression system consistently showed the highest levels of soluble expression; however this was only the case for PLCXD3 with no soluble expression being seen for PLCXD1 or 2. The best levels of soluble expression were obtained for full-length versions of PLCXD3 containing an N- or C-terminal $(His)_6$ tag and expressed in *Sf9* insect cells and therefore these cells were chosen for scale-up purification. Given that the best levels of soluble expression were only observed for PLCXD3, further optimisation of the recombinant production of PLCXD1 and 2 is required. Future strategies to enhance soluble expression could include co-expression with chaperones and the screening of more fusion tags. An alternatively method may be to recover native recombinant protein from inclusion bodies through a process known as refolding. Indeed this strategy has already proven successful for a number of proteins with poor soluble expression in *E. coli*, however the optimal conditions for refolding are protein-dependent and cannot be predicted and therefore this strategy is often challenging (Tsumoto *et al*., 2003).

Scale-up purification of hPLCXD3 was performed using *Sf9* cells in a total 1 litre culture volume, using the predetermined optimal growth conditions for the soluble expression of N- and C-terminally $(His)_6$-tagged PLCXD-3. The highest levels of soluble expression were seen with an N-terminal hexa-His-tagged version of PLCXD3. Purification of both N- and C-terminal $(His)_6$ tagged-PLCXD3 was successful from insect cells with the presence of a band of the expected size following affinity and gel permeation chromatography. Unfortunately, enzymatic cleavage of the N-terminal $(His)_6$-tag from PLCXD3 resulted in complete protein precipitation, rendering the protein unsuitable for further biochemical and crystallographic studies. Interestingly, sequence analysis predicts an intrinsically disordered region (IDR) formed by the first 10 amino acids within the N-terminal regions of hPLCXD3, which therefore suggest that the N-terminus of PLCXD3 does not assume a unique three-dimensional structure under physiological conditions. IDRs have generally been shown to be involved in a variety of functions including molecular recognition, molecular assembly and protein modification (Dunker *et al*., 2002). It is therefore possible that the inclusion of a $(His)_6$-tag at the N-terminus of PLCXD3 may cause a disorder-to-order transition within this region, which could be associated with enhanced solubility of purified PLCXD3. This opens up the possibility that under physiological conditions an N-terminal IDR may mediate interactions with other proteins, which act as binding partners to stabilise PLCXD3 or alternatively proteins involved in post translation modifications. Future experiments should aim to express and purify PLCXD3 lacking the predicted N-terminal IDR to assess its effect on the solubility of the protein. Also, future work could involve pull-down experiments and two-hybrid assays to characterise the existence of

potential binding partners of PLCXD3 and the effect of removal of the predicted N-terminal IDR on protein-protein interactions.

In-order to prevent potential precipitation of PLCXD3, cleavage of the C-terminal $(His)_6$-tag was not performed. As expected, there were no signs of precipitation following purification and concentration (to 5 mg/mL) of the protein. Failure to cleave large affinity tags from purified proteins has been noted to make crystallisation and structure determination more of a challenge as multi-domain proteins are usually less conducive to forming well-ordered, diffracting crystals, presumably due to the conformational heterogeneity allowed by the flexible linker region (Smyth *et al*., 2002). The presence of a small affinity tag, such as the $(His)_6$, is not expected to affect the structure of PLCXD3 as it does not significantly increase the size or charge. Due to these characteristics His-tagged proteins may be more conducive for structure determination, indeed more than 100 structures of $(His)_6$-tagged proteins having been deposited in the Protein Data Bank (Carson *et al*., 2007).

Chapter 8: Conclusions and future directions

The work described herein suggests that PLCXDs are ubiquitous enzymes present in all species from bacteria to man. At least three tissue-specific PLCXDs (PLCXD1-3) were identified in most mammals and four (PLCXD1-4) in teleost fishes. PLCXDs only contain an X-domain in their structure and lack all other domain structures present in mammalian PI-PLCs. PLCXDs are therefore more similar in primary structure to bacterial PI-PLCs and possibly represent the evolutionary precursor of mammalian PI-PLCs. As mentioned at the start of the thesis, "Science never solves a problem without creating 10 more", therefore this Chapter discusses the questions raised by this thesis and suggests future experiments that could be conducted.

8.1. Are PLCXDs active phospholipase C enzymes?

Based on the multiple sequence alignments described in Chapter 3, key amino acids known to be essential for the catalytic functioning of bacterial PI-PLCs were found to be conserved in the X-domain sequences of all PLCXDs, with the exception of ePLCXD4. Bacterial PI-PLCs use these residues to catalyse the hydrolysis of PI by a mechanism involving general acid, general base catalysis. Based on this data, it is therefore speculated that PLCXDs may possess a similar catalytic mechanism to bacterial PI-PLCs and that the catalytic activity of ePLCXD4 may be distinct from other PLCXDs. Whether PLCXDs also contain residues that would enable them to interact with PI and possible $PI(4,5)P_2$ was difficult to predict given the low overall sequence homologies with the bacterial PI-PLCs. The ability of human PLCXDs to catalyse the hydrolysis of $PI(4,5)P_2$ and PI was tested in this thesis. Although expression of human PLCXD1, 2 and 3 in HeLa cells was associated with a 3- to 7-fold increase in endogenous phospholipase C activity, it was found in Chapter 6 that purified hPLCXD3 was not able to hydrolyse either

$PI(4,5)P_2$ or PI. One interpretation of this data is that human PLCXDs may function to increase the activity of other endogenous PI-PLCs and are themselves not catalytically active. Future experiments could screen the catalytic activities of individually purified mammalian PI-PLCs in the presence and absence of purified PLCXD3 to test whether PLCXD3 can increase the rate of $PI(4,5)P_2$ hydrolysis. Alternatively, the observed results may suggest that our expression and purification protocols are not sufficient for the production of active PLCXDs. Indeed, we experienced great difficulties to express human PLCXDs as soluble proteins in *E. coli,* mammalian and insect cells with the recombinant proteins mainly being localised within insoluble inclusion bodies. Although our small-scale expression trials carried out at OPPF identified insect cells as giving the best soluble expression of human PLCXD3, this expression was found to be inconsistent following scale-up purification with repeated purification attempts failing to gain any soluble protein. Future experiments could further optimise the recombinant expression of PLCXDs to gain sufficient protein for enzymatic analysis and crystallography. Obtaining the crystal structures of human PLCXDs would prove useful in determining the substrate specificity of PLCXDs. This way we could model the X-domain structure with that of known bacterial PI-PLCs and mammalian PI-PLCs structures to predict whether PI and/or $PI(4,5)P_2$ would be able to interact with the active site of PLCXDs.

8.2. What is the role of ePLCXD4 in the intestine of the eel during developmental transitions?

Based on microarray data from the intestine of sexually immature yellow eels and sexually mature silver eels, a novel PI-PLC family member was identified which

exhibited differential expression following sexual maturation. The deduced amino acid sequence of the eel protein shares a maximum of 33% with an uncharacterised PLCXD from the bicolour damselfish (*Stegastes partitus*) and less than 20% with all other PLCXDs, including eel PLCXD1, 2 and 3. Subsequently, the eel PLCXD gene identified in the microarray was denoted as PLCXD4. The original microarray data was validated by real time PCR analysis which found a 30-fold decrease in the expression of PLCXD4 mRNA in the intestine of silver compared to yellow eels. Immunofluorescence revealed PLCXD4 to be present in unknown epithelial cells and western blotting analysis found an increase in PLCXD4 levels in the intestine of SW-acclimated silver eels, contrasting the RT-qPCR data. This data therefore suggests that PLCXD4 protein levels are up-regulated by salinity changes in the gut associated with the ingestion of SW, but only in silver eels. Physiologically this may suggest a possible role for PLCXD4 in osmoregulation in the intestine of eels; however this seems unlikely given that PLCXD4 protein expression levels were not affected by salinity transfer in yellow eels. Future experiments could test the effect of salinity changes on the expression of PLCXD4 in cultured epithelial cells from both the yellow and silver eels. Another possible explanation is that the observed increases in PLCXD4 protein levels are associated with the morphological and physiological changes that occur late on during the silvering process as the eel enters the sea. Further studies using cultured epithelial cells from the eel intestine involving PLCXD4 overexpression and knockdown are required to gain better insight into the physiological functions of ePLCXD4 in the intestine.

8.3. What is the role of PLCXDs in the brain?

Data described within this thesis provides evidence that PLCXDs may be important for brain function. Quantitative PCR analysis using a number of mouse tissues found PLCXD1, 2 and 3 mRNA to be predominantly expressed in the brain. More specifically, *in situ* hybridisation data available within the Allen brain atlas revealed PLCXD1 and 2 to have distinct expression profiles within the brain. PLCXD1 was particularly expressed in neurons within the hippocampal formation and the cerebellum suggesting that PLCXD1 could be involved in signal transduction in these brain regions and potential association with learning and memory formation. PLCXD2 mRNA was predominantly located in neurons within the main olfactory bulb and visual cortex suggesting that PLCXD2 might specifically be involved the neural pathways underlying the transduction and processing of sensory stimuli within higher brain regions. No *in situ* hybridisation data for PLCXD3 was available within the Allen brain atlas and therefore the localisation of PLCXD3 mRNA within the brain is currently unknown. More work is required to further characterise the significance of these results. The specific functions of PLCXDs within the brain could be assessed by the generation of knock-out mice. To investigate the functions of PLCXDs in neuronal function, the expression and localisation of PLCXDs in primary neurons could be characterised. Experiments could also study the effect of PLCXD overexpression and/or knockdown on the function of primary neurons.

Expression analysis using a mouse model of neurodegeneration, known as the Harlequin (*Hq*) mouse, revealed a potential role for PLCXDs in neurodegeneration. The levels of PLCXD mRNA and protein were found to differ in tissues that were associated

with significant neurodegeneration attributed to the *Hq* mutation. Both PLCXD2 and PLCXD3 were found to be significantly down-regulated in retinal samples extracted from *Hq* mutant mice compared to control mice. Furthermore, immunofluorescence suggested that PLCXD3 is localised in amacrine cells within the retina and that protein levels are also be reduced in *Hq* mutant mice, although these reductions need to be confirmed by quantitative immunofluorescent experiments. In the cerebellum, although mRNA levels were consistent between control and mutant mice, levels of PLCXD3 protein were significantly reduced in *Hq* mutant mice compared to control mice. Taken together, although these results are compelling, further studies are required to clarify the association between the disease phenotype and PLCXD mRNA and protein expression levels. Future experiments are required to test whether increases in oxidative stress could reduce the levels of PLCXD2 and 3 mRNA in the retina and PLCXD3 protein in the cerebellum of *Hq* mice. This could be tested by RT-qPCR and western blotting analysis of primary neuron cultures with or without chemically induced oxidative stress. Interestingly, a paper was recently published which suggested that three intronic SNPs within PLCXD3 were associated with an increased risk of variant CJD. Although we are yet to further characterise the importance of these SNPs with regard to the expression and catalytic activity of PLCXD3, this data may also suggest a potential role for PLCXDs in neurodegeneration. It is hoped that the worked described within this thesis would stimulate further research into the role of PLCXDs in neurodegenerative disorders. Experiments could use RT-qPCR and western blotting experiments to test whether PLCXDs show differential expression profiles in other neurodegenerative disorders, such as

Alzheimer's disease (AD), Huntingdons disease (HD) and Parkinson's disease (PD). Furthermore, primary neuron cultures could be used to test the functional impact of overexpression and knockdown of PLCXDs in neuronal function.

8.4. Optimisation of the recombinant expression of PLCXDs

A major focus of this thesis was to determine the optimal conditions required for the expression and purification of sufficient amounts of soluble PLCXD for enzymatic analysis and structurally analysis by X-ray crystallography. Although PLCXD1, 2 and 3 were found to express well in *E. coli*, significant formation of inclusion bodies was found in all cases, with PLCXD3 showing the highest solubility. PLCXD3 was therefore chosen for scale-up purification however a 30 L culture was required to obtain sufficient soluble protein for crystallography. This prompted a visit to the Oxford Protein Production Facility to test the effect of fusion tags and different host organisms on the solubility of recombinantly expressed PLCXDs. Initial success was achievedd with PLCXD3 expressed in insect cells however this expression was found to be inconsistent with repeated attempst failing to obtain any expression at all. It is clear from work carried out in this thesis that further work is required to optimise to conditions required for soluble recombinant expression of human PLCXDs. One possibility is to recover native recombinant protein from inclusion bodies through a process known as refolding. Although this strategy has proved successful for a number of proteins with poor soluble expression in *E.coli*, the optimal conditions for refolding are protein-dependent and cannot be predicted making this strategy challenging. Another possible strategy is co-expression with chaperones in *E. coli*. Recombinant cells experience a high substrate load and therefore it is expected that the availability

of chaperones, which are critically important for protein folding, might be a limiting factor. Future experiments could express individual chaperones or chaperone sets, including GroEL, DNak and their associated co-chaperones (de Marco *et al*., 2007) along with PLCXDs.

References

Abnet, C.C., Freedman, N., Hu, Z., Wang, K., Yu, X., Shu, O., Tuan, J.M., Zheng, W., Dawsey, S.M.,Dong, L.M., *et al.,* (2010). A shared susceptibility locus in *PLCE1* at 10q23 for gastric adenocarcinoma and esophageal squamous cell carcinoma. *Nat. Gen.* 42: 764-767.

Adamski, F.M., Timms, K.M. and Sieh, B.H. (1999). A unique isoform of phospholipase CBETA4 highly expressed in the cerebellum and eye. *Biochim. Biophys. Acta.* 1444:55-60.

Anderson, R.J. and Roberts, E.G. (1930). The chemistry of the lipoids of tubercle *bacilli.* XX. The occurrence of mannose and inosite in the phosphatide fractions from the human, avian, and bovine tubercle bacilli. *J. Biol. Chem.* 89: 611-617.

Antonescu, C.N., Aguet, F., Danuser, G., and Schmid, S.L. (2011). Phosphatidylinositol-(4,5)-bisphosphate regulates clathrin-coated pit initiation, stabilization, and size. *Mol. Biol. Cell* 22: 2588-2600.

Avalos, A.M and Ploegh, H.L. Early BCR events and antigen capture, processing, and loading on MHC class II on B cells. *Front. Immunol* 5: 1-5.

Bae, S.S., Lee, Y.H., Chang, J.S., Galadari, S.H., Kin, Y.S., Ryu, S.H. and Sug, P.G. (1998) Src homology domains of phospholipase C gamma1 inhibit nerve growth factor-induced differentiation of PC12 cells. *J. Neurochem.* 71:178-185.

Bahk, Y.Y., Lee, Y.H., Lee, T.G., Seo, J., Ryu, S.H., and Suh, P.G. (2004). Two forms of phospholipase C-beta 1 generated by alternative splicing. *J. Biol. Chem.* 269: 8240-8245.

Bai, Y., Edamatsu, H., Maeda, S., Saito, H., Suzuki, N., Satoh, T. and Kataoka, T. (2005) Crucial role of phospholipase Cepsilon in chemical carcinogen-induced skin tumour development. *Cancer. Res.* 64: 8808-8810.

Balla, T. (2013). Phosphoinositides: Tiny lipids with giant impact on cell regulation. *Physiol Rev* 93: 1019-1337.

Baneyx, F (1999). Recombinant protein expression in *Escherichia coli. Curr. Opin. Biotechnol.* 10: 411-421

Berridge, M.J. (2009). Inositol trisphosphate and calcium signalling mechanisms. *Biochim. Biophys. Acta.* 1793: 933-940.

Berridge, M.J., Lipp, P., Bootman, M.D. (2000). The versatility and universality of calcium signalling. *Nat. Rev. Mol. Cell. Biol.* 1: 11-21.

Bishop, M.T., Sanchez-Juan, P. and Knight, R.S.G. (2013). Splice site SNPs of PLCXD3 are significantly associated with variant and sporadic Creutzfeldt-Jakob disease. *BMC Medical Genetics.* 14: 1-7.

Blaschke, R.J., and Rappold, G. (2006). The pseudoautosomal regions, *SHOX* and disease. *Genetics of disease.* 16, 233-239.

Blis, T.V. and Collingridge, G.L. (1993). A synaptic model of memory: Long-term potentiation in the hippocampus. *Nature.* 361: 31-39.

Blum, S. and Dash, P.K. (2004). A cell-permeable phospholipase Cgamma 1-binding peptide transduces neurons and impairs long-term spatial memory. *Learn. Mem.* 11: 239-243.

Bolanos, C.A., Neve, R.L. and Nestler, E.J. (2005). Phospholipase C gamma in distinct regions of the ventral tegmental area differentially regulates morphine-induced locomotor activity. *Synapse* 56: 166-169.

Bootman, M.D. (2012). Calcium signalling. *Cold Spring Harb Perspect Biol.* 4: 1-3.

Bottomley, M.J., Surdo, P.L., and Driscoll, P.C. (1999). Endocytosis: How dynamin sets vesicles PHree! *Cur. Biol.* 9: 301-304.

Bouaita, A., Agustin, S., Lechauve, C., Cwerman-Thibault, H., Benit, P., Simonutti, M., Paques, M., Rustin, P., Sahel, J-A and Corral-Debrinski, M. (2012). Downregulation of apoptosis-inducing factor in Harlequin mice induces progressive and severe optic atrophy which is durably prevented by AVV2-AIF1 gene therapy. *Brain.* 135: 35-52.

Brose, N., and Rosenmund, C. (2002). Move over protein kinase C, you've got company: alternative cellular effectors of diacylglycerol and phorbol esters. *J. Cell. Sci.* 115: 4399-4411.

Brown, F.D., Rozelle, A.L., Yin, H.L., Balla, T., and Donaldson, J.G. (2001). Phosphatidylinositol 4,5-bisphosphate and Arf6-regulated membrane traffic. *J. Cell. Biol.* 154: 1007-1017.

Bruel-Jungerman, E., Davis, S., and Laroche, S. (2007). Brain Plasticity Mechanisms and Memory: A Party of Four. *Neuroscientist.* 13: 492-505.

Bunney, T.D., Opaleye, O., Roe, S.M., Vatter, P., Baxendale, R.W., et al. (2009). Structural insights into formation of an active signalling complex between Rac and phospholipase C gamma 2. *Mol. Cell.* 34:223-233.

Camilli, A., Goldfinem H. and Portnoy, D.A. (1991). Listeria monocytogenes mutants lacking phosphatidylinositol-specific phospholipase C are avirulent. *JEM.* 173: 751-754.

Carson, M., Johnson, D.H., McDonald, H., Brouillette, C., DeLucas, L.J. (2007). His-tag impact on structure. *Biol. Crystallogr.* 63: 295-301.

Chalfant, M.L., Denton, J.S., Langloh, A.L., Karlson, K.H., Loffing, J., Benos, D.J., and Stanton, B.A. (1999). The NH2 terminus of the epithelial sodium channel contains an endocytic motif. *J. Biol. Chem.* 274: 32889-32896.

Chandrasekar, I., Stradal, T.E.B., Holt, M.R., Entschladen, F., Jockusch, B.M., and Ziegler, W.H. (2005). Vinculin acts as a sensor in lipid regulation of adhesion-site turnover. *J. Cell. Sci.* 118: 1461-1472.

Chuang, S., Bianchi, R., Kim, D., Shin, H.S., and Wong, R.K. (2001). Group 1 Metabotropic Glutamate Receptors Elicit Epileptiform Discharges in the Hippocampus Through PLCbeta1 Signalling. *J. Neurosci,* 21, 6387-6394.

Cifuentes, M.E., Honkanen, L. and Rebecchi, M.J. (1993). Proteolytic fragments of phosphoinositide-specific phospholipase C-δ1. *J. Biol. Chem.* 268: 11586-11593.

Clarke, A.J. and Witcomb, D.M. (1980). A study of the histology and morphology of the digestive tract of the common eel (Anguilla anguilla). *Journal of Fish Biology.* 16: 159-170.

Dawson, R.M. (1959). Studies on the enzymic hydrolysis of monophosphoinositide by phospholipase preparations from P. notatum and ox pancreas. *Biochim. Biophys. Acta.* 33: 68-77.

De Camilli, P., Emr, S.D., McPherson, P.S., and Novick, P. (1996). Phosphoinositide as regulators in membrane traffic. *Science.* 271: 1533-1539.

De Marco, A. (2007). Protocol for preparing proteins with improved solubility by co-expressing with molecular chaperones in Escherichia coli. *Nat Protoc.* 10: 2632-2639.

Dove, S.K., Cooke, F.T., Douglas, M.R., Sayers, L.G., Parker, P.J., and Mitchell, R.H. (1997). Osmotic stress activates phosphatidylinositol-3,5-bisphosphate synthesis. *Nature.* 390: 187-192.

Drin, G., Douquet, D. and Scarlata, S. (2006). The pleckstrin homology domain of phospholipase C eta transmits enzymatic activation through modulation of the membrane-domain orientation. *Biochemistry.* 45: 5712-5724.

Dunker, A.K., Brown, C.J., Lawson, J.D., Iakoucheva, L.M., Obradovic, Z. (2002). Intrinsic Disorder and Protein Function. *Biochemistry.* 41: 6573-6582.

Durif, C., Dufour, S. and Elie, P. (2005). The silvering process of Anguilla anguilla: a new classification from the yellow resident to the silver migrating stage. *J. Fish Biol.* 66: 1025-1043.

Ellis. M.V., James, S.R., Perisic, O., Downes, C.P., Willams, R.L and Katan, M. (1998). Catalytic domain of phosphoinositide-specific phospholipase C (PLC): Mutational analysis of residues within the active site and hydrophobic ridge of PLCδ1. *J. Biol. Chem.* 275: 11650-11659.

Essen, L.O., Perisic, O., Cheung, R., Katan, M., William, R.L. (1996). Crystal structure of a mammalian phosphoinositide-specific phospholipase C delta. *Nature.* 380: 595-602.

Essen, L-O., Perisic, O., Katan, M., Wu, Y., Roberts, M.F., William, R.L. (1997). Structural Mapping of the Catalytic Mechanism for a Mammalian Phosphoinositide-Specific Phospholipase C. *Biochemistry.* 36: 1704-1718.

Essen, L-O., Perisic, O., Lynch, D.E., Katan, M. Williams, R.L. (1997). A ternary binding site in the C2 domain of phosphoinositide-specific phospholipase C-δ1. *Biochemistry* 36: 2753-2762.

Ferguson, K.M., Lemmon, M.A., Schlessinger, J., Sigler, P.B. (1995). Structure of the high affinity complex of inositol trisphosphate with a phospholipase C pleckstrin homology domain. *Cell.* 83: 1037-1046.

Folch, J. (1949). Complete fractionation of brain cephalin; isolation from it of phosphatidyl serine, phosphatidyl ethanolamine, and diphosphoinositide. *J Biol Chem* 177: 497-504.

Ford, M.G., Pearse, B.M., Higgins, M.K., Vallis, Y., Owen, D.J., Gibson, A., Hopkins, C.R., Evans, P.R., and McMahon, H.T. (2001). Simultaneous binding of PtdIns(4,5)P2 and clathrin by AP180 in the nucleation of clathrin lattices on membranes. *Science.* 291: 1051-1055.

Fukami, K., Makao, K., Inoue, T., Kataoka, Y., Kurokawa, M., Fissor, R.A., Nakamura, K., Katsuki, M., Mikoshiba, K., Yoshida, N. and Takenawa, T. (2001). Requirement of phospholipase Cdelta4 for the zona pellucida-induced acrosome reaction. *Science.* 292: 920-923.

Fukami, K., Yoshida, M., Inoue, T., Kurokawa, M., Fissore, R.A., Yoshida, N., Mikoshiba, K. and Takenawa, T. (2003). Phospholipase C delta 4 is required for Ca2+ mobilization essential for acrosome reaction in sperm. *J. Cell Biol.* 161: 79-88.

Fukudome, Y., Ohno-Shosaku, t., Matsui, M., Omori, Y., Fukaya, M., Hiroshi, T., Taketo, M.M., Watanabe, M., Manabe, T., Kano, M. (2004). Two distinct classes of muscarinic action on hippocampal inhibitory synapses: M2-mediated direct suppression and M1/M3- mediated indirect suppression through endocannabinoid signalling. *Euro. J. Neurosci.* 19: 2682-2692.

Gifford, J.L., Walsh, M.P. and Vogel, H.J. (2007) Structures and metal-ion-binding properties of the Ca^{2+}-binding helix-loop-helix EF-hand motifs. *Biochem. J.* 405: 199-221.

Gonzales, M.L., Anderson, R.A. (2006). Nuclear phosphoinositides, kinases and inositol phospholipids. *J. Cell. Biochem.* 97: 252-260.

Grobler, J.A., Essen, L.O., William, R.L., and Hurley, J.H. (1996). C2 domain conformational changes in phospholipase C-δ1. *Nat. Struct. Biol.* 3: 788-795.

Grosell, M. (2010). 4-The role of the gastrointestinal tract in salt and water balance. *Fish physiology*. 30: 135-164.

Hangen, E., Blomgren, K., Benit, P., Kroemer, G. and Modjtahedi, N. (2009). Life with or without AIF. *Trends in Biochemical Sciences.* 35: 278-287.

Hannig, G., Makrides, S.C. (1998). Stretegies for optimizing heterologous protein expression in *Escherichia coli*. *Trends Biotechnol.* 16: 54-60.

Hanrahan, O., Webb, H., O'Byrne, R., Brabazon, E., Treumann, A., Sunter, J.D., Carrington, M. and Voorheis, H.P. (2009). Theglycosylphosphatidylinositol-PLC in Trypanosoma brucei forms a linear array on the exterior of the flagellar membrane before and after activation. *PLoS Pathog.* 5: 1-16.

Harden, T.K., Hicks, S.N. and Sondek, J. (2009). Phospholipase C isozymes as effectors of Ras superfamily GTPases. *J. Lipid. Res.* 50: 243-248.

Hashimoto, A., Takeda, K., Inaba, M., Sekimata, M., Kasiho, T., Ikehara, S., Homma, Y., Akira, S., Kurosaki, T. (2000). *J. Immunol.,* 165, 1738-1742.

Haslam, R.J., Koide, H.B., Hemmings, B.A. (1993). Pleckstrin domain homology. *Nature.* 27: 363: 306-310.

Hawkins, P.T., Anderson, K.E., Davidson, K. and Stephen, L.R. (2006). Signalling through Class 1 PI3Ks in mammalian cells. *Biochem Trans.* 34: 647-662.

Heacock, A.M. and Agranoff, B.W. (1997). CDP-diacylglycerol synthase from mammalian tissues. *Biochim. Biophy. Act.* 1348: 166-172.

Heinz, D.W., Essen, L-O., and William, R.L. (1998). Structural and mechanistic comparison of prokaryotic and eukaryotic phosphoinositide-specific phospholipase C. *J. Mol. Biol.* 275: 635-650.

Hemmings, B.A. (1997). UPDATE: PH domains—A universal membrane adapter. *Science.* 275: 1899

Heytens, E., Parrington, J., Coward, K., Young, C., Lambrecht, S., *et al.,* (2009). Reduced amounts and abnormal forms of phospholipase C zeta (PLCζ) in spermatozoa from infertile men. *Hum. Reprod.* 24: 2417-2428.

Hicks, S.N., Jezyk, M.R., Gershburg, S., Seifert, J.O., Harden, T.K. and Sondek, J. (2008). General and versatile autoinhibition of PLC isozymes. *Mol. Cell* 31: 383-394.

Higgs, H.N., and Pollard, T.D. (2000). Activation by Cdc42 and PIP2 of Wiskott-Aldrich Syndrome protein (WASp) stimulats actin nucleation by Arp2/3 complex. *J. Cell. Biol.* 150: 1311-1320.

Hilgemann, D.W., and Ball, R. (1996). Regualtion of cardiac Na^+, Ca^{2+} exchange and KATP potassium channels by PIP_2. *Science* 273: 956-959.

Hinkles, B., Wiggins, R.C., Gbadegesin, R., Vlangos, C.N., Seelow, D., Nurnberg, G., Garg, P., Verma, R., Chaib, H., Hoskins, B.E, *et al*., (2006). *Nat Gen.* 38: 1397-1405.

Hokin, M.R., and Hokin, L.E. (1953). Enzyme secretion and the incorporation of P32 into phospholipids of pancreas slices. *J Biol Chem* 203: 967-977.

Homma, Y., Takenawa, T., Emori, Y., Sorimachi, H., and Suzki, K. (1989). Tissue- and cell type-specific expression of mRNAs for four types of inositol phospholipid-specific phospholipase C. *Biochem. Biophys. Res. Commun.* 164: 406-412.

Hondal, R.J., Zhao, Z., Kravchuk, A.V., Liao, H., Riddle, S.R., Yue, X., Bruzik, K.S. and Tsai, M-D. (1997). Mechanism of phosphatidylinositol-specific phospholipase C: A unified view of the mechanism of catalysis. *Biochemistry* 37: 4568-4580.

Huang, C.L., Feng, S., Hilgemann, D.W. (1998). Direct activation of inward rectifier potassium channels by PIP2 and its stabilization by Gβγ. *Nature* 391: 803-806.

Hurley, J.H., Misra, S. (2000). Signalling and subcellular targeting by membrane-binding domains. *Annu. Rev. Biophys. Biomol. Struct.* 29: 49-79.

Hwang, J-IK., Oh, Y-S., Shin, K-J., Kim, H., Ryu, S.H., Suh, P-G. (2005). Molecular cloning and characterisation of a novel phospholipase C, PLC-*η*. *J. Biochem.* 389: 181-186.

Ichinohe, M., Nakamura, Y., Sai, K., Nakahara, M., Yamaguchi, H. and Fukami, K (2007). Lack of phospholipase C-delta 1 induces skin inflammation. *Biochem Biophys Res Commun.* 356: 912-918.

Illenberger, D., Schwald, F. and Gierschik, P. (1997). Characterization and purification from bovine neutrophils of a soluble guanin-nucleotide-binding protein that mediates isozymes-specific stimualtion of phospholipase C β_2. *Eur. J. Biochem.* 246: 71-77.

Illenberger, D., Schwald, F., Pimmer, D., Binder, W., and Maier G. (1998). Stimulation of phospholipase C-β_2 by Rho GTPases Cdc42Hs and Rac1. *EMBO J.* 17: 6241-6249.

Irvine, R.F. (2003). Nuclear lipid signalling. *Nat. Rev. Mol. Cell. Biol.* 4: 349-361.

Izquierdo, I. and Medina, J.H. (1997). Memory Formation: The sequences of Biochemical Events in the Hippocampus and Its Connection to Activity in Other Brain Structures. *Neurobiology of Learning and Memory.* 68: 285-316.

Jarrard, L.E. (1993) On the role of the hippocampus in learning and memory in the rat. *Behav. Neual Biology.* 60: 9-26.

Jezyk, M.R., Snyder, J.T., Gershberg, S., Worthylake, D.K., Harden, T.K. and Sondek, J. Crystal structure of Rac1 bound to its effector phospholipase C-beta1. *Nat Struc & Mol Biol.* 13: 1135-1139.

Jhon, D.Y., Lee, H.H., Park, D., Lee, C.W., Lee, K.H., Yoo, O.J. and Rhee, S.G. (1993). Cloning, sequencing, purification, and Gq-dependent activation of phospholipase C-beta 3. *J. Biol. Chem.* 268: 6654-6661.

Ji, Q.S., Winnier, G.E., Niswender, K.D., Horstman, D., Wisdom, R., Magnuson, M.A and Carpenter, G. (1997). Essential role oft he tyrosine kinase substrate phospholipase C-gamma1 in mammalian growth and development. *Proc. Natl. Acad. Sci. USA.* 94: 2999-3003.

Jiang, H., Kuang, Y., Wu, Y., Smrcka, A., Simon, M.I and W, D. (1996). Pertussis toxin-sensitive activation of phospholipase C by the C5a and fMET-Leu-Phe-receptors. *J. Biol. Chem.* 271: 13430-13434.

Jiang, H., Kuang, Y., Wu, Y., Xie, W., Simon, M.I. and Wu, D. (1997). Roles of phospholipase C beta2 in chemoattractant-elicited responses. *Proc. Natl. Acad. Sci. U. S. A.* 94: 7971-7975.

Jiang, H., Lyubarsky, A., Dodd, R., Vardi, N., Pugh, E., Baylor, D., Simon, M.I. and Wu, D. (1996). Phospholipase C beta 4 is involved in modulating the visual response in mice. *Proc. Natl. Acad. Sci. U. S. A.* 93: 14598-14601.

Jin, T-G., Satoh, T., Liao, Y., Song, C., Gao, X., Kariya, K-I., Hu, C-D., Kataoka, T. (2001). Role of the CDC_{25} Homology Domain of Phospholipase Cε in AMplifcation of Rap1-dependent Signaling. *J. Biol. Chem.* 276: 30301-30307.

Jones, K.T. (2005). Mammalian egg activation: from Ca^{2+} spiking to cell cycle progression. *Reproduction.* 130: 813-823.

Jorntell, H., Hansel, C. (2006). Synaptic memories upside down: bidirectional plasticity at cerebellar parallel fiber-Purkinje cell synapses. *Neuron.* 52: 227-238.

Kabachinski, G., Yamaga, M., Kielar-Grevstad, D.M., Bruinsma, S., Martin, T.F. (2014). CAPS and Munc13 utilize distinct PIP2-linked mechanisms to promote vesicle exocytosis. *Mol. Biol. Cell.* 25: 508-521.

Kadamur, G., Ross, E.M. (2013). Mammalian phospholipase C. *Annu. Rev. Physiol.* 75: 127-154.

Kelley, G.G., Reks, S.E., Ondrako, J.M. and Smrcka, A.V. (2001). Phospholipase Cε: A novel Ras effector. *EMBO J.* 20: 743-754.

Kim, D., Jun, K.S., Lee, S.B., Kang, N.G., Min, D.S., Kim, Y.H., Ryu, S.H., Suh, P.G. and Shin, H.S. (1997). Phospholipase C isozymes selectively couple to specific neurotransmitter receptors. *Nature.* 389: 290-293.

Kim, Y.J., Sekiya, F., Poulin, B., Bae, Y.S and Rhee, S.G. (2004). Mechanism of B-Cell Receptor phosphorylation and activation of phospholipase C-γ2. *Mol Cell Biol.* 24: 9986-9999.

Kirk, C.J. (1990). Recent devlopments in our understanding of the inositol lipid signalling system. *Symp. Soc. Exp. Biol.* 44: 173-180.

Kirkman-Brown, J.C., Punt, E.L., Barratt, C.L.R. and Publicover, S.J. (2002). Zona pellucida and progesterone-induced Ca2+ signalling and acrosome reaction in human spermatozoa. *J. andrology.* 23: 306-315.

Klein, J.A. and Ackerman, S.L. (2003). Oxidative stress, cell cycle, and neurodegeneration. *J. Clin. Invest.* 111: 785-793.

Klein, J.A., Longo-Guess, C.M., Rossmann, M.P., Seburn, K.L., Hurd, R.E., Frankel, W.N., Bronson, R.T. and Ackerman, S.L. (2002). The harlequin mouse mutation downregulates apoptosis-induing factor. *Nature.* 419: 367-374.

Klichko, V.I., Miller, J., Wu, A., Popov, S.G. and Alibek, K. (2003). Anaerobic induction of *Bacillus anthracis* haemolytic activity. *Biochem. Biophys. Res. Commun.* 303: 855-862.

Kouchi, Z., Fukami, K., Shikano, T., Oda, S., Nakamura, Y., Takenawa, T. and Miyazaki, S. (2004). Recombinant phospholipase C zeta has a high Ca^{2+} sensitivity and induces Ca^{2+} oscillations in mouse egge. *J . Biol. Chem.* 279: 10408-10412.

Kouchi, Z., Skikano, T., Nakamura, Y., Shirakawa, H., Fukami, K. and Miyazaki, S. (2005). The role of EF-hand domains and C2 domain in regulation of enzymatic activity of phospholipase Cζ. *J. Biol. Chem.* 280: 21015-21021.

Kretsinger, R.H., Nockold, C.E. (1973). Carp muscle calcium-binding protein. II. Structure determination and general description. *J. Biol. Chem.* 248: 3313-3326.

Kunzevitzky, N.J., Willeford, K.T., Feuer, W.J., Almeida, M.V. and Goldberg, J.L. (2013). Amacrine cell subtypes differ in their intrinsic neurite growth capacity. *Invest. Ophthalmol. Vis. Sci.* 54: 7603-7613.

Kuppe, A., Evans, L.M., McMillen, D.A. and Griffith, O.H. (1989). Phosphatidylinositol-specific phospholipase C of Bacillus cereus: cloning, sequencing, and relationship to other phospholipases. *J. Bacteriol.* 171: 6077-6083.

Lange, A., Mills, R.E., Lange, C.J., Stewart, M., Devine, S.E. and Corbett, A.H. (2007). Classical nuclear localisation signals: Definitions, function, and interaction with Importin α. *J. Biol. Chem.* 282: 5101-5105.

Lee, CH., Park, D., Wu, D., Rhee, S.G. and Simon, M.I. (1992). Members of the Gq alpha subunit gene family activate phospholipase C beta isozymes. *J. Biol. Chem.* 267: 16044-16047.

Lee, S.B. and Rhee, S.G. (1996). Molecular cloning, splice variants, expression, and purification of phospholipase C-delta 4. *J. boil. Chem.* 274: 25-31.

Lee, W.K., Kin, J.K., Seo, M.S., Cha, J.H., Lee, K.J., Rha, H.K., Min, D.S., Jo, Y.H. and Lee, K.H. (1999). Molecular cloning and expression analysis of a mouse phospholipaseC-delta1. *Biochem. Biophys. Res. Commun.* 261: 393-399.

Lemmon, M.A. (2007). Pleckstrin homology (PH) domains and phosphoinositides. *Biochem. Soc. Symp.* 74: 81-93.

Lemmon, M.A., Ferguson, K.M., O'Brien, R., Sigler, P.B. and Schlessinger, J. (1995). Specific and high-affinity binding of inositol phosphates to an isolated pleckstrin homology domain. *Proc. Natl. Acad. Sci. USA* 92: 10472-10476.

Li, D., Lyons, J.A., Pye, V.E., Vogeley, L., Argao, D., Kenyon, C.P., Shah, S.T.A., Doherty, C., Aherne, M and Caffrey, M. (2013). Crystal structure of the integral membrane diacylglycerol kinase. *Nature.* 497: 521-524.

Lin, F.G., Cheng, H.F., Lee, I.F., Kao, H.J., Loh, S.H. and Lee, W.H. (2001). Downregulation of phospholipase C delta3 by cAMP and calcium. *Biochem. Biophys. Res. Commun.* 286: 274-280.

Lin, H.Y., Xu, J., Ischenko, I., Ornitz, D.M., Halegoua, S. and Hayman, M.J. (1998). Identification of the cytoplasmic regions of fibroblast growth factor (FGF) receptor 1 which play important roles in induction of neurite outgrowth in PC12 cells by FGF-1. *Mol. Cell. Biol.* 18: 3762-3770.

Lomasney, J.W., Cheng, H.F., Kobayashi, M., and Ling, K. (2012). Structural basis for calcium and phosphatidylserine regulation of PLCδ1. *Biochemistry* 51: 2246-2257.

Lomasney, J.W., Cheng, H-F., Roffer, S.R. and King, K. (1999). Activation of phospholipase C δ1 through C2 domain by Ca^{2+}-enzyme-phosphatidylserine ternary complex. *J. Biol. Chem.* 274: 21995-22001.

Lopez, I., Mak, E.C., Ding, J., Hamm, H.E. and Lomasney, J.W. (2001). A novel bifunctional phospholipase C that is regulated by Gα12 and stimulates the Ras/mitogen-activated protein kinase pathway. *J. Biol. Chem.* 276: 2758-2765.

Ma, H.P., Saxena, S., Warnock, D.G. (2002). Anionic phospholipids regulate native and expressed epithelial sodium channel (ENaC). *J. Biol. Chem.* 277: 7641-7644.

Macneil, M.A., Heussy, J.K., Dacheux, R.F., Raviola, E. and Masland, R.H. (1999). The Shapes and Numbers of Amacrine Cells: Matching of Photofilled With Golgi-stained Cell in the Rabbit Retina and Comparison with Other Mammalian Species. *J. Comp. Neurol.* 413: 305-326.

Mangat, R., Singal, T., Dhalla, N.S. and Tappia, P.S. (2006). Inhibition of phospholipase c-gamma 1 augments the decrease in cardiomyocyte viability by H2O2. *Am. J. Physiol. Heart Circ. Physiol.* 291: 854-860.

Marrero, M.B., Paxton, W.G., Duff, J.L., Berk, B.C and Bernstein, K.E. (1994) Angiotensin II stimulates tyrosine phosphorylation of phospholipase C-gamma1 in vascular smooth muscle cells. *J. Biol. Chem.* 269: 10935-10939.

Mate, M.J., Ortiz-Lonbardia, M., Boitel, B., Haouz, A., Tello, D., Susin, S.A., Penninger, J., Kroemer, G. and Alzari, P.M. (2002). The crystal structrure of the mouse apoptosis-inducing factor AIF. *Nature Structural Biology.* 9: 442-446.

Mayer, B.J., Ren, R., Clark, K.L., Baltimore, D. (1993). A putative modular domain present in diverse signalling protein. *Cell.* 73: 629-630.

McLaughlin, S., Wang, J., Gambhir, A., and Murray, D. (2002). PIP_2 and proteins: Interaction, Organization and Information Flow. *Annu. Rev. Biophys. Biomol. Struct.* 31: 151-175.

McNeill, E., Conway, S.J., Roderick, H.L., Bootman, M.D. and Hogg, N. (2007). Defective chemoattractant-induced calcium signalling in s100A9 null neutrophils. *Cell Calcium* 41: 107-121.

Mengaud, J., Braun-Breton, C. and Cossart, P. (1991). Identification of phosphatidylinositol-specific phospholipase C activity in *Listeria monocytogenes*: a novel type of virulence factor? *Mol Microbiol.* 5: 367-372.

Mitchell, R.H. (1975). Inositol phospholipids and cell surface receptor function. *Biochim Biophys Acta* 415: 81-47.

Mitchell, R.H. (2008). Inositol derivatives: evolution and functions. *Nat Rev Mol Cell Biol* 9: 151-161.

Mizuguchi, M., Yamada, M., Kim, S.U. and Rhee, S.G. (1991). Phospholipase C isozymes in neurons and glial cells in culture: an immunocytochemical and immunochemical study. *Brain Res.* 548: 35-40.

Modjtahedi, N., Gioranetta, F., Madeo, F. and Kroemer, G. (2006). Apoptosis-inducing factor: vital and lethal. *Trends in Cell Biology.* 16: 264-272.

Moews, P.C., Kretsinger, R.H. (1975). Terbium replacement of calcium in carp muscle calcium-binding parvalbumin: An X-ray crystallographic study. *J. Mol. Biol.* 91: 229-232.

Munk, P., Hansen, M.M., Maes, G.E., Nielsen, T.G., Castonguay, M., Riemann, L. and Bachler, M (2010). Oceanic fronts in the Sargasso Sea control the early life and drift of Atlantic eels. *Porceeding of the Royal Society B: Biological Sciences.* rspb20100900.

Nagy, Z.S., Esiri, M.M. and Smith, A.D. (1998). The cell division cycle and the pathophysiology of Alzheimers disease. *Neuroscience.* 87: 731-739.

Nakahara, M., Shimozawa, M., Nakamura, Y., Irino, Y., Morita, M., Kudo, Y. and Fukami, K. (2005). A novel phospholipase C, PLC(eta)2, is a neuron-specific isozyme. *J. Biol. Chem.* 280: 29128-29134.

Nalefski, E.A., and Falke, J.J. (1996). The C2 domain calciu-binding motif: Structural and functional diversity. *Prot Sci.* 12: 2375-2390.

Nelson, M.R., Thulin, E., Fagan, A., Forsen, S., and Chazin, W,J, (2002). The EF-hand domain: A globally cooperative structural unit. *Protein Sci.* 2: 198-205.

Nettleship, J.E., Assenberg, R., Diprose, J.M., Rahman-Huq, N., Owen, R.J. (2010). Recent advances in the production of proteins in insect and mammalian cells for structural biology. *J. Struct. Biol.* 172: 55-65.

Nomikos, M., Blayney, L.M., Larman, M.G., Campbell, K., Rossbach, A., Saunders, C.M., Swann, K., and Lai, F.A. (2005). Role of PLC-zeta domains in Ca^{2+}-dependent PIP2 hydrolysis and cytoplasmic Ca^{2+} oscillations. *J. Biol. Chem.* 280: 31011-31018.

Nomikos, M., Mulgrew-Nesbitt, A., Pallavi, P., Mihalyne, G., Zaitseva, I., *et al.* (2007). Binding of phosphoinositide-specific phospholipase C-ζ (PLC-ζ) to phospholipid membrane. *J. Biol. Chem.* 282: 16644-16653.

Nuwayhid, S.J., Vega, M., Walden, P.D., Monaco, M.E. (2006). Regulation of de novo phosphatidylinositol synthesis. *J. Lipid. Res.* 47: 1449-1456.

Oh, J.E., Nook, J.K., Park, K.H., Lee, G., Seo, B.M and Min, B.M. (2003). Phospholipase C-gamma1 is required for subculture-induced terminal differentiation of normal human oral keratinocytes. *Int. J. Mol. Med.* 11: 491-498.

Pamer, E.G. (2004). Immune responses to *Listeria monocytogenes. Nat Rev Immun.* 4: 812-823.

Park, D., Jhon, D.Y., Lee, C.W., Lee, K.H. and Rhee, S.G. (1993). Activation of phospholipase C isozymes by G protein beta gamma subunits. *J. Biol. Chem.* 268: 4573-4576.

Pears, C. (1995). Structure and function of the protein kinase C gene family. *J. Biosci.* 20: 311-332.

Petersen, T.N., Brunak, S., von H.G. and Nielsen, H. (2011). SignalP 4.0: discriminating signal peptides from transmembrane regions. *Nat Methods.* 8: 785-786.

Piechulek, T., Rehlen, T., Walliser, C., Vatter, P., Moepps, B and Gierschik, P. (2005). Isozyme-specific stimulation of phospholipase C-γ2 by Rac GTPases. *J. Biol. Chem.* 280: 38923-38931.

Popovics, P., Lu, J., Kamil, L.N., Morgan, K., Millar, R., Schmid, R., Blindauer, C.A. and Stewart, A.J. (2014). A canonical EF-loop directs Ca^{2+} sensitivity in Phospholipase C-ɳ2. *J. Cell. Biochem.* 115: 557-565.

Poussin, M.A., Leitges, M. and Goldfine, H. (2009). The ability of Listeria monocytogenes PI-PLC to facilitate escape from the macrophage phagosome is dependent on host PKCbeta. *Microb Pathog.* 46: 1-5.

Rakotoarisoa, L., Carricaburu, V., Leblanc, C., Mironneau, J. and Macrez, N. (2006). Angiotensin II-induced delayed stimulation of phospholipase C gamma1 requires activation of both phosphatidylinositol 3-kinase gamma and tyrosine kinase in vascular myocytes. *J. Cell. Mol. Med.* 10: 734-748.

Rameh, L.E., Tolias, K.F., Duckworth, B.C., and Cantley, L.C. (1997). A new pathway for synthesis of phosphatidylinositol-4,5-bisphosphate. *Nature.* 390: 192-196.

Rebecchi, M.J. and Pentyala, S.N. (2000). Structure, function, and control of phosphoinositdie-specific phospholipase C. *Physiol Rev.* 80: 1291-1335.

Reyes-Harde, M., Stanton, P.K. (1998). Postsynaptic phospholipase C activity is required for the induction of homosynaptic long-tern depression in rat hippocampus. *Neurosci. Let.* 252: 155-158.

Rheenen, J.V., Achame, E.M., Janssen, H., Calafat, J., and Jalink, K. (2005). PIP2 signalling in lipid domains: a critical re-evaluation. *EMBO. J.* 24: 1664-1673.

Rizo, J., and Sudhof, T.C. (1998). C_2-domains, structure and function of a universal Ca^{2+}-binding domain. *J. Biol. Chem.* 273: 15879-15882.

Sano, A., Zhu, X., Sano, H., Munoz, N.M., Boetticher, E. and Leff, A.R. (2001). Regulation of eosinophil function by phosphatidylinositol-specific PLC and cytosolic PLA (2). *Am J Physiol Lung Cell Mol Physiol* 281: 844-851.

Satterwaite, A.B., Li, Z and Witte, O.N. (1998). Btk function in B cell development and response. *Semin. Immunol.* 10: 309-316.

Saunders, C.M., Larman, M.G., Parrington, J., Cox, L.J., Royse, J., Blayney, L.M., Swann, K. and Lai, F.A. (2002). PLC zeta: a sperm-specific trigger of Ca(2+) oscillations in eggs and embryo development. *Development* 129: 3533-3544.

Sechi, A.S., and Wehland, J. (2000). The actin cytoskeleton and plasma membrane connection: PtdIns(4,5)P(2) influences cytoskeletal protein activity at the plasma membrane. *J. Cell. Sci.* 113: 3685-3695.

Seifert, J.P., Wing, M.R., Snyder, J.T., Gershburg., Sondek, J. and Harden, T.K. (2004). RhoA activates purified phospholipase Cε by a guanine nucleotide-dependent mechanism. *J. Biol. Chem.* 279: 47992-47997.

Sekiya, F., Poulin, B., Kin, Y.J. and Rhee, S.G. (2004). Mechanism of tyrosine phosphorylation and activation of phospholipase C-gamma 1. Tyrosine 783 phosphorylation is not sufficient for lipase activation. *J. Biol. Chem.* 279: 32181-32190.

Sharom, F.J. and Lehto, M.T. (2002). Glycosylphosphatidylinositol-anchored proteins: structure, function, and cleavage by phosphatidylinositol-specific phospholipase C. *Biochemistry and Cell Biology.* 80: 535-549.

Shen, H., and Dowhan, W. (1996). Reduction of CDP-diacylglycerol synthase activity results in the excretion of inositol by Saccharomyces cerevisiae. *J. Biol. Chem.* 271: 29043-29048.

Shibatohge, M., Kariya, K., Liao, Y., Hu, C.D., Watari, Y., Goshima, M., Shima, F. and Kataoka, T. (1998). Identification of PLC210, a Caenorhabditis elegans phospholipase C, as a putative effector of Ras. *J. Biol. Chem.* 273: 6218-6222.

Shimohama, S., Matsushima, H., Fujimoto, S., Takenawa, T., Taniquchi, T., Kameyama, M. and Kimura, J. (1995). Differential involvement of Phospholipase C isozymes in Alzheimer's disease. *Gerontology.* 41: 9-13.

Shimohama, S., Perry, G., Richey, P., Takenawa, T., Whitehouse, P.J., Miyoshi, K., Suenaga, T., Matsumoto, S., Nishimura, M. and Kinura, J. (1993). Abnormal accumulation of phospholipase C-delta in filamentous inclusions of human neurodegenerative diseases. *Neurosci Lett.* 162: 183-186.

Shulga, Y.V., Topham, M.K., Epand, R.M. (2011). Substrate specificity of diacylglycerol kinase-epsilon and the phosphatidylinositol cycle. *FEBS Letters.* 585: 4025-4028.

Singh, S.M., and Murray, D. (2003). Molecular modelling of the membrane targeting phospholipase C pleckstrin homology domains. *Protein Sci.* 12: 1934-1953.

Sloane-Stanley, G.H. (1953). Anaerobic reactions of phospholipids in brain suspensions. *Biochem. J.* 53: 613-619.

Smrcka, A.V., Brown, J.H., Holz, G.G. (2012). Role of phospholipase Cε in physiological phosphoinositide signalling networks. *Cellular signalling.* 24: 1333-1343.

Smyth, D.R., Mrozkiewicz, M.K., Mcgrath, W.J., Listwan, P., Kobe, B. (2002). Crystal structures of fusion proteins with large-affinity tags. *Protein Sci.* 12: 1313-1322.

Song, C., Hi, C.D., Masago, M., Kariyai, K., Yamawaki-Kataoka, Y., Shibatohge, M., Wu, D., Satoh, T. and Kataoka, T. (2001). Regulation of a novel human phospholipase C, PLCε, through membrane targeting by Ras. *J. Biol. Chem.* 276: 2752-2757.

Sorensen, H.P., Mortensen, K.K. (2005). Advanced genetic strategies for recombinant protein expression in *Escherichia coli. J. Biotechnol.* 115: 113-128.

Sorkin, A., Heling, K., Water, C.M., Carpenterm G. and Geuinot, L. (1991). Multiple autophosphorylation sites of the epidermal growth factor receptor are essential for receptor kinase activity and internalization. *J. Biol. Chem.* 267: 8672-8678.

Sorli, S.C., Bunney, T.D., Sugden, P.H., Paterson, H.F. and Katan, M. (2005). Signalling properties and expression in normal and tumor tissues of two phospholipase C epsilon slice variants. *Oncogene.* 24: 90-100.

Stewart, A.J., Mukherjee, J., Roberts, S.J., Lester, D. and Farquharson, C. (2005). Identification of a novel class of mammalian phosphatidylinositol-specific phospholipase C eznymes. *Int. J. Mol. Med.* 15:117-121.

Suh, P.G., Park, J.I., Manzoli, L., Cocco, L., Peak, J.C., Katan, M., Fukami, K., Kataoka, T., Yun, S., and Ryu, S.H. (2008). Multiple roles of phosphoinositide-specific phospholipase C isozymes. *BMB. Rep.* 41: 415-434.

Sun, L., Mao, G., Kunapuli, S.P., Dhanasekaran, D.N. and Rao, A.K. (2007). Alternative splice variants of phospholipase C-beta2 are expressed in platelets: effect Galpha-dependent activation and localization. *Platelets.* 18: 217-223.

Susin, S.A., Lorenzo, H.K. Zamzami, N., Marzo, I., Snow, B.E., Brothers, G.M., Mangion, J., Jacotot, E., Costantini, P., Loeffler, M., Larochette, N, Goodlett, D.R., Aebersold, R., Siderovski, D.O., Penninger, J.M. and Kroemer, G. (1999). Molecular characterisation of mitochondrial apoptosis-inducing factor. *Nature.* 397: 441-446.

Takai, Y., Sasaki, T. and Matozaki, T. (2001) Small GTP-binding proteins. *Physiol. Rev.* 81: 153-208.

Takano, M., and Kuratomi, S. (2003). Regulation of cardiac inwardly rectifying potassium channels by membrane lipid metabolism. *Prog. Biophys. Mol. Biol.* 81: 67-79.

Takei, K., Haucke, V. (2001). Clathrin-mediated endocytosis: membrane factors pull the trigger. *Trends in Cell Biology.* 9: 385-391.

Tamura, K., Peterson, D., Peterson, N., Stecher, G., Nei, M. and Kumar, S. (2011). MEGA5: Molecular Evolutionary Genetics Analysis using Maximum Likelihood, Evolutionary Distance, and Maximum Parsimony Methods. *Molecular Biology and Evolution.* 28: 2731-2739.

Tanaka, O. and Kondo, H. (1994). Localization of mRNAs for three novel members (beta 3, beta 4 and gamma 2) of phospholipase C family in mature rat brain. *Neurosci. Lett.* 182: 17-20.

Taylor, S.J., Exton, J.H. (1991). Two alpha subunits of the Gq class of G proteins stimulate phosphoinositide phospholipase C-beta 1 activity. *FEBS Lett.* 286: 214-216.

Tdano, M., Edamatsu, H., Minamisawa, S., Yokoyama, U., Ishikawa, Y., Suzuki, N., Saito, H., Wu, D., Masagotoda, M., Yamawaki-Kataoka, Y., Setsu, T., Terashima, T., Maeda, S., Satoh, T. and Kataoka, T. (2005). Congenital semilunar valvulogenesis defect in mice deficient in phospholipase C epsilon. *Mol. Cell. Biol.* 25: 2191-2199.

Tomas, A., Yermen, B., Regazzi, R., Pessin, J.E., and Halban, P.A. (2009). Regulation of insulin secretion of phosphatidylinositol-4,5-bisphosphate. *Traffic* 11: 123-137.

Traynor-Kaplan, A.E., Harris, A.L., Thompson, B.L., Taylor, P., and Sklar, L.A. (1988). An inositol tetrakisphosphate-containing phospholipid in activated neutrophils. *Nature* 334: 353-356.

Tsumoto, K., Ejima, D., Kumagai, I., Arakawa, T. (2003). Practical consideration in refolding from inclusion bodies. *Protein Expr. Purif.* 28: 1-8.

Turecki, G., Grof, P., Cavazzoni, P., Duffy, A., Grof, E., Ahrens, B., Berghofer, A., Muller-Oerlinghausen, B., Dvorakova, M., Libigerova, E., Vojtechovsky, M., Zvolsky, P., Jppber, R., Nilsson, A., Prochazka, H., Licht, R.W., Rasmussen, N.A., Schou, M., Vestergaard, P., Holzinger, A., Schumann, C., Thau, K., Rouleau, G.A. and Alda, M. (1998) Evidence for a role of phospholipase C-gamma1 in the pathogenesis of bipolar disorder. *Mol. Psychiatry.* 3: 534-538.

Valius, M., Bazenet, C. and Kazlauskas, A. (1993). Tyrosine 1021 and 1009 are phosphorylation sites in the carboxy terminus of the platelet-derived growth factor receptor beta suunit and are required for binding of phospholipase C gamma and a 64-kilodalton protein, respectively. *Mol. Cell. Biol.* 13: 133-143.

Van Ginneken, V.J.T. and Maes, G.E. (2005). The European eel (*Anguilla anguilla,* Linnaeus), its lifecycle, evolution and reproduction: a literatura review. *Reviews in Fish Biology and Fisheries.* 15: 367-398.

Van Ginneken, V.J.T., Durif, C., Balm, S.P., Boot, R., Verstegen, M.W., Antonissen, E. and van Den Thillart, G. (2007). Silvering of European eel (Anguilla anguilla L.): seasonal changes of morphological and metabolic parameters. *Animal Biology.* 57: 63-77.

Varnai, P., Lin, X., Lee, S.B., Tuymetova, G., Bondeva, T., Spat, A., Rhee, S.G., Hajnoczky, G., and Balla, T. (2002). Inositol lipid binding and membrane localisation of isolated pleckstrin homology (PH) domains. Studies on the PH domains of phospholipase C delta 1 and p130. *J. Biol. Chem.* 277: 27412-27422.

Venema, V.J., Ju, H., Sun, J., Eaton, D.C., Marrero, M.B. and Venema, R.C. (1998). Bradykinin stimulates the tyrosine phosphorylation and bradykinin B2 receptor association of phospholipase C gamma 1 in vascular endotelial cells. *Biochem Biophys Res Commun* 246: 70-75.

Volwerk, J. J., Koke, J.A., Wetherwax, P.B. and Griffith, O.H. (1989). Functional characteristics of phosphatidylinositol-specific phospholipase C from *Bacillus cereus* and *Bacillus thuringiensis. FEMS Microbiol. Lett.* 52: 237-241.

Waldo, G.L., Ricks, T.K., Hicks, S.N., Cheever, M.L., Kawano, T., Tsuboi, K., Wang, X., Montell, C., Kozasa, T., Sondek, J. and Harden, T.K. (2010). Kinectic scaffolding mediated by a phospholipase C-beta and Gq signalling complex. *Science.* 330: 974-980.

Wang, D., Feng, J., Wen, R., Marine, J.C., Sangster, M.Y., Parganas, E., Hoffmeyer, A., Jackson, C.W., Cleveland, J.L., Muraay, P.J., Ihle, J.N. (2000) Phospholipase C gamma 2 is essential in the functions of B cell and several Fc receptors. *Immunity.* 13: 25-35.

Wang, T., Dowal, L., El-Maghrabi, M.R., Rebecchi, M. and Scarlata, S. (2000). The pleckstrin homology domain of phospholipase C-β2 links the bidning of Gβγ to activation of the catalytic core. *J. Biol. Chem.* 275: 7466-7469.

Wang, T., Pentyala, S., Rebecchi, M.J. and Scarlata, S. (1999). Differential association of the pleckstrin homology domains of phospholipases C-β_1, C-β_2, and Cδ_1 with lipid bilayers and the βγ subunits of heterotrimeric G proteins. *Biochemistry* 38: 1517-1524.

Wassarman, P., Chen, J., Cohen, N., Litscher, E., Liu, C., Huayu, Q. and William, Z. (1999). Structure and function of the mammalian egg zona pellucida. *J. Exp. Zoo.* 285: 251-258.

Watanabe, M., Nakamura, M., Sato, K., Kamo, M., Simon, M.I. and Inoue, Y. (1998). Patterns of expression for the mRNA corresponding to the four isoforms of phospholipase Cβ in mouse brain. *Eur. J. Neurosci.* 10: 2016-2025.

Webb, H., Carnall, N. and Carrington, M. (1994). The role of GPI-PLC in Trypanosoma brucei. *Braz. J. Med. Biol. Res..* 27: 349-356.

Webb, H., Carnall, N., Vanhamme, L., Rolin, S., Abbeele, J. V. D., Welburn, S., Pays, E. and Carrington, M. (1997). The GPI-phospholipase C of *Trypanosoma brucei* is nonessential but influences parasitemia in mice. *JCB.* 139: 103-114.

Whitman, M., Downes, C.P., Keeler, M., Keller, T., and Cantley, L. (1988). Type I phosphatidylinositol kinase makes a novel inositol phospholipid, phosphatidylinositol-3-phosphate. *Nature.* 332: 644-646.

Wilde, J.I. and Watson, S.P. (2001). Regulation of phospholipase C gamma isoforms in haematopoietic cells: why one, not the other? *Cell. Signal.* 13: 691-701.

Wing, M.R., Snyder, J.T., Sondek, J. and Harden, T.K. (2003). Direct activation of phospholipase Cε by Rho. *J. Biol. Chem.* 278: 41253-41258.

Xie, W., Samoriski, G.M., McLaughlin, J.P., Romoser, V.A., Smrcka, A., Hinkle, P.M., Bidlack, J.M., Gross, R.A., Jiang, H. and Wu, D. (1999). Genetic alteration of phospholipase C beta3 expression modulates behavioural and cellular responses to mu opioids. *Proc. Natl. Acad. Sci. U. S. A.* 96: 10385-10390.

Yin, H.L., and Janmey, P.A. (2002) Phosphoinositide regulation of the actin cytoskeleton. *Annu. Rev. Physiol.* 65: 761-789.

Yoon, S-Y., Jellerett, T., Salicioni, A.M., Lee, H.C., Yoo, M., *et al.,* (2008). Human sperm devoid of PLC zeta 1 fail to induce Ca^{2+} release and are unable to initiate the first steps of embryo development. *J. Clin. Investig.* 118: 3671-3681.

Yugo, I., Shinobu, N., Hideo, N., Tom, N. and Tsuneo, Y. (1994). Purification and properties of phosphatidylinositol-specific phospholipase C from *Streptomyces antibioticus. Biochim. Biophys. Acta.* 1214: 221-228.

Zhou, Y., Wing, M.R., Sondek, J. and Harden, T.K, (2005). Molecular cloning and characterization of PLC-eta2. *Biochem. J.* 391: 667-676.

Appendices

Appendix A- Sequences of primers used for the amplification of eel PLCXDs

Marathon adaptor primer 1 (AP1)	5'-CCATCCTAATACGACTCACTATAGGGC-3'
Marathon adaptor primer 2 (AP2)	5'-ACTCACTATAGGGCTCGAGCGGC-3'
Eel PLCXD4 AS1	5'-TGCCAGCGAAAAGTATTACAAAG-3'
Eel PLCXD4 AS2	5'-CTTCATGACCATTTGGGAGATCAAGC-3'
Eel PLCXD4 AS3	5'-CATGAGGGTGAGCAATCAAACG-3'

>Anguilla anguilla PLCXD4 protein mRNA, partial coding sequence.

GTACTTTGTAATACTTTTCGCTGGCAGTGAAGGGGATCCCTATTTCAATGATTTAGAAAAGCTTGATCT
CCCAAATGGTCATGAAGTAAACTGGATGAAAAGTATAGATGATGAAACACTTCTCTCAGCAGTCACCAT
TCCAGGCACATGCCAAAGCATGAAAATGAATACTCTTGATCAACACCAAGCATGGACAGTAACACAGCA
GTTTACAGCAGGGGTGCGATTCTTTGATATCTCCCTGGATAATTCAGTTGTCAAAGATGGTTCTCTTAC
ACGTAGAAAATTTGCAGATGTCATGGAAAAGATGAGAGAACGTTTGATTGCTCACCCTCATGAAGTAAT
TTTGATAAGATTGACCCCAGAAAATGGCAAAGCTGAAAAGGAAATAGAAAAATTCATACAAGTGAATGA
CAATGTGTGGAAGGATAAAAAAGTGCCCAAAATGAAAGAAGTAAGGGGTAAGATAGTGTTGGTGCAGAG
CAGCAAGTTCAGTAAAGGGCTCCCGGTGGACCTTCATGTGGGTGGGAAGGAGTTTAAAGATAAGCACTC
AAAAAAGTACATGGAAGCGATTTATAATCATCTAAAGGCAGCAGAAAATGCAGGTGACCATATTGTAGT
GACTGAAACAAGCGCATATTTTGGATTCACAAAATCATCAAAAAATGCAGCTGTAAAAATTAATCCCAT
GCTCCAAAAATACATAGACAACCAGCCGCATGCTAATAAACCAAAAGGTTTGGGGGTGATTGTCATGGA
CTATCCAGGCATTGATCTCATCCAGAAAATCATAGATATCAACCCTAAATCAGAAGGCTCACCTGAATC
CTCCCCAGAAGAAGGTGAGAACCCACCTGAAACTGATGGGGAACCCGAATGA

Figure 1/Table 1: Partial coding sequence of the sense strand of ePLCXD4, prior to the onset of this project. Primers used to amplify and sequence the 5' end within this thesis were: AS1, AS2 and AS3.

Primer seqeunecs used for determination of tissues distribution by real-time quantitative PCR.

	Sense (5’-3’)	Antisense (5’-3’)
PLCXD1	GCAGCATGGCTTGACTCCCACC’	CGTCGTCATCGTAGGACAGCACG
PLCXD2	GTGCGTGACGGCCTCCATGAAATC	CATCAGCCAGTGGGTGGTGGTAG
PLCXD3	CGACGAGGCGTCGCCGGTG	GAGGCCGTGCGCGAAGTAGAG
PLCXD4	CGTTTGATTGCTCACCCTCATGA	GAGCCCTTTACTGAACTTGCTGCTCT

Appendix B- Accession numbers for proteins in used in ClustalW and phylogenetic analyses.

Protein	Species	EMBL Accession number
PLCXD1	*Homo sapiens*	AAH05028.1
	Mus musculus	AAH39627.1
	Bos Taurus	AA151475.1
	Danio rerio	AAH93162.1
	Anguilla anguilla	N/A
	Xenopus tropicalis	AAMC01064598
	Gallus gallus	AADN03001397
PLCXD2	Homo sapiens	AA1211156.1
	Mus musculus	AA151060.1
	Bos Taurus	DAAA02001335
	Anguilla anguilla	N/A
	Xenopus laevis	AAH42310.1
PLCXD3	Homo sapiens	CAH56160.1
	Mus musculus	NP_796329.2
	Bos Taurus	NP_001096774.1
	Anguilla anguilla	N/A
	Danio rerio	AAH91866.1
PLCXD4	Anguilla anguilla	JX101676
	Takifugu rubripes	XP_003969411.1
	Oreochromis niloticus	XP_003452509.2
	Stegastes partitus	XP_008286913.1
	Danio rerio	XP_005158485.1
PI-PLC	Bacillus cereus	NP_833485.1
	Bacillus thuringiensis	ZP_04103399.1
	Listeria monocytogenes	CAA38438.1
	Trypanosoma cruzi	CAA03904.1

Appendix C- Sequences of primers used for molecular cloning of PLCXDs in *E.coli*

hPLCXD isoform	Primer Pair (5'→3')	Extension	Target Vector
hPLCXD1	Sense- ATGGGTGGCAGGTGAGCGCTTC Antisense- TCAGCACCACAGCAGCTTCTGCATTGAG	**NcoI HindIII**	**pET M11**
	Sense- ATGGGTGGGCAGGTGAGCGCTTC Antisense- TCAGCACCACAGCAGCTTCTGATTGAG	**SpeI NdeI**	**pdlNotI'nPk 'MCS'R**
	Sense- ATGGGTGGGCAGGTGAGCG Antisense-TCAGCACCACAGCAGCTTCTGATTG	**See Table 2.5 Chapter 2**	**pOPIN (N-terminal fusion)**
	Sense- ATGGGTGGGCAGGTGAGCG Antisense- GCACCACAGCAGCTTCTGATTGAGC	**See Table 2.5 Chapter 2**	**pOPIN (C-terminal fusion)**
hPLCXD-2.1	Sense- ATGCTAGCAAGTTAGGAAGGCCAGGAG Antisense- GGATCTTCTGCTGAATCTCAAAGG	**NdeI HindIII**	**pET 22b+**
	Sense- ATGCTAGCAAGTTAGGAAGGCCAGGAG Antisense TCAGGATCTTCTGCTGAATCTCAAAGG	**SpeI NdeI**	**pdlNotI'nPk 'MCS'R**
	Sense- ATGCTAGCAGTTAGGAAGGCCAGGAGG Antisense- TCAGGATCTTCTGCTGAATCTCAAAGG	**See Figure 2.5 Chapter 2**	**pOPIN (N-terminal fusion)**
	Sense- ATGCTAGCAGTTAGGAAGGCCAGGAGG Antisense- GGATCTTCTGCTGAATCTCAAAGGATAAACTGG	**See Figure 2.5 Chapter 2**	**pOPIN (C-terminal fusion)**
hPLCXD3	Sense- ATGGCCTCGTCTCAGGGGAAAACG Antisense- TCAAAGTGTTGGCTTCTCCTTCATCAAAG	**NcoI HindIII**	**pET M11**
	Sense- ATGGCCTCGTCTCAGGGGAAAAACG Antisense- TCAAAGTGTTGGCTTCTCCTTCATCAAAG	**SpeI NdeI**	**pdlNotI'nPk 'MCS'R**
	Sense- ATGGCCTCGTCTCAGGGGAAAAAC Antisense- TCAAGTGTTGGCTTCTCCTTCATCAAAG	**See Table 2.5 Chapter 2**	**pOPIN (N-terminal fusion)**
	Sense- ATGGCCTCGTCTCAGGGGAAAAAC Antisense- GTTGGCTTCTCCTTCATCAAAGACATAG	**See Table 2.5 Chapter 2**	**pOPIN (C-terminal fusion)**

Appendix D- Primers used for semi-quantitative and quantitative PCR experiments to determine tissue expression patterns

Mouse PLCXD1 Sense	5’-GTACCTGGACCTGCGGATCGCGCAT-3’
Mouse PLCXD1 Antisense	5’-GGCCAGAGCTGATCATAACGGCTGACTGT-3’
Mouse PLCXD2 Sense	5’-GAGACACTGACCAGGAGATCTACTTCATC-3’
Mouse PLCXD2 Antisense	5’-GCTCGCTCACTCAGGGTGCTCTCCAAG-3’
Mouse PLCXD3 Sense	5’-CAGACGATGAGCTTCACTGGTCAGC-3’
Mouse PLCXD3 Antisense	5’-CTGTGGTAGAAGACCAGTACTTGATAGTG-3’
Mouse Rpl-P0 Sense	5’-GAGTGATGTGCAGCTGATAAAGACTGG-3’
Mouse Rpl-P0 Antisense	5’-CTGCTCTGTGATGTCGAGCACTTCAG-3’
Human PLCXD1 Sense	5’-CGCCCTGTCGTGCTGAAATGGTC-3’
Human PLCXD1 Antisense	5’-GATACAGGCGACCAGGTACTCGTG-3’
Human PLCXD2.1 Sense	5’-CGCTACTTTGACCTGCGTGTGTC-3’
Human PLCXD2.1 Antisense	5’-CGCAGCGTCAAACTTTCCACACTG-3’
Human PLCXD3 Sense	5’-GCGGAAATGGTTAGCCACTCAGAC-3’
Human PLCXD3 Antisense	5’-CAGCACTTGATAGTCCTTCTCCCAC-3’
Human Rpl-P0 Sense	5’-GAGTGATGTGCAGCTGATCAAGACT-3’
Human Rpl-P0 Antisense	5’-GTTCCTCTGTGATATCAAGCACTTCAG-3’

Appendix E- Sequencing primers for pCR 4-TOPO

M13 sense	5’-GGAACAAACGGCATGTGAGC-3’
M13 antisense	5’-AAGCAGTGGTAACAACGCAGAGTACGCGGG-3’
T3 sense	5’-ATTAACCCTCACTAAAGGGA-3’
T7 antisense	5’-TAATACGACTCACTATAGGG-3’
pETM11 Sense	5’-CCATGAAACATCACCATCACCATCACC-3’
pETM11 Antisense	5’-GCTAGTTATTGCTCAGCGGTGGCAG-3’
pET22b+ Sense	5’-CTTAAGAAGAGATATACCATGAAACATCAC-3’
pET22b+ Antisense	5’-AGCTTGTCGACGGAGCTCGAATT-3’

Appendix F- Specific primers for RT-qPCR assays using cDNA prepared from Harlequin mice tissues

Gene name	Sense primer (5'-3')	Antisense primer (5'-3')
AIF1	GGGGGCAAAATGGATAATTC	CTGTTCTCTTCTGGGGACAG
AIF2	GTCATCTCCTAGGATCCCCTTC	TTGGTCTTCTTTTATAGTTTTGTAGGC
BRN3A	GAGGCCTATTTTGCCGTACA	CAGTAAGTGGCAGAGAATTTCA
PLCXD1	GTACCTGGACCTGCGGATCGCGCAT	GGCCAGAGCTGATCATAACGGCTGACTGT
PLCXD2	GAGACACTGACCAGGAGATCTACTTCATC	GCTCGCTCACTCAGGGTGCTCTCCAAG
PLCXD3	CTCAGGTGGTGCTGACACCCAAA	GTACGGATCCACTGCATCATGGCG